



City Research Online

City, University of London Institutional Repository

Citation: Navaratnarajah, V. (1982). Variation of transfer bond in concrete under lateral restraint. (Unpublished Doctoral thesis, The City University)

This is the accepted version of the paper.

This version of the publication may differ from the final published version.

Permanent repository link: <https://openaccess.city.ac.uk/id/eprint/35300/>

Link to published version:

Copyright: City Research Online aims to make research outputs of City, University of London available to a wider audience. Copyright and Moral Rights remain with the author(s) and/or copyright holders. URLs from City Research Online may be freely distributed and linked to.

Reuse: Copies of full items can be used for personal research or study, educational, or not-for-profit purposes without prior permission or charge. Provided that the authors, title and full bibliographic details are credited, a hyperlink and/or URL is given for the original metadata page and the content is not changed in any way.

VARIATION OF TRANSFER BOND IN CONCRETE UNDER LATERAL RESTRAINT

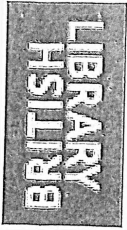
by

VELUPPILLAI NAVARATNARAJAH

Submitted in fulfilment of the requirements
for the degree of Doctor of Philosophy

THE CITY UNIVERSITY
Department of Civil Engineering

NOVEMBER, 1982.



IMAGING SERVICES NORTH

Boston Spa, Wetherby
West Yorkshire, LS23 7BQ
www.bl.uk

BEST COPY AVAILABLE.

VARIABLE PRINT QUALITY

**PAGINATED BLANK PAGES
ARE SCANNED AS FOUND
IN ORIGINAL
NO INFORMATION IS
MISSING**

CONTENTS

	<u>Page</u>
Notation	vii
Terminology	x
List of Tables	xii
List of Figures	xiv
Acknowledgement	xix
Abstract	xx
CHAPTER 1 : INTRODUCTION	1
1.1 Outline of investigation	1
1.2 Preliminary background to the study	3
1.3 Organisation of the thesis	5
CHAPTER 2 : REVIEW OF BOND BEHAVIOUR OF REINFORCING STEEL	8
2.1 Bond tests	9
2.2 Parameters influencing bond strength	19
2.2.1 Effects of bar profile	20
2.2.2 Diameter of bar and embedment length	23
2.2.3 Strength of concrete	24
2.2.4 Confinement	26
2.3 Choice of parameters in the present study.	28

	<u>Page</u>
CHAPTER 3 : EXPERIMENTAL INVESTIGATION OF THE EFFECT OF TENSION RELEASE ON BOND BEHAVIOUR	30
3.1 Object and scope of test programme	30
3.2 Test specimen	31
3.2.1 Philosophy of choice of test specimen	31
3.2.2 Details of test programme	33
3.2.3 Details of test specimen	34
3.2.4 Casting of specimens	34
3.2.4.1 Details of mould	34
3.2.4.2 Materials	36
A. Concrete	36
B. Steel	38
3.2.5 Control tests	38
3.3 Test arrangement	39
3.4 Instrumentation	41
3.5 Test procedure	41
CHAPTER 4 : EXPERIMENTAL INVESTIGATION OF THE EFFECT OF LATERAL COMPRESSION ON BOND BEHAVIOUR	46
4.1 Object and scope of test programme	46
4.2 Test specimen	46
4.2.1 Philosophy of choice of test specimen	46
4.2.2 Details of test programme	47
4.2.3 Details of test specimen	47
4.2.4 Casting of specimen	49

4.2.4.1	Details of mould	49
4.2.4.2	Materials and casting procedure	52
	A. Concrete	52
	B. Steel	53
	C. Casting procedure	53
4.2.5	Control tests	56
4.3	Test arrangement	57
4.4	Instrumentation	60
4.5	Test procedure	62
CHAPTER 5	: THEORETICAL ANALYSIS	69
5.1	Bond mechanism	69
5.2	Failure mechanism of deformed bars	69
5.2.1	Splitting failure mechanism	74
5.2.1.1	Bond action in partly cracked elastic stage	76
5.2.1.2	Concrete ring with external pressure	80
5.2.2	Plough-through failure mechanism	86
5.2.3	Definition of bond failure	88
5.2.4	Empirical theory of bond failure under lateral pressure	89
5.2.5	Failure mechanism under tension release	92

	<u>Page</u>
CHAPTER 6 : PRESENTATION AND DISCUSSION OF RESULTS OF EXPERIMENTS WITH LATERAL TENSION RELEASE	99
6.1 Load slip characteristics	99
6.1.1 Effect of type of bar	100
6.2 Ultimate bond resistance	105
6.2.1 Effect of concrete cover and tension release	107
6.2.2 Interaction between concrete cover and tension release	111
6.3 Critical bond stress	115
6.3.1 Effect of concrete cover and tension release	118
6.3.2 Interaction between concrete cover and tension release	127
6.4 Modes of ultimate failure	129
CHAPTER 7 : PRESENTATION AND DISCUSSION OF RESULTS OF EXPERIMENTS WITH LATERAL COMPRESSION	136
7.1 Load-slip characteristics	136
7.2 Ultimate bond resistance	139
7.2.1 Effect of location of bars	143
7.2.2 Effect of cover	145
7.2.3 Effect of lateral pressure	149
7.2.4 Interaction between concrete cover and lateral pressure	151
7.3 Critical bond stress	161
7.3.1 Effect of location of bars	161
7.3.2 Effect of cover	161
7.3.3 Effect of lateral pressure	168
7.3.4 Interaction between concrete cover and lateral pressure	171

7.4	Comparison of experimental results with theory	175
7.5	Modes of ultimate failure	184
CHAPTER 8	: COMPARISON OF RESULTS WITH DESIGN CODE PROVISIONS IN C.P. 110	196
8.1	Factor of safety under lateral tension release	197
8.2	Factor of safety under lateral compression	199
8.3	Outlook for design	201
CHAPTER 9	: CONCLUSIONS	202
9.1	Main conclusions relating to lateral tension release	202
9.2	Main conclusions relating to lateral compression	203
9.3	Bond efficiency of the different types of bars	204
9.4	Recommendations for further study	205
REFERENCES		207
APPENDIX A	: LOAD SLIP CHARACTERISTICS	217
APPENDIX B	: DATA RELATING TO TENSION RELEASE TESTS	247
B.1	Details of concrete mix and concrete strength	247
B.2	Calibration tables of load cells	249
B.3	Properties of test bars and steel studs	250
APPENDIX C	: DATA RELATING TO LATERAL COMPRESSION TESTS	255
C.1	Details of concrete mix and concrete strength	255
C.2	Calibration table of load cell	257
C.3	Investigation for loading system	258
APPENDIX D	: CALCULATIONS OF BOND FORCE	260

NOTATION

A	distance from face of concrete to centre of reinforcement bar
A_{tr}	area of cross-section of transverse reinforcement/stirrup
B	defined by the equation $B = \frac{2p_o A^2}{f_t}$
a } b }	power indices in formulae
a'	half-width of bearing pad on an anchor block
B_1, B_2, B_3, B_4	regression coefficients
C	cover of concrete to reinforcement bar
D	diameter of reinforcement bar
D_c	diameter of cylindrical 'core' of the bar
d	diameter of transverse reinforcement/stirrup
e	centre to centre spacing of ribs in deformed reinforcement bar
F	force developed in reinforcement bar at bond failure
F_{cr}	component of F due to ring tension cracking
F_{fr}	frictional component of F
f_b	bond stress at a slip 0.1 mm at the free-end
f_{bb}	bond stress in the absence of transverse reinforcement/stirrup
f_{bo}	bond stress at 0.1 mm slip at maximum concrete cover and zero tension release or lateral pressure
f_{br}	coefficient of friction between steel and concrete
f_{btr}	bond stress attributable due to transverse reinforcement/stirrup
f_{bu}	ultimate bond stress
f'_c	cylinder strength of concrete

f_{cp}	prism strength of concrete
f_{cu}	cube strength of concrete
f_s	punching shear strength of concrete
f_t	splitting tensile strength of concrete
f_{yt}	yield strength of transverse reinforcement/stirrup
G	a coefficient
h	height of rib in deformed reinforcement bar
K_1	initial bond slip modulus
K_2	bond slip modulus after ring tension cracking
K_b	a factor which is a function of type of deformed bar and concrete
K_c	a factor which is a function of concrete cover
k	a factor depending on strength of concrete
L	embedment length of reinforcement bar
M	a constant
m n }	power indices in formulae
p	lateral pressure
p_{av}	average pressure at bar/concrete interface
p_i	internal pressure
p_o	outside pressure
p_2	pressure on internal surface of cracked ring
R	radius of internal cracking in concrete surrounding the bar
r	radius at any point in the wall of a thick ring
r_1	inside radius of thick ring

r_2	outside radius of thick ring
s	spacing of transverse reinforcement/stirrup
w	effective width of dispersion of compressive stress at level of bar
x_1, x_2, x_3 x_4, x_5, x_6	regression coefficients
α	angle between bond forces and the axis of the reinforcement bar
β	a constant
ϵ_t	tensile strain in concrete surrounding bar
ϵ_{tm}	limiting tensile strain of 4250 microstrains
γ	a factor depending on slope of the stirrups to the axis of the longitudinal bar
σ_θ	tangential stress in the wall of a thick cylinder at an angle θ
σ_x	vertical compressive stresses due to concentrated load on an anchor block
σ_y	bursting tensile stress in an anchor block

TERMINOLOGY

A number of terms used in other bond studies as well as in this investigation need to be defined precisely for the sake of clarity.

1. Bond strength is used to denote the maximum or ultimate load that is obtained before bond failure. This may be expressed as the ultimate bond load or the ultimate bond stress which is the maximum average bond stress over the bonded length.
2. Critical bond stress denotes the average bond stress over the bonded length at a slip of 0.1 mm at the free end of the bar.
3. Bond failure is defined in this study as occurring at a free-end slip of 0.1 mm.
4. Ultimate failure implies a failure in which the concrete surrounding the reinforcing bar fails and the bar is unable to hold the load applied.
5. Resistance to slip of a reinforcing bar is its resistance to slip or movement relative to the surrounding concrete.
6. Slip denotes the relative displacement between the reinforcement bar and the surrounding concrete that occurs upon loading of the bar. The loaded-end slip is a measure of the slip at the loaded end of a bond test specimen. The free-slip is a measure of the slip at the unloaded end of a bond test specimen.
7. Rib is used to denote the bar deformation which is oriented essentially normal to the axis of a reinforcing bar.
8. The term concrete key is used to denote the concrete between two ribs of a deformed bar.

9. Top cast and bottom cast are used to denote whether a horizontal bar has been so placed that more (top cast) or less (bottom cast) than 300 mm of concrete has been cast below the bar.
10. Initial slip modulus is taken as the slope of the line joining the origin of the load-slip curve to the point on the curve corresponding to the load at 0.1 mm slip.
11. Cracked slip modulus is given by the slope of the line joining the points on the load-slip curve corresponding to the loads at 0.1 mm slip and ultimate load respectively.
12. Tension release ($\mu\epsilon$) is the strain applied in the studs in order to induce a tensile strain field in the concrete. Hence the stated value of tension release is a general indication only of the level of tensile strain in the concrete in the region of the bar under test.

LIST OF TABLES

<u>Table</u>		Page
3.1	Designation code used for specimen numbers - tension release.	35
3.2	Typical record of observations - tension release.	44
4.1	Designation code used for specimen numbers - lateral pressure.	51
4.2	Typical record of observations - lateral pressure.	67
6.1	Slip moduli - Torbar.	102
6.2	Slip moduli - Hybar.	103
6.3	Slip moduli - Square-twisted bar.	104
6.4	Pull-out force at failure.	106
6.5	Ultimate bond stress.	108
6.6	Pull-out force at 0.1 mm slip.	116
6.7	Critical bond stress.	117
6.8	Values of K_b in Equation 6.1.	126
7.1	Maximum slip recorded in top and bottom bars under lateral pressure.	138
7.2	Ultimate pull-out force and concrete strength - Torbar.	140
7.3	Ultimate pull-out force and concrete strength - Hybar.	141
7.4	Ultimate pull-out force and concrete strength - Square-twisted bar.	142
7.5	Ultimate bond stress under lateral pressure.	144
7.6	Ratio of ultimate bond stress/splitting tensile stress.	157
7.7	Correlation of experimental values of ultimate bond stress.	158
7.8	Ratios of bond stresses with different covers and lateral pressure.	160
7.9	Bar force at 0.1 mm slip - Torbar.	162
7.10	Bar force at 0.1 mm slip - Hybar.	163

<u>Table</u>		<u>Page</u>
7.11	Bar force at 0.1 mm slip - Square-twisted bar.	164
7.12	Critical bond stress under lateral pressure.	165
7.13	Variation of critical bond stress with cover.	169
7.14	Ratio of critical bond stress/splitting tensile stress.	172
7.15	Correlation of experimental values of critical bond stress.	174
7.16	Bursting tensile stresses at level of bar.	177
7.17	Pressure at level of bar due to vertical load.	177
7.18	Comparison of bar force at critical bond stress - Torbar.	181
7.19	Comparison of bar force at critical bond stress - Hybar.	182
7.20	Comparison of bar force at critical bond stress - Square-twisted bar.	183
8.1	Safety factors on allowable stresses - tension release.	198
8.2	Safety factors on allowable stresses - lateral pressure.	200

APPENDICES

B.1	Strength of concrete - tension release.	248
B.2	Calibration of load cells.	249
B.3	Properties of test bars.	251
C.1	Strength of concrete - lateral pressure.	256
C.2	Calibration of load cell.	257

LIST OF FIGURES

<u>Figure</u>		<u>Page</u>
2.1	The geometry of a deformed reinforcing bar and the mechanical interaction between the bar and concrete (after Rehm).	13
2.2	Deformation of concrete around ribbed reinforcing bar (schematic diagram) after Goto.	13
2.3	Schematic representation of how the radial components of the bond forces are balanced against tensile stress rings in the concrete in an anchorage zone (after Tepfers).	13
3.1	Pull-out test arrangement.	32
3.2	Details of test specimen - lateral tension release.	32
3.3	Details of mould.	37
3.4	Types of reinforcement bars studied.	37
3.5	Schematic diagram of test arrangement.	40
3.6	Photograph showing bond test under lateral tension release.	42
4.1	Details of test specimen - lateral compression.	48
4.2	Assembled secondary reinforcement cage.	50
4.3	Assembled steel mould.	50
4.4	Specimen assembly before casting.	55
4.5	Schematic diagram of test arrangement.	58
4.6	Photograph showing bond test under lateral compression.	59
4.7	Pulling of test bar.	55
4.8	Jacks applying lateral pressure.	61
4.9	Transfer of lateral pressure to concrete.	61
4.10	Arrangement for slip measurement.	63

4.11	Device for rotating test block	63
4.12	Sequence of testing of top and bottom bars.	66
5.1	Bearing of rib against concrete.	72
5.2	Crushing under rib (after McClure).	72
5.3	Effect of thickness of concrete cover upon bond capacity (after Tepfers).	77
5.4	Internal cracking surrounding reinforcement bar.	77
5.5	Thick ring under internal and external pressure.	81
5.6	Internal cracking in concrete ring under uniform external pressure.	81
5.7	Plough-through shear mechanism.	87
5.8	Internal cracking in concrete ring under unidirectional pressure.	87
5.9	Stress on bar/concrete interface due to lateral pressure.	93
5.10	Section through reinforcing bar and concrete showing separation that occurs near a primary crack.	93
5.11	Magnified deformation showing separation between concrete and bar.	95
5.12	Deformation of concrete around reinforcing steel after formation of internal cracks (schematic diagram).	95
5.13	Graph showing initial and cracked slip modulus.	97
6.1	Variation of ultimate bond stress with cover - Torbar.	109
6.2	Variation of ultimate bond stress with cover - Square-twisted bar.	109
6.3	Variation of ultimate bond stress with cover - Hybar.	110
6.4	Variation of bond stress with cover and tension release - Torbar.	112
6.5	Variation of bond stress with cover and tension release - Hybar.	113
6.6	Variation of bond stress with cover and tension release - Square-twisted bar.	114

<u>Figure</u>		<u>Page</u>
6.7	Variation of critical bond stress with cover - Torbar.	119
6.8	Variation of critical bond stress with cover - Square-twisted bar.	119
6.9	Variation of critical bond stress with cover - Hybar.	120
6.10	Variation of critical bond stress with tension release - Hybar.	120
6.11	Variation of critical bond stress with tension release - Torbar.	121
6.12	Variation of critical bond stress with tension release - Square-twisted bar.	121
6.13	Variation of ratio of critical bond stress with tensile release in concrete - Hybar.	122
6.14	Variation of ratio of critical bond stress with tensile release in concrete - Square-twisted bar.	123
6.15	Variation of ratio of critical bond stress with tensile release in concrete - Torbar.	124
6.16	Variation of ratio of critical bond stress with ratio of tensile strain in concrete.	128
6.17	Typical failure modes under tension release - Torbar.	130
6.18	Typical failure modes under tension release - Hybar.	131
6.19	Typical failure modes under tension release - Square-twisted bar.	132
6.20	Crack patterns at ultimate failure - Torbar.	133
6.21	Crack patterns at ultimate failure - Hybar.	134
7.1	Variation of ultimate bond stress with concrete cover - Torbar.	147
7.2	Variation of ultimate bond stress with concrete cover - Hybar.	147
7.3	Variation of ultimate bond stress with concrete cover - Square-twisted bar.	148
7.4	Variation of ultimate bond stress with lateral pressure - Torbar.	148
7.5	Variation of ultimate bond stress with lateral pressure - Hybar.	150

<u>Figure</u>		<u>Page</u>
7.6	Variation of ultimate bond stress with lateral pressure - Square-twisted bar.	150
7.7	Variation of bond stress with cover and lateral pressure - Torbar.	152
7.8	Variation of bond stress with cover and lateral pressure - Hybar.	153
7.9	Variation of bond stress with cover and lateral pressure - Square-twisted bar.	154
7.10	Variation of critical bond stress with concrete cover - Torbar.	166
7.11	Variation of critical bond stress with concrete cover - Hybar.	166
7.12	Variation of critical bond stress with concrete cover - Square-twisted bar.	167
7.13	Variation of critical bond stress with lateral pressure - Torbar.	167
7.14	Variation of critical bond stress with lateral pressure - Hybar.	170
7.15	Variation of critical bond stress with lateral pressure - Square-twisted bar.	170
7.16	Bursting stress due to concentrated load in an anchor block.	178
7.17	Longitudinal sectional profile of Square-twisted bar.	178
7.18	Typical failure modes - Torbar - Plate 1.	188
7.19	Typical failure modes - Torbar - Plate 2.	189
7.20	Typical failure modes - Hybar - Plate 1.	190
7.21	Typical failure modes - Hybar - Plate 2.	191
7.22	Typical failure modes - Hybar - Plate 3.	192
7.23	Typical failure modes - Square-twisted bar - Plate 1.	193
7.24	Typical failure modes - Square-twisted bar - Plate 2.	194

APPENDICES

Page

A.1 - A.6	Load slip characteristics - lateral tension release.	217
A.7 - A.30	Load slip characteristics - lateral compression.	223
B.1	Details of test bars.	252
B.2	Stress-strain characteristic of high-tensile steel stud.	253

ACKNOWLEDGEMENT

The author wishes to thank the advice and guidance offered by his supervisors Dr. N.P. Roberts and Dr. P.R.S. Speare. The author feels particularly thankful to Dr. P.R.S. Speare for his constructive criticism and suggestions during the writing of the thesis. Thanks are also due to the technical staff of the Civil Engineering Departments of The City University and University of Malaya for their assistance in the experiments and the secretarial staff of the Faculty of Engineering, University of Malaya in the preparation of the thesis in its present form. The free samples of reinforcement bars provided for the tests at the University of Malaya by GKN Reinforcements Limited, Square Grip Limited and Welbond Reinforcements Limited, all of the United Kingdom, are gratefully acknowledged.

The author is especially indebted to [REDACTED] who was instrumental in making this study possible and for his constant encouragement throughout the study. The author wishes to thank [REDACTED] for his continued interest in this work.

Special thanks are due to [REDACTED], who endured patiently during the long period of study. Her endless help, inspiration and encouragement made the attainment of this thesis possible. It is to her that this thesis is dedicated.

ABSTRACT

The thesis describes a study of the effects of lateral restraint on the bond behaviour of reinforcement bars. Bond performance of three types of deformed bars, namely Torbar, Hybar and Square-twisted bars has been investigated experimentally both under varying levels of lateral tension release and lateral compression. The tests included different values of concrete cover to the reinforcement bars and the study of the bond behaviour of top and bottom cast reinforcement bars under lateral compression.

Ultimate bond stress and critical bond stress defined as at the serviceability limit state are shown to increase progressively with cover and the square-root of the lateral compression, the cover affecting the ultimate bond stress more significantly than the lateral pressure. However, a limiting cover of 3.5 bar diameters and a lateral compression of about 25 per cent of the compressive strength of concrete are shown to give the maximum bond resistance. The bursting effects of lateral compression are suggested to affect the bond performance of reinforcement bars under lateral compression. Torbar and Hybar are shown to develop higher ultimate bond resistance under lateral compression than the Square-twisted bars. Top cast bars are demonstrated to be inferior in bond resistance than bottom cast bars.

Ultimate bond stress and critical bond stress are shown to decrease with decreasing cover and increasing lateral tension release. Complete loss of bond is suggested at a tension release of about 4250 micro-strains. A limiting cover of 3.5 bar diameters is shown to offer the maximum bond resistance. Torbar and Hybar are again demonstrated to perform better under tension release than Square-twisted bar.

The interactive behaviour of cover with either lateral tension release or lateral compression has been studied and relationships between bond stress, concrete cover and lateral restraint have been formulated based on the experimental results, both at ultimate and serviceability limit states. A theoretical model for the bond behaviour of reinforcement bars under lateral compression at serviceability limit state has been proposed and verified with the experimental results. The safety factors under lateral tension release and lateral compression are examined based on the provisions for bond design in the current Code of Practice C.P. 110.

CHAPTER 1

INTRODUCTION

1.1 Outline of investigation

The main thrust of the present investigation is towards studying the effects of lateral restraint, both lateral pressure and tension release on the development of transfer bond behaviour of deformed reinforcement steel bars. A comprehensive study would include concrete of various strength levels, different types of deformed bars, effects of varying sizes of deformed bars and the corresponding concrete cover to the deformed bars. It was not possible to cover all of these variables nor was it possible to examine fully the selected variables. However the study helps to obtain a better understanding of the behaviour of the bond of deformed bars under lateral restraint.

There are two basic areas which are covered in this investigation:-

1. the bond performance of deformed bars under lateral pressure,
2. the bond behaviour of deformed bars in regions of tension release or transverse cracking.

Both areas were investigated experimentally. The tests were confined to a single size of deformed bar but of three different types very commonly used in construction in the United Kingdom. Various concrete covers were provided in the test specimens and meaningful levels of lateral pressure and tension release were applied. The amount of secondary lateral reinforcement in the test blocks was kept constant.

The bonded length of the reinforcement subjected to the lateral restraint was kept at a fixed value and the length was chosen so as to enable a uniform distribution of stress in the region of the bonded length. Behaviour of both top and bottom cast bars was studied under lateral pressure.

The experimental work on tension release was carried out in the Civil Engineering Laboratories of the City University. The work involved the design and instrumentation of the experimental set up to apply the various levels of tension release in the specimen.

The experimental work on lateral pressure was carried out in the Civil Engineering Laboratories of the University of Malaya in Kuala Lumpur, Malaysia. The design of the specimen and the apparatus including the instrumentation to apply varying levels of lateral pressure was carried out in Malaysia. This included the design of a simple device to rotate the specimen through 180° so that the bottom cast bars may be turned to the top for testing.

The detrimental effect of tension release in the concrete surrounding a reinforcement bar on its bond resistance is demonstrated. It is shown that there exists a limiting value of tension release in the concrete at which bond resistance completely disappears. A basis for design has been developed.

The limited beneficial effects of lateral pressure are compared with an empirical theory based on the modes of failure.

1.2 Preliminary background to the study

Bond performance of reinforcement steel in reinforced concrete has been the subject of close study since the advent of reinforced concrete. Although the earliest recorded experimental study of bond was made by Hyatt (1) in 1877, exhaustive tests by Abrams (2) in 1913 contributed largely towards shaping the thought and practice relating to bond stress and bond design. The appearance of the deformed bars and their superior bond performance over round bars as shown by the tests of Slater (3) in 1920 led to the further development of high bond deformed bars with improved rib formation. The development of increased ultimate bond strength in deformed bars is essentially manifested due to an adequate composite action. The deformed bars also performed better in the size, width and distribution of cracks in comparison to round bars. However, the recent development of high strength reinforcing bars, the wide spread use of high-strength concrete and the introduction of new large diameter bars have caused designers of reinforced concrete to examine the subject of bond more closely. Recent studies have led the Codes to approach the subject of bond performance of bars differently from that in the past, laying more emphasis on the length of the bar required to develop the force in the bar at points of anchorage and curtailment.

A parallel development to the study of bond has been an increased awareness amongst designers of the importance of detailing correctly the reinforcement at joints and supports in structural frames so that the joints would develop completely the design moments and forces. Research and study of such joints and supports have raised

new questions about the behaviour and bond performance of reinforcement bars at such locations. For example, recent research at the Cement and Concrete Association on beam-column joints (4) has shown that a favourable concrete strut action may enhance the bond of the beam reinforcement bars at the column. It would seem that the lateral compression of the strut would lead to possible reduced anchorage length of this reinforcement and help in the improved detailing at the joint. A similar enhanced bond performance due to a favourable lateral compressive strut is suggested in a study of pile caps (5). The subject of enhancement of bond stress due to lateral compressive stresses is not new and was initially suggested by Leonhardt (6) as a factor to be investigated before accepting results of pull-out bond tests. Experimental work by Untrauer and Henry (7) has shown that the bond strength increases with increased normal pressures. The necessity to design heavier structures and the need to provide a greater quantity of reinforcement at joints have focussed the attention of designers to the bond behaviour of reinforcement bars and the beneficial contribution of lateral restraints needed a closer look.

One of the major concerns of designers is the behaviour in bond of reinforcement bars in regions that are in tension, both cracked and uncracked. This concern which was mainly related to reinforcement bars in flexural members has been highlighted during the increased amount of research effort in torsion in structural reinforced concrete. Navaratnarajah (8) has shown that closed welded stirrups in torsion beams enhanced the torsional strength of beams compared to beams reinforced with tied stirrups. Work at the Otto-Graf

Institut in Stuttgart (9) has confirmed the necessity to have closed loop stirrups in torsion beams since torsion beams are extensively cracked in the regions in which the stirrups are anchored. The tension release in these regions due to cracking is considered as responsible for the ineffectiveness of stirrups that do not have closed loops.

Hence a study of the effects of lateral restraint on the transfer bond of steel reinforcement, in particular that of deformed reinforcement bars would be useful in order to understand the transfer bond behaviour of reinforcements in reinforced concrete members.

1.3 Organization of the thesis

Chapter 2 gives a review of some of the major contributions on the bond strength and bond resistance of deformed bars. The first part is a record of the various bond researches and the main findings of these studies. The second part discusses in detail the parameters influencing bond strength and the different formulations suggested for bond strength as a function of these parameters.

Chapter 3 describes in detail the experimental details of the present study relating to bond resistance of deformed bars under conditions of transverse tensile release in the concrete surrounding a reinforcement bar. Details of the apparatus used including the measurement techniques adopted in the study are described. Similarly, Chapter 4 gives the details of the experimental study relating to the study of bond resistance of a deformed bar subjected to lateral compression.

The failure mechanisms of deformed bars are discussed in detail in Chapter 5. After a consideration of the factors contributing to the mechanism of bond development, failure mechanisms of deformed bars under normal bond behaviour are discussed and theoretically analysed. The theoretical study is extended to bond action when the concrete surrounding the bar is subjected to uniform external pressure. Based on the results of this analysis and a definition of bond failure, an empirical theory of bond failure under lateral pressure in one direction is formulated. The behaviour of deformed bars under lateral tension release is also analysed with a critical examination of the contribution of the rib profiles in the failure mechanism.

The experimental results of deformed bars subjected to bond tests under lateral tension release are examined in Chapter 6. The effects of the variations of concrete cover and the various levels of tension release on critical bond stress and ultimate bond stress are discussed. Based on the experimental results, expressions are derived for critical bond stress of deformed reinforcement bars under lateral tension release.

In Chapter 7 are presented the results of the experiments on bond tests of deformed bars under unidirectional lateral compression. Effects of varying the concrete cover and the lateral compression on the bond stress are discussed. The experimental results are compared with the values of the force in the bar at bond failure calculated on the basis of the theory proposed in Chapter 5.

Chapter 8 gives a comparison of the critical bond stress and ultimate bond stress values with the values of bond stress permitted in the British Code of Practice, C.P.110: 1972: (Amended 1979).

The main conclusions relating to the study of transfer bond behaviour of deformed reinforcements under lateral tension release and compression are presented in Chapter 9.

CHAPTER 2

REVIEW OF BOND BEHAVIOUR OF REINFORCING STEEL

Early interest in bond was concentrated mainly towards understanding the mechanism by which the reinforcing steel and the surrounding concrete contributed to resist tensile forces in reinforced concrete members. While bond enables the reinforcement to co-operate with concrete before cracking occurs, thereafter it ensures distribution of the cracks and makes it possible for the reinforcement to absorb the tensile forces by maintaining connection between the steel and concrete in the regions between the cracks. The greater interest evinced in the distribution of cracks and therefore reduction in size of cracks and crack widths led to the development of high bond deformed reinforcement bars. The bond behaviour of deformed bars is intrinsically different from that of round smooth bars.

Bond between the smooth round reinforcement bars and concrete is attributed to both physical and mechanical causes. The physical phenomenon of adhesion is attributed to shrinkage of the concrete (10, 11, 12) and chemical effects (13) whereas Dutron (14) explains the adhesiveness as due to the capillary and molecular forces in the cement paste surrounding the reinforcement surface. Additional resistance is manifested when the cement paste engages mechanically with the irregularities on the surface of the bar. The resistance to sliding is ensured by the surface shear strength of the sheath of concrete in contact with the bar and by the frictional resistance that comes into action after that sheath has sheared. These frictional forces are far greater than the adhesion forces and vary considerably with the surface condition of the bar and upon the

magnitude of the transverse stresses acting upon the bars due either to the shrinkage of the concrete or to external actions that can increase the grip exerted upon the reinforcement.

The bond of deformed bars is much greater than that of plain round bars due to the mechanical interlocking of the ribs formed on the bars with the surrounding concrete. The magnitude of the bearing resistance involves both the shear strength and the compressive strength of the concrete surrounding the bar and is also affected by the factors which determine the amount of grip that the concrete exerts upon the bar.

This review is mainly concerned with the mechanism of bond of deformed reinforcement bars as affected by the various factors including lateral restraint. Bond research has been extensive and hence the review is confined only to the parameters that are of direct relevance to this study.

2.1 Bond tests

Pull-out bond test samples have been the most popular in bond studies. Abrams (2) made a very exhaustive study of the bond of plain and deformed bars using both pull-out and beam tests. He tested deformed bars with transverse ribs and twisted bars. The twisted bars acted similar to a wedging tapered bar due to the reliance on lateral pressure for slip resistance. Improvement of slip resistance with increased bearing area of rib per unit length of bar was observed which prompted the recommendation that the ribs be spaced closely. Concrete strength, embedment length, concrete cover and bar diameter were some of the important variables studied. Improvement of slip resistance with increased bearing area of rib per unit length was

observed.

Menzel (15) in 1939 examined the various factors which influence bond of deformed bars using pull-out tests. The results indicated the superiority of deformed bars with transverse ribs over deformed bars with longitudinal ribs thus supporting the efficacy of the larger rib bearing area of deformed bars with transverse ribs. However, little or no difference in slip resistance was observed for bars with different rib face angles. Slip resistance was observed to depend on the position of the rib during casting and the direction of pull in the pull-out tests. Increase of slip resistance with age of concrete and in proportion to the cement content reflected the influence of the improved concrete strength on the slip resistance.

Clark (16) examined 17 different types of $7/8$ in. diameter deformed bars of which 16 had transverse ribs and showed that the bond performance of the bars improved consistently with increase of rib bearing area per unit length of bar. Top cast bars (depth of concrete below bar was 15 ins.) were found to be $2/3$ as effective as the corresponding bottom cast bars (depth of concrete below bar was 2 ins.) Clark (17) conducted a similar series of tests in 1949 in which he compared the results of beam bond tests and pull-out tests with different embedment lengths and concluded that the pull-out tests gave a reliable estimate of the bonding efficiency of deformed bars in beams. Based on his tests, Clark concluded that good slip resistance is developed with a ratio of the shearing area of concrete between the ribs to the bearing area of the ribs of 5 or 6.

Watstein (18) measured the distribution of bar stresses in pull-out specimens over different embedment lengths. He observed that the maximum bond stress for deformed bars was twice the minimum bond stress even at high loads in the 8 in. embedment length and three times the minimum bond stress in the 12 in. embedment length at high loads i.e. more stress variation was observed in the longer embedment lengths as compared with the shorter embedment lengths. Mathey and Watstein (19) showed that the bond stress varied with the D/L ratio i.e. ratio of diameter of bar to embedment length.

Mains (20) determined the bond stress distribution in beam and pull-out bond specimens by using electrical strain gauges placed inside the reinforcing bar. His results confirmed earlier tests of Watstein and the maximum bond stress was often more than twice the average bond stress. The maximum local bond stress in deformed bars was observed to occur at or near the loaded end at all stages of loading while the location of the maximum local bond stress in plain bars moved from the loaded end to the unloaded end with increasing load.

The tendency of the deformed bars to split the concrete at failure prompted Ferguson and his research team (21, 22, 23) to examine the influence of spacing of bars in beams, stirrups, development length and the concrete cover on the bond strength. While an improvement of ultimate bond stress with increasing effective bar spacing was noticed, the presence of stirrups produced a marked improvement on the ultimate bond stress which was found to vary with $\sqrt{f'_c}$, where f'_c is the cylinder strength of concrete. The depth of clear cover was found to increase the ultimate bond stress which varied with the ratio D/L as in the Mathey and Watstein tests (19).

The influence of different types of deformations was investigated comprehensively by Rehm (24, 25) followed by Lutz (26) and Lutz and Gergely (27). The studies showed that the slip of deformed bars could occur as a result of splitting of the concrete caused by the wedging action of the ribs or due to crushing of the concrete under bearing of the ribs. It was also observed that ribs with a face angle between 40° and 105° produced about the same movement indicating that for these angles the friction between the rib face and the concrete is sufficient to prevent relative movement at the interface. Consequently, slip is due almost entirely to the crushing of the concrete in front of the ribs. When concrete is crushed to a powder, it becomes lodged in front of the ribs. This in effect produces ribs with face angles of 30° to 40° (Figure 2.1). The slip movement is therefore independent of the rib face angle when this exceeds about 40° . But transverse and longitudinal cracking preceded such movements. Rehm found that the slip was a function of only the rib height until the average shear across the concrete key became larger than about half the concrete strength at which time the concrete key began to crack leading eventually to shear of the concrete key or form a wedge of concrete in front of the rib. Lutz observed similar behaviour in his tests. The effect of impairing the frictional and adhesive properties on the surface of the bar was examined by Lutz and it was observed that though a significant slip occurred initially as compared with bars having good frictional properties, at high loads when crushing became extensive in front of the ribs, the slip of the bars with impaired surface properties approached the slip of bars with good surface properties. While it

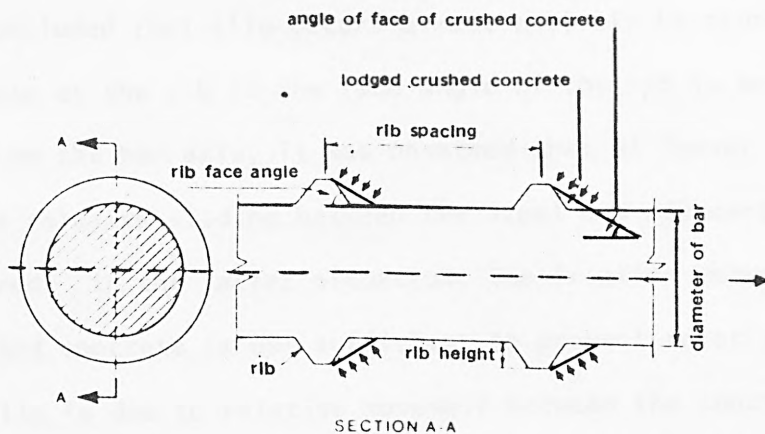
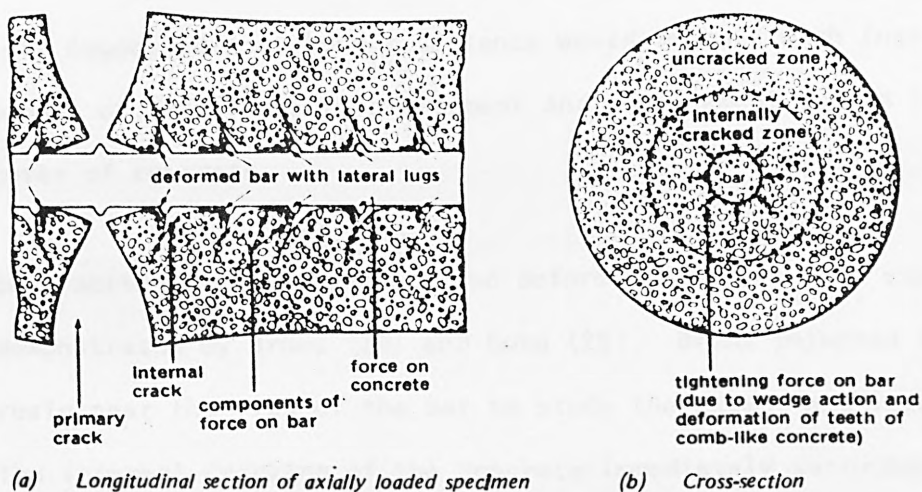


Fig. 2.1: The geometry of a deformed reinforcing bar and the mechanical interaction between the bar and the concrete. (after Rehm)



(a) Longitudinal section of axially loaded specimen (b) Cross-section
 Fig. 2.2: Deformation of concrete around ribbed reinforcing bar (schematic diagram) after Goto

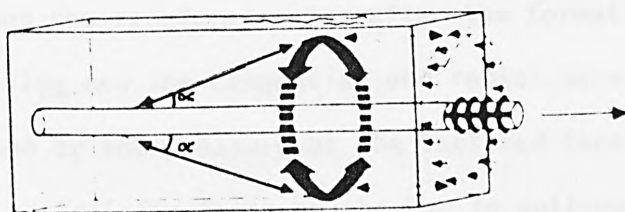


Fig. 2.3: Schematic representation of how the radial components of the bond forces are balanced against tensile stress rings in the concrete in an anchorage zone. (after Tepfers)

was concluded that slip occurs almost entirely by crushing of the concrete at the rib if the face angle of the rib is more than about 45° from the bar axis, it was observed that at lesser rib face angles relative sliding between the steel and adjacent concrete also occurred. In the latter situation, the friction between the rib face and concrete is not sufficient to prevent relative movement and slip is due to relative movement between the concrete and steel along the face of the rib and secondarily to some crushing of the mortar. Transverse reinforcement in the form of stirrups reduced the splitting of the concrete and thereby increased bond resistance was developed due to improved confinement of the deformed bar. Lutz suggested that bond resistance would improve with increased amount of transverse reinforcement and confinement due to increased cover of concrete.

Bond action between concrete and deformed bars has been experimentally demonstrated by Broms (28) and Goto (29). Broms injected a coloured resin near the ribs of the bar to study the extent and location of the internal cracking of the concrete immediately surrounding the bar whereas Goto used red ink. The slopes of the internal cracks, from 45° to 80° indicate the trajectories along which the compressive forces leave the ribs of the deformed bar and spread into the concrete (Figure 2.2). The deformation of the concrete around the reinforcing bar after the formation of the internal cracking and the tangential and radial stresses in the concrete caused by the pressure at the inclined faces of the ribs constitute the restraining force on the bar to pull-out. Goto's experiments also confirmed the destruction of the adhesive bond in the early stages causing separation between the concrete and steel followed by wedging of the ribs on the teeth of cracked concrete.

Tepfers in his study (30) of bond action of deformed bars suggested the occurrence of rings of tensile stress in the concrete around reinforcing bars in an anchorage zone to balance the radial components of the bond forces. The rings are thinnest in the concrete cover protecting the reinforcement and when the ring is stressed to rupture, it fails at this point resulting in the appearance of longitudinal cracks. At cracking, the resistance of the concrete ring falls and increased movement between the concrete and steel is possible. The angle α between the bond forces (Figure 2.3) and the bar axis may change from the initial value of 45° in the uncracked elastic stage. The radial components of the bond forces impose a load on the concrete cantilevers surrounding the bar (teeth of cracked concrete) which when loaded to their ultimate capacity break, resulting in bond failure. Tepfers compared his concrete ring theory with test results and concluded that the ring theory based on a partly cracked elastic stage gave values of bond stresses on the safe side (31). He used pull-out specimens with short bond length so that the bond stress was almost evenly distributed along the length.

Losberg and Olsson (32) devised a special steel ring pull-out test with strain gauges placed on a steel ring surrounding the anchorage length of a deformed bar in order to measure the splitting component of the bond forces, following the ring theory of Tepfers. They observed that inclined ribs produced more ring tension than transverse ribs probably due to the fact that the splitting effect for the inclined ribs is greater depending on the extra force component due to the inclination.

The influence of the geometry of deformed steel bars on their bond strength in concrete was studied by Skorobogatov and Edwards (33) on 16 mm diameter bars with ribs of 48.5° and 57.8° angles of slope. The study showed that the magnitude of the slope of the rib faces did not affect the final value of the bond stress. The value of the maximum bond stress was the same for both types of bar investigated, because the bar with the greater slope was modified by crushed concrete wedges (truncated cones) in the rib fillet which effectively reduced the angle to the smaller value. This confirmed the earlier results of Rehm (25), Lutz (26) and Tepfers (31).

Cairns (34) in his study of ultimate strength of lapped joints of compression reinforcement concluded that bond failure of ribbed reinforcing bars is due to failure of concrete caused by the bearing of the ribs on the concrete. He excluded bond failure that occurs by shearing along a surface across the tops of the bar ribs caused by ribs which are closely spaced in relation to their height or where confining forces are great. He suggested an inclined failure surface passing through the top of the bearing face of the rib and developed the ultimate bond strength as the sum of two components, namely the one due to the confining force on the bar and associated with the splitting of the concrete cover to the reinforcement and the other dependent on the strength of the concrete based on the Coulomb-Mohr failure criterion over the inclined failure surface.

Recently, Mirza and Houde (35) have disputed the generally accepted view that slip results due to crushing of the concrete in front of the ribs as a result of high bearing and shearing stresses based on their experimental observations that examination of sliced specimens

did not reveal evidence of polished areas due to sliding or powdery areas on account of crushing. They explained the slip at the steel-concrete interface as due to the bending of the comb-like structures of the first concrete layers surrounding the bar. However, their study showed that bond resistance increased with concrete cover due to increased confinement of the deformed bar against cracking by the surrounding concrete. The effect of concrete cover on maximum bond stress was also studied by Edwards and Yannopoulos (36) on bond specimens with short embedment lengths (in order to obtain evenly distributed stress) which showed that the size of the concrete cover has a significant effect on the maximum bond stress.

The need to consider the effects of confinement of reinforcing bar in bond tests was first stated by Leonhardt (6) arising from his concern for the effect of lateral stresses caused by testing machine plattens on the results of pull-out bond specimens. However, Untrauer and Henry (7) studied the influence of lateral pressure in one direction and found the bond strength to increase with increase in normal pressure. The increase was approximately proportional to the square root of the normal pressure and the square root of the compressive strength. The increase was greater for 1-1/8 in. diameter bar compared to a 3/4 in. diameter bar. The slip at ultimate bond stress increased with increased normal pressure. Gvozdev (37) showed that a transverse compression of the order of one-third the compressive strength may double the bond of plain bars and cause a 50% increase in the bond of deformed bars.

A comprehensive Dutch bond study (38) included besides variables such as type of steel (4 types), bar diameters (3 different sizes) also three different concrete covers to the bars and different

positioning of the bars in the specimen, placed in two diametrically opposite corners so that one was at the top and the other was at the bottom. The tests showed that for all the types of bars tested, increased cover enhanced the bond resistance of the bar. Ferguson's tests (21, 22) showed that the bond strength increases with the thickness of the concrete cover. Plowman (13) basing himself on pull-out test results considers the bond strength to vary with the ratio of concrete cover to bar diameter. According to Chamberlin (39) the results obtained in beam tests show that the full bond capacity is attained only for ratio of cover to bar diameter equal to 3. He also reports that increasing the cover not only increases the bond strength but also reduces the slip of the bars.

Various authors have investigated the effect of the transverse reinforcement such as stirrups which help to confine the bursting of the concrete surrounding the bar. Ferguson concluded based on his tests (18, 19) that the ultimate bond stress increases linearly with the percentage of transverse reinforcement and this increase may amount to about 50% for a percentage of 0.2%. Plowman (12) noted that the spacing of the stirrups had an effect on bond. A recent study by Kemp and Wilhelm (40) which included tests with open and closed stirrups showed that closed stirrups increased the bond resistance more significantly than open stirrups particularly with increased concrete cover. With concrete cover equal to the bar diameter, the bond force was sensibly the same for the different stirrup patterns. As the cover was increased to 3 bar diameters, the capacity of the closed stirrups was nearly twice the capacity of the open stirrup specimens. Further support is found in the recent studies by Jimenez et al (41) and Morita and Kaku (42) which

showed that transverse reinforcement are beneficial in increasing the ultimate dowel force.

The influence of the position of the reinforcement bars in the bond test specimen on bond resistance has been reported by Clark (16), Menzel (43), Welch (44) and Brettle (45, 46). Bond resistance of bars in the horizontal position and placed in the bottom part of the specimen was observed to be greater than those placed near the top by about 30% by Clark. Tests performed by Welch showed the influence of concrete sedimentation on bond strength. Differences in indicated bond strength of about 50% for deformed bars were observed with concretes of similar strengths but different settlements. Concretes with large settlement and bleeding characteristics were shown to cause loss of bond strength even with small depths of concrete below horizontally cast bars. Brettle observed that the maximum average bond stress of horizontally cast deformed bars reduced by about 30% as the ratio of the distance of the bar from the bottom to the total depth of concrete varied from 0.1 to 0.9.

2.2 Parameters influencing bond strength

Bond development between steel and concrete as well as the distribution of bond stress depend on several factors. The influence of some of these factors is very well established. However, explanation of bond behaviour advanced by various researchers have tended to be based on the influence of only certain factors. This is not very satisfactory, either because the various factors act in different ways upon bond behaviour or because they directly influence one another. For example, bond studies have been made for varying diameter of bars, different strengths of concrete, different embedment lengths (without relevance to bar diameter) and varying concrete cover to reinforcement

(without a fixed cover to bar diameter ratio). In some of the studies, more than one of these variables were sometimes varied at the same time thus clouding the effects of any single parameter. In studying embedment lengths, some researchers used a constant embedment length for different bar diameters whereas others chose constant multiples of bar diameter as embedment length. The conclusions arrived at by the two groups have not been the same and hence not very helpful. Varying the strength of concrete in the same studies further complicated the understanding as it is known that embedment length is a function of diameter of bar and the strength of concrete.

A general concept may, however, be obtained by examining the variables that principally affect bond behaviour such as the bond quality of the bar profile, the diameter and embedment length of the bar, the strength of the concrete, the confinement of the bar caused by the concrete cover or the amount of transverse reinforcement and the position of the bars in the test specimen.

2.2.1 Effects of bar profile

The bond properties of a bar may be divided into two categories, namely (1) the geometric properties relating to the bar size and the ribs, and (2), the surface properties such as friction and adhesion. Adhesive resistance must be overcome before true sliding or frictional resistance becomes effective, though mechanical interlocking can occur before slipping takes place between the steel and concrete. Tests have shown that the adhesion resistance between concrete and a deformed bar is often small compared to the resistance due to the mechanical interlocking of the ribs in the concrete. The adhesive resistance is significant only when compressive force and shear are

applied to a bar but rather negligible where tension and high shear exist at the bar-concrete interface.

The sliding resistance due to friction and to mechanical interlocking of the irregularities on the bars depends not only on the surface condition or roughness of the bars but more particularly on the profile of the deformed bars which include the cross-sectional shape of the bar, the arrangement of their projections, and the height and spacing of these projections along the length.

Saillard (12) established a relationship between the bond strength f_{bu} of deformed bars and the height and spacing of the ribs as

$$f_{bu} = f_{br} + \frac{h}{e} \cdot f_{cu} \quad \dots \quad 2.1$$

where f_{br} = frictional resistance between steel and concrete

f_{cu} = compressive strength of concrete

h = height of the ribs

e = spacing of the ribs

Djabry (47) also considered the bond capacity of a deformed bar to be proportional to the degree of irregularity defined by a relationship of the form h^m/e^n where h denotes the average height of the ribs and e their average spacing, m and n being constants.

According to Rehm (24, 25), the local bond stress of deformed bars varies with the ratio of the bearing surface of a rib to the bond surface area between two ribs. He proposed an expression of the form

$$f_{bu} = G \cdot \Delta^\beta \cdot f_{cu} \frac{(D_c + h)h}{D_c \cdot e} \quad \dots \quad 2.2$$

where Δ = slip of the bar

$\beta < 1$ = a constant

f_{cu} = compressive strength of concrete

D_c = diameter of the cylindrical 'core' of the bar

h, e = height and spacing of the ribs

G = a coefficient

Rehm (25, 48) also reported that, for a given contact pressure of the ribs, the slip decreases if the height of the ribs decreases and that the rib spacing has no effect upon the contact pressure as long as the shear strength of the concrete does not exceed $0.4 f_{cu}$.

Lutz (26) also observed that increasing the height of the rib can cause a significant increase in the bond strength and slip resistance due to reduction of the bearing pressure on the rib. His conclusions on the effect of rib spacing confirmed the earlier work of Rehm.

Soretz and Holzenbein (49) have recently studied the influence of rib dimension on bond resistance. They confirmed earlier studies and showed that with simultaneous decrease of rib height and spacing, the bond characteristic remains unchanged up to about 1 mm slip. The type of failure changes from exclusive splitting to mainly excessive slip without splitting. Increased inclination of the rib to the bar axis improved the bond characteristic slightly and changing the rib cross section from a rectangle to a 45° trapezoid had no significance on the bond characteristics.

2.2.2 Diameter of bar and embedment length

It would be incomplete not to mention the influence of diameter of bars and the bond length on bond stress. Many investigators have studied these aspects on the basis of pull-out tests or beam tests in which either the bond length was kept constant or the ratio of bond length to bar diameter was constant. The ultimate bond stress decreases with increasing bar diameter and Djabry (47) reports that the decrease in the ultimate bond stress as a function of the increase in bar diameter is less pronounced in the case where the bond length is kept constant than in the case where that length is a constant multiple of the bar diameter. He proposes the following expression for bond stress

$$f_{bu} \left(\frac{L}{D}\right)^a \cdot D^b = \text{a constant} \quad \dots \quad 2.3$$

where L = embedment length

D = diameter of reinforcement bar

a, b = constants

Mathey and Watstein (19) found that the bond strength varied linearly with D/L . Similar behaviour was noted by Ferguson and Thompson (22). Lutz (50) has confirmed this behaviour and suggested a relationship to fit his results and those of the above mentioned two investigations as

$$f_{bu} = 1.70 + 9.70 D/L \quad \dots \quad 2.4$$

in imperial units for a concrete cylinder strength of 3910 psi. However, the Dutch test reports (38) show that the bond stress is independent of L/D .

Orangun, Jirsa and Breen (51) derived the following equation from a non-linear regression analysis of test data :

$$\frac{f_{bu}}{\sqrt{f'_c}} = 1.2 + 3.0 \frac{C}{D} + 50 \frac{D}{L} \quad \dots \quad 2.5$$

where f_{bu} = is the bond stress, psi

f'_c = concrete cylinder strength, psi

C = smallest clear concrete cover or half-bar spacing

D, L = bar diameter and embedment length respectively

2.2.3 Strength of concrete

Variation of the ultimate bond strength as a function of the strength of the concrete was earlier considered to be of the form

$$f_{bu} = A_1 \cdot f_{cu} + A_2 \quad \dots \quad 2.6$$

where A_1 , A_2 denote constants which depend on various factors such as the type of bar, the diameter, the bond length, method of testing etc. Rehm (24) adopts the relationship of the form

$$f_{bu} = A_3 \cdot f_{cu}$$

for concretes having a strength between 80 and 430 kg/cm². Some authors however, relate the bond stress to the tensile strength of the concrete. Rusch and Rehm (48) based on the results of pull-out tests performed on deformed bars suggested:

$$\begin{aligned}
 f_b &= 0.62 (f_{cp})^{0.77} \text{ for Tor bars or deformed bars with low projections;} \\
 \text{and } f_b &= 0.55 (f_{cp})^{0.91} \text{ for deformed bars with pronounced profiling;}
 \end{aligned}
 \quad \dots \quad 2.7$$

where f_b is the bond stress corresponding to a slip of 0.1 mm and f_{cp} is the prism strength of the concrete. Tensile strength of concrete is commonly taken as proportional to the square root of compressive strength. Ferguson (22) also adopts an expression of the form

$$f_{bu} = A_4 \sqrt{f_{cu}} \quad \dots \quad 2.8$$

Based on the results of 18 eccentric pull tests, Lutz (50) derived the expression for ultimate bond stress f_{bu} as

$$f_{bu} = \frac{6.1 \sqrt{f'_c}}{D} + 1080 \frac{D}{L} + 1080 \frac{d^3 L}{s} \quad \dots \quad 2.9$$

where f'_c = cylinder strength of concrete in psi

D = diameter of bar, ins.

d = diameter of transverse reinforcement, ins.

L = embedment length of reinforcement bar

s = spacing of transverse reinforcement, ins.

Recently Kemp and Wilhelm (40) have shown that the average bond stress varies with concrete strength according to

$$f_{bu} = \sqrt{f'_c} \left[E_1 + E_2 \left(\frac{C}{D} \right) \right] \quad \dots \quad 2.10$$

where f'_c = concrete cylinder strength, psi

C = concrete cover, ins.

D = diameter of reinforcement bar, ins.

E_1, E_2 = experimental constants

2.2.4 Confinement

Confinement of the deformed bars in the anchorage zone usually takes the form of concrete cover or transverse reinforcement in the form of stirrups.

Although the beneficial effect of concrete cover in bond development had been recorded by various researchers, the first formulation of a relationship was developed by Ferguson (22, 23) in the form

$$f_{bu} = 3C + M \quad \dots \quad 2.11$$

where C is the thickness of the cover and M is a constant depending on the embedment length and diameter of the bar. The C.U.R. tests (38) provided a linear relationship between bond stress and the ratio of concrete cover to bar diameter of the form:

$$f_{bu} = B_1 \frac{C}{D} f_{cu} + B_2 f_{cu} + B_3 \frac{C}{D} + B_4 \quad \dots \quad 2.12$$

where f_{cu} = compressive strength of concrete and B_1, B_2, B_3, B_4 are coefficients which vary with the type of bar (profile) and the location of the bar (top or bottom). Equation (2.10) shows the correlation obtained by Kemp and Wilhelm (40) between bond stress,

the compressive strength and the ratio of concrete cover to the diameter of the bar based on their experimental results. Analysis of test data by Orangun, Jirsa and Breen (51) shown in Equation (2.5) also indicates the influence of concrete cover on bond strength. However, it was suggested that the value of C/D used should not exceed 2.5.

It has been shown (52) that a statistical analysis of a large number of results yields a relationship between the bond strength of a given bar and the characteristics of the transverse reinforcement in the form

$$f_{bu} = f_{bb} + \gamma \cdot \frac{d^k}{s} \quad \dots \quad 2.13$$

where f_{bb} = bond strength of bars in the absence of transverse reinforcement

d = diameter of transverse reinforcement (stirrup)

s = stirrup spacing

k = factor depending on strength of concrete

γ = a factor depending on the slope of the stirrups in relation to the axis of the longitudinal bars

Lutz (50) deduced a relationship for the ultimate bond stress f_{bu} as given in Equation (2.9) in which the third term gives the contribution due to the transverse reinforcement.

The effect of transverse reinforcement was also studied by Orangun, Jirsa and Breen (51) who assessed the additional bond strength f_{btr} attributable to the transverse reinforcement as

$$\frac{f_{btr}}{\sqrt{f'_c}} = \frac{l}{500} \cdot \frac{A_{tr} f_{yt}}{s \cdot D} \quad \dots \quad 2.14$$

where A_{tr} is the area of transverse steel (in²) with yield strength f_{yt} (psi) and spacing s (in.). However, the contribution of the transverse steel is limited to a maximum of $3\sqrt{f'_c}$.

Kemp and Wilhelm (40) based on their results of bond tests with closed stirrups developed the expression for ultimate bond stress

f_{bu} as

$$f_{bu} = \sqrt{f'_c} \left[6.57 + 2.9 \frac{C}{D} \right] + 0.191 \frac{A_{tr} f_{yt}}{s \cdot D} \quad \dots \quad 2.15$$

where D = diameter of bar, ins.

A_{tr} = area of transverse steel of yield strength f_{yt}

s = spacing of stirrup, ins.

C = cover of concrete, ins.

2.3 Choice of parameters in the present study

The important variables in bond study are the strength of concrete, the geometric properties of the bar, the diameter of the bar, its embedment length and the confinement of the bar both due to concrete cover and transverse reinforcement. The embedment length of a bar is related to its diameter. However, in studies where the object is to study the mechanism of bond development, it is preferable to keep the embedment length as small as possible as found in the studies of Rehm (25), Lutz (50), Tepfers (30) and Edwards and Yannopoulos (36). The different parameters influencing bond also influence one another and hence studies relating to specific parameters are best carried

out with the other variables kept constant.

In the present study relating to the effects of lateral restraint on bond, a single size of bar with a constant embedment length and constant amount of transverse reinforcement will be chosen. The variable parameters chosen for the study, namely the cover to the reinforcement bar, the degree of lateral restraint (pressure or release) and the different profiles of the three types of bars are independent of each other in bond behaviour. The concrete strength for the study is kept constant and the embedment length is kept at 4 times the diameter of the bar. X

EXPERIMENTAL INVESTIGATION OF THE EFFECT OF TENSION RELEASE ON
BOND BEHAVIOUR

3.1 Object and scope of test programme

This part of the study is confined to the bond behaviour of deformed reinforcement bars in regions of tension release in concrete. Different levels of tension release are studied together with varying concrete cover to the deformed bars. The choice of a suitable embedment length poses a problem in bond studies as the embedment length influences the bond stress distribution. A short embedment length helps to avoid the bond stress variation obtained in long embedment lengths and to understand more of the basic bond behaviour. Rehm (25) and Lutz and Gegerly (27) used very short embedment lengths in their study towards understanding the basic mechanism of bond. Since this study is concerned with the basic bond behaviour of reinforcement bars under lateral restraint, a short embedment length is preferred. Recently Edwards and Yannopoulos (36) adopted an embedment length of 38 mm which was four times the rib spacing of the 16 mm diameter Wellbond deformed bar used in their tests, whereas Rehm and Eligehausen (53) used a bond embedment length of 3 bar diameters in their study of bond of ribbed bars under repeated loads. Whilst acknowledging the desirability of using an embedment length as small as practicable, the need for very accurate method of measuring the slip and load values as in the tests of Edwards and Yannopoulos has to be considered. In the present tests, based on practical considerations an embedment length of four bar diameters is chosen.

3.2 Test specimen

3.2.1 Philosophy of choice of test specimen

The concern of various investigators of bond performance of reinforcement bars has been the effect of the types of tests and bond specimens on the results. The pull-out specimen has been generally preferred in view of its simplicity but one of its drawbacks is the suspected influence of the lateral compression induced in the concrete surrounding the test bar by the platten of the testing machine (6). Fig. 3.1 shows the lateral compressive stresses which are due to the friction of the base of the specimen on the platten of the machine, whereby the lateral expansion of the concrete in compression is prevented. Even if this friction is obviated by lubrication or interposition of a sheet of rubber between the specimen and the platten of the testing machine, there nevertheless remains an arching effect which also increases the bond. The beam test had been extensively used in the studies at the University of Texas (21, 22) and in Holland (38). A recent study by Losberg and Olsson (32) has shown that the pull-out test does not give any direct information about the bond strength in a real situation compared to the beam test. A major argument against the pull-out type of test is that although the bar is under a tensile load, the concrete surrounding it is in a state of compression. In order to overcome such a stress-field in the specimen, a double tension pull-out type of specimen has been successfully used in the studies (54, 55) at the City University. In a double tension pull-out test, two bars are embedded in a specimen in line in a concrete block and pulled in opposite directions simultaneously thus creating a tensile stress-field in the concrete surrounding the

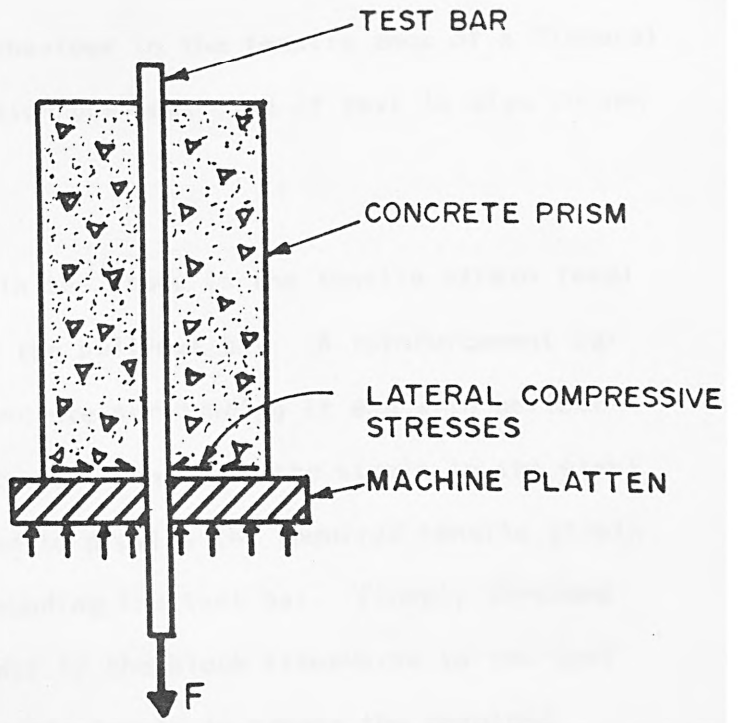


FIG. 3.1 PULL - OUT TEST ARRANGEMENT

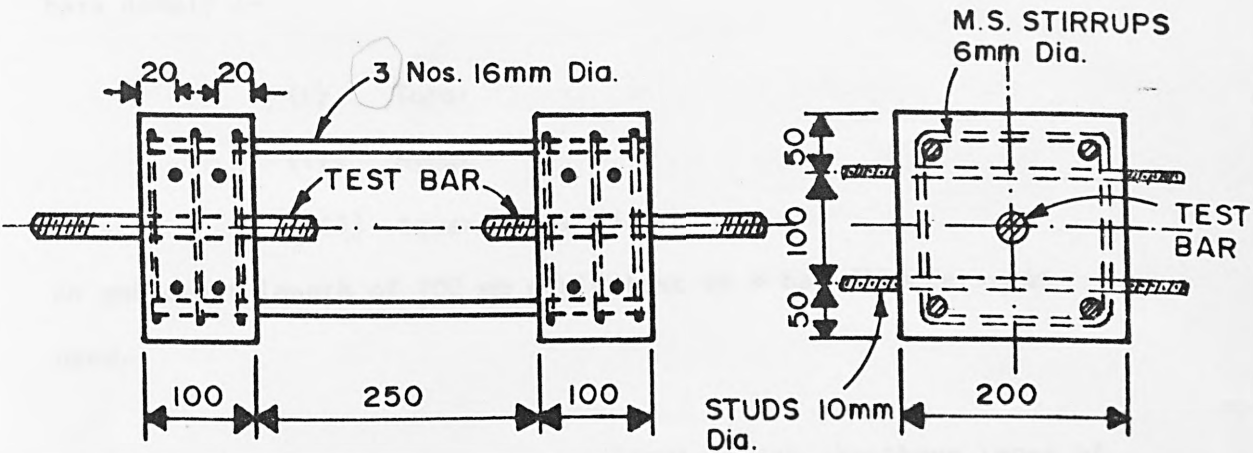


FIG. 3.2 DETAILS OF TEST SPECIMEN - LATERAL TENSION RELEASE

test bars, similar to the behaviour in the tensile zone of a flexural member. Thus, a double tension pull-out type of test is also chosen for the present study.

One of the major variables in the study is the tensile strain level in the concrete surrounding the pull-out bar. A reinforcement bar under stress strains the concrete surrounding it and with perfect bond the strain in the concrete is equal to the strain in the steel bar. This principle is used to provide the required tensile strain in the concrete block surrounding the test bar. Closely threaded high tensile steel studs cast in the block transverse to the test bars were tensioned to suitable levels to create the required tensile stress in the concrete.

3.2.2 Details of test programme

The study was carried out with deformed reinforcement bars of 25 mm nominal diameter consisting of three different types of profiled bars namely :-

(i) Tobar

(ii) Hybar

and (iii) Square-twisted bar.

An embedment length of 100 mm equivalent to 4 bar diameters was used.

The following concrete covers were studied with the three types of bars: 25 mm; 50 mm; 63 mm and 88 mm.

Three levels of tension release were applied in the tests which gave tensile strain levels of 1180, 1770 and 2360 micro strains in

the concrete surrounding the test bars. The entire programme was studied with a concrete strength of 35N/mm^2 .

The test specimens were designated numbers to indicate the type of bar, the concrete cover and the level of tension release according to a code as shown in Table 3.1.

3.2.3 Details of test specimen

The details of the test specimen are as shown in Fig. 3.2. The test bars 250 mm long with both ends threaded over a length of 50 mm were cast centrally in concrete blocks 200 mm square by 100 mm thick at each end such that the bar projected 50 mm on the inside. The embedment length of the test bar in the concrete was maintained at 100 mm. The two concrete blocks at the ends of the specimen and separated by 250 mm were interconnected with 3 Nos. 16 mm deformed Torbars each at top and bottom as shown. The ends of the test bars projecting 50 mm on the inside were drilled and tapped to receive a stud for attaching dial gauges to obtain slip measurements at the unloaded ends. 4 Nos. 10 mm diameter high tensile studs threaded uniformly and closely over their length of 350 mm were located symmetrically at depths of 50 mm and 20 mm from the face of the concrete block and transversely to the test bar as shown. The 3 Nos. 16 mm deformed Torbars were enclosed in 3 Nos. 6 mm diameter closed mild steel stirrups at 50 mm centres in the end blocks to form the secondary reinforcement cage for the specimen.

3.2.4 Casting of specimens

3.2.4.1 Details of mould

The specimens were cast in timber moulds. The reinforcement cage

Example Specimen Number

T 50 - 60A

Type of bar

Concrete cover to reinforcement bar

Tension applied to studs

Letter A or B indicates the two bars in each specimen

Types of bar

- T - Torbar
- U - Hybar
- S - Square-twisted

Tension applied to studs and tension release in concrete

- 0 - Zero tension force and zero tension release
- 40 - 40 kN tension force to produce tension release
 $\epsilon = 1180 \times 10^{-6}$
- 60 - 60 kN tension force to produce tension release
 $\epsilon = 1770 \times 10^{-6}$
- 80 - 80 kN tension force to produce tension release
 $\epsilon = 2360 \times 10^{-6}$

TABLE 3.1: DESIGNATION CODE USED FOR SPECIMEN NUMBERS

and the positioning of the test bars and the steel studs in the timber mould are shown in Fig. 3.3. During casting of the specimen, the test bars were coupled together at their inner threaded ends with a central coupler (as shown) having internal threads to ensure that the test bars remained in the same line as the central axis of the specimen. Clearances between the test bar and the holes in the mould through which they were threaded were sealed with plasticine to prevent egress of cement grout during compaction. The studs were located tight in the timber mould with specially made circular nuts at the ends. The nuts fitted snugly against recesses made in the side faces of the timber mould so that they did not work themselves loose and cause dislocation or loosening of the studs during compaction of the concrete.

The inner faces of the timber mould were brushed with a thin layer of mould oil before placing the assembled reinforcement inside the mould.

3.2.4.2 Materials

A. Concrete

The concrete was made with Portland cement mixed with river sand and river gravel of maximum size 20 mm in the proportions 1:1.84:3.53 with a water-cement ratio of 0.50. The concrete mix was designed to obtain an average strength of 35 N/mm^2 at an age of 14 days. The specimens were cast and compacted on a table vibrator. The specimens together with the mould were covered with wet burlap for two days after which the forms were removed and the specimens continuously immersed in water until the day prior to testing. The specimens were tested at a strength of 35 N/mm^2 . The strength of

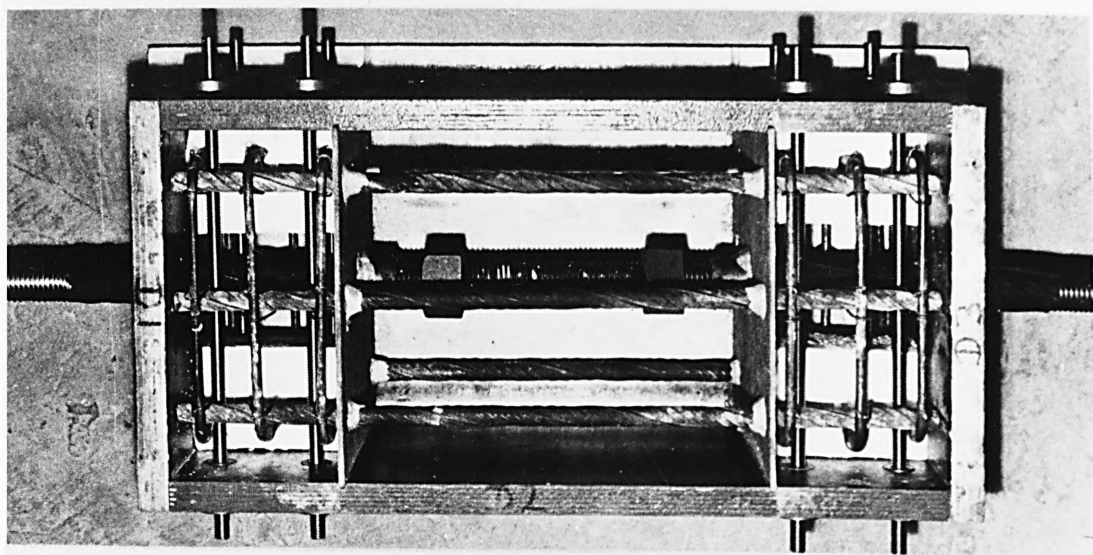


FIG. 3.3 DETAILS OF MOULD

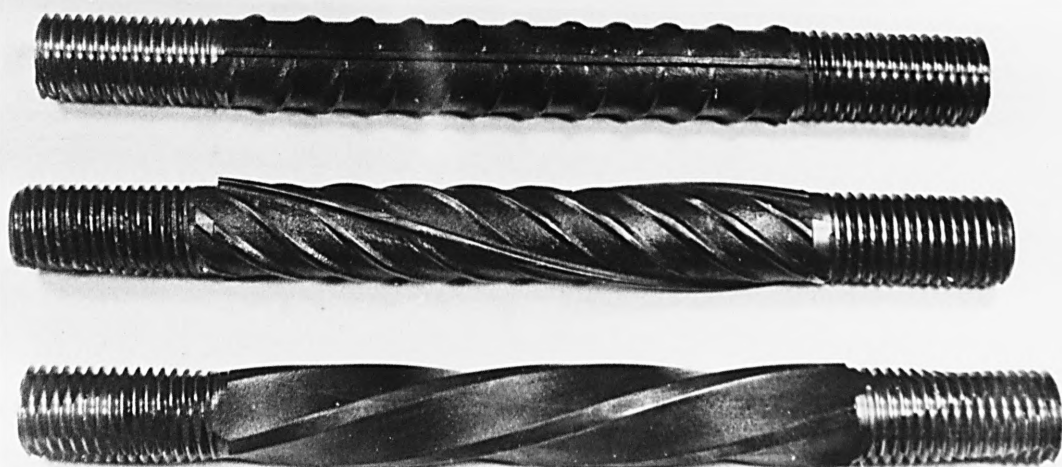


FIG. 3.4 TYPES OF REINFORCEMENT BARS STUDIED

the concrete was monitored by progressively testing control cubes cast with the same batch of concrete in the specimens and cured besides the specimens.

Details of mix and concrete strength are given in Appendix B.

B. Steel

All test bars were high strength deformed bars conforming to B.S. 4449: 1978. The mechanical properties of the bars together with details of rib dimensions and spacing of ribs are given in Appendix B. The three types of bars used, namely Torbar, Hybar and Square-twisted bar are shown in the photograph in Fig. 3.4.

The test bars were cut to the required length and the ends were threaded to a length of 50 mm. The surfaces of the test bars were thoroughly cleaned of all oil and grease. Just prior to the threading of the bars in the mould and securing them in position, the bonding length of the deformed bars was cleaned with trichloroethylene.

The stress-strain characteristic of the high strength studs was determined. This is given in Appendix B.

3.2.5 Control tests

12 Nos. concrete cubes 100 x 100 x 100 mm and 2 Nos. cylinders
150 ^{diam} mm x 300 ^{long} mm were cast together with every batch of specimens. ✕

A batch of two cubes was periodically tested to monitor the increase in strength in order to estimate the age at which the concrete would attain a strength of 35 N/mm^2 . On the day of the test, the

remaining cubes (usually 3 to 4 cubes) were tested for compressive strength. The cylinders were tested for splitting tensile strength. The results are given in Appendix B.

3.3 Test arrangement

The test set-up consists of a closed frame A as shown in Fig. 3.5. The test bars were pulled in tension through tie rods $T_1 - T_2$ which were pulled against the closed frame using two hollow cylindrical jacks 1 and 2 of same type and capacity. The tie rods were connected to the test bars through screwed couplers $C_1 - C_2$ which have internal threads at either end. The couplers were also mounted with electrical strain gauges in a closed bridge circuit so as to serve as load cells to measure the pull applied to the test-bars through the tie rods. The hydraulic jacks pulling the tie-rods were coupled together in parallel so that the same level of pull was simultaneously applied on the test bars.

The required tension release in the concrete surrounding the test bars was obtained by tensioning the studs through cross-heads $H_1 - H_4$ bolted to the studs. It was essential that the cross-heads were secured tight to the studs so that when tension was applied, all the four studs were tensioned equally at the same time. Tie-rods $T_3 - T_6$ screwed into cross-heads $H_1 - H_4$ were pulled against the closed frame using hollow cylindrical jacks 3 - 6 of same type and capacity at their ends. The four jacks were hydraulically coupled together so that all the four cross-heads were pulled in unison as pressure was applied. The tie rods $T_3 - T_6$ were each mounted with electrical strain gauges in a bridge circuit to measure the pull applied to the studs through the cross-heads.

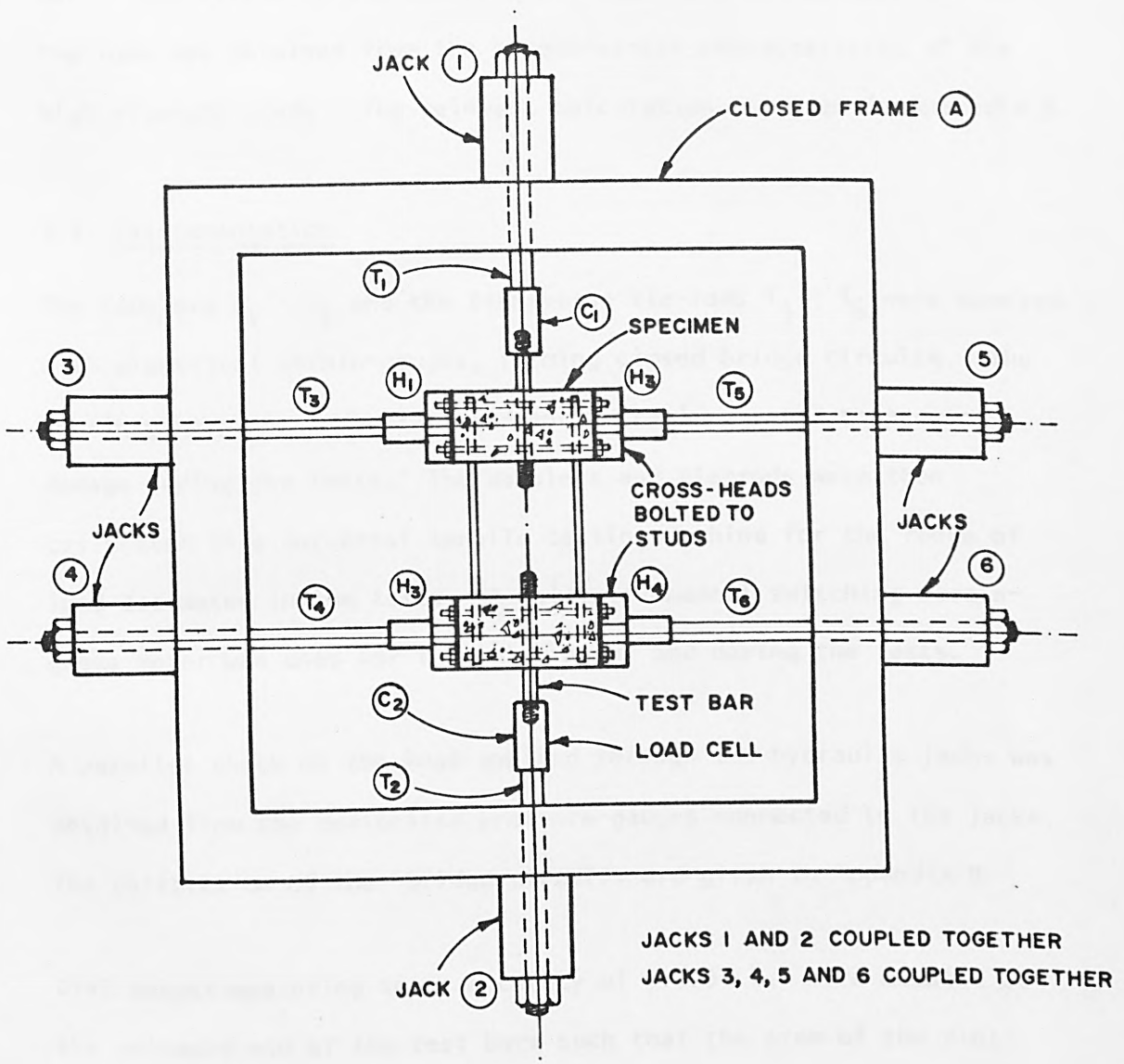


FIG. 3.5 SCHEMATIC DIAGRAM OF TEST ARRANGEMENT

The pull applied to the tie rods $T_3 - T_6$ was varied from 0 to 40 kN, 60 kN and 80 kN in order to provide the required tension release of 1180, 1770 and 2360 micro-strain in the concrete surrounding the test bars. The strain in the concrete corresponding to the pull in the tie-rods was obtained from the stress-strain characteristic of the high strength studs. The relevant calculation is given in Appendix B.

3.4 Instrumentation

The couplers $C_1 - C_2$ and the transverse tie-rods $T_3 - T_6$ were mounted with electrical strain-gauges, forming closed bridge circuits. The strain-gauges were water-proofed and suitably covered to prevent damage during the tests. The couplers and tie-rods were then calibrated in a universal tensile testing machine for the range of load estimated in the tests. A multiple channel switching strain-gauge meter was used for the calibration and during the tests.

A parallel check on the load applied through the hydraulic jacks was obtained from the calibrated pressure-gauges connected to the jacks. The calibration of the bridge circuits are given in Appendix B.

Dial gauges measuring to an accuracy of 0.0001 in. were mounted at the unloaded end of the test bars such that the stem of the dial gauges resting against the concrete face enabled measurement of the relative movements between the bar and the surrounding concrete. The general arrangement during the test of a specimen is shown in the photograph in Fig. 3.6.

3.5 Test procedure

The cross-heads were initially connected to the studs and properly

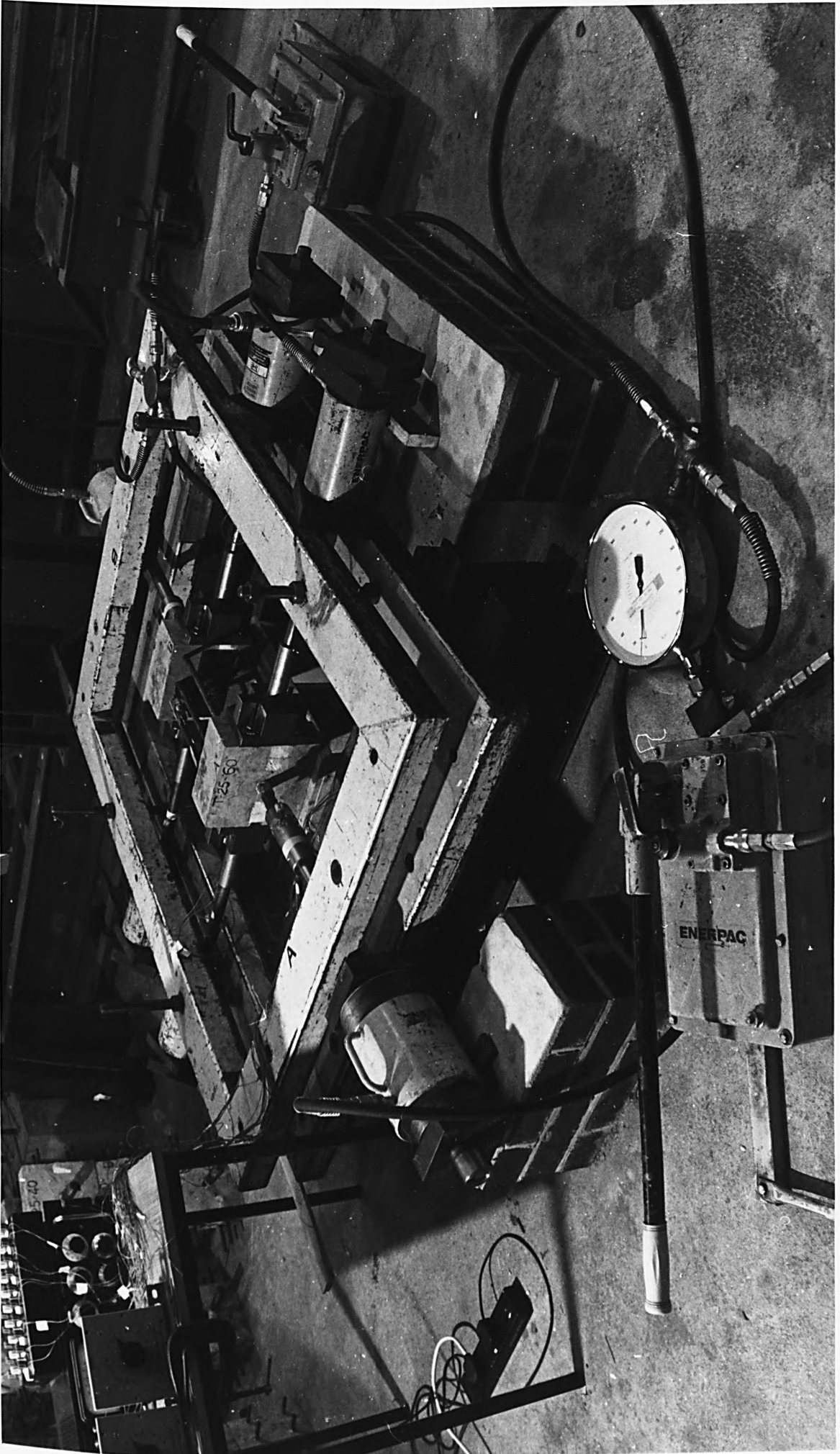


FIG. 3.6 PHOTOGRAPH SHOWING BOND TEST UNDER LATERAL TENSION RELEASE

secured and tightened. The tie-rods connecting to the cross-heads as well as the test-bar were secured hand-tight against the frame through the hydraulic jacks. The zero readings of the dial gauges, load cells and the pressure gauges were taken.

The required level of tension was then applied to the studs and locked in. Load was then progressively applied to the test bars while the applied tension on the studs was maintained at the specified level. Observations of load and dial-gauge readings were recorded as loading progressed with particular attention to initial slip, on-set of cracking and propagation of cracks. Observation of cracking was facilitated by white-washing the faces of the concrete before the test.

Loading was continued until one of the test bars pulled out. The ultimate load at pull-out was recorded. The bar that pulled out was locked with a nut at its free-end and loading was resumed till the second bar also pulled out. The pull-out ultimate load of this bar was also recorded. Thus, a single specimen yielded two results.

A typical record of the observations is shown in Table 3.2.

Reinforcement type = HYBAR
 Tension applied = 40 kN
 Cover = 63 mm

Date cast = 10.1.77
 Date tested = 18.1.77
 Least Count of Dial Gauge = 0.0001 ins.

Pressure Gauge Reading (psi)	Dial Gauge No. of divisions		Strain Meter Divisions	Load kN	Slip (mm)		Remarks
	Bar A	Bar B			Bar A	Bar B	
0	0	0	0	0	0	0	Loading commenced
160 X	$\frac{1}{4}$	-	4	7.33	0.0006	0	Initial slip in A
80	$\frac{1}{4}$	$\frac{1}{4}$		8.49	0.0006	0.0006	Initial slip in B
200 O	$\frac{3}{4}$	$\frac{1}{2}$	5	9.66	0.002	0.001	
20	$1\frac{1}{2}$	1		10.82	0.004	0.003	
40	2	2		11.98	0.005	0.005	
60	$3\frac{1}{2}$	4		13.14	0.009	0.010	
80	$4\frac{1}{2}$	$5\frac{1}{2}$		14.30	0.011	0.014	
300	7	9	8	15.45	0.018	0.023	
20	10	11		16.61	0.025	0.028	
40	13	14		17.77	0.033	0.036	
60	18	19		18.93	0.046	0.048	
80	21	23		20.09	0.053	0.58	
400	25	28	11	21.25	0.064	0.071	
20	$31\frac{1}{2}$	33		22.41	0.080	0.083	
40	39	40	12	23.57	0.099	0.101	
60	46	48		24.72	0.117	0.122	
80	55	57		25.88	0.140	0.145	
500	64	65	14	27.64	0.163	0.165	
20	78	73		28.20	0.198	0.185	
40	89	79		29.36	0.226	0.201	
60	98	86		30.52	0.249	0.218	
80	107	92		31.68	0.272	0.234	
600 O	116	97	17	32.84	0.295	0.246	
20	125	104		34.00	0.318	0.264	
40 X	135	110		35.15	0.343	0.279	
60	146	117		36.31	0.371	0.297	
80	157	123		37.47	0.399	0.312	

Pressure Gauge Reading (psi)	Dial Gauge No. of divisions		Strain Meter Divisions	Load kN	Slip (mm)		Remarks
	Bar A	Bar B			Bar A	Bar B	
700	170	131	20	38.63	0.432	0.333	Crack at end A
20	180	138		39.79	0.457	0.351	
40	194	147		40.95	0.493	0.373	
60	210	156		42.11	0.533	0.396	
80	225	168		43.27	0.572	0.427	
800	246	186	23	44.42	0.625	0.472	Crack at end B
820	271	200		45.58	0.688	0.508	
40	292	214		46.74	0.742	0.544	
60	330	240	25	47.90	0.838	0.610	Dial gauges removed.
1020	-	-	30	57.94			Pull-out of bar A
1040	-	-	31	59.87			Pull-out of bar B

Readings of Load Cells

Load Cell No.	No. of Divisions		
	Initial zero	Beginning of test	End of Test
T ₃	0	32	30
T ₄	-18	12	9
T ₅	-10	16	14
T ₆	0	32	30

TABLE 3.2: TYPICAL RECORD OF OBSERVATIONS - TENSION RELEASE

EXPERIMENTAL INVESTIGATION OF THE EFFECT OF LATERAL
COMPRESSION ON BOND BEHAVIOUR

4.1 Object and scope of test programme

This part of the study relates to the bond behaviour of deformed reinforcement bars in regions of lateral restraint or under lateral compressive stresses. Besides investigating the effects of varying levels of compressive stresses and varying concrete side cover to the deformed bars, the study also includes the performance of top and bottom cast bars in bond tests. The embedment length is kept short for the reasons given in Chapter 3.

4.2 Test Specimen

4.2.1 Philosophy of choice of test specimen

A double pull-out type of specimen was chosen for the study similar to the specimen in the tests for tension release for the reasons given earlier in Chapter 3. However, in view of the study relating to top and bottom cast bars, two sets of bars, one for the top casting and another for the bottom were cast together in the same block one below the other. Sufficient depth of the block was chosen so that the failure of the top bars would not affect the bond performance of the bottom bars and vice versa. In order that the variation in the casting of the concrete may be kept to a minimum, two levels of compression were tested with one test block and the test sequence was arranged such that if the top bars were tested under high compression, the bottom bars directly below them were tested under low compression and vice versa. In this manner, the

failure regions of the top and bottom bars did not extend into one another. The bars were cast at equal depths from the top and bottom faces of the concrete block and this depth was kept constant throughout the test programme.

4.2.2 Details of test programme

The study was again confined to deformed reinforcement bars of 25 mm nominal diameter of the same three different types of profile used in the tension tests namely

(i) Torbar

(ii) Hybar

and (iii) Square-twisted bar

An embedment length of 100 mm equivalent to 4 bar diameters was used.

The concrete covers studied with the three types of bars were 25 mm, 50 mm, 75 mm and 100 mm.

The compression was applied on the top of the concrete surface 50 mm above the centre of the test bar. Three levels of compression were studied corresponding to compressive stresses of 3.92 N/mm^2 , 7.84 N/mm^2 and 11.76 N/mm^2 on the concrete surface.

The concrete used in the test programme had an average compressive strength of 35 N/mm^2 .

4.2.3 Details of test specimen

The details of the test specimen are as shown in Fig. 4.1. It consists of a concrete block 500 mm wide, 500 mm high and 375 mm

deep with test bars located with their centres at depths 50 mm from the top and bottom surface of the block and set in from the side faces with their centres at distances varying from 37 mm to 113 mm as the cover varied from 25 mm to 100 mm. The test bars 300 mm long with both ends threaded over a length of 50 mm were embedded in the concrete block over a length of 100 mm such that the bars projected 50 mm inside the inset steel box as shown in figure. The test bars were threaded through rubber washers located in circular openings in the metal box whose centres were at the same distance from the side face as the centre of the test bar.

The block was reinforced with a reinforcement cage consisting of 25 mm diameter secondary reinforcement bars located as shown around 6 mm diameter mild steel closed welded stirrups. A photograph of the assembled secondary reinforcement cage is shown in Fig. 4.2.

The test specimens were designated a number to indicate the type of bar, the position of bar, the concrete cover and the intensity of lateral pressure applied according to a code as shown in Table 4.1.

4.2.4 Casting of specimen

4.2.4.1 Details of mould

The concrete test block was cast in a steel mould which consisted of a steel box of internal dimensions 500 mm x 375 mm and 500 mm high made of steel plates 15 mm thick and bolted together. Steel boxes open on two adjacent longitudinal faces and measuring 175 mm long and 100 mm deep with varying width depending on the cover required to the reinforcing bar, were fixed symmetrically at the centre of the sides 375 mm long on the inside such that the top of the boxes

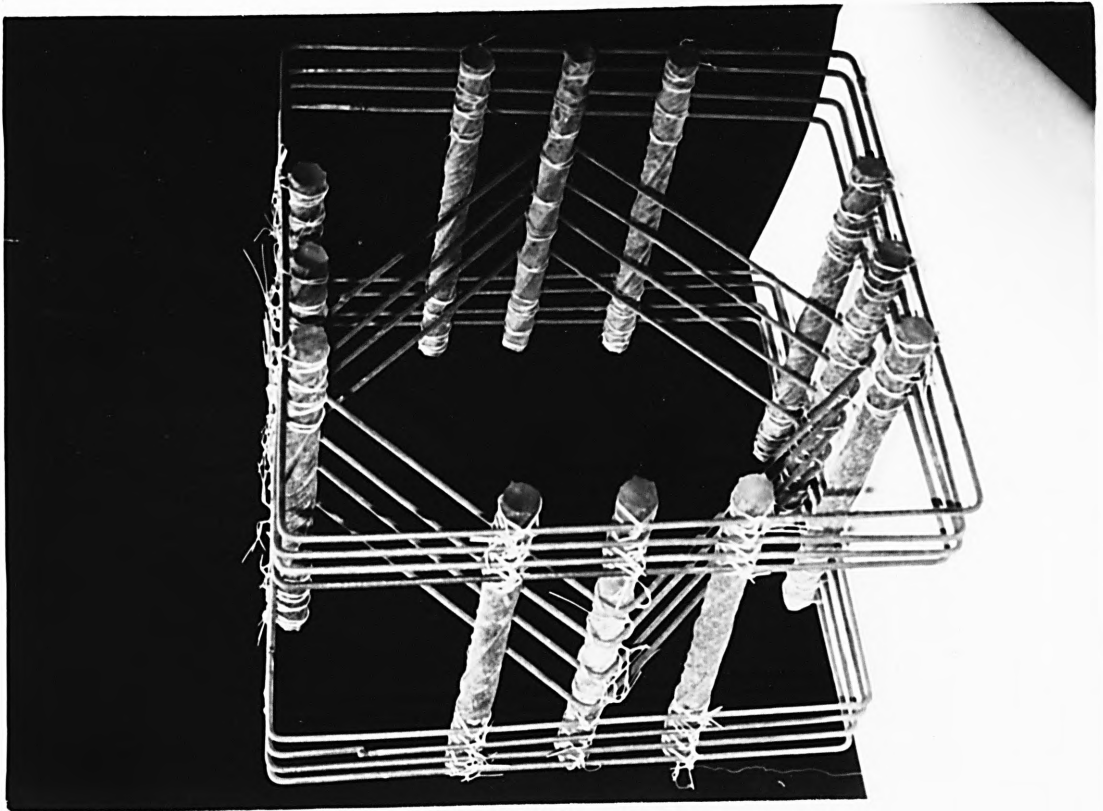


FIG. 4.2 ASSEMBLED SECONDARY REINFORCEMENT CAGE

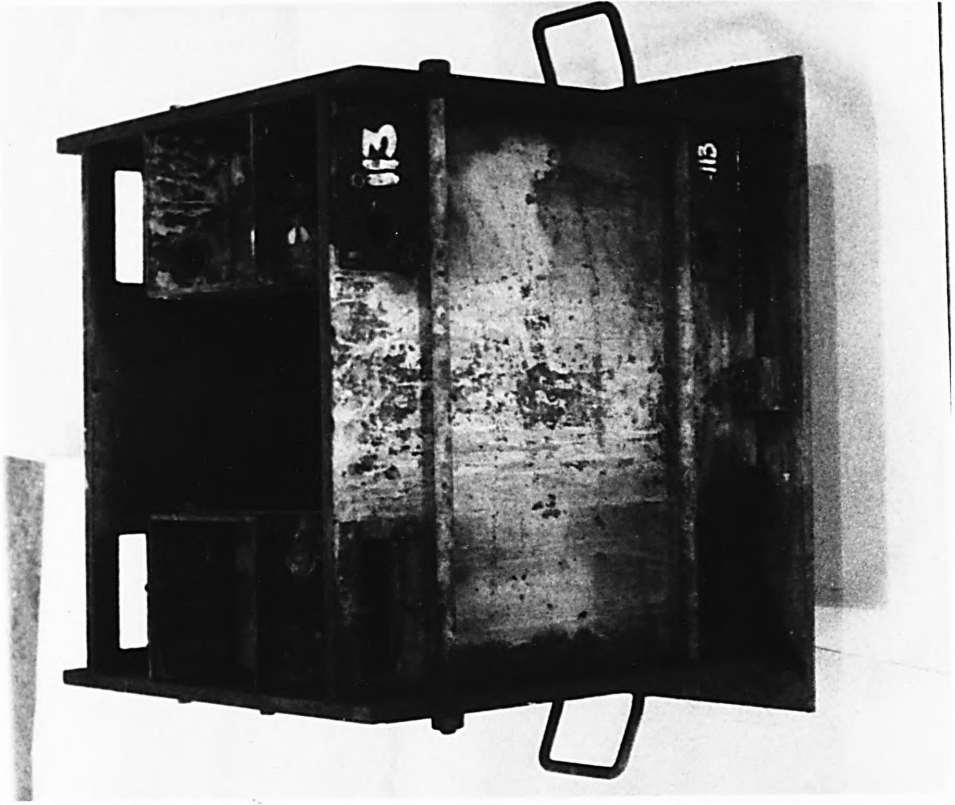


FIG. 4.3 ASSEMBLED STEEL MOULD

Example Specimen Number

T 88 - B 41

Type of bar

Distance from side face of concrete
to centre of reinforcement bar

Location of bar

Lateral applied force

Numbers 1, 2 indicate the two bars
in each test

Types of Bar

T - Torbar

H - Hybar

S - Square-twisted

Location of Bar

B - Bottom of Specimen

T - Top of specimen

Distance from side face of concrete to centre of reinforcement bar

37 - 37 mm to give effective concrete cover of 25 mm

63 - 63 mm to give effective concrete cover of 50 mm

88 - 88 mm to give effective concrete cover of 75 mm

113 - 113 mm to give effective concrete cover of 100 mm

Lateral force applied and lateral pressure developed in concrete

0 - Zero lateral force and zero lateral pressure.

2 - Lateral force of 2 Tons to produce lateral pressure of 3.92 N/mm^2

4 - Lateral force of 4 Tons to produce lateral pressure of 7.84 N/mm^2

6 - Lateral force of 6 Tons to produce lateral pressure of 11.76 N/mm^2

TABLE 4.1 : DESIGNATION CODE USED FOR SPECIMEN NUMBERS

were flush with the top of the side plates of the mould. The end plates of the mould measuring 500 mm x 500 mm on the inside were provided with windows measuring 110 mm x 40 mm at the top and bottom corners. The windows were covered and bolted with cover plates carrying a circular hole 25 mm diameter through which the test bar was threaded. The centre of the circular hole was positioned on the plate such that attachment of the plate to the window on the end plate provided the required cover to the test bar threaded through this hole. With a set of different cover plates and metal box insets corresponding to one particular cover, it was possible to use the same mould for casting the different test specimens for varying concrete cover. The assembled steel mould is shown in photograph in Fig. 4.3.

The test bars were threaded through the circular hole in the end plates of the mould and the circular hole in the inset metal box with the end of the bar projecting 50 mm inside the metal box inset. The bar was threaded through rubber washers in the circular holes in order to locate the bar centrally in the holes and also to prevent the bars jamming against the sides of the circular holes in the mould end plate or in the side wall of the inset box.

4.2.4.2 Materials and casting procedure

A. Concrete

The concrete was made with Malaysian make Tiger Brand Portland cement mixed with mining sand and granite of maximum size 20 mm in the proportions 1:2:3.45 with a water-cement ratio of 0.55. The concrete was designed to give an average crushing strength of 35 N/mm² at an age of 14 days. The aggregates were washed and

oven-dried before use to minimise variations in strength and eliminate impurities which would impair the bond properties of the steel. Details of the mix and concrete strength for the various batches are given in Appendix C.

B. Steel

All test bars were high strength deformed bars conforming to B.S. 4449: 1978. The mechanical properties of the bars together with details of rib dimensions and spacing of ribs are given in Appendix B. The types of bars used were the same as in the tests with tension release (Fig. 3.4) and were obtained for the tests from England.

The test bars were cut to the required length and the ends were threaded to a length of 50 mm. The surfaces of the test bars were thoroughly cleaned of all oil and grease. Just prior to the threading of the bars in the mould and securing them in position, the bonding length of the deformed bars was cleaned with trichloroethylene.

C. Casting procedure

The assembled mould was coated with a thin coat of mould oil on the inside. The secondary reinforcement cage was assembled (Fig. 4.2), lowered into the mould and located with the required cover to the stirrups from the bottom plate. Each test bar was then threaded into position and was held against the metal inset on the inside with a nut. Any clearance between the bar and the hole on the end plate of the mould was sealed with plasticine to prevent egress of cement grout. Similarly all the eight test bars

in a test block were located in the mould.

Although the test bar was held against the metal inset on the inside with a nut, there was the possibility that the bar may fall out of alignment due to lack of restraint at the face of the mould and the possibility of the bar moving away from its intended position either side-ways or vertically. This was prevented by threading the bars at the free end through templates (Fig. 4.4). These templates were made of plywood 25 mm thick and had windows cut out at the top and bottom corners at positions identical to those on the end plates of the mould. These windows were covered and bolted with cover plates in steel carrying circular holes 25 mm diameter such that they could be positioned at various positions on the window to provide the required cover to the bar. Care was taken during assembly of the moulds and casting of the specimen so that the cover to the test bar provided at the end plate and the wooden template were the same. In order to ensure that the test bars were level, the templates were suitably wedged from the casting floor and checked for correct level of the bar. Care was taken to ensure that the templates were not disturbed during casting of the test block. The completed assembly ready for casting is shown in the photograph in Fig. 4.4.

Aggregates, cement and water by weight were placed in a tilting drum and mixed for about 5 minutes. The concrete was placed in layers in the mould and compacted using a petrol driven immersion vibrator. Care was taken to ensure that the test bars were secure in position whilst the concrete was being vibrated. At the top of the block, a hook bolted to an end plate, immersed in the top concrete and resting below the secondary reinforcement cage was located in the centre of

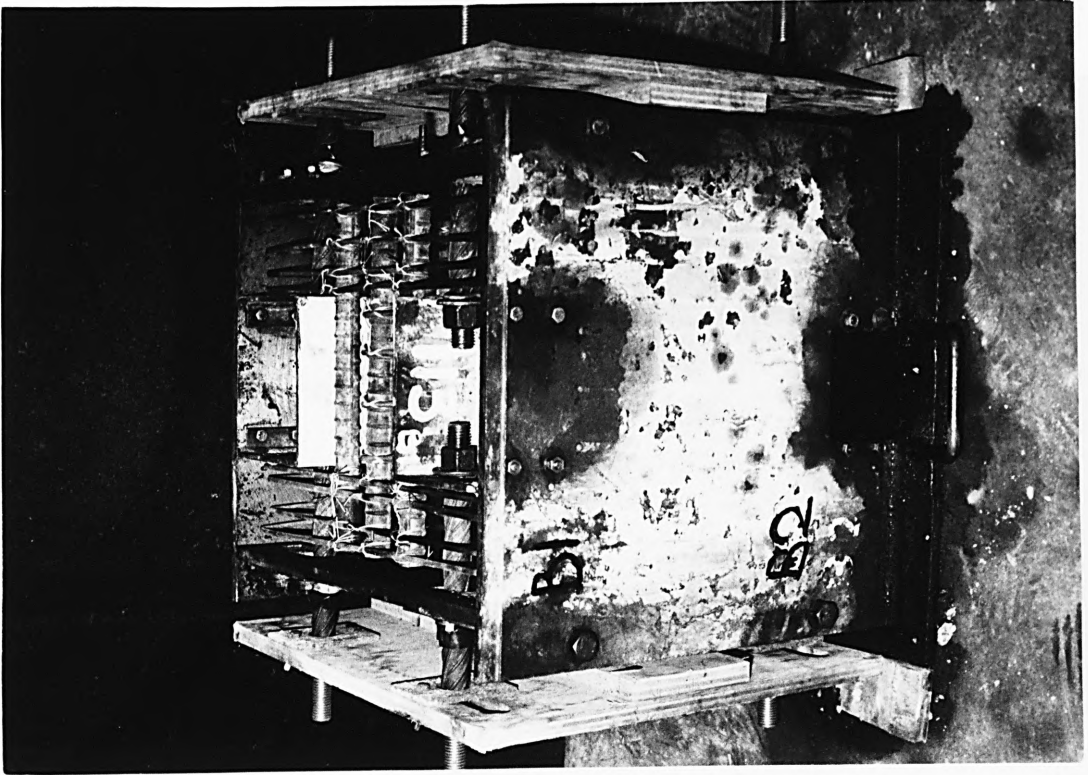


FIG. 4.4 SPECIMEN ASSEMBLY BEFORE CASTING

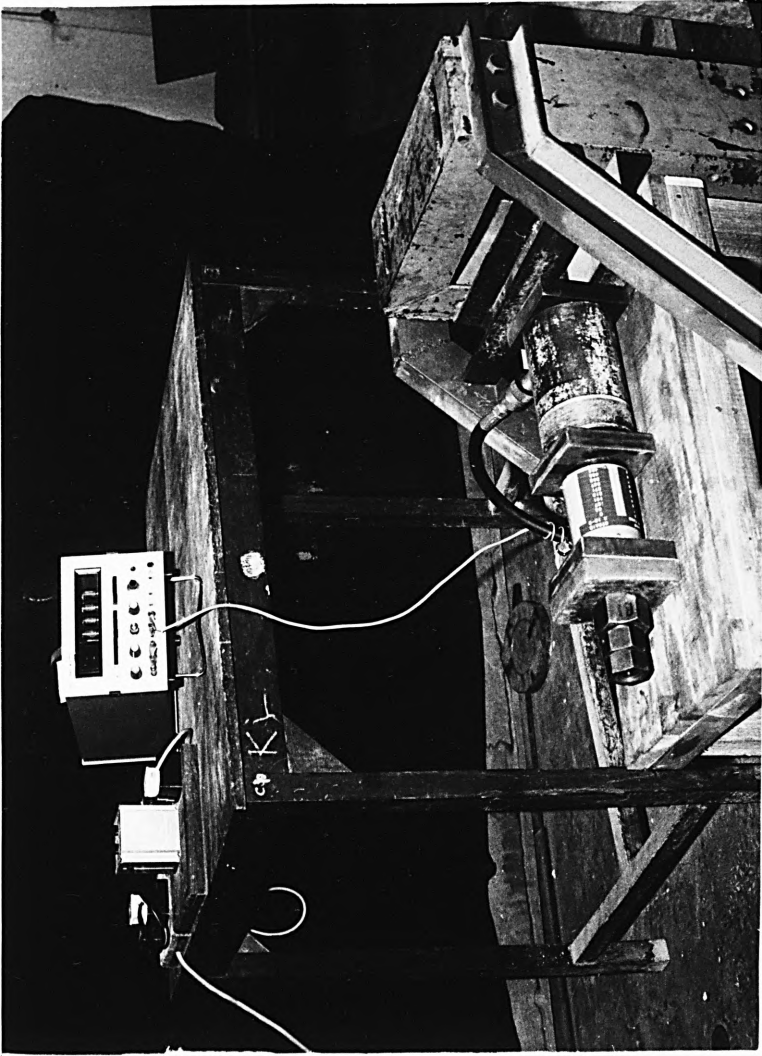


FIG. 4.7 PULLING OF TEST BAR

the block. The hook was cast to enable the lifting of the block during transport and assembly in the test frame. The hook would be unbolted after correct placing of the block in the testing frame, leaving the top surface free of obstruction.

The test block assembly was covered with a wet burlap after one day and the burlap was kept moist with a continuous drip of water. After 3 days, the timber templates and the side faces of the moulds were removed after which the top and exposed faces of the test block were covered with burlap and the water curing was continued. At an age of 5 days, the end plates of the mould were also removed and the complete test block was again covered with burlap and cured until the day before the test. Care was taken to ensure that the test bars were not disturbed during the demoulding operations. The bolts connecting the metal box insets to the side of the mould were removed prior to the demoulding of the side of the mould. The insets would remain through the test and are recovered only after the tests have been completed and the test bars have been pulled out of the test block. The specimens were tested when the concrete attained a strength of 35N/mm^2 . The strength of the concrete was monitored by progressively testing control cubes cast with the same batch of concrete and cured according to the same regime as the test block.

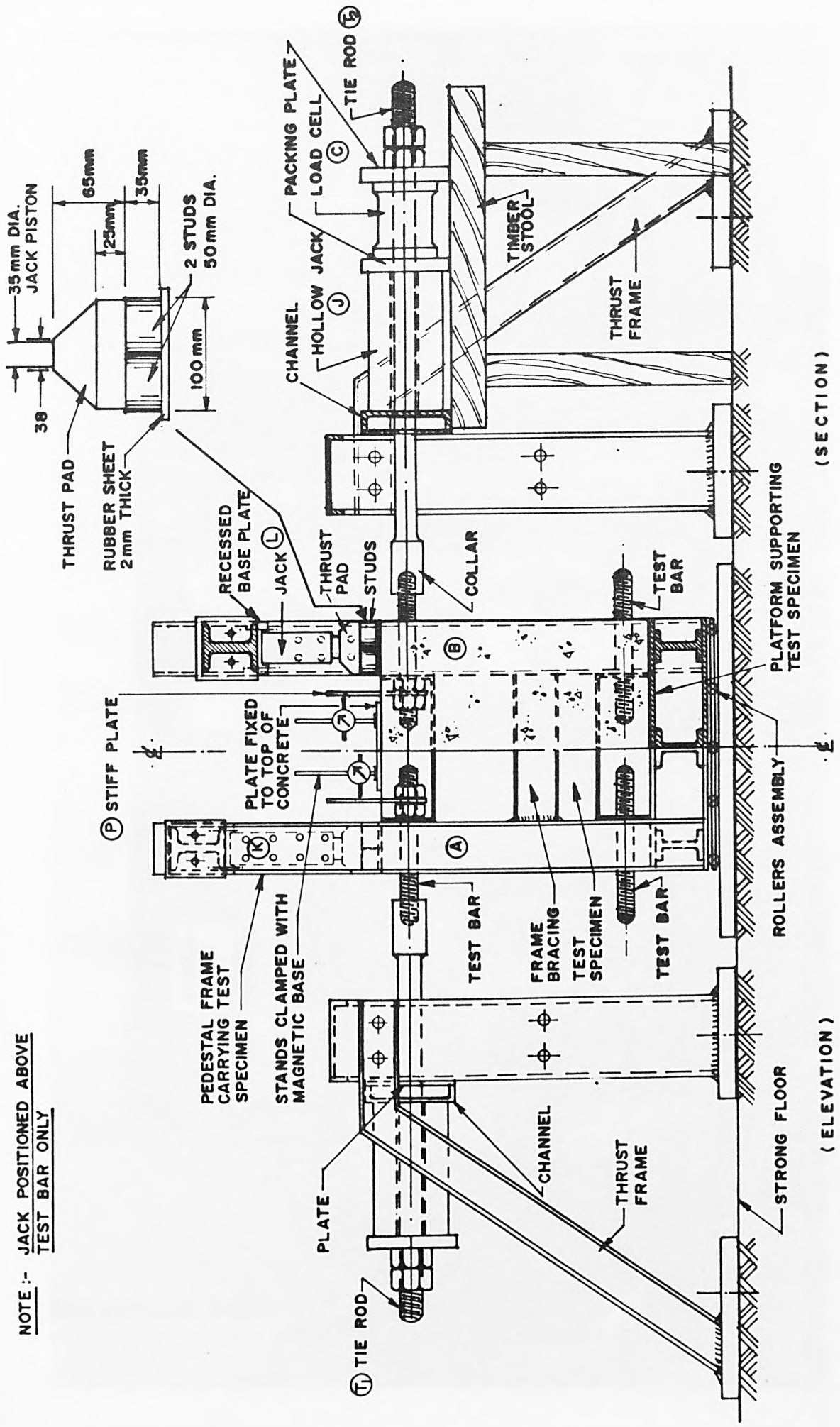
4.2.5 Control tests

12 Nos. concrete cubes $100 \times 100 \times 100$ mm and 2 Nos. cylinders $150 \text{ mm} \times 300 \text{ mm}$ were cast together with every test block. A batch of two cubes was periodically tested to monitor the increase in strength in order to estimate the age at which the concrete would

attain a strength of 35 N/mm^2 . On the day of the test, the remaining 3 or 4 cubes were tested for compressive strength. The cylinders were tested for splitting tensile strength. The results are given in Appendix C.

4.3 Test arrangement

The test set-up is shown in the schematic diagram in Fig. 4.5 and the photograph in Fig. 4.6. The concrete test block was placed on a pedestal frame resting on a roller assembly on top of a steel plate placed on the strong floor of the testing laboratory. The roller assembly enables the test bars to be pulled in either direction without any restraint due to friction between the pedestal frame and the bottom steel plate. The pedestal frame consists of a platform for supporting the test block with 4 Nos. vertical legs A, B of channel section in the four corners. The two legs at A were bolted together at the top with a cross-beam thus forming a portal frame. Similarly the legs at B were bolted with another cross-beam to form a portal frame. The portals A and B were braced together above the common platform with welded channel sections. The cross-beams were capable of being shifted to different levels on the vertical legs to allow for the necessary clearance required between the bottom of the cross-beams and the top of the concrete block. The test bars were pulled in tension through tie rods, $T_1 - T_2$ which were threaded to the test bars through collars having internal threads. The tie rods were pulled through a hydraulic hollow jack J against vertical frames which were attached to the strong floor and held against vertical movement by thrust frames as shown (Figs. 4.5, 4.7).



NOTE :- JACK POSITIONED ABOVE TEST BAR ONLY

FIG. 4.5 SCHEMATIC DIAGRAM OF TEST ARRANGEMENT

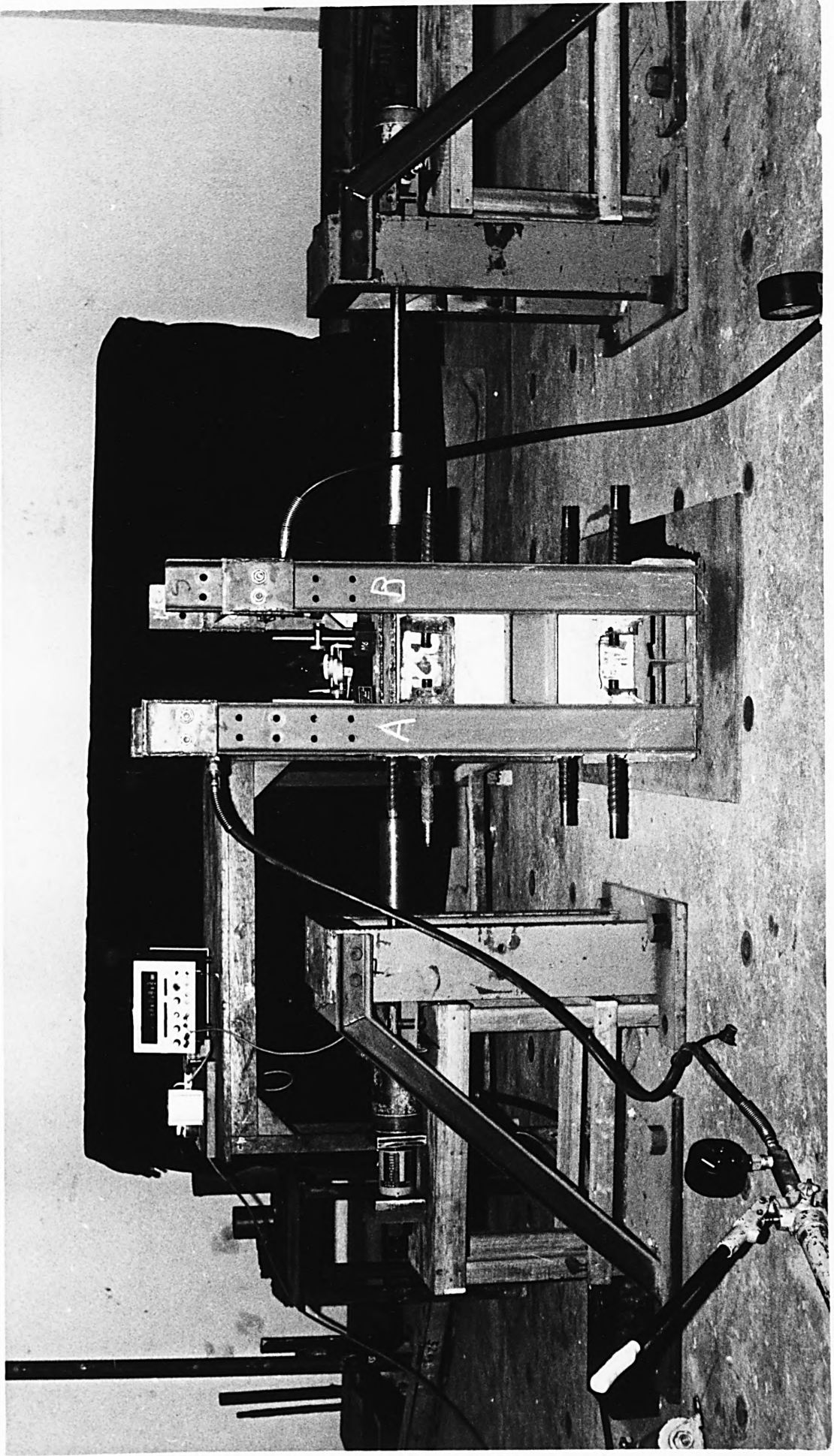


FIG. 4.6 PHOTOGRAPH SHOWING BOND TEST UNDER LATERAL COMPRESSION

The required lateral compression was applied to the top of the block above the embedded length of the test bar with a system of jack, thrust pad and studs as shown in the figure. The jacks K, L applying the vertical thrust were held against the cross-beams at A, B, (Fig. 4.8). The bases of the jacks were held inside recessed base plates which were bolted with studs to the bottom of the cross-beam at different locations. The positions of these plates were altered to suit the respective cover of the concrete to the test bar in the test block. The piston of each jack rested symmetrically on a thrust pad which has a base 100 mm x 50 mm x 25 mm thick reducing to 38 mm square over a depth of 40 mm. The thrust pad in turn rested on two steel studs 50 mm diameter and 35 mm thick placed as shown (Fig. 4.9). A rubber sheet 2 mm thick and measuring 105 mm x 50 mm was placed immediately below the studs to help to even out any irregularities on the surface of the concrete which may lead to uneven bearing of the studs. An investigation was carried out to ensure that the system of applying the thrust adopted in the tests produced an even pressure on the embedded length of the bar. Details of this investigation are given in Appendix C.

4.4 Instrumentation

The loads applied to the test bars were measured using a prior calibrated load cell C connected to a digital strain meter. The load cell was connected in series with the hydraulic jack as shown. The slip in the bars at the unloaded end was measured with the help of a stiff plate P fixed to the free-end of the test-bar sandwiched between a nut and a locking nut. Care was taken that the nut close to the test block provided sufficient clearance to allow the slip

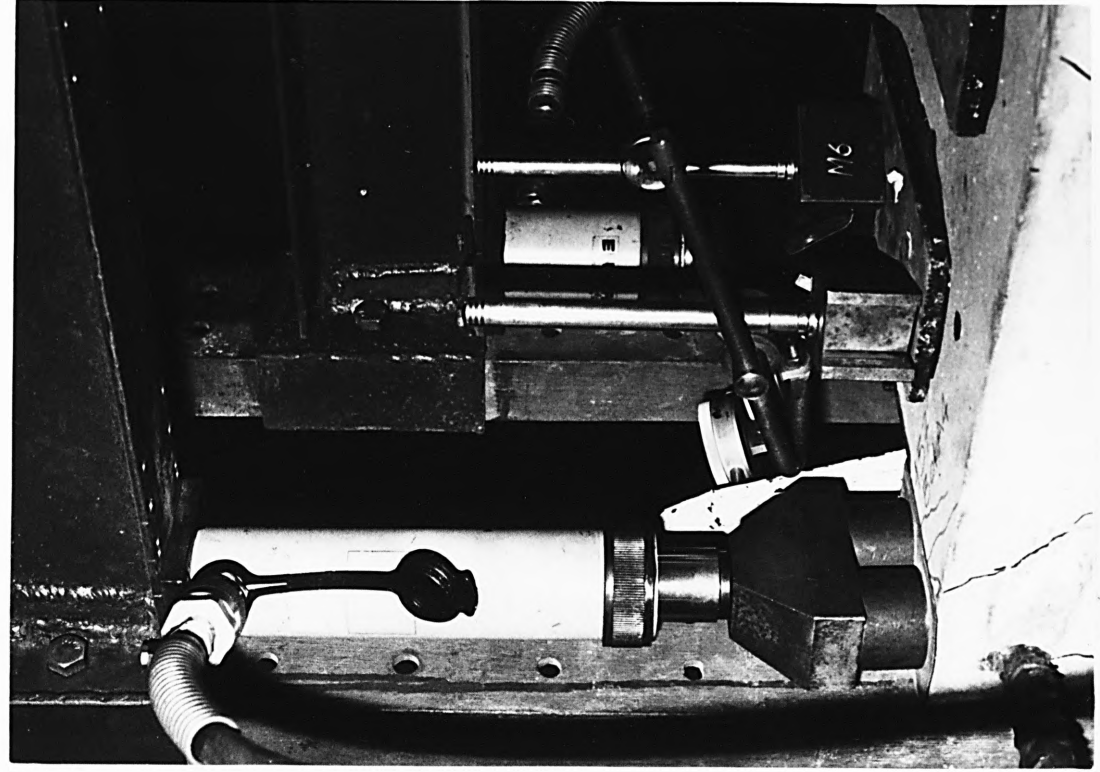


FIG. 4.8 JACKS APPLYING LATERAL PRESSURE

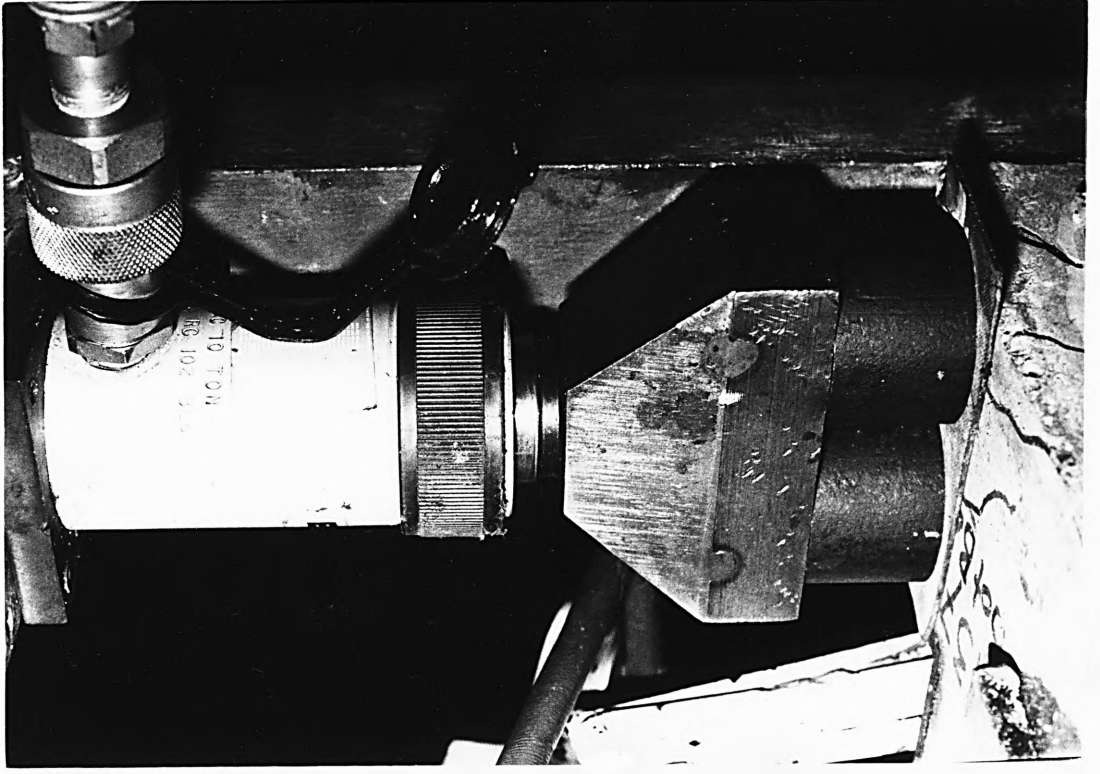


FIG. 4.9 TRANSFER OF LATERAL PRESSURE TO CONCRETE

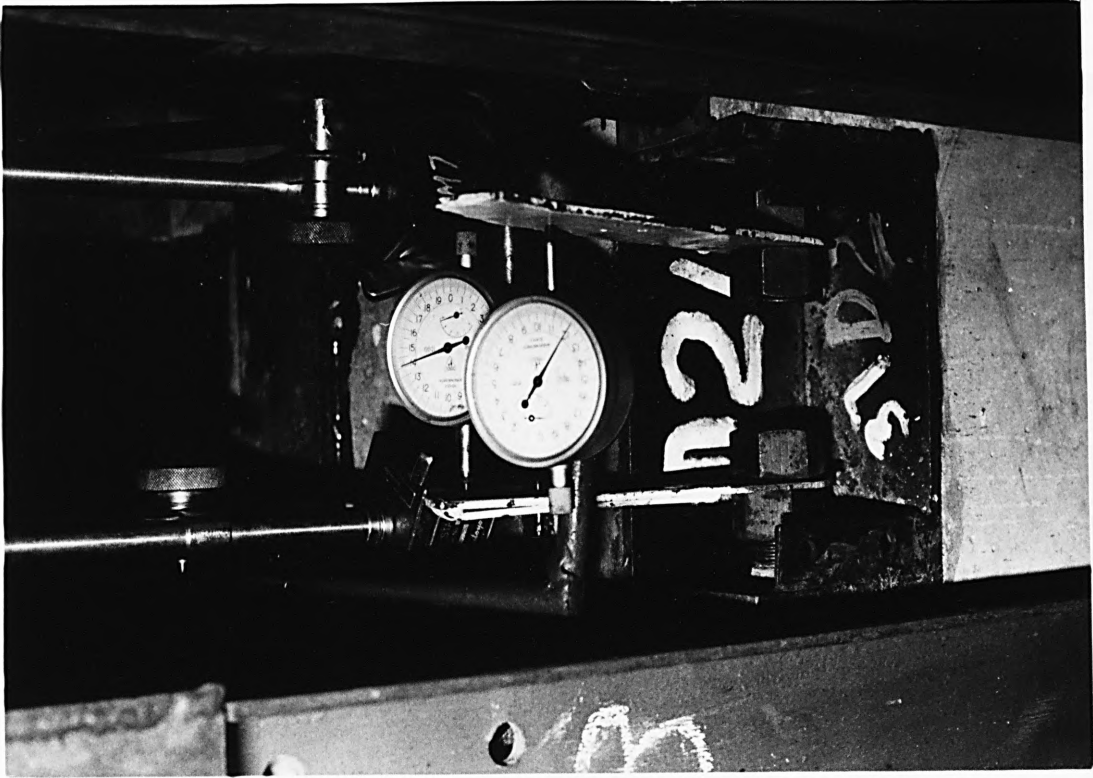


FIG. 4.10 ARRANGEMENT FOR SLIP MEASUREMENT

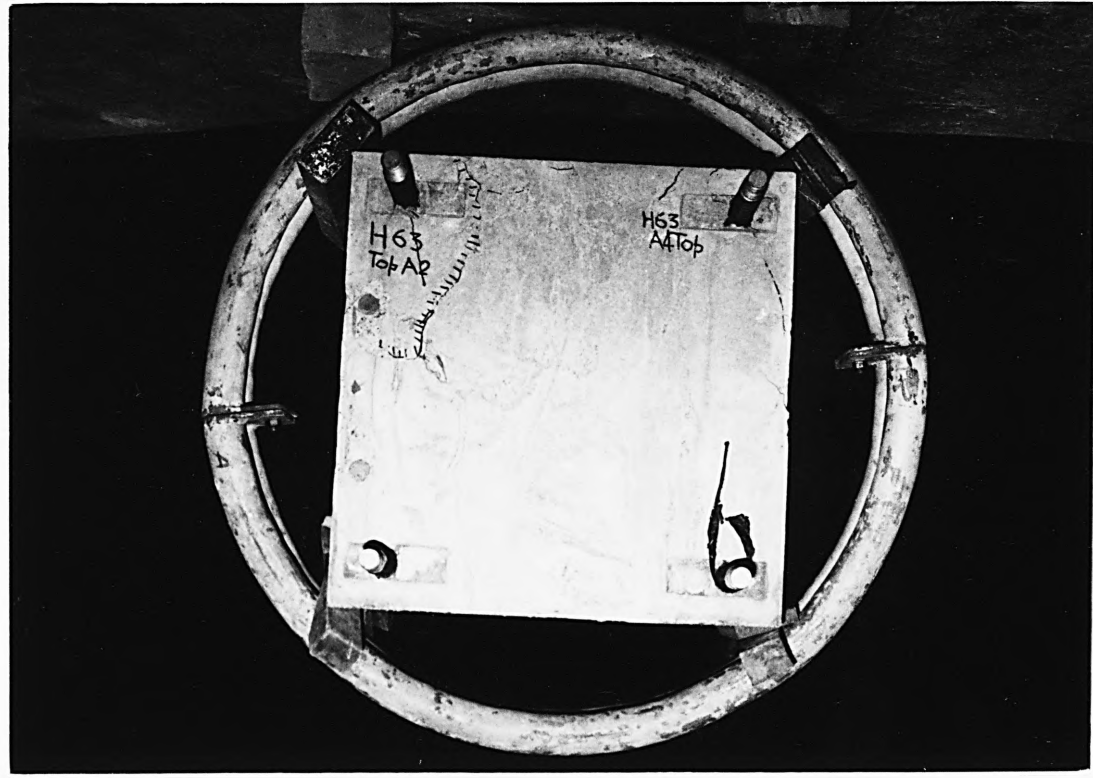


FIG. 4.11 DEVICE FOR ROTATING TEST BLOCK

the embedded test bars. Care was taken to ensure that the jacks were vertical and were in the same line as the axes of the tie rods. The dial gauges to measure slip of the free ends of the bars were then mounted such that their stems pressed against the stiff plates fixed to the ends of the bars for the purpose.

The required pressure was then applied to the jacks providing the vertical thrust and the pressure was maintained at the same level during the test. Load was gradually applied to the test bars by increasing the pressure on the hydraulic jack connected to the tie rod and observations of slip were made at different load stages. Particular attention was paid to initial slip, on-set of cracking and propagation of cracks as the test progressed. As soon as one of the test bars had reached its ultimate bond strength, load began to fall as indicated on the digital strain meter connected to the load cell. At this point, the loading was temporarily stopped. The dial gauge reading the slip of the bar that had failed was removed together with the stiff plate connected to the end of the bar. The nut at the end of the bar was then tightened against the test block with a view of preventing further pull-out of this bar. The loading was then resumed and observations of slip were taken until the other bar also failed.

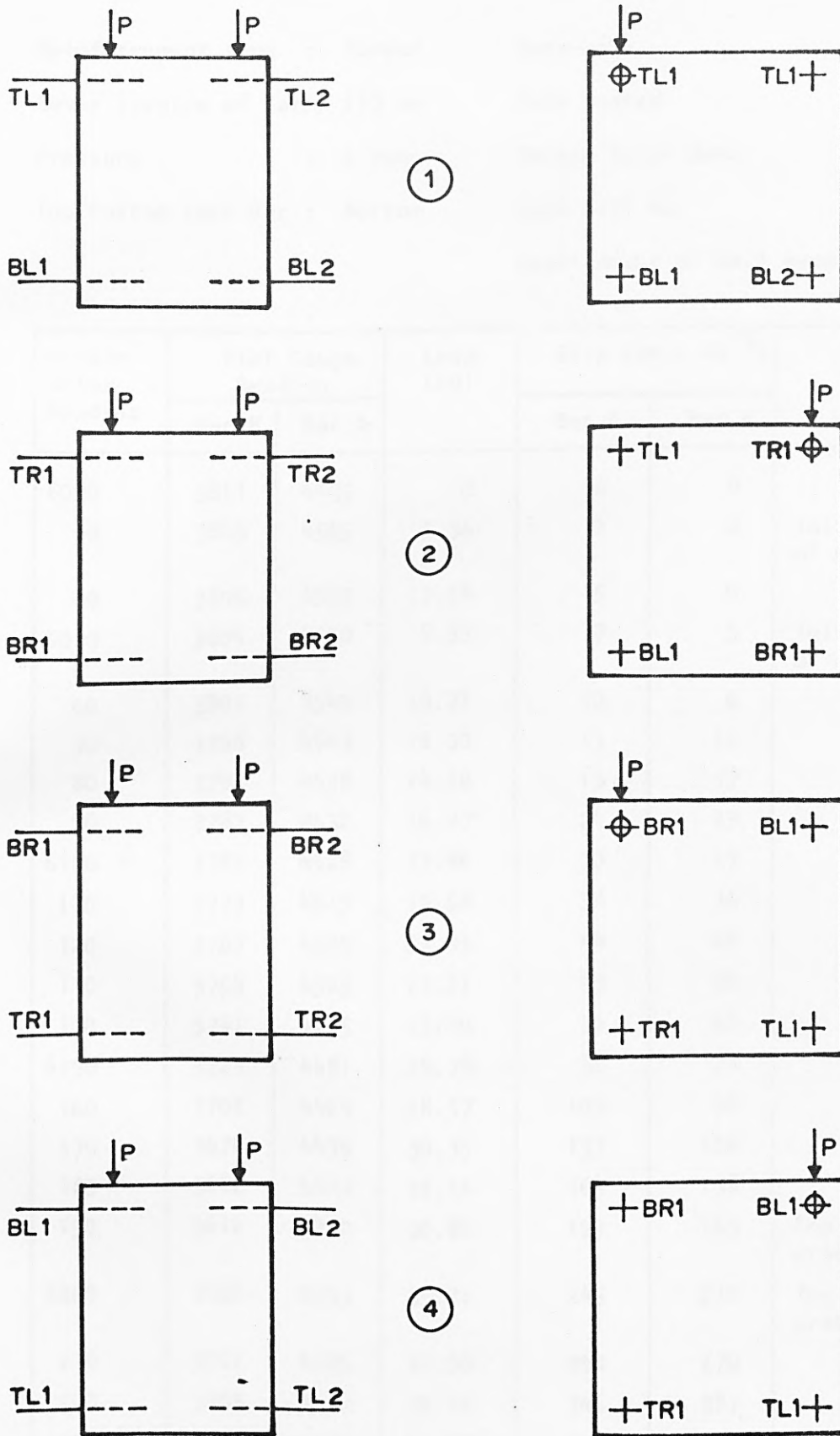
The block was then moved side ways so that the other set of bars on the top were in the line of the testing frame. The test was repeated on the bars until they failed.

In order to test the bottom bars, the test block had to be rotated so that the bottom bars presented themselves at the top. The test

block was removed from the pedestal frame after the top bars have been tested and placed in a circular frame (Fig. 4.11). The circular frame with the test block secured in it was rotated through 180° to enable the bottom of the block to be turned over. The test block was then transferred back to the pedestal frame to continue the test on the other two sets of bars (bottom-cast bars). The entire operation was performed using a hand-pulley mounted on a movable A-frame with manilla rope to go round the test block during lifting operations. Care was taken to ensure that the test bars were not knocked or otherwise disturbed during these operations. The sequence of testing of the bars is given in Fig. 4.12.

A typical record of the observations is shown in Table 4.2.





T = TOP BARS ; B = BOTTOM BARS
 L = BAR TO LEFT ; R = BAR TO RIGHT

FIG. 4.12 SEQUENCE OF TESTING OF TOP AND BOTTOM BARS

Reinforcement type : Torbar Date cast : 10.3.81
 Cover (centre of bar): 113 mm Date tested : 28.3.81
 Pressure : 2 tons Strain Meter Zero : 6000
 Top/Bottom cast-Bar : Bottom Load Cell No. : 2
 Least count of dial gauge: 0.001 mm

Strain Meter Reading	Dial Gauge Reading		Load (kN)	Slip (mm x 10 ⁻³)		Remarks
	Bar B	Bar A		Bar B	Bar A	
6000	3811	4555	0	0	0	
30	3809	4555	5.36	2	0	Initial slip of B
40	3806	4555	7.14	5	0	
6050	3804	4550	8.93	7	5	Initial slip of A
60	3801	4549	10.71	10	6	
70	3798	4543	12.50	13	12	
80	3792	4538	14.28	19	17	
90	3787	4532	16.07	24	23	
6100 +	3781	4528	17.86	30	27	
110	3773	4519	19.64	38	36	
120	3767	4509	21.43	44	46	
130	3758	4505	23.21	53	50	
140	3741	4495	25.00	70	60	
6150	3725	4481	26.78	86	74	
160	3702	4465	28.57	109	90	
170	3674	4435	30.35	137	120	
180	3642	4417	32.14	169	138	
190	3612	4390	30.89	199	165	Top cover crack bar B
6200 +	3566	4343	35.71	245	212	Top cover crack bar A
210	3521	4285	37.50	290	270	
220	3465	4168	39.28	346	387	
230	3405	3845	41.07	406	710	
6231	3386	2521	41.25	425	1034	Bar A failed - Bar A locked.

Strain Meter Reading	Dial Gauge Reading		Load (kN)	Slip (mm x 10 ⁻³)		Remarks
	Bar B	Bar A		Bar B	Bar A	
6190	3379	-	33.92	432	-	Re-loading commenced
220	3375	-	39.28	436	-	
230	3356	-	41.07	455	-	
240	3299	-	42.85	512	-	
6250	3185		44.64	626		
260	3035		46.42	776		
270	2712		48.21	1099		
6272	2035		48.57	1776		
						Bar B failed

TABLE 4.2: TYPICAL RECORD OF OBSERVATIONS - LATERAL PRESSURE

CHAPTER 5

THEORETICAL ANALYSIS

5.1 Bond Mechanism

Studies of bond resistance of plain and deformed reinforcing bars have shown that in general bond resistance is developed due to three factors, namely :

1. adhesion (chemical) or gluing of the cement gel to the surface of the bar;
2. friction between the concrete and bar surface;
3. mechanical interlocking between the concrete and the deformations of the bar.

Bond resistance of plain bars depends primarily on resistance to shearing of the cement gel adhering to the bar surface before initial slip and thereafter on friction between the bar surface and the surrounding concrete. The roughness of the bar surface would determine this resistance. Rehm (25) has shown that for plain smooth bars with or without rolling skin, the maximum frictional resistance attained is only about 4% of the cube strength of concrete.

Bond resistance of deformed bars depends primarily on the mechanical interlock between the ribs and the surrounding concrete.

5.2 Failure mechanism of deformed bars

As load is applied to the reinforcement bar, there is loss of adhesion due to shearing of the cement gel. Any further resistance to pull-out of the bar is provided by the frictional resistance between the bar

surface and the concrete surrounding it. However, due to the tension applied to the bar, the diameter of the bar would tend to decrease at all points and the reinforcing bar would tend to separate radially from the concrete thereby destroying the adhesive stress between the reinforcing bar and concrete at low stresses. This is supported by the work of Lutz (50) and Ferguson (7). Further frictional bond stresses which are manifested by the interlocking of the surface of the reinforcing bar with the surrounding concrete would thus be reduced due to the bar tension. This was confirmed by McClure (56) in a finite element study of a model consisting of a reinforcing bar and the surrounding concrete for a distance of two and three bar radii and over a bonded length of one rib spacing.

As slip begins to take place due to failure in adhesion and friction, the ribs of the deformed bars bear against the concrete surrounding it and the crushing strength of the mortar comes into play.

The ribs bearing against the concrete produce very high bearing (compressive) stresses (25) which tend to crush the concrete resulting in further slip of the reinforcement bar. However, the ribs by their wedging action into the concrete would also cause splitting of the concrete surrounding it depending on the restraint provided by this concrete.

The interlocking of the ribs and the forces developed in the concrete in resisting the slip of the bar are dependent on the geometric properties of the surface profile of the deformed bar which include the rib height, rib spacing and rib face angle (given with respect to the bar axis). Rehm (25) found from his single rib pull-out tests

that slip resistance increased with increasing height of the rib. This was later confirmed by Lutz (50) in similar single rib tests. It is believed that the major portion of the improved slip resistance is due to the reduction in bearing pressure caused by the increased height of the rib. The increased bearing area significantly reduced the bearing pressure and consequent crushing of the concrete next to the rib.

The rib spacing plays an equally important part as the rib height in the bond failure mechanism. For a bar of given diameter, the rib bearing area for a given length of embedment can be increased by increasing the rib heights or by increasing the number of ribs in this given length of bar. In both situations, the shearing area of the concrete 'teeth' or key between the ribs is essentially constant, being roughly proportional to the product of the outside bar diameter (inclusive of rib height) and the embedment length. The area in shear increases slightly with increasing rib height and decreases slightly with closer rib spacing and more ribs in the same length. With a large rib spacing, the bearing pressure against the concrete key dominates over the shear stress across the base of the concrete key. The portion of the concrete key just in front of the rib is severely crushed and acts as a wedge by moving with the rib (Fig. 5.1). This wedge usually makes an angle between 30° and 45° with the bar axis and exerts high lateral pressure on the concrete which is still intact. Rehm (25) observed in his tests that the concrete key failed in a region with a length equal to 5 to 7 times the rib height. Similar observations of the concrete wedge were made by Lutz (50). The failure plane was seen to extend between adjacent ribs when well

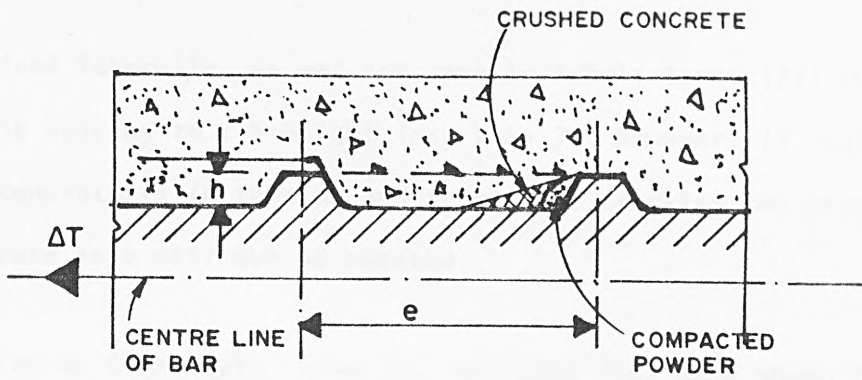
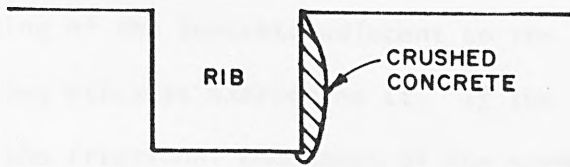
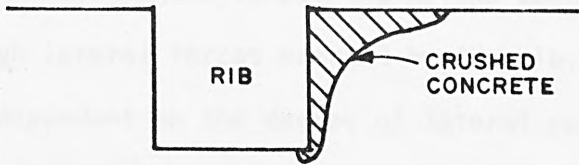


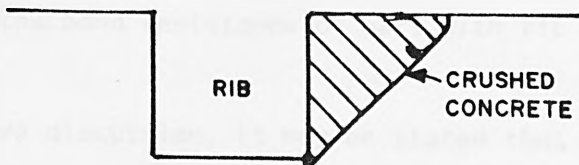
FIG. 5.1 BEARING OF RIB AGAINST CONCRETE



a. INITIAL CRUSHING



b. INTERMEDIATE CRUSHING



c. FINAL CRUSHING

FIG. 5.2 CRUSHING UNDER RIB (after McClure)

confined laterally, as was the case in Rehm's tests (25) for ratios of rib spacing to rib height less than 7. However, in regions where the concrete is in tension and transverse cracking can occur, the concrete keys will not be sheared.

Studies by Clark (17), Rehm (25) and Lutz (50) have shown that there was little difference between the slip resistance exhibited by bars with rib face angles greater than 40° and the resistances were significantly greater than those of bars with face angles of less than 30 to 40° . When the rib face angle is greater than about 40° , the frictional component of the force normal to the rib face is sufficient to prevent the rib from sliding with respect to the concrete key. The slip observed is due almost entirely to the gradual crushing of the concrete adjacent to the rib as a result of the high bearing stresses exerted on it. If the rib face angle is 30° or less, the frictional component of the normal force is not sufficient to prevent movement of the rib with respect to the adjacent portion of the concrete key. The slip observed in such a situation is primarily due to pushing of the concrete outward as a result of high lateral forces exerted by the rib. This outward movement is dependent on the degree of lateral restraint provided to the reinforcement bar. This was demonstrated in the tests of Rehm (25) in which the bond resistance of flat ribbed bars of rib face angle 24° under effective lateral restraint was found to be better than the bond resistance of bars with rib face angle of 45° .

From the above discussion, it may be stated that bond failure may be either of splitting failure of the concrete or plough-through shear

failure of the concrete depending on the lateral restraint provided by the concrete surrounding the reinforcement bar. However, Tepfers (30, 31) has treated bond failure as occurring in one of three modes, namely the uncracked elastic, the plastic or the partly cracked elastic modes as a result of cover cracks longitudinal to the reinforcing bar. It would seem that Tepfers considers plough through failures as a form of partly cracked elastic type of failure in which only a ring round the reinforcement bar is cracked leaving the outer concrete intact and the pull-out of the bar is caused by the cracking in the immediate region surrounding it.

In the following, the two modes of failure, namely the splitting and plough-through types, would be examined in detail.

5.2.1 Splitting failure mechanism

As the load on the bar is increased and the resistance due to adhesion and friction are exceeded, the bar rib bears against the concrete key and crushes the concrete in front of the rib (Fig. 5.1). The completely compacted concrete powder and the partly crushed concrete forms a wedge of concrete in front of the rib. The concrete in front of the rib can sustain a bearing pressure several times the crushing strength of concrete because of the confined condition of the concrete.

Further loading of the bar causes this wedge of concrete in front of the rib to press against the concrete surrounding it which is intact. This results in a radial component of the bearing stress between the rib plus the wedge of crushed concrete and the intact

concrete which causes splitting failures.

McClure (56) carried out an analysis using finite element models to study crushing of the concrete with varying rib face angles of 90, 60 and 45° and found essentially the same results for all the three face angles. This is in agreement with the work of Lutz (50) which also showed that the rib face angle had no apparent effect on the final extent of crushing. The different stages in the crushing of the concrete under the ribs are shown in Fig. 5.2. The final surface of the crushed concrete is slightly curved and extends slightly beyond the end of the rib with the surface making an approximate angle of 45° with the bar axis. McClure concluded that the stresses at the surface of the crushed concrete wedge are normal to the surface and therefore the radial component of this normal stress would be equal to the longitudinal component.

The radial component due to bond action on the intact concrete can be regarded as a hydraulic pressure acting on a thick-walled ring. The concrete surrounding the bar behaves like a thick ring and the ring thickness is determined by the smallest possible dimension, as the ring would crack at the thinnest point due to the ring tensile stresses. Tepfers (31) has suggested that the failure of the concrete ring may be of perfectly elastic, perfectly plastic or partly cracked elastic mode depending on the thickness of the concrete ring (cover). He developed expressions for the concrete stress when the cover cracked due to splitting tension based on the bond forces between the reinforcing bar and the concrete making an angle α with the bar. Experimental results obtained by Tepfers (31)

and Tilantera and Rechart (57) fell within the range of the plastic theory and partly cracked elastic theory expression when α was taken as 45° (Fig. 5.3).

Cairns (34) based on his study of lapped joints in compression reinforcement suggested that the angle α was less than 45° and was given by the expression :

$$\alpha = 45^\circ - \theta/2, \text{ when } \theta = \text{angle of internal friction of concrete.}$$

However, recent work by Skorobogatov and Edwards (33) justifies the assumption of the lateral splitting force and longitudinal pull-out force as being equal to each other.

5.2.1.1 Bond action in partly cracked elastic stage (31)

Considering a concrete ring loaded internally and radially by the radial bond stress components from a reinforcing bar (Fig. 5.4), internal cracks are formed when the circumferential stresses reach the ultimate tensile strength of concrete. The bond force is now transferred through the concrete 'teeth' between the internal cracks to the uncracked part of the ring. The pressure from the reinforcing bar on the inner surface area on the internally cracked ring must be reduced in comparison with the pressure on the inner surface of the initial uncracked ring.

For the cylinder subjected to internal pressure p_i the tangential stress equation at a radius r is given by

$$\sigma_\theta = \frac{p_i r_1^2}{r_2^2 - r_1^2} \left[1 + \frac{r_2^2}{r^2} \right] \text{ where } \begin{array}{l} r_1 = \text{internal radius} \\ r_2 = \text{external radius} \end{array} \dots (5.1).$$

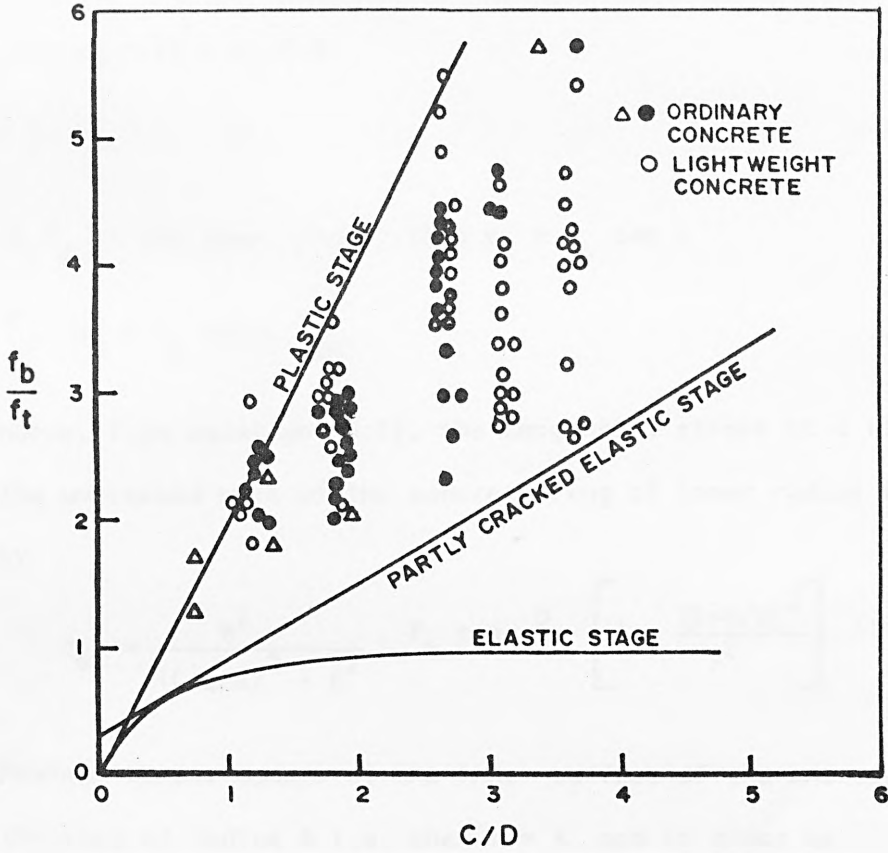


FIG. 5.3 EFFECT OF THICKNESS OF CONCRETE COVER UPON BOND CAPACITY (after Tefpers)

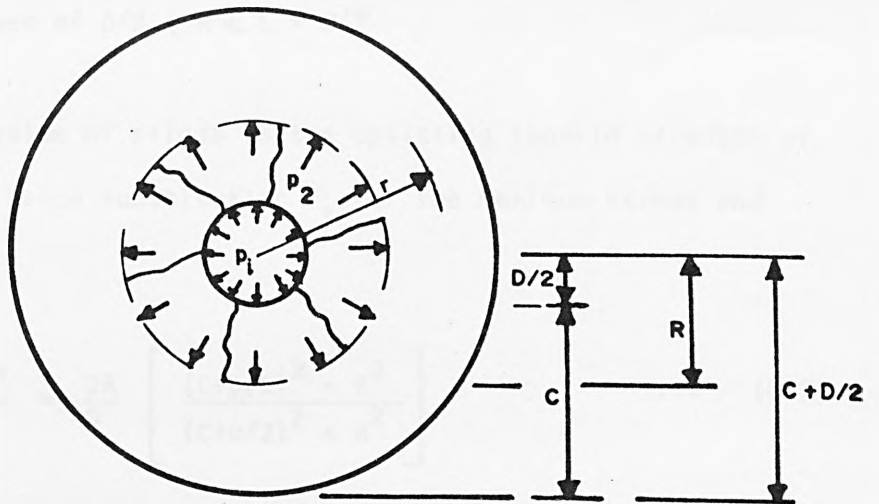


FIG. 5.4 INTERNAL CRACKING SURROUNDING REINFORCEMENT BAR

The pressure p_2 on the inner surface of the internally cracked ring of radius R is given by

$$p_2 \cdot \pi \cdot 2R = p_i \cdot \pi \cdot D \quad \dots \quad (5.2)$$

$$\text{i.e. } p_2 = p_i \cdot \frac{D}{2R} \quad \dots \quad (5.3)$$

If f_b is the bond stress, then $p_i = f_b \tan \alpha$

$$\therefore p_2 = f_b \tan \alpha \cdot \frac{D}{2R} \quad \dots \quad (5.4)$$

Hence, from equation (5.1), the tangential stress at a radius ' r ' in the uncracked part of the concrete ring of inner radius R is given by

$$\sigma_\theta = \frac{R^2}{(C+D/2)^2 - R^2} \cdot f_b \tan \alpha \frac{D}{2R} \left[1 + \frac{(C+D/2)^2}{r^2} \right] \quad \dots \quad (5.5)$$

Maximum stress occurs at the inner surface of the uncracked part of the ring of radius R i.e. when $r = R$, and is given by

$$\sigma_{\theta(\max)} = \frac{D}{2R} \cdot f_b \tan \alpha \left[\frac{(C+D/2)^2 + R^2}{(C+D/2)^2 - R^2} \right] \quad \dots \quad (5.6)$$

for values of $D/2 \ll R \ll C + D/2$

The maximum value of stress is the splitting tensile strength of concrete and hence substituting f_t for the maximum stress and rearranging

$$\frac{f_b \tan \alpha}{f_t} = \frac{2R}{D} \left[\frac{(C+D/2)^2 - R^2}{(C+D/2)^2 + R^2} \right] \quad \dots \quad (5.7)$$

In order to obtain the value of R for maximum lateral pressure from the bar, equation (5.7) is differentiated with respect to R to give

$$\frac{d(f_b \tan \alpha / f_t)}{dR} = \frac{2}{D[(C+D/2)^2 + R^2]} \left\{ \frac{(C+D/2)^2 - 3R^2 - 2R^2}{(C+D/2)^2 + R^2} [(C+D/2)^2 - R^2] \right\}$$

Equating the differential coefficient to zero :

$$R^4 + 4 (C+D/2)^2 R^2 - (C+D/2)^4 = 0$$

Solving, in order to obtain the maximum bond capacity of the ring,

$$R = 0.486 (C+D/2) \quad \dots \quad (5.8)$$

$$\text{Therefore, optimum crack depth} = R - D/2 = 0.486C - 0.257D \quad \dots \quad (5.9)$$

When this depth is exceeded, the crack penetrates right through the concrete cover. Therefore, the minimum thickness of concrete cover at which the crack immediately penetrates the cover is when

$$0.486C - 0.257D = 0 \quad \dots \quad (5.10)$$

$$\text{i.e. } C = 0.529D$$

The maximum tangential stress in the concrete ring at the partly cracked stage is given by substituting in equation (5.6) for R from equation (5.8) as

$$\sigma_{\theta}(\text{max}) = \frac{1.664 f_b \tan \alpha \cdot D}{(C+D/2)} \quad \dots \quad (5.11)$$

Hence the maximum bond stress when the cracking is initiated in the concrete cover is given when the maximum tangential stress is equal

to the tensile strength of concrete

$$\text{i.e. } f_t = \frac{1.664 f_b \tan \alpha \cdot D}{(C+D/2)} \quad \dots \quad (5.12)$$

$$\text{If } \alpha = 45^\circ, \text{ then } f_b = f_t \frac{(C+D/2)}{1.664D} \quad \dots \quad (5.13)$$

5.2.1.2 Concrete ring with external pressure

Consider a thick cylinder subjected to an internal pressure p_i and outside pressure p_o . (Fig. 5.5).

The tangential stress σ_θ is given by Timoshenko (58) as :

$$\sigma_\theta = \frac{-r_1^2 r_2^2 (p_o - p_i)}{r_2^2 - r_1^2} \cdot \frac{1}{r^2} + \frac{p_i r_1^2 - p_o r_2^2}{r_2^2 - r_1^2} \quad \dots \quad (5.14)$$

where r_1 = internal radius; r_2 = external radius.

This is maximum when $r = r_1$;

$$\sigma_{\theta(\max)} = \frac{-r_2^2 (p_o - p_i)}{r_2^2 - r_1^2} + \frac{p_i r_1^2 - p_o r_2^2}{r_2^2 - r_1^2} \quad \dots \quad (5.15)$$

Now, consider a concrete ring loaded internally and radially by the bond stress components from the reinforcing bar as a thick cylinder and the external lateral pressure applied as uniformly applied around the circumference of the concrete ring. (Fig. 5.6).

The ring has internal cracks where the circumferential stresses have reached the ultimate concrete tensile stress. The bond force is now transferred through the concrete 'teeth' between the internal cracks

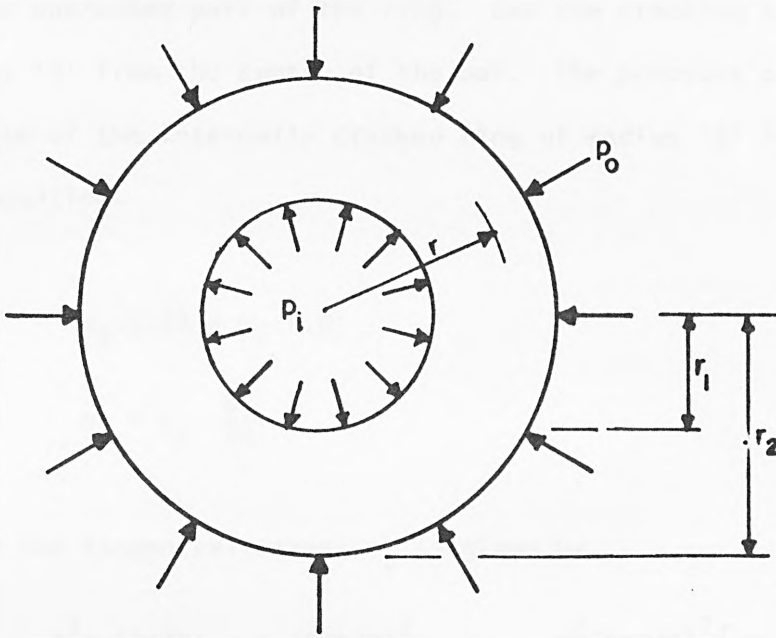


FIG. 5.5 THICK RING UNDER INTERNAL AND EXTERNAL PRESSURE

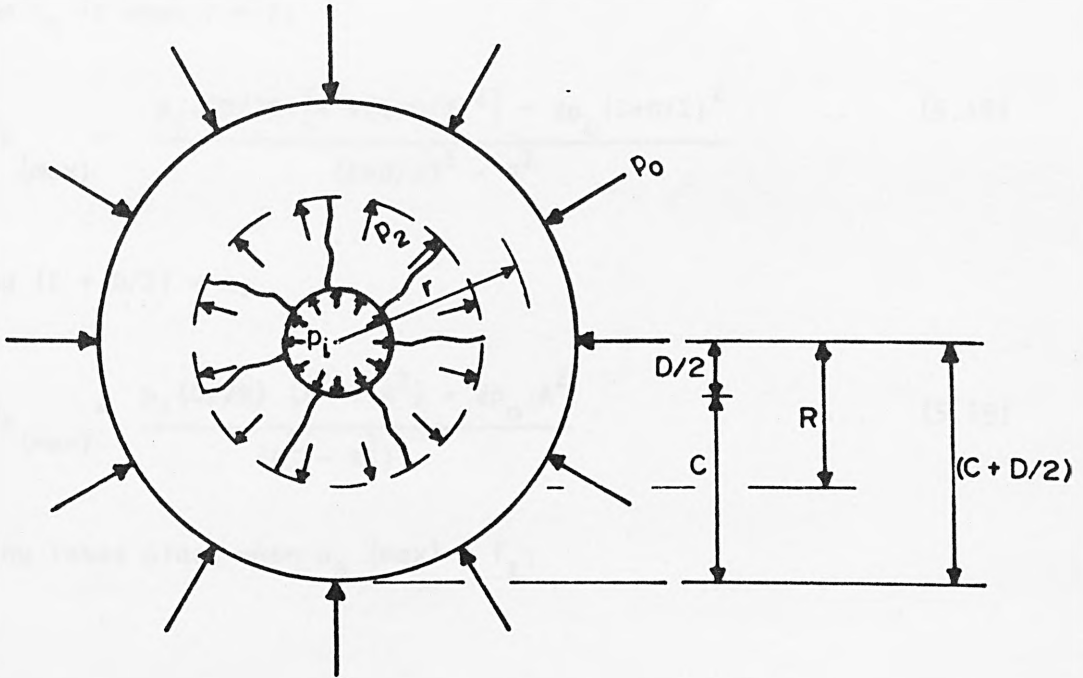


FIG. 5.6 INTERNAL CRACKING IN CONCRETE RING UNDER UNIFORM EXTERNAL PRESSURE

to the uncracked part of the ring. Let the cracking extend to a radius 'R' from the centre of the bar. The pressure p_2 on the inner surface of the internally cracked ring of radius 'R' is obtained from the equation.

$$p_2 \cdot \pi \cdot 2R = p_i \cdot \pi \cdot D \quad \dots \quad (5.16)$$

Hence
$$p_2 = p_i \cdot \frac{D}{2R}$$

Hence the tangential stress σ_θ is given by

$$\frac{R^2 p_i (D/2R) - p_o (C+D/2)^2}{(C+D/2)^2 - R^2} - \frac{1}{r^2} \cdot \frac{R^2 (C+D/2)^2 [p_o - p_i (D/2R)]}{(C+D/2)^2 - R^2} \quad \dots \quad (5.17)$$

Maximum σ_θ is when $r = R$;

$$\sigma_{\theta(\max)} = \frac{p_i \cdot (D/2R) [R^2 + (C+D/2)^2] - 2p_o (C+D/2)^2}{(C+D/2)^2 - R^2} \quad \dots \quad (5.18)$$

Putting $(C + D/2) = A$;

$$\sigma_{\theta(\max)} = \frac{p_i (D/2R) (R^2 + A^2) - 2p_o \cdot A^2}{(A^2 - R^2)} \quad \dots \quad (5.19)$$

Cracking takes place when $\sigma_\theta (\max) = f_t$;

Hence substituting f_t for σ_θ (max) ;

$$p_i (D/2R) \cdot (R^2 + A^2) - 2p_o A^2 = f_t \cdot (A^2 - R^2)$$

$$p_i (D/2R) \cdot (R^2 + A^2) = 2p_o A^2 + f_t (A^2 - R^2)$$

$$= f_t \left[\frac{2p_o A^2}{f_t} + (A^2 - R^2) \right]$$

$$\therefore \frac{p_i}{f_t} = \frac{2R}{D} \cdot \frac{1}{(A^2 + R^2)} \left[\frac{2p_o A^2}{f_t} + (A^2 - R^2) \right]$$

Putting $\frac{2p_o A^2}{f_t} = B = \frac{2p_o (C + D/2)^2}{f_t}$, we have

$$\frac{p_i}{f_t} = \frac{2R}{D(A^2 + R^2)} [B + (A^2 - R^2)]$$

Differentiating with respect to 'R' the function $\left(\frac{p_i}{f_t}\right)$ and simplifying;

$$\frac{d}{dR} \left(\frac{p_i}{f_t}\right) = \frac{2}{D} \frac{1}{(A^2 + R^2)^2} \cdot [A^4 - 4A^2 R^2 - R^4 + B(A^2 - R^2)]$$

Equating the differential coefficient to zero, we get

$$A^4 - 4A^2 R^2 - R^4 + B(A^2 - R^2) = 0 \quad \dots (5.20)$$

But $B = \frac{2p_o A^2}{f_t}$

$$\therefore \text{Equation (5.20) becomes } A^4 - 4A^2 R^2 - R^4 + \frac{2p_o A^2}{f_t} (A^2 - R^2) = 0 \quad \dots (5.21)$$

R may be solved for different values of p_o

Case 1

$$\text{Take } p_o = f_t/2$$

Equation (5.21) becomes $A^4 - 4A^2R^2 - R^4 + A^2(A^2 - R^2) = 0$

Simplifying we get, $R^4 + 5A^2R^2 - 2A^4 = 0$

$$\text{Solving, } R = 0.61A$$

From equation (5.19),

$$\begin{aligned}\sigma_{\theta(\max)} &= \frac{p_i \cdot \frac{D}{2 \times 0.61A} A^2 (1 + 0.372) - 2p_o A^2}{0.628A^2} \\ &= p_i \cdot D \cdot \frac{1.79}{A} - 3.18p_o\end{aligned}$$

$$\text{But } \sigma_{\theta(\max)} = f_t$$

$$\text{i.e. } f_t = p_i \cdot D \cdot \frac{1.79}{A} - 3.18p_o$$

$$\text{Rearranging: } p_i = \frac{A}{1.79D} [f_t + 3.18p_o]$$

$$\text{Since } p_o = \frac{f_t}{2}; \therefore p_i = \frac{A}{1.79D} \times 2.59 f_t$$

$$= f_t \cdot \frac{(C + D/2)}{0.691D}$$

But $p_i = f_b \tan \alpha$ where f_b is the bond stress

$$= f_b \text{ when } \alpha = 45^\circ$$

$$\text{i.e. } f_b = \frac{f_t (C + D/2)}{0.691D}$$

$$\text{when } \frac{C + D/2}{D} = 1.5; f_b = 2.17 f_t = 6.03 \text{ N/mm}^2 \text{ where } f_t = 2.78 \text{ N/mm}^2$$

$$= 2.5; f_b = 3.62 f_t = 10.06 \text{ N/mm}^2$$

$$= 3.5; f_b = 5.07 f_t = 14.09 \text{ N/mm}^2$$

$$= 4.5; \quad f_b = 6.51 \quad f_t = 18.10 \text{ N/mm}^2$$

Case 2

Take $p_o = f_t$

Equation (5.21) becomes $A^4 - 4A^2R^2 - R^4 + 2A^2(A^2 - R^2) = 0$

i.e. $3A^4 - 6A^2R^2 - R^4 = 0$

or $R^4 + 6A^2R^2 - 3A^4 = 0$

Solving, $R = 0.68A$

$$\sigma_{\theta(\max)} = \frac{p_i \cdot \frac{D}{2 \times 0.68A} \cdot A^2 (1 + 0.4624) - 2p_o A^2}{0.5376A^2}$$

$$= p_i \cdot D \cdot \frac{2}{A} - 3.72p_o$$

Putting $\sigma_{\theta(\max)} = f_t$ and re-arranging, we have

$$p_i = \frac{A}{2D} \left[f_t + 3.72p_o \right]$$

But $p_o = f_t$; and $p_i = f_b$ as before;

i.e. $f_b = f_t \frac{(C + D/2)}{0.424d}$

when $\frac{C + D/2}{D} = 1.5$; $f_b = 3.54 f_t = 9.83 \text{ N/mm}^2$

$= 2.5$; $f_b = 5.90 f_t = 16.40 \text{ N/mm}^2$

$= 3.5$; $f_b = 8.25 f_t = 22.94 \text{ N/mm}^2$

$= 4.5$; $f_b = 10.6 f_t = 29.47 \text{ N/mm}^2$

1500 4800 psi

5.2.2 Plough-through failure mechanism

It has been shown (25) that when the ribs are high and spaced too closely (less than 7 times the rib height) the shear stress acting on the cylindrical concrete surface between the adjacent ribs would govern the behaviour and the bar will pull-out with a failure surface at this cylindrical surface. It has already been shown that when the rib spacing is larger than approximately 10 times the rib height, the partly crushed concrete in front of the rib forms a wedge which exerts a splitting radial pressure on the concrete. However, if this radial pressure is restrained by the concrete surrounding the bar, the bar would eventually pull-out due to the shear failure at the cylindrical surface as in the case of bars with closely spaced ribs (Fig. 5.7).

The pull-out force ΔT is given by

$$\Delta T = \pi(D_c + 2h) \cdot f_s, \text{ where } f_s = \text{punching shear stress}$$
$$D_c = \text{diameter of 'core' of bar}$$
$$h = \text{height of rib.}$$

As determined by Mohr's envelope, this punching shear stress is given approximately by (38)

$$f_s = 0.5 \sqrt{f_t \cdot f_{cu}} \quad \dots \quad (5.22)$$

$$\text{Therefore, } \Delta T = \pi(D_c + 2h) \times 0.5 \sqrt{f_t \cdot f_{cu}}$$

If f_b is the bond stress, then

$$\pi D \cdot f_b = \Delta T = \pi(D_c + 2h) \times 0.5 \sqrt{f_t \cdot f_{cu}}$$
$$\therefore f_b = 0.5 \sqrt{f_t \cdot f_{cu}} \cdot \frac{(D_c + 2h)}{D} \quad \dots \quad (5.23)$$

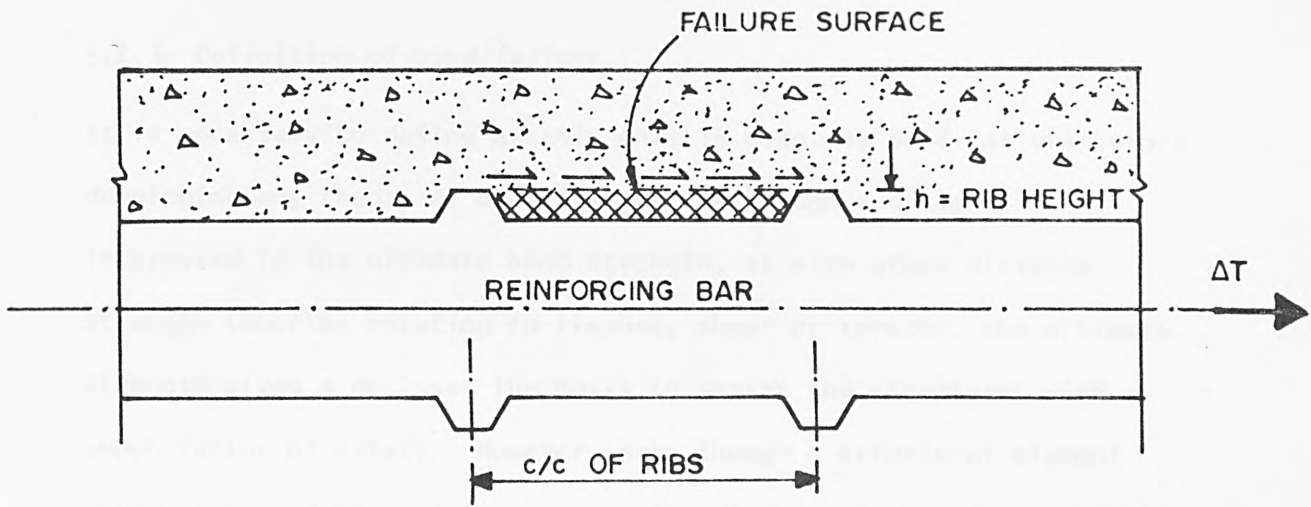


FIG. 5.7 PLOUGH-THROUGH SHEAR MECHANISM

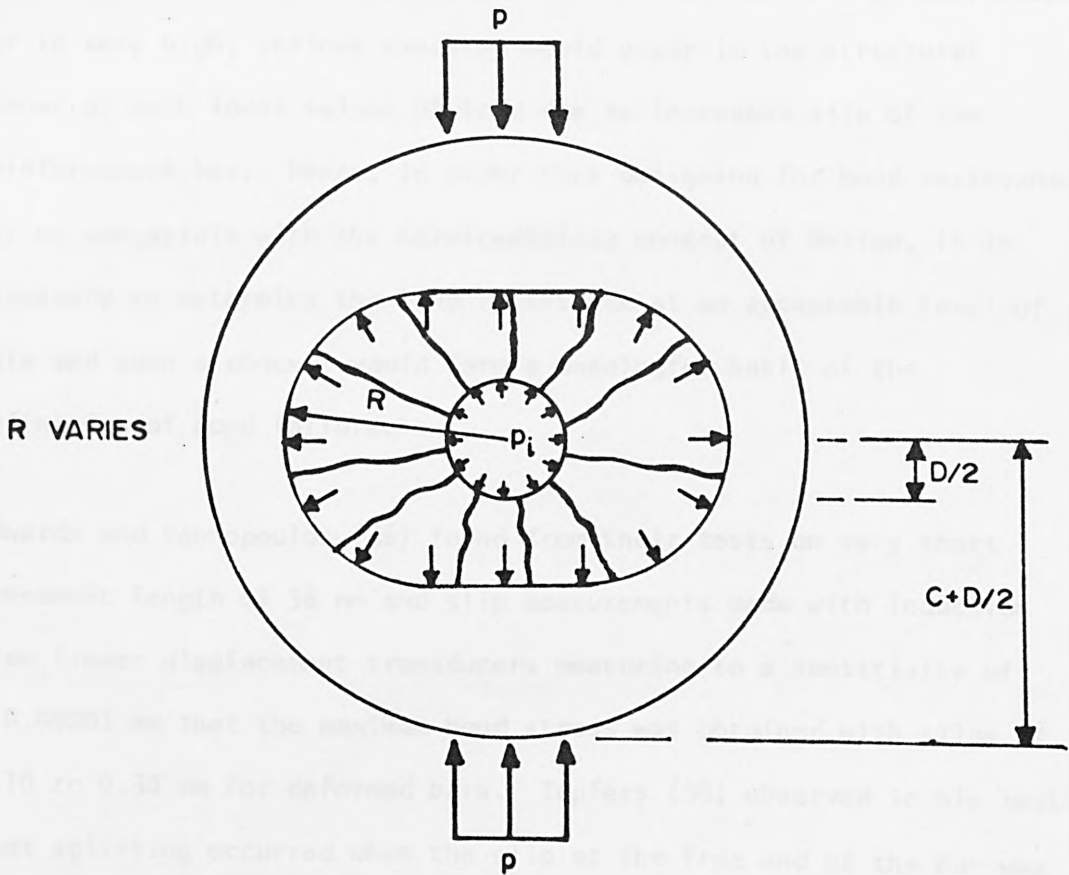


FIG. 5.8 INTERNAL CRACKING IN CONCRETE RING UNDER UNIDIRECTIONAL PRESSURE

5.2.3 Definition of bond failure

It is necessary to define exactly what is meant by bond failure before developing any theory of bond failure. Although a designer is interested in the ultimate bond strength, as with other ultimate strength theories relating to flexure, shear or torsion, the ultimate strength gives a designer the basis to design the structures with a known factor of safety. However, even though a structural element would withstand high ultimate strength, distress in the element either in the form of excessive cracking or deflection would make it unserviceable and unacceptable aesthetically. This indeed is the basis of the serviceability approach in modern design codes.

Hence, even in designing for bond, although the ultimate bond resistance as obtained from the pull-out resistance of a reinforcement bar is very high, serious cracking would occur in the structural member at much lower values of load due to increased slip of the reinforcement bar. Hence, in order that designing for bond resistance may be compatible with the serviceability concept of design, it is necessary to determine the bond resistance at an acceptable level of slip and such a concept would form a meaningful basis of the definition of bond failure.

Edwards and Yannopoulos (36) found from their tests on very short embedment length of 38 mm and slip measurements made with induction type linear displacement transducers measuring to a sensitivity of ± 0.00001 mm that the maximum bond stress was obtained with slips of 0.10 to 0.30 mm for deformed bars. Tepfers (30) observed in his tests that splitting occurred when the slip at the free end of the bar was

about 0.1 mm. Soretz and Holzenbein (49) have stated that "... it is absolutely impossible to fully utilize the bond resistance over 0.1 mm slip at the free end of the bar due to the corresponding increase of the crack width". Djabry (47) suggested that a suitable characteristic value of bond stress would be that corresponding to a slip of 0.1 mm. Rusch and Rehm (48) also recommended the bond stress at a slip of 0.1 mm as the criterion of bond failure.

Based on the above supporting evidence, it seems prudent to define bond failure for purposes of this study as occurring at a free end slip of 0.1 mm and the corresponding bond stress may be referred to as the "critical bond stress". The extra resistance that would be available at ultimate failure may be considered as an additional margin of safety for design purposes.

5.2.4 Empirical Theory of bond failure under lateral pressure

The foregoing discussion has shown that the failure mechanism of deformed bars is complex. The introduction of a uniform external radial pressure on the outer surface of the concrete ring surrounding the bar would enhance greatly the bond capacity of the bar as shown in 5.2.1.2. However, in a normal situation, it is not always possible to obtain a uniform external pressure round the circumference of the ring but only pressure applied in a single direction. For example, if a pressure was applied to the concrete ring in a vertical direction, then the tendency is for the internal cracking to be resisted in the region of the vertical direction but unrestrained in the other directions. Under such a system of forces, the region of cracking around the bar would take an elliptical form of a circle flattened in the direction of the lateral pressure as seen in Fig. 5.8. The

actual shape of this region would be dependent on the magnitude of the lateral pressure and the cover to the concrete both in the direction of the lateral pressure and at right angles to it. In order to define the shape of this region of tensile cracking, an analytical approach using finite elements may be used to obtain the different stress contours due to a diametral compression (external to the concrete ring) for varying covers and different levels of lateral compression. However, till such analytical solutions are available, in order to deal with the practical design detailing problem relating to the effects of lateral compression on bond resistance such as at beam-column joints, it seems justifiable to adopt an approximate approach supported with experimental verification to determine the bond force at critical bond failure which has been defined to occur at a slip of 0.1 mm at the free end.

An approximate assessment of the critical pull-out force may be obtained by applying the weak-link theory to the partially cracked elastic theory of Tepfers. According to Tepfers (30), it has been shown that the critical bond failure begins when the region close to the bar starts cracking and extends to an annular area around the bar. The cracking of concrete surrounding a bar subjected to a lateral pressure would be restrained in a direction parallel to the direction of the pressure but unrestrained in the other directions. Hence, the concrete in the other regions would crack early leading to bond failure. Furthermore, when a pressure is applied to concrete in one direction, this pressure causes bursting tensile stresses to develop in a direction at right angles to the pressure. The magnitude of these bursting stresses has been shown to be substantial by Iyengar (59) and Yettram and Robins (60) in their study of anchorage zone stresses in

axially post-tensioned members. These bursting tensile stresses would cause cracking to be developed in the direction of the applied pressure (vertical cracks were noticed to develop below the bar in the direction of the pressure in the test specimens). Hence, it may be argued that the initiation of bond failure is caused by the development of cracks due to the presence of the bursting tensile stresses which aggravate the tensile splitting ring tensile stresses caused due to the bond pull-out force. This results in the early tensile failure of the concrete surrounding the reinforcement bar. The theory developed for uniform ring tension around the bar would thus be modified such that cracking is caused at a tensile stress level that is lower than the tensile strength of the concrete by an amount equal to the bursting tensile stresses. The pull-out force in such a situation would be lower than when no lateral pressure is present. However, the presence of the lateral pressure would itself cause additional resistance to the pull-out of the bar manifested in the enhanced frictional resistance caused by the lateral pressure. Hence, the force in bar at bond failure would be composed of two parts and may be written as :

Force in bar at bond failure = force causing tensile cracking +
frictional force due to lateral
pressure.

$$\text{i.e. } F = F_{cr} + F_{fr} \quad \dots \quad (5.24)$$

This force F would however be limited by the restraint to cracking and in such situations a plough-through shear type of failure would be initiated. This would be expected in cases where cracking of cover is restrained by increased concrete cover or increased lateral

pressure. The pull-out force in such situations would be evaluated as in 5.2.2.

The frictional force due to lateral pressure could be obtained by multiplying the average pressure on the circumference of the bar by the coefficient of friction between concrete and steel. The average pressure on the perimeter of the bar is shown to be half of the lateral pressure applied, as follows :

Consider a reinforcement bar under lateral pressure p (Fig. 5.9)

Then the pressure on segment $ds = p \cdot ds \cos \theta$

Pressure radially on segment ds is $p \cdot \cos^2 \theta \cdot ds$

If the average pressure on the bar/concrete interface is

designated p_{av} , then $p_{av} = \frac{4}{\pi D} \int_0^{\frac{\pi D}{4}} p \cdot \cos^2 \theta \cdot ds$.

Putting $ds = \frac{D}{2} \cdot d\theta$

$$p_{av} = \frac{4}{\pi D} \int_0^{\pi/2} p \cdot \cos^2 \theta \cdot \frac{D}{2} \cdot d\theta = \frac{2p}{\pi} \int_0^{\pi/2} \cos^2 \theta \cdot d\theta$$

Integrating and simplifying, we have $p_{av} = p/2$

5.2.5 Failure mechanism under tension release

In order to understand the failure mechanism under tension release, one has to examine the conditions prevailing in the immediate vicinity of a deformed bar in a tensile stress zone. This is readily seen by studying a concrete cylinder of finite length containing a concentrically embedded bar which is pulled in tension. Initially, the stresses in the concrete surrounding the bar result in cracks leading to separation of the bar from the concrete in the vicinity

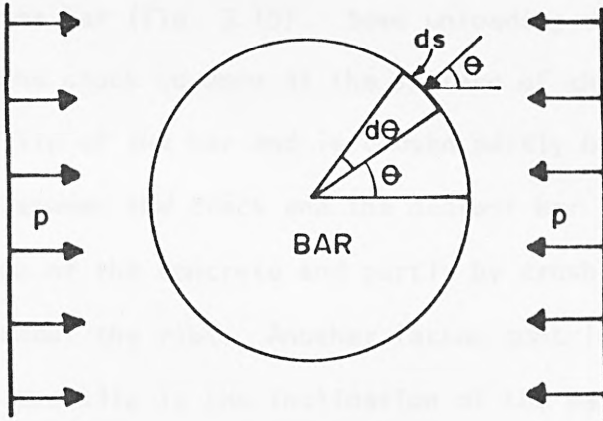


FIG. 5.9 STRESS ON BAR/CONCRETE INTERFACE
DUE TO LATERAL PRESSURE

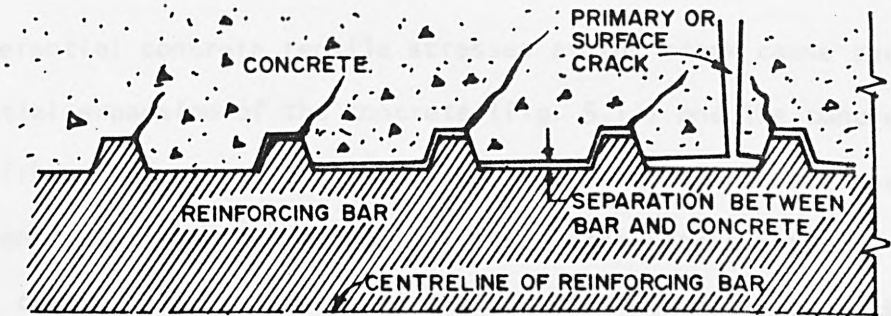


FIG. 5.10 SECTION THROUGH REINFORCING BAR AND CONCRETE
SHOWING SEPARATION THAT OCCURS NEAR A
PRIMARY CRACK

of the crack. However, since the reinforcing bar has ribs, separation does not produce complete unloading of the concrete adjacent to the bar in as much as the bar ribs prevent much of the opening of the crack at the bar (Fig. 5.10). Some unloading does occur at the bar, allowing the crack to open at the surface of the bar. This opening leads to slip of the bar and is caused partly by the unloading of the concrete between the crack and the nearest bar rib producing a relative contraction of the concrete and partly by crushing due to bearing stresses under the ribs. Another factor contributing to the opening and hence the slip is the inclination of the bar ribs and the movement of the concrete along the inclined bar rib face. Lutz and Gergely (27) reported a finite element study of a model of such a cylindrical specimen the results of which indicated that slip due to the rib inclinations amounted to about one-quarter of the elongation of the steel between two primary cracks and the separation of the bar from the concrete amounted to about 0.3 times the elongation of the steel between cracks.

The circumferential concrete tensile stresses at the crack cause the circumferential expansion of the concrete (Fig. 5.11) and the concrete bends away from the bar. As the bar slips, the longitudinal stresses are sufficiently large to cause internal transverse cracks between the primary cracks. The existence of such internal transverse cracks has been demonstrated by Broms (28) and Goto (29). Broms injected a coloured resin to study the extent and locations of the internal cracks whereas Goto used red ink. The deformation of concrete around reinforcing bars after formation of internal cracking is shown schematically in Fig. 5.12. Further movement of the bar would cause butting of the bar rib faces against the inclined faces of the cracks

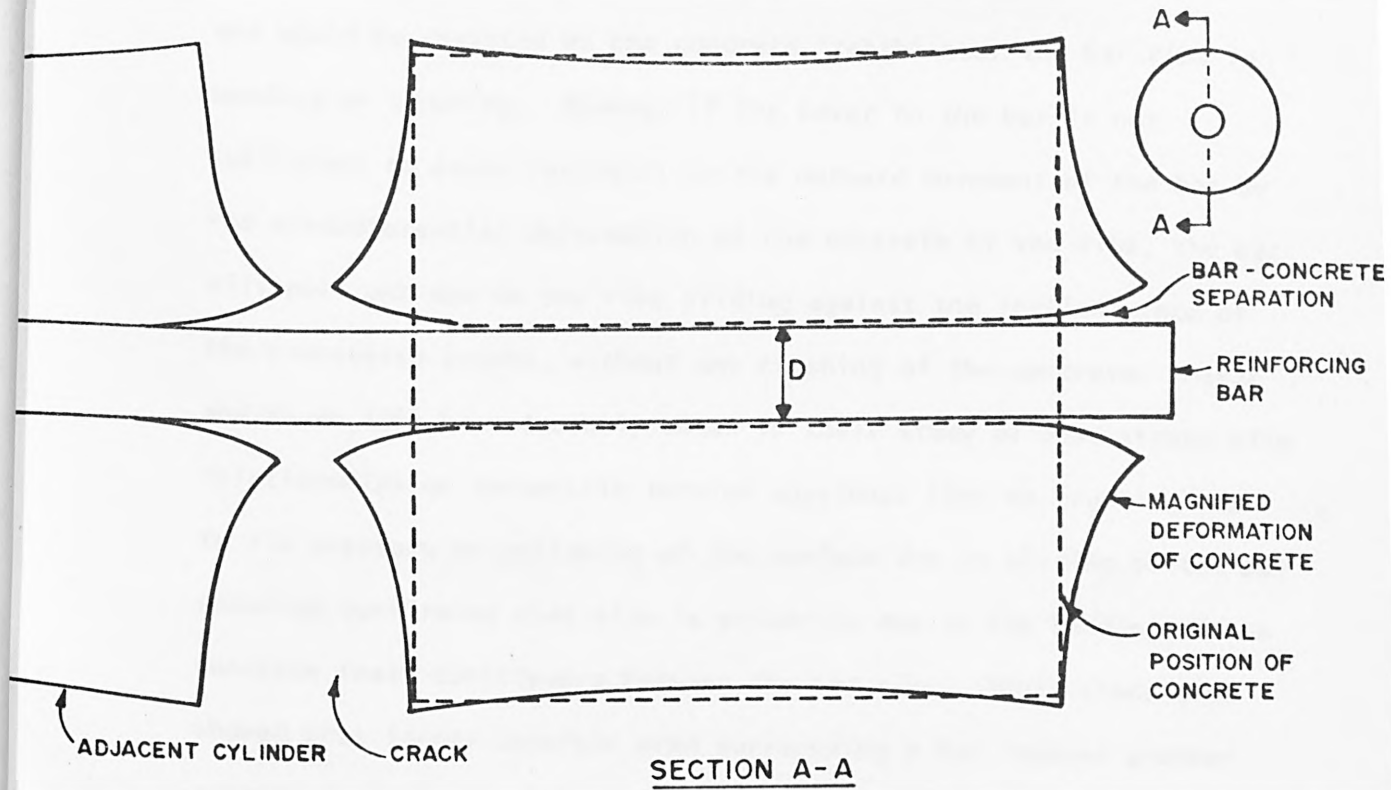


FIG. 5.11 MAGNIFIED DEFORMATION SHOWING SEPARATION BETWEEN CONCRETE AND BAR (After Lutz)

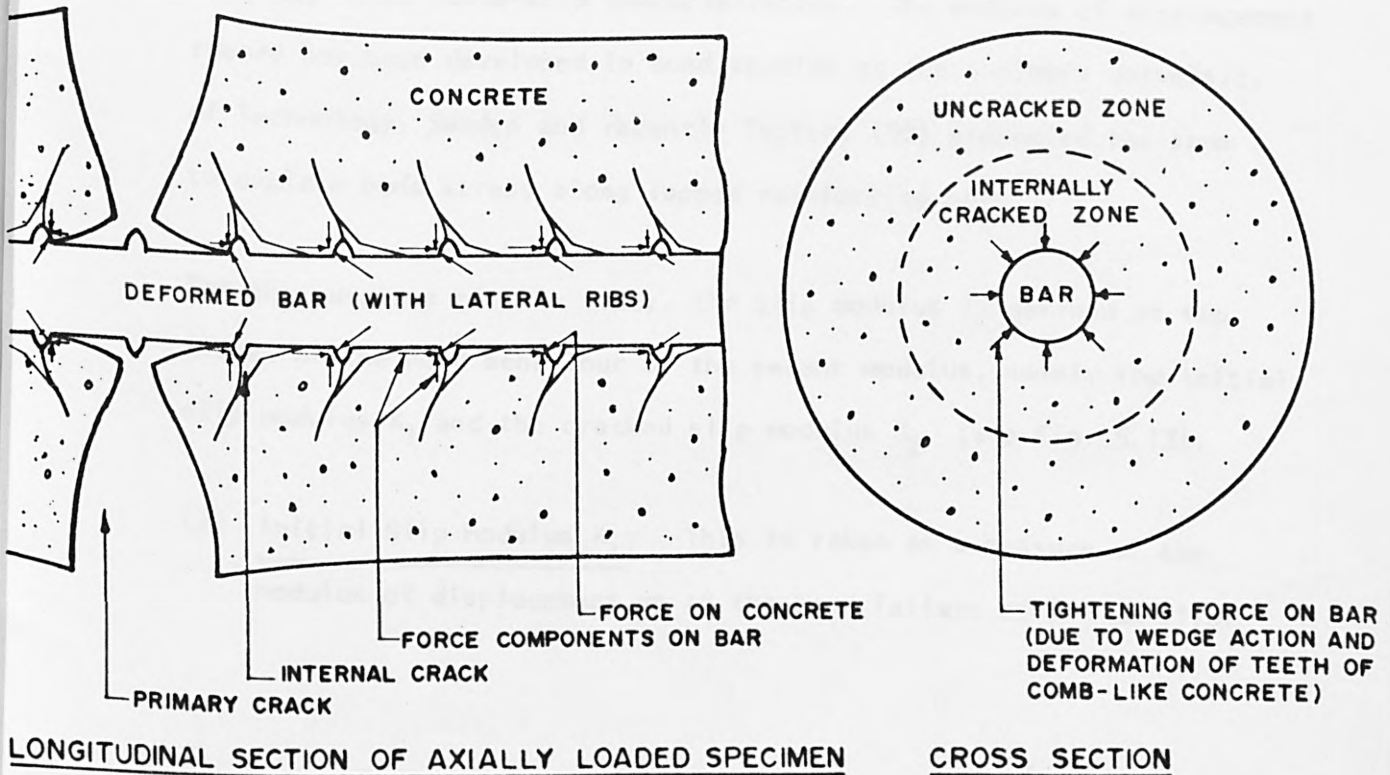


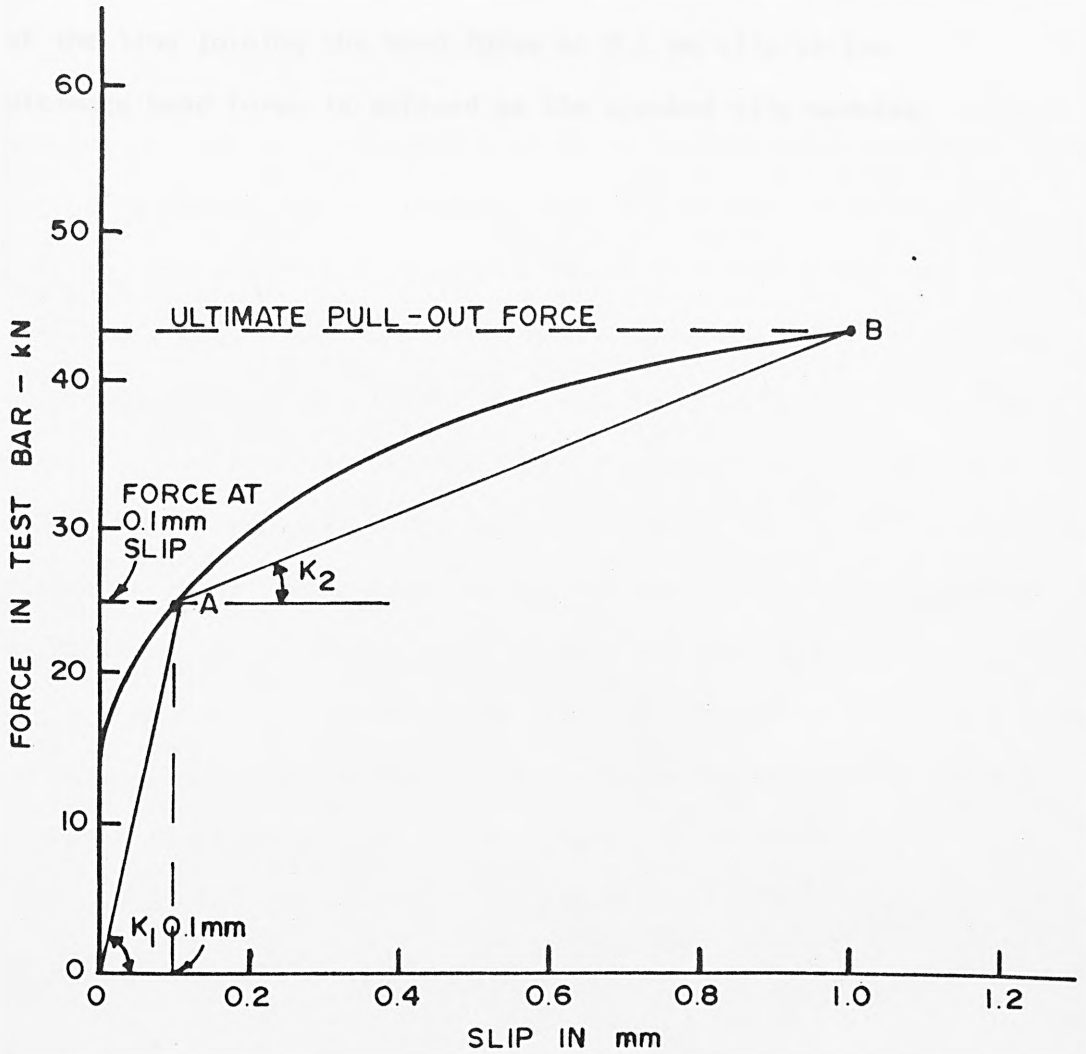
FIG. 5.12 DEFORMATION OF CONCRETE AROUND REINFORCING STEEL AFTER FORMATION OF INTERNAL CRACKS (Schematic Diagram)

and would be resisted by the concrete 'teeth' near the bar ribs in bending or crushing. However if the cover to the bar is not sufficient to cause restraint to the outward movement of the bar by the circumferential deformation of the concrete by the ribs, the bar will pull out due to the ribs sliding against the inclined face of the transverse cracks, without any crushing of the concrete. Mirza and Houde (36) have recently shown in their study of bond stress slip relationships on concentric tension specimens that no crushing due to rib pressure or polishing of the surface due to sliding of the bar occurred confirming that slip is primarily due to the bending of the concrete teeth cantilevers between the bar ribs. Their study also showed that larger concrete area surrounding a bar imposed greater restraint on the bar thereby causing a decrease in slip of the steel-concrete interface.

The resistance offered by the cracked concrete 'teeth' cantilevers may be studied by obtaining the slip modulus or modulus of displacement from the bond force-slip characteristics. The modulus of displacement theory has been developed in bond studies at the Chalmers University of Technology, Sweden and recently Tepfers (30) presented the same to explain bond stress along lapped reinforcing bars.

For the purposes of this study, the slip modulus is defined at two stages of the bond behaviour by the secant modulus, namely the initial slip modulus K_1 and the cracked slip modulus K_2 (see Fig. 5.13).

- (a) Initial Slip Modulus K_1 : This is taken as a measure of the modulus of displacement up to the bond failure at 0.1 mm slip.



K_1 - INITIAL SLIP MODULUS - SLOPE OF OA
 K_2 - CRACKED SLIP MODULUS - SLOPE OF AB

FIG. 5.13 GRAPH SHOWING INITIAL AND CRACKED SLIP MODULUS

(b) Cracked Slip Modulus K_2 : Critical bond stress has been defined as the bond resistance at 0.1 mm slip when internal cracking takes place in the concrete surrounding the bar. In order to study the resistance offered by the cracked concrete, the slope of the line joining the bond force at 0.1 mm slip to the ultimate bond force is defined as the cracked slip modulus.

PRESENTATION AND DISCUSSION OF RESULTS OF EXPERIMENTS WITH LATERAL
TENSION RELEASE

6.1 Load-slip characteristics

Initially as the test bars were pulled, no changes were recorded on the dial gauges at the unloaded end till the initial slip occurred. Thereafter the end of the bar continued to slip with progressive increase of load on the test bar. As the load was further increased, cracking occurred at the loaded ends with the cracks radiating from the bar surface towards the boundaries of the concrete block. When cracking became extensive, the test bar slipped rapidly and eventually pulled out. Load-slip curves for the specimens with varying covers and for the three different types of deformed bars are given in Figs. A.1 to A.6. It is seen that each test specimen yielded two load-slip curves, one for each of the test bars cast in the specimen. The graphs for the two bars are designated, A and B and the origin of the graphs for bars designated B are shifted by 0.1 mm on the slip axis.

The load-slip characteristics deviated from the load axis with the onset of initial slip and moved away from the load axis due to the increasing load which caused progressive increase in slip at the unloaded end of the bar. The load-slip curve was terminated at ultimate pull-out of the bar which was indicated by a drop in the load. The shape of the characteristic depended on the type of reinforcement namely the profile of the reinforcement bar and the level of tension release in the concrete. These are discussed in the following sections.

6.1.1 Effect of type of bar

The Square-twisted bars behaved substantially differently from the other two bars, namely the Torbar and Hybar reinforcement bars. The load-slip characteristic of the Square-twisted bars deviated from the the load axis with the onset of initial slip and thereafter gradually curved towards the slip-axis with increase of slip but without appreciable resistance to pull-out. Beyond a slip value of 0.1 mm the load increased less rapidly and the characteristics curved towards the slip axis culminating in the eventual pull-out of the bar. As the tension release in the concrete surrounding the test bar was increased, the characteristics curved towards the slip axis much earlier indicating the disruptive effects of the transverse cracking in the surrounding concrete on the bond characteristics of the bar. No discernible difference was seen in the shapes of the load-slip characteristics obtained for the different concrete covers. The initial slip modulus determined at the limiting slip of 0.1 mm and the cracked slip modulus determined at ultimate pull-out are tabulated in Table 6.3. The initial modulus decreased with increasing tensile release in the concrete as expected. However, it is noticed that the residual modulus, namely the cracked modulus as a percentage of the initial modulus generally increased with the level of cracking indicating that the cracked 'teeth' in the concrete offered additional pull-out resistance. This is not true for concrete cover of 25 mm equal to one bar diameter in which case the cracked modulus dropped drastically and in three cases to zero suggesting that for Square-twisted bars greater care must be exercised when concrete cover of one bar diameter is used.

In the case of the Torbar and Hybar too, the load-slip characteristics deviated from the load axis with the onset of initial slip. The bars continued to resist pull-out with increased slip and the load-slip characteristics moved away gradually from the load axis. At about 0.1 mm slip and beyond, the characteristics are noticed to take on a curve of nearly uniform slope for each type of bar suggesting that the mechanism of bond in ribbed bars changed at about this value of slip and the load-slip characteristic beyond this value of slip is dependent on the profile of the bar. The load-slip characteristics of the Hybar show a steeper slope in the region beyond 0.1 mm slip compared to the Torbar. This is explained by the heavier rib on the Hybar with a rib height of 1.50 mm compared to a rib height of 1.20 mm in the Torbar.

Tables 6.1 and 6.2 give the initial moduli and the cracked moduli for the Torbar and Hybar respectively. It is observed that Hybar offers greater resistance to pull-out than the Torbar as shown by the greater values of initial modulus. However their performance is very much superior to the Square-twisted bars after cracking as indicated by the ratio of the cracked modulus to the initial modulus. The residual cracked modulus is substantially higher for the Torbar and Hybar compared to the Square-twisted bar.

It is also noticed that the ratio of the cracked modulus to the initial modulus increased with the level of tensile release in the concrete for covers of 50, 63 and 88 mm both for Torbar and Hybar although the ratios for the Hybar are observed to be higher than that for Torbar. It is again noticed that the cover of 25 mm, or one bar diameter does not show any noticeable difference suggesting that the cracking in the cover is already extensive and that the transverse cracking therefore does not affect the pull-out resistance.

Tension Release	$\epsilon = 0$				$\epsilon = 1180 \times 10^{-6}$				$\epsilon = 1770 \times 10^{-6}$				$\epsilon = 2360 \times 10^{-6}$			
	K_1	K_2	$\frac{K_2}{K_1} \times 100$		K_1	K_2	$\frac{K_2}{K_1} \times 100$		K_1	K_2	$\frac{K_2}{K_1} \times 100$		K_1	K_2	$\frac{K_2}{K_1} \times 100$	
88	312	27.27	8.74		255	21.55	8.45		160	31.75	19.84		120	31.25	26.04	
	315	26.79	8.50		275	38.46	13.90		215	54.41	25.31		156	23.59	15.12	
63	185	32.26	17.44		170	34.82	20.48		170	37.74	22.2		110	36.36	33.05	
	258	28.13	10.90		162	33.33	20.57		150	35.71	23.81		90	40.18	44.64	
50	245	19.23	7.85		186	27.11	14.57		180	25.81	14.34		185	32.26	17.43	
	248	18.18	7.33		205	31.25	15.24		176	26.67	15.15		187	24.66	13.33	
25	183	25.00	13.66		184	22.73	12.35		198	37.50	18.94		164	26.67	16.26	
	193	27.17	14.08		175	31.25	17.86		200	21.74	10.87		257	39.47	15.36	

K_1 - initial slip modulus - kN/mm

K_2 - cracked slip modulus - kN/mm

TABLE 6.1 : SLIP MODULI - TORBAR

Tension Release	$\epsilon = 0$			$\epsilon = 1180 \times 10^{-6}$			$\epsilon = 1770 \times 10^{-6}$			$\epsilon = 2360 \times 10^{-6}$		
	K_1	K_2	$\frac{K_2}{K_1} \times 100$	K_1	K_2	$\frac{K_2}{K_1} \times 100$	K_1	K_2	$\frac{K_2}{K_1} \times 100$	K_1	K_2	$\frac{K_2}{K_1} \times 100$
88	345	23.57	6.83	280	41.18	14.71	282	33.33	11.82	160	45.46	28.41
	390	22.50	5.77	240	37.50	15.63	250	40.00	16.00	212	47.62	22.46
63	332	47.62	14.34	235	42.86	18.24	218	42.31	19.41	305	77.27	25.33
	282	35.71	12.66	235	54.39	23.14	210	51.89	24.71	200	55.83	27.92
50	300	46.51	15.50	257	40.82	15.88	175	34.09	19.48	128	45.83	35.80
	235	41.10	17.49	233	39.68	17.03	186	41.67	22.40	137	38.33	27.98
25	280	40.00	14.29	252	35.71	14.17	216	37.88	17.54	235	31.25	13.30
	240	47.17	19.65	248	41.67	16.80	227	30.77	13.56	240	31.75	13.23

K_1 - initial slip modulus - kN/mm

K_2 - cracked slip modulus - kN/mm

TABLE 6.2 : SLIP MODULI - HYBAR

Tension Release	$\epsilon = 0$			$\epsilon = 1180 \times 10^{-6}$			$\epsilon = 1770 \times 10^{-6}$			$\epsilon = 2360 \times 10^{-6}$		
	K_1	K_2	$\frac{K_2}{K_1} \times 100$	K_1	K_2	$\frac{K_2}{K_1} \times 100$	K_1	K_2	$\frac{K_2}{K_1} \times 100$	K_1	K_2	$\frac{K_2}{K_1} \times 100$
88	272	5.0	1.84	176	5.55	3.15	167	8.88	5.32	143	9.00	6.29
	186	2.0	1.08	175	7.00	4.00	162	6.67	4.12	134	7.50	5.60
63	217	10.0	4.61	222	8.46	3.81	170	8.33	4.90	125	16.25	13.00
	185	10.0	5.41	172	6.98	4.06	160	10.00	6.25	77	9.78	12.70
50	277	6.67	2.41	257	13.04	5.07	160	23.53	14.71	142	4.00	2.82
	232	6.67	2.88	204	5.26	2.58	181	13.16	7.27	143	3.33	2.33
25	225	3.49	1.55	250	0.00	0.00	200	0.00	0.00	180	3.0	1.67
	136	4.88	3.59	165	3.30	2.00	170	0.00	0.00	160	1.25	0.78

K_1 - initial slip modulus - kN/mm

K_2 - cracked slip modulus - kN/mm

TABLE 6.3 : SLIP MODULI - SQUARE TWISTED BAR

However, it is observed that the residual modulus for Torbar and Hybar in the case of 25 mm cover are still higher than those obtained for the Square-twisted bar.

The increase in the ratio of the cracked modulus to the initial modulus with increasing level of tension release (causing increased transverse cracking in the surrounding concrete) is explained as due to the increased resistance to pull-out obtained when the face of the rib profile butts against the inclined faces of the cracks. The increased resistance is manifested in the bending of the concrete 'teeth' cantilevers between the bar ribs. Similar observations were made by Mirza and Houde (36) in their study of test specimens under tension pull and with varying concrete covers. It is also observed that with increasing cover, such as at 88 mm, the ratio decreases suggesting that the mechanism of pull-out is different in this case. In such a case, the larger concrete area surrounding the bar imposed greater restraint on the bar leading to crushing of the concrete between the ribs and causing a plough-through type of failure. In the present tests, this type of failure was only noticed in the specimens with zero tension release and tension release of 1180 microstrain for 88 mm cover with Torbar. With Hybar, even with 88 mm cover, failure was primarily due to side-cover cracking (see under modes of failure).

6.2 Ultimate bond resistance

The ultimate bond resistances recorded by the maximum pull-out for the three different types of reinforcement bars are tabulated in Table 6.4. The tables show the tension applied to the tie rods T₃ - T₆ ranging from 0 to 80 kN and the corresponding tension release obtained in the concrete surrounding the test bars ranging from

Torbar

Cover (mm)	Tension applied - kN/Tension release				f_{cu} (N/mm ²)
	0	40	60	80	
	$\epsilon = 0$	$\epsilon = 1180 \times 10^{-6}$	$\epsilon = 1770 \times 10^{-6}$	$\epsilon = 2360 \times 10^{-6}$	
88	54.08; 54.08	56.0; 46.35	56.0; 57.94	44.42; 52.15	34.95
63	56.5; 56.0	57.94; 54.08	50.22; 54.08	46.35; 54.08	34.87
50	59.87; 50.99	57.94; 59.68	49.83; 53.31	50.99; 53.31	36.30
25	40.56; 34.76	34.76; 44.42	50.22; 42.49	42.49; 48.28	35.98

Hybar

Cover (mm)	Tension applied - kN/Tension release				f_{cu} (N/mm ²)
	0	40	60	80	
	$\epsilon = 0$	$\epsilon = 1180 \times 10^{-6}$	$\epsilon = 1770 \times 10^{-6}$	$\epsilon = 2360 \times 10^{-6}$	
88	54.85; 65.28	66.63; 57.94	52.15; 57.94	50.22; 59.87	36.13
63	54.85; 59.87	57.94; 59.87	56.00; 54.85	61.79; 59.87	35.23
50	50.22; 54.85	56.01; 57.94	52.15; 52.15	45.39; 44.40	34.35
25	53.12; 53.70	46.16; 50.22	52.54; 48.48	49.06; 45.58	36.44

Square-twisted

Cover (mm)	Tension applied - kN/Tension release				f_{cu} (N/mm ²)
	0	40	60	80	
	$\epsilon = 0$	$\epsilon = 1180 \times 10^{-6}$	$\epsilon = 1770 \times 10^{-6}$	$\epsilon = 2360 \times 10^{-6}$	
88	29.36; 22.41	18.93; 21.25	21.25; 18.93	17.77; 17.77	34.23
63	30.52; 29.36	27.04; 22.41	22.41; 23.57	23.57; 16.61	35.17
50	29.94; 29.36	27.04; 21.25	22.41; 20.09	15.45; 16.61	35.2
25	16.61; 23.57	25.30; 16.61	20.09; 17.19	18.93; 16.61	35.8

Note: ϵ in units of strain

TABLE 6.4 : PULL-OUT FORCE AT FAILURE - kN

0 to 2360 microstrains. The strengths of concrete in different specimens as obtained from representative test cubes are also shown. Each specimen yielded two results as given in the table. In order that a comparative study of the different parameters may be made, it is necessary to obtain results of the same concrete strength which had been earlier fixed at 35 N/mm^2 . Table 6.5 shows the ultimate bond resistance of each specimen obtained as the average of the two results and corrected for strength. It is accepted that bond resistance varies with concrete strength as the tensile strength or square-root of the compressive strength of concrete. The results tabulated in Table 6.5 are obtained from the ultimate pull-out force given in Table 6.4 by correcting for the varying concrete strength in the ratio of the square-root of the compressive strengths. Based on these corrected pull-out force values and the bond surface of the reinforcement bar obtained by the multiple of the bond length of 100 mm and the perimeter of the bar, ultimate bond stress values have been calculated and tabulated in Table 6.5.

6.2.1 Effect of concrete cover and tension release

It is seen that for all the three types of reinforcement, the ultimate bond stress dropped at a concrete cover of one bar diameter. This is more prominent in the specimens where there was no tension release. Hybar and Torbar performed much better than the Square-twisted bar for all values of cover and tension release.

The variation of ultimate bond stress with varying concrete cover for the three types of bars is shown in Figs. 6.1, 6.2 and 6.3. The graphs show that for all the three types of bars, in the absence of tension release in the surrounding concrete, the ultimate bond stress

Torbar

Cover (mm)	Pull-out force (corrected) -kN				Ultimate bond stress - N/mm ²			
	$\epsilon = 0$	$\epsilon = 1180$	$\epsilon = 1770$	$\epsilon = 2360$	$\epsilon = 0$	$\epsilon = 1180$	$\epsilon = 1770$	$\epsilon = 2360$
88	54.12	51.22	57.00	48.32	6.84	6.47	7.21	6.11
63	56.36	56.12	52.25	50.31	7.12	7.09	6.60	6.36
50	54.43	57.75	50.64	49.44	6.88	7.30	6.40	6.25
25	36.64	38.51	45.09	44.14	4.63	4.87	5.70	5.58

Hybar

Cover (mm)	Pull-out force (corrected) -kN				Ultimate bond stress - N/mm ²			
	$\epsilon = 0$	$\epsilon = 1180$	$\epsilon = 1770$	$\epsilon = 2360$	$\epsilon = 0$	$\epsilon = 1180$	$\epsilon = 1770$	$\epsilon = 2360$
88	59.10	61.31	54.19	54.19	7.47	7.75	6.85	6.85
63	57.20	58.70	55.22	60.68	7.23	7.42	6.98	7.67
50	53.00	57.51	52.61	45.33	6.70	7.27	6.65	5.73
25	52.37	47.23	49.52	46.44	6.62	5.97	6.26	5.87

Square-twisted

Cover (mm)	Pull-out force (corrected) -kN				Ultimate bond stress - N/mm ²			
	$\epsilon = 0$	$\epsilon = 1180$	$\epsilon = 1770$	$\epsilon = 2360$	$\epsilon = 0$	$\epsilon = 1180$	$\epsilon = 1770$	$\epsilon = 2360$
88	26.18	20.32	20.32	18.00	3.16	2.45	2.45	2.17
63	29.85	24.71	22.97	20.07	3.60	2.98	2.79	2.42
50	29.60	24.13	21.33	16.00	3.57	2.91	2.56	1.93
25	19.82	20.73	18.49	17.58	2.39	2.50	2.23	2.12

Note: ϵ in units of microstrain

TABLE 6.5 : ULTIMATE BOND STRESS

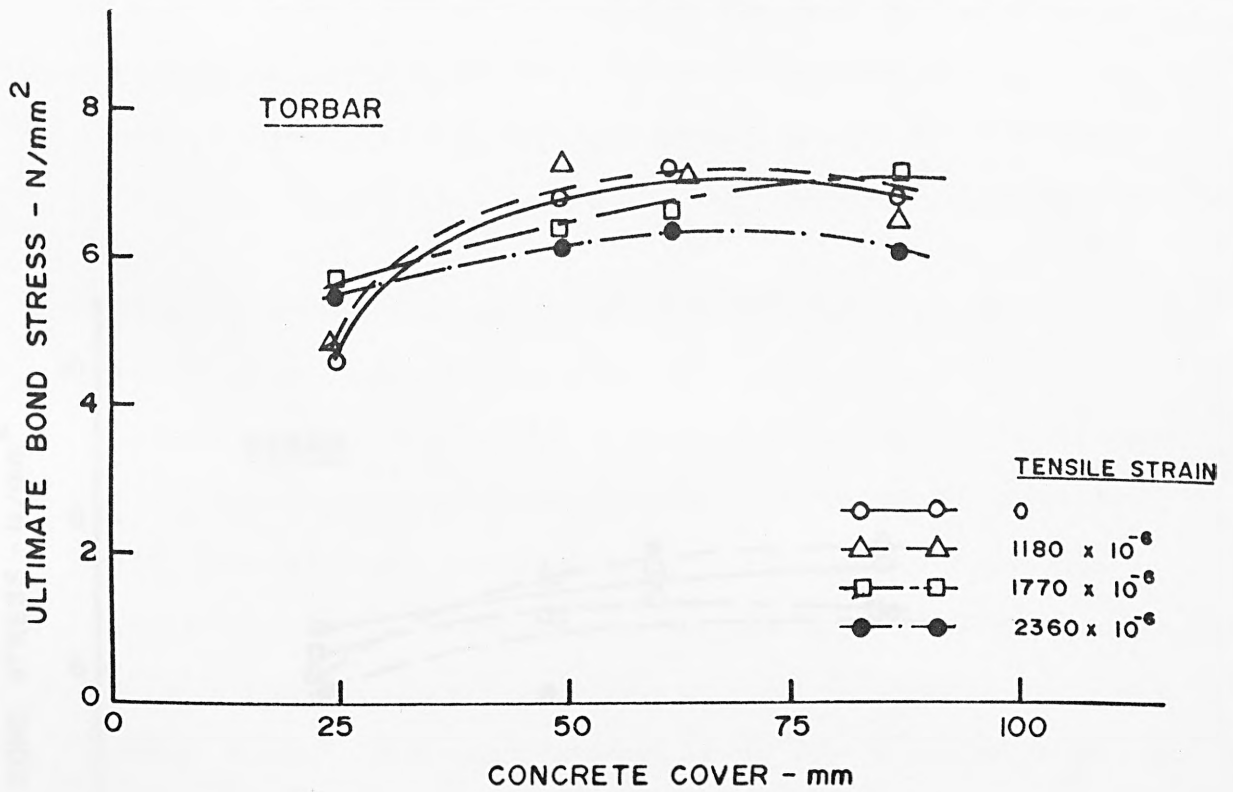


FIG. 6.1 VARIATION OF ULTIMATE BOND STRESS WITH COVER - TORBAR

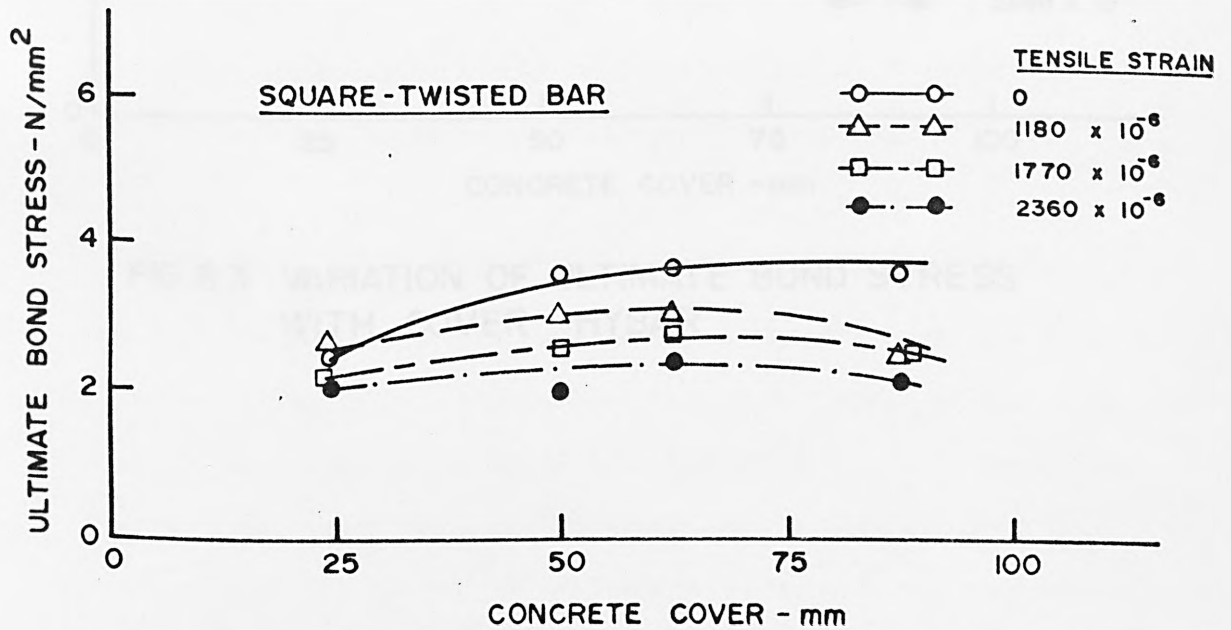


FIG. 6.2 VARIATION OF ULTIMATE BOND STRESS WITH COVER - SQUARE-TWISTED BAR

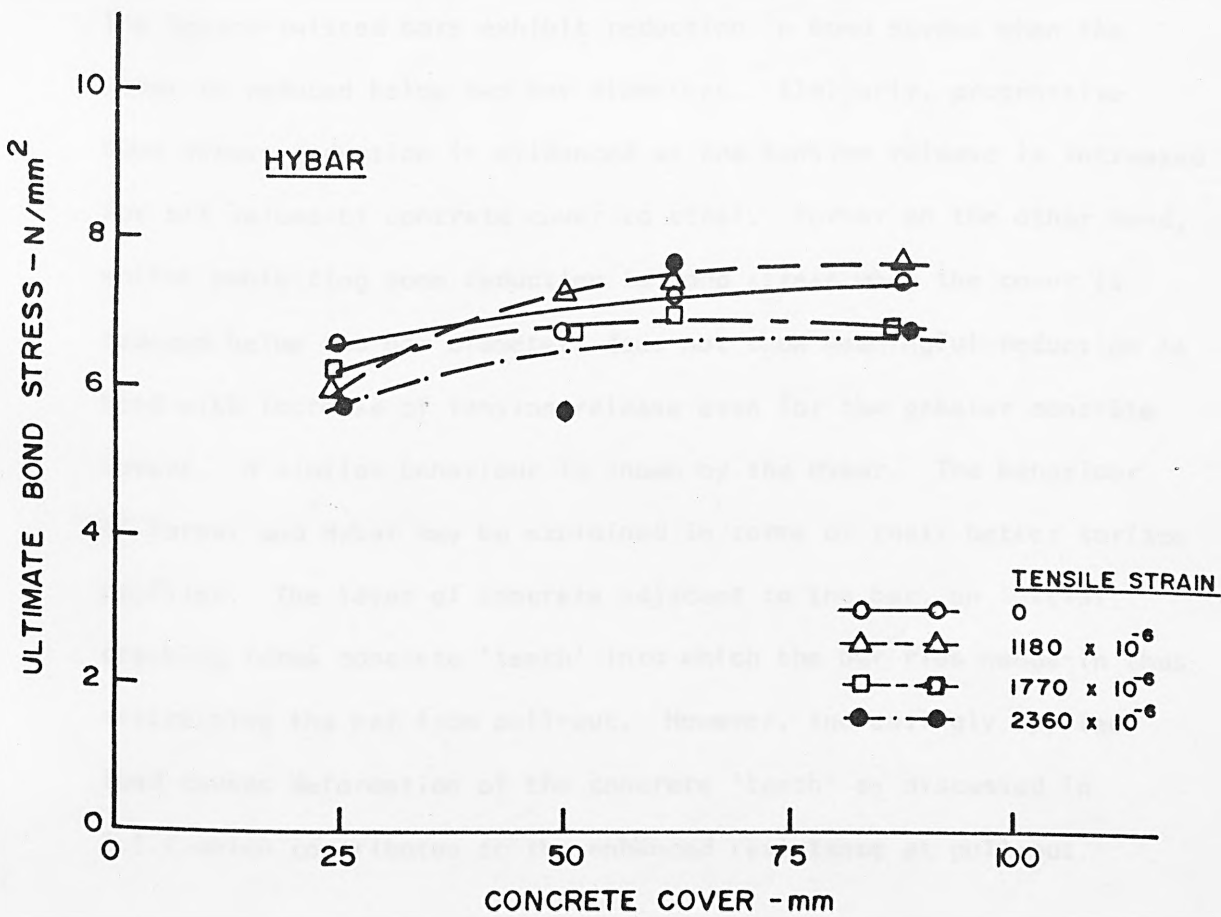


FIG. 6.3 VARIATION OF ULTIMATE BOND STRESS WITH COVER - HYBAR

increases with increasing cover reaching a plateau at a value of cover of approximately 3.5 times bar diameter. McClure (56) has shown in his investigation using frozen stress techniques that the splitting stress in the area surrounding an internally pressurised cylinder becomes small as the cover to diameter ratio exceeds a value of 3.5.

The Square-twisted bars exhibit reduction in bond stress when the cover is reduced below two bar diameters. Similarly, progressive bond stress reduction is evidenced as the tension release is increased for all values of concrete cover to steel. Torbar on the other hand, whilst exhibiting some reduction in bond stress when the cover is reduced below two bar diameters does not show meaningful reduction in bond with increase of tension release even for the greater concrete covers. A similar behaviour is shown by the Hybar. The behaviour of Torbar and Hybar may be explained in terms of their better surface profiles. The layer of concrete adjacent to the bar, on initial cracking forms concrete 'teeth' into which the bar ribs wedge-in thus restraining the bar from pull-out. However, increasingly applied load causes deformation of the concrete 'teeth' as discussed in 6.1.1 which contributes to the enhanced resistance at pull-out.

6.2.2 Interaction between concrete cover and tension release

The combined effects of the variations of concrete cover and level of tension release on ultimate bond stress in respect of the three types of bars are seen in Figs. 6.4, 6.5 and 6.6. It is again seen that concrete cover has a marked effect on the ultimate bond resistance whilst the effect of tension release is not so prominent. However, both Hybar and Torbar show a definite tendency to lose bond resistance at higher levels of tension release such as at 2360

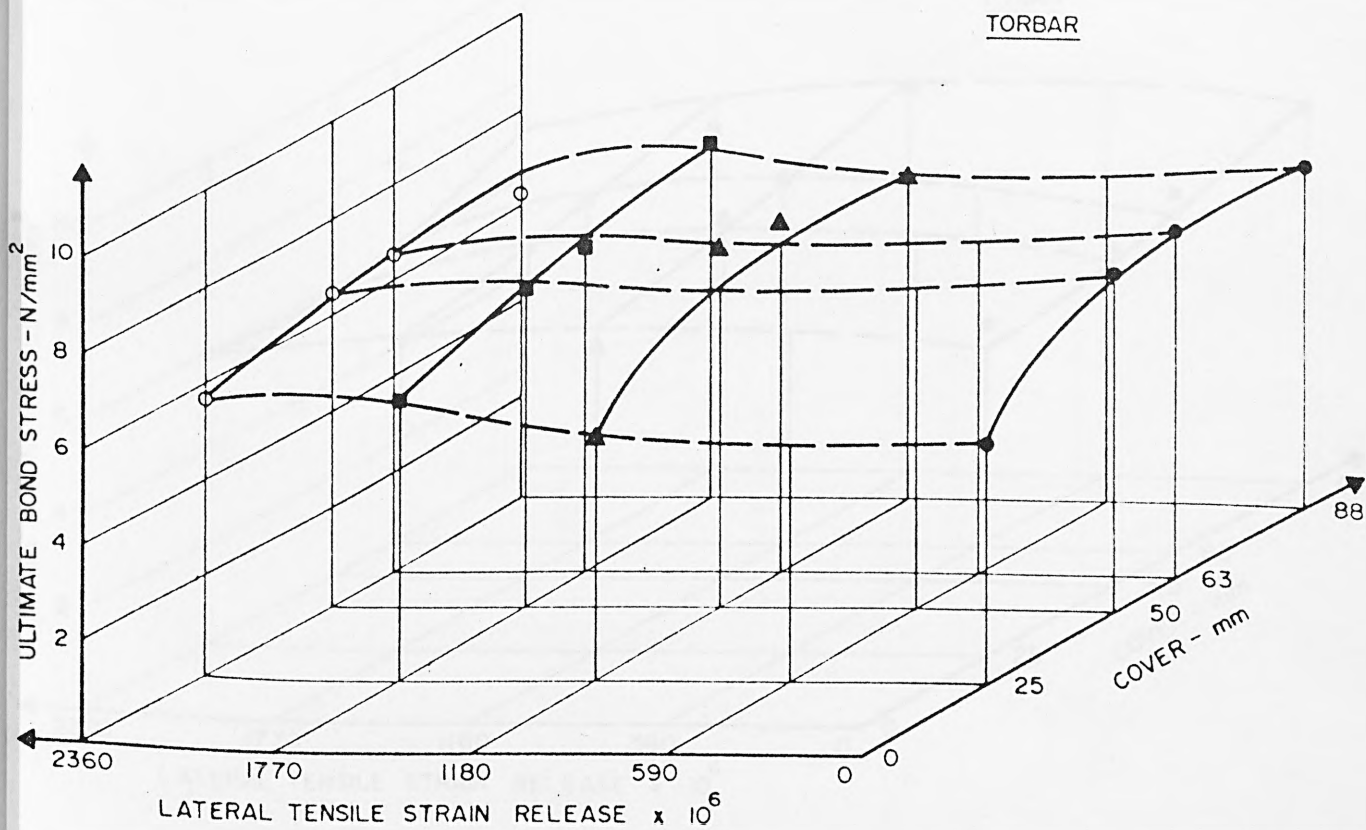
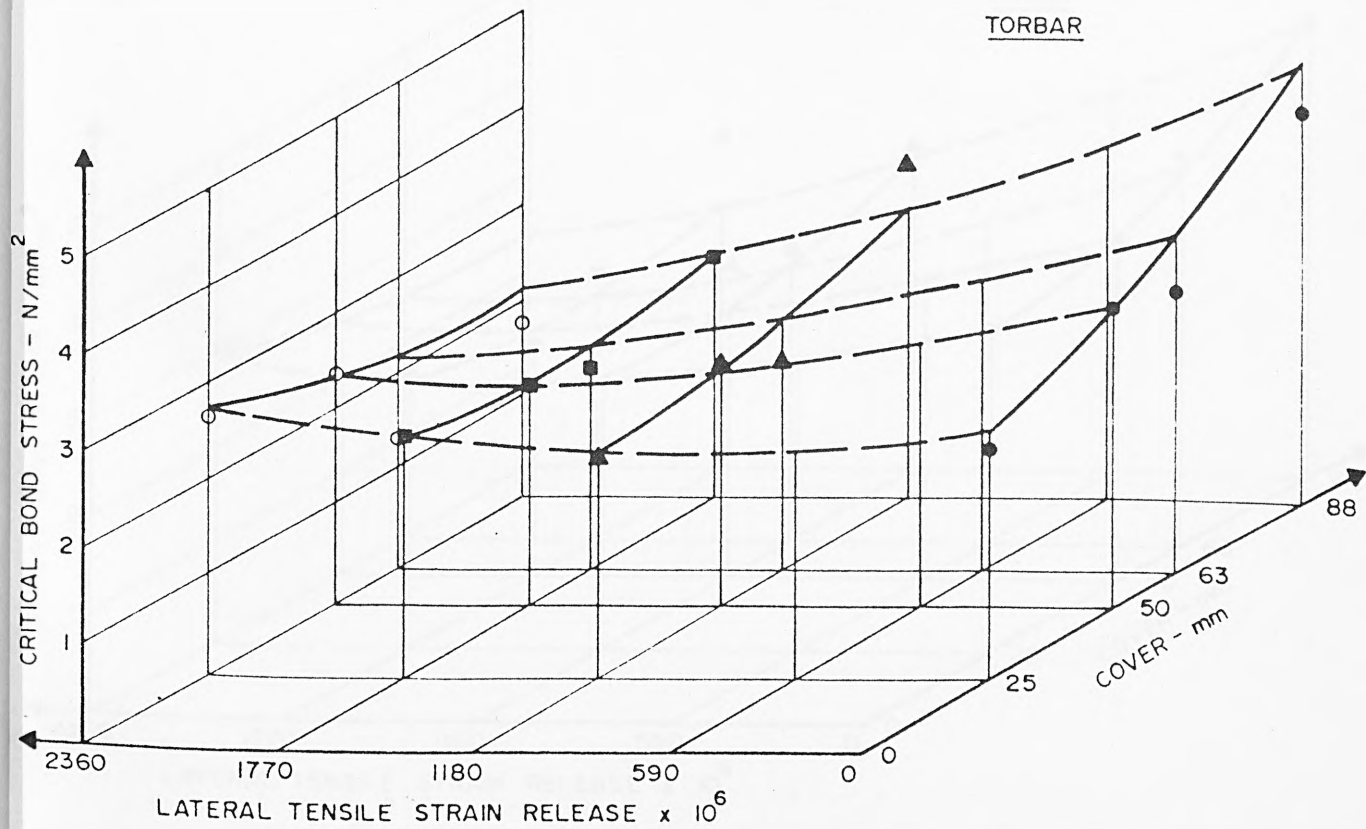


FIG 6.4 VARIATION OF BOND STRESS WITH COVER AND TENSION RELEASE
 (Top) CRITICAL BOND STRESS, (Bottom) ULTIMATE BOND STRESS

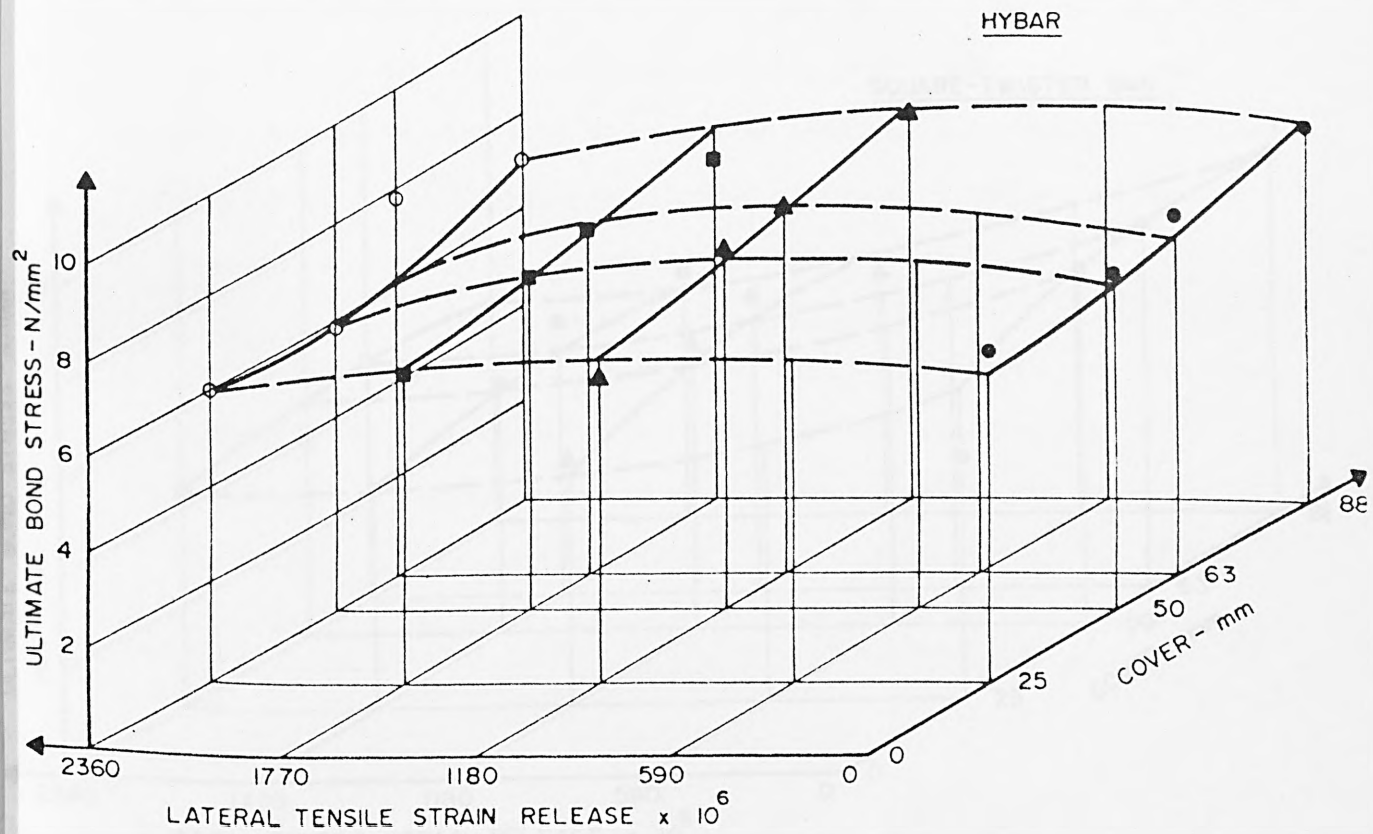
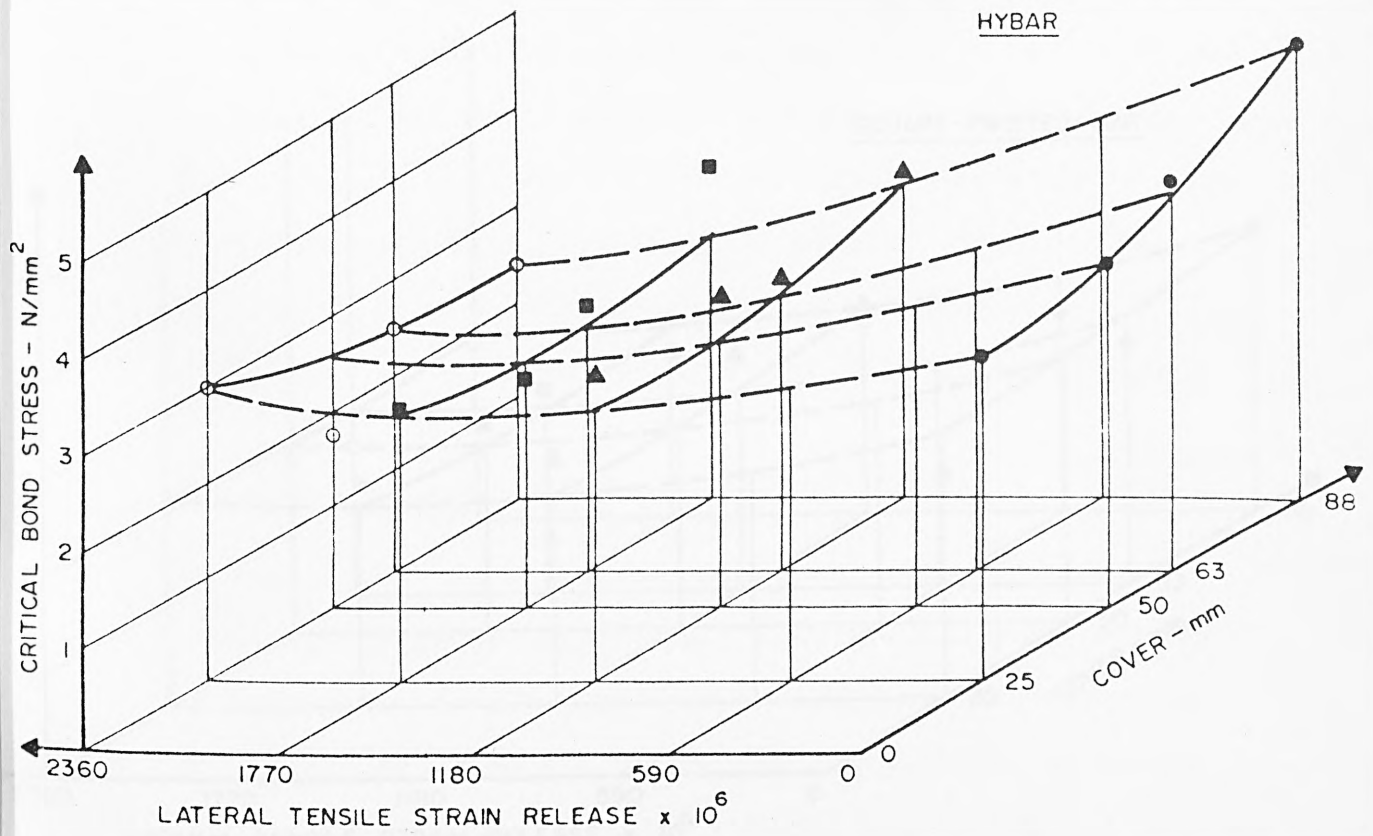


FIG 6.5 VARIATION OF BOND STRESS WITH COVER AND TENSION RELEASE
(Top) CRITICAL BOND STRESS, (Bottom) ULTIMATE BOND STRESS

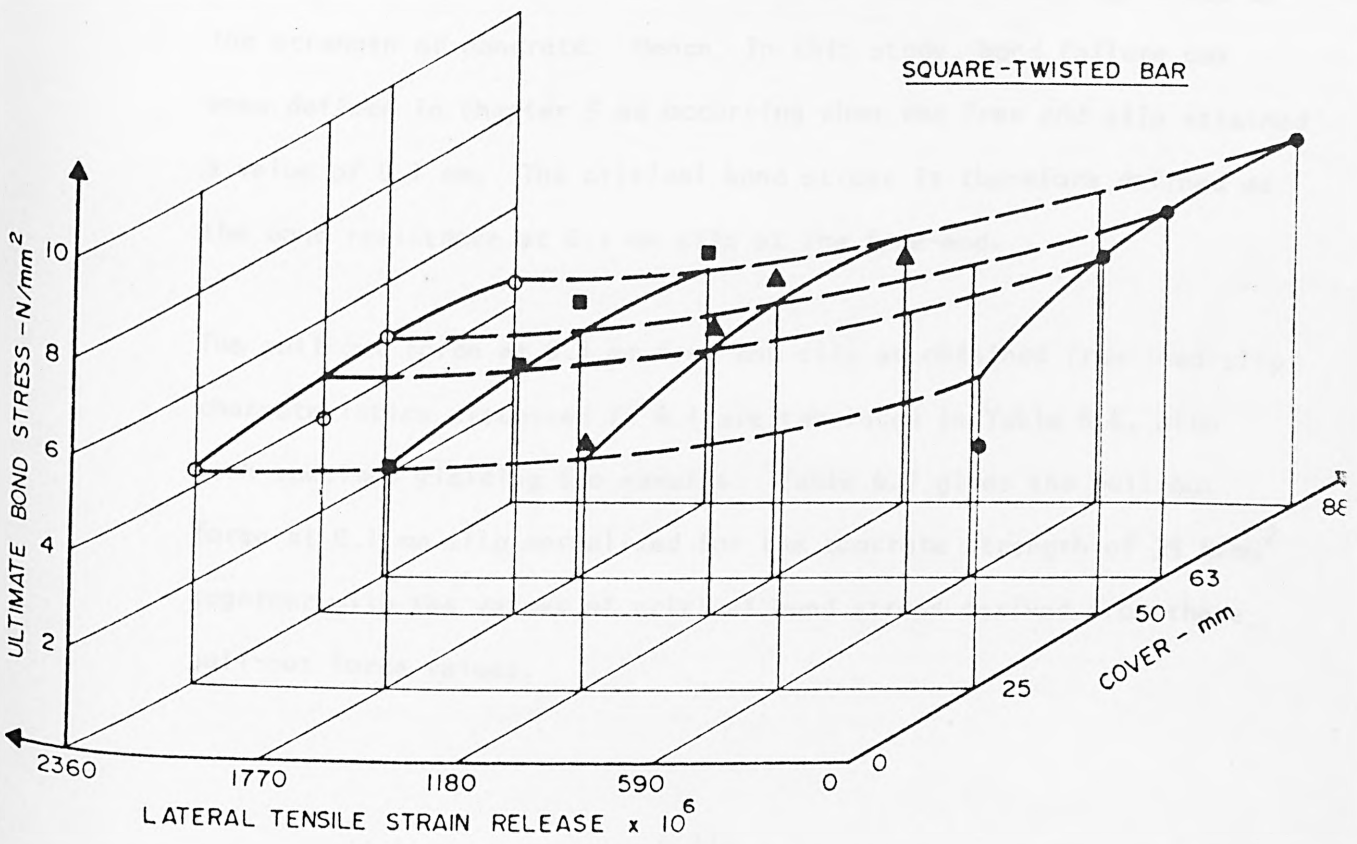
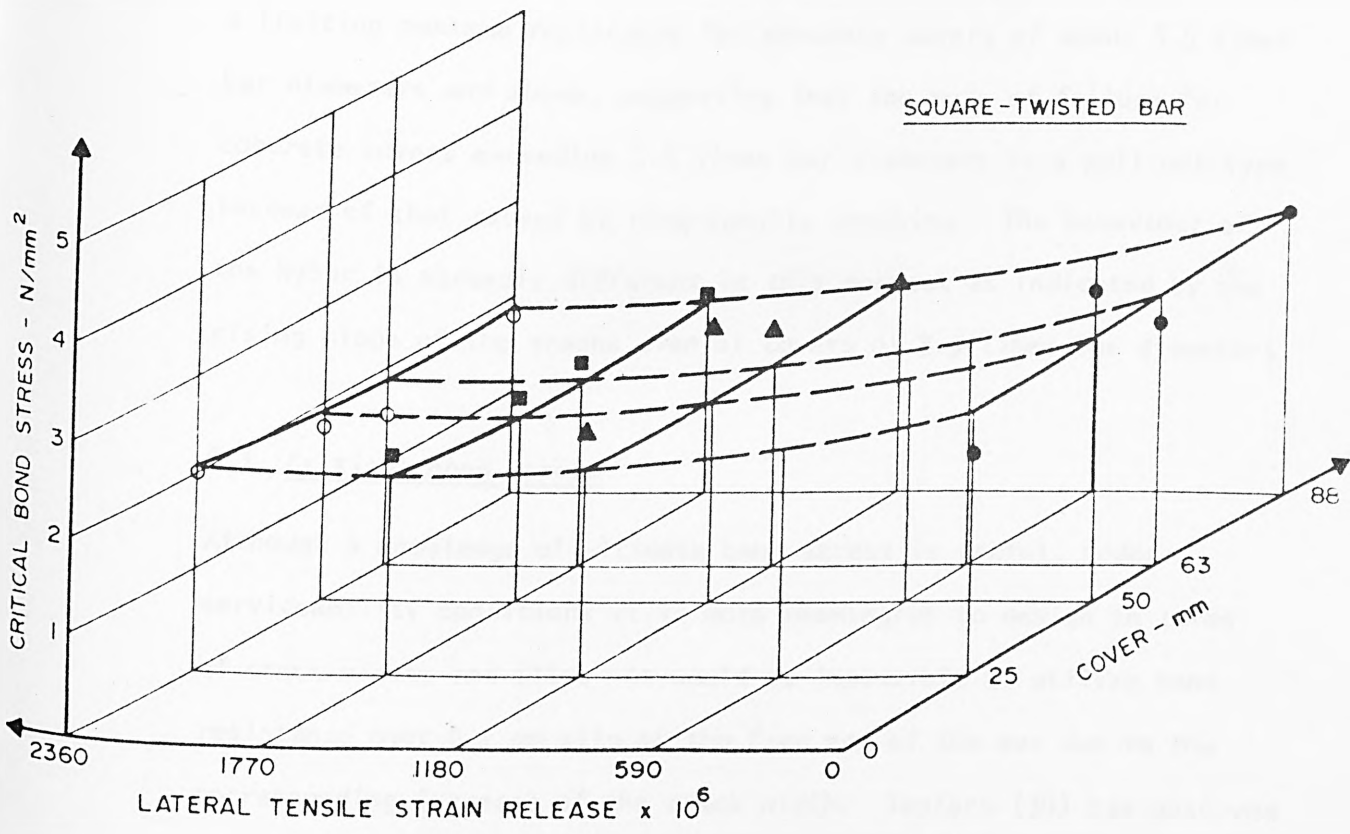


FIG. 6.6 VARIATION OF BOND STRESS WITH COVER AND TENSION RELEASE
 (Top) CRITICAL BOND STRESS, (Bottom) ULTIMATE BOND STRESS

microstrains. The curves for Torbar and Square-twisted bar indicate a limiting maximum resistance for concrete covers of about 3.5 times bar diameters and above, suggesting that the mode of failure for concrete covers exceeding 3.5 times bar diameters is a pull-out type instead of that caused by ring-tensile cracking. The behaviour of the Hybar is markedly different in this respect as indicated by the rising slope of the graphs even at covers of 3.5 times bar diameters.

6.3 Critical bond stress

Although a knowledge of ultimate bond stress is useful, under serviceability conditions it is more meaningful to design in terms of crack widths and slip. It would be impossible to utilize bond resistance over 0.1 mm slip at the free end of the bar due to the corresponding increase of the crack width. Tepfers (30) has observed that splitting occurred when the slip was about 0.1 mm regardless of the strength of concrete. Hence in this study, bond failure has been defined in Chapter 5 as occurring when the free end slip attained a value of 0.1 mm. The critical bond stress is therefore defined as the bond resistance at 0.1 mm slip at the free-end.

The pull-out force at 0.1 mm free-end slip as obtained from load-slip characteristics discussed in 6.1 are tabulated in Table 6.6, with each specimen yielding two results. Table 6.7 gives the pull-out force at 0.1 mm slip normalised for the concrete strength of 35 N/mm^2 together with the values of critical bond stress derived from these pull-out force values.

Torbar

Cover (mm)	Tension applied - kN/Tension release				f_{cu} (N/mm ²)
	0	40	60	80	
	$\epsilon = 0$	$\epsilon = 1180 \times 10^{-6}$	$\epsilon = 1770 \times 10^{-6}$	$\epsilon = 2360 \times 10^{-6}$	
88	31.20; 31.50	25.5; 27.5	16.0; 21.5	15.6; 12.0	34.95
63	25.80; 18.50	17.0; 16.2	17.0; 15.0	11.0; 9.0	34.87
50	24.50; 24.80	18.6; 20.5	18.0; 17.6	18.5; 18.7	36.30
25	18.40; 19.30	18.4; 17.5	19.8; 20.0	16.4; 25.7	35.98

Hybar

Cover (mm)	Tension applied - kN/Tension release				f_{cu} (N/mm ²)
	0	40	60	80	
	$\epsilon = 0$	$\epsilon = 1180 \times 10^{-6}$	$\epsilon = 1770 \times 10^{-6}$	$\epsilon = 2360 \times 10^{-6}$	
88	39.0; 34.5	28.0; 24.0	28.2; 25.0	16.0; 21.2	36.13
63	33.2; 28.2	23.5; 23.5	21.8; 21.0	30.5; 20.0	35.23
50	30.0; 23.5	25.7; 23.3	17.5; 18.6	12.8; 13.7	34.35
25	28.0; 24.0	25.2; 24.8	21.6; 22.7	23.5; 24.0	36.44

Square-twisted

Cover (mm)	Tension applied - kN/Tension release				f_{cu} (N/mm ²)
	0	40	60	80	
	$\epsilon = 0$	$\epsilon = 1180 \times 10^{-6}$	$\epsilon = 1770 \times 10^{-6}$	$\epsilon = 2360 \times 10^{-6}$	
88	27.2; 18.6	17.6; 17.5	16.7; 16.2	14.30; 13.4	34.23
63	18.5; 21.7	22.2; 17.2	17.0; 16.0	7.7; 12.5	35.17
50	27.7; 23.2	25.7; 20.4	16.0; 18.1	14.2; 14.3	35.20
25	22.5; 13.6	25.0; 16.5	20.0; 17.0	18.0; 16.0	35.8

ϵ in units of strain

TABLE 6.6 : PULL-OUT FORCE AT 0.1mm SLIP - kN

Torbar

Cover (mm)	Force at 0.1mm Slip(corrected)-kN				Critical bond stress - N/mm ²			
	$\epsilon = 0$	$\epsilon = 1180$	$\epsilon = 1770$	$\epsilon = 2360$	$\epsilon = 0$	$\epsilon = 1180$	$\epsilon = 1770$	$\epsilon = 2360$
88	31.33	26.58	18.75	13.84	3.96	3.36	2.37	1.75
63	22.23	16.61	15.98	10.05	2.81	2.10	2.02	1.27
50	24.21	19.22	17.48	18.27	3.06	2.43	2.21	2.31
25	18.35	17.48	19.38	20.49	2.32	2.21	2.45	2.59

Hybar

Cover (mm)	Force at 0.1mm Slip(corrected)-kN				Critical bond stress - N/mm ²			
	$\epsilon = 0$	$\epsilon = 1180$	$\epsilon = 1770$	$\epsilon = 2360$	$\epsilon = 0$	$\epsilon = 1180$	$\epsilon = 1770$	$\epsilon = 2360$
88	36.15	25.55	26.19	18.27	4.57	3.23	3.31	2.31
63	30.62	23.42	21.36	20.09	3.87	2.96	2.70	2.54
50	27.06	24.76	18.20	13.37	3.42	3.13	2.30	1.69
25	25.47	24.52	21.68	23.26	3.22	3.10	2.74	2.94

Square-twisted

Cover (mm)	Force at 0.1mm Slip(corrected)-kN				Critical bond stress - N/mm ²			
	$\epsilon = 0$	$\epsilon = 1180$	$\epsilon = 1770$	$\epsilon = 2360$	$\epsilon = 0$	$\epsilon = 1180$	$\epsilon = 1770$	$\epsilon = 2360$
88	23.22	17.74	16.67	14.01	2.80	2.14	2.01	1.69
63	20.07	19.65	16.42	12.44	2.42	2.37	1.98	1.50
50	25.37	22.97	17.00	14.18	3.06	2.77	2.55	1.71
25	17.83	20.56	18.33	16.83	2.15	2.48	2.21	2.03

Note: ϵ in units of microstrain

TABLE 6.7 : CRITICAL BOND STRESS

6.3.1 Effect of concrete cover and tension release

The Torbar and Hybar show better bond performance than the Square-twisted bar. The variation of critical bond stress with increasing cover is shown in Figs. 6.7, 6.8 and 6.9. While the Square-twisted bar shows increased bond stress with cover in the absence of tension release, Hybar and Torbar in particular show increased bond stress not only in the absence of tension but with low level of tension release such as at 1180 microstrains with increasing cover. This aspect is particularly interesting and useful for design purposes.

The variation of critical bond stress with the level of tension release is shown in Figs. 6.10, 6.11 and 6.12. In the case of all the three types of bars, bond resistance deteriorates with increase in the tensile transverse cracking in the concrete surrounding the test bar for all concrete covers except the 25 mm cover, or one bar diameter. In this case, the concrete cover cracked very early in the loading and hence additional cracking due to tension release does not seem to materially affect the bond resistance of the bar.

In order to study the effects of the different levels of tension release and the various concrete covers, the variation of the ratio of the bond resistance, f_b to the bond resistance obtained with maximum concrete cover and zero tension, f_{bo} , is plotted in Figs. 6.13, 6.14 and 6.15 for the Hybar, Square-twisted bar and Torbar respectively. In all cases, it is seen that there is a definite correlation between the bond strength and the level of tensile strain in the concrete surrounding the bar except when the cover is equal to one bar diameter. The relationship may be given in the form :

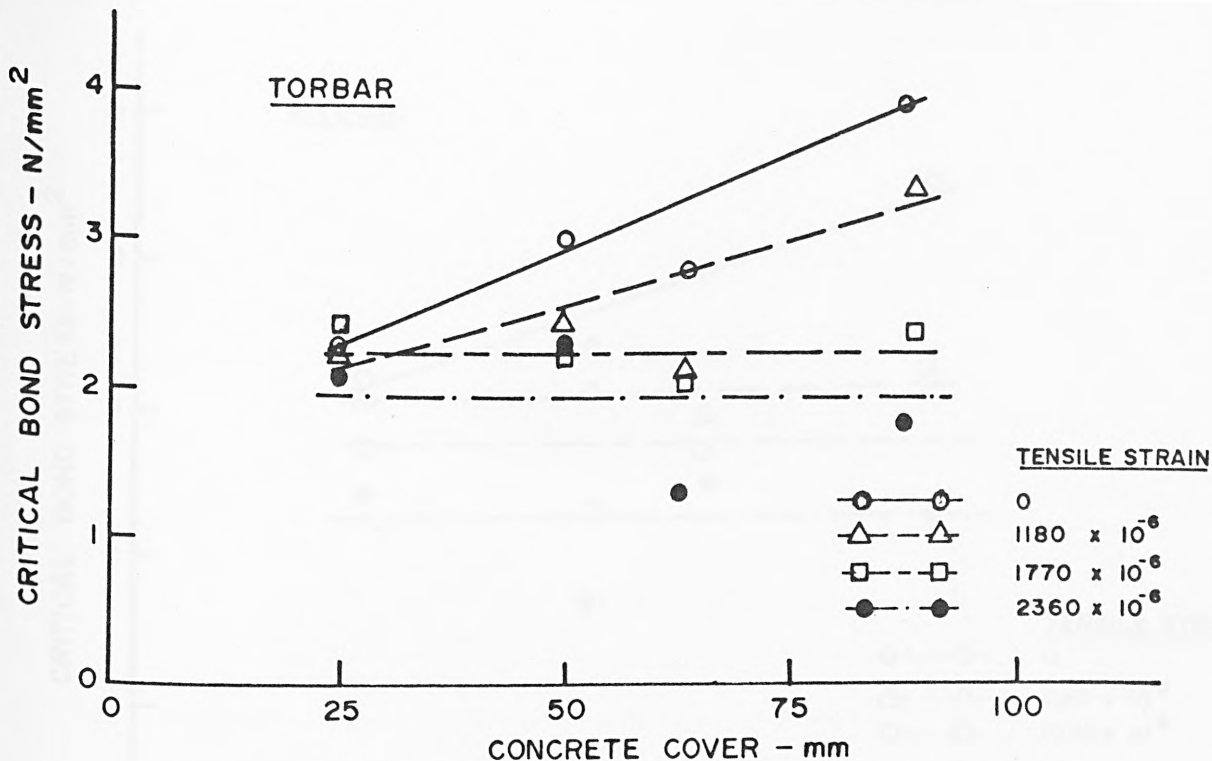


FIG. 6.7 VARIATION OF CRITICAL BOND STRESS WITH COVER - TORBAR

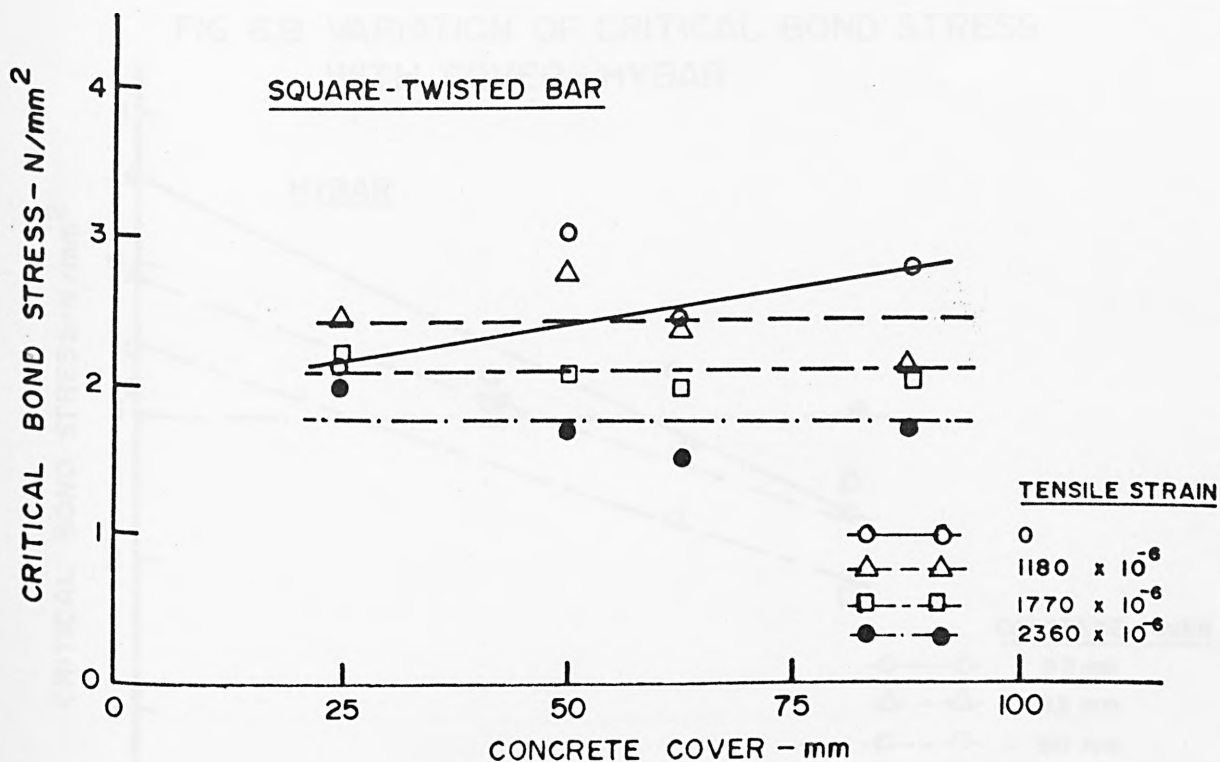


FIG. 6.8 VARIATION OF CRITICAL BOND STRESS WITH COVER - SQUARE-TWISTED BAR

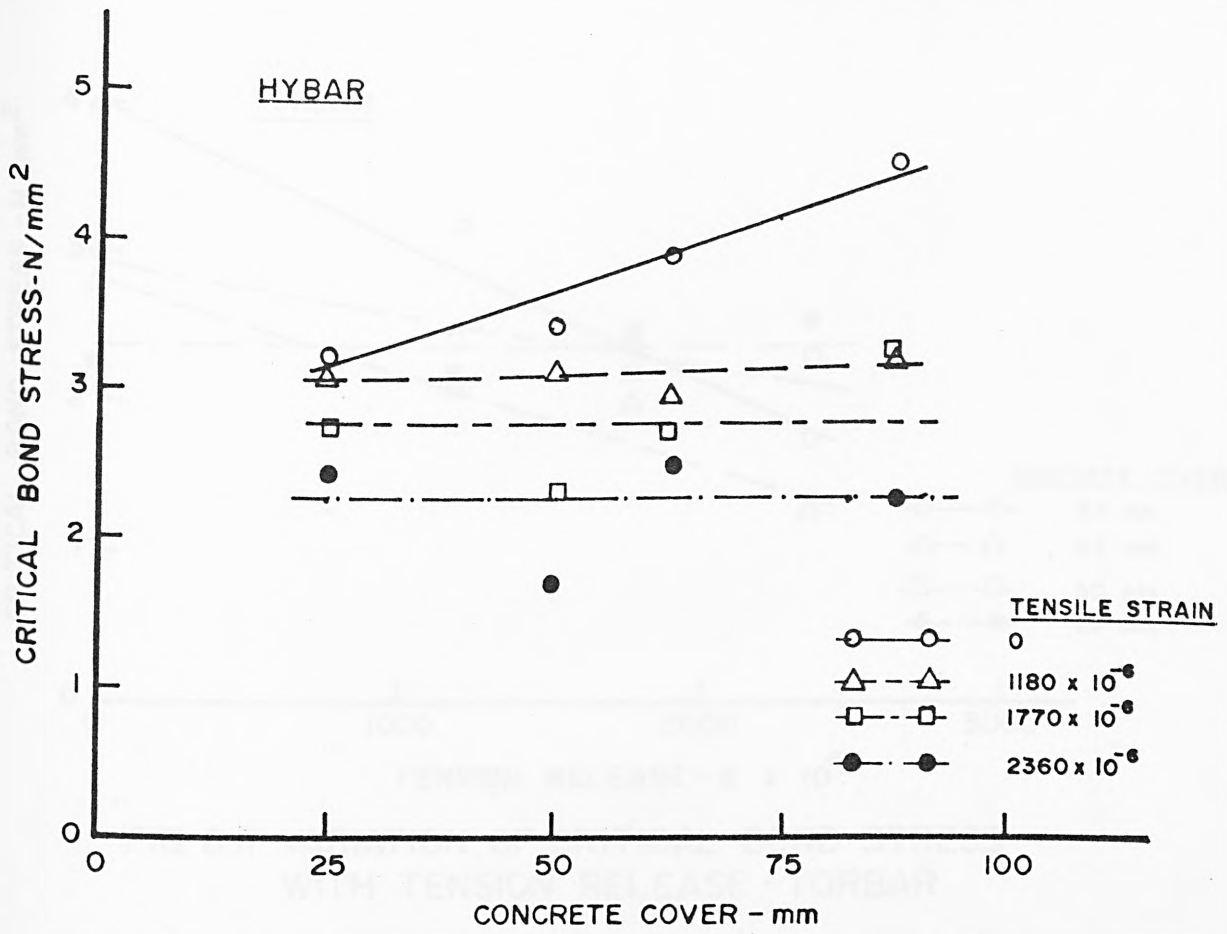


FIG. 6.9 VARIATION OF CRITICAL BOND STRESS WITH COVER - HYBAR

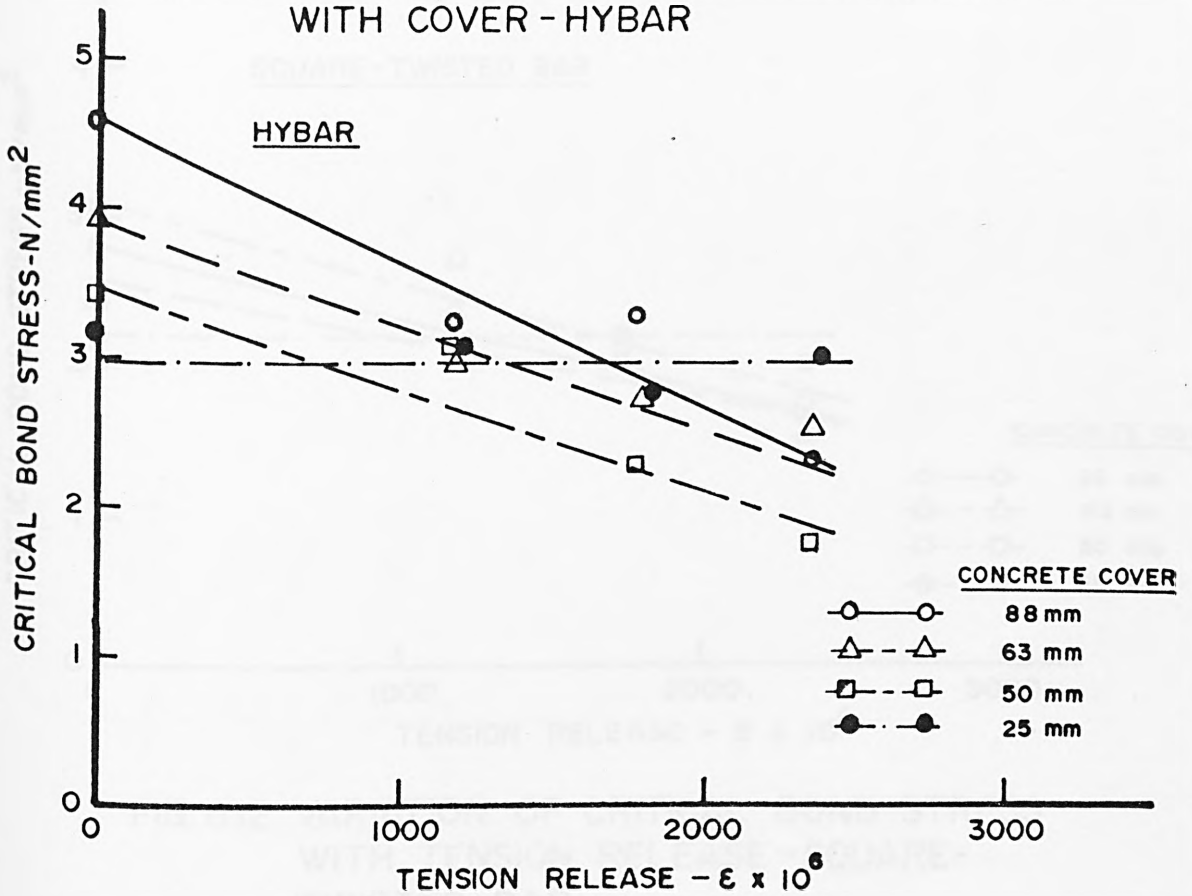


FIG. 6.10 VARIATION OF CRITICAL BOND STRESS WITH TENSION RELEASE - HYBAR

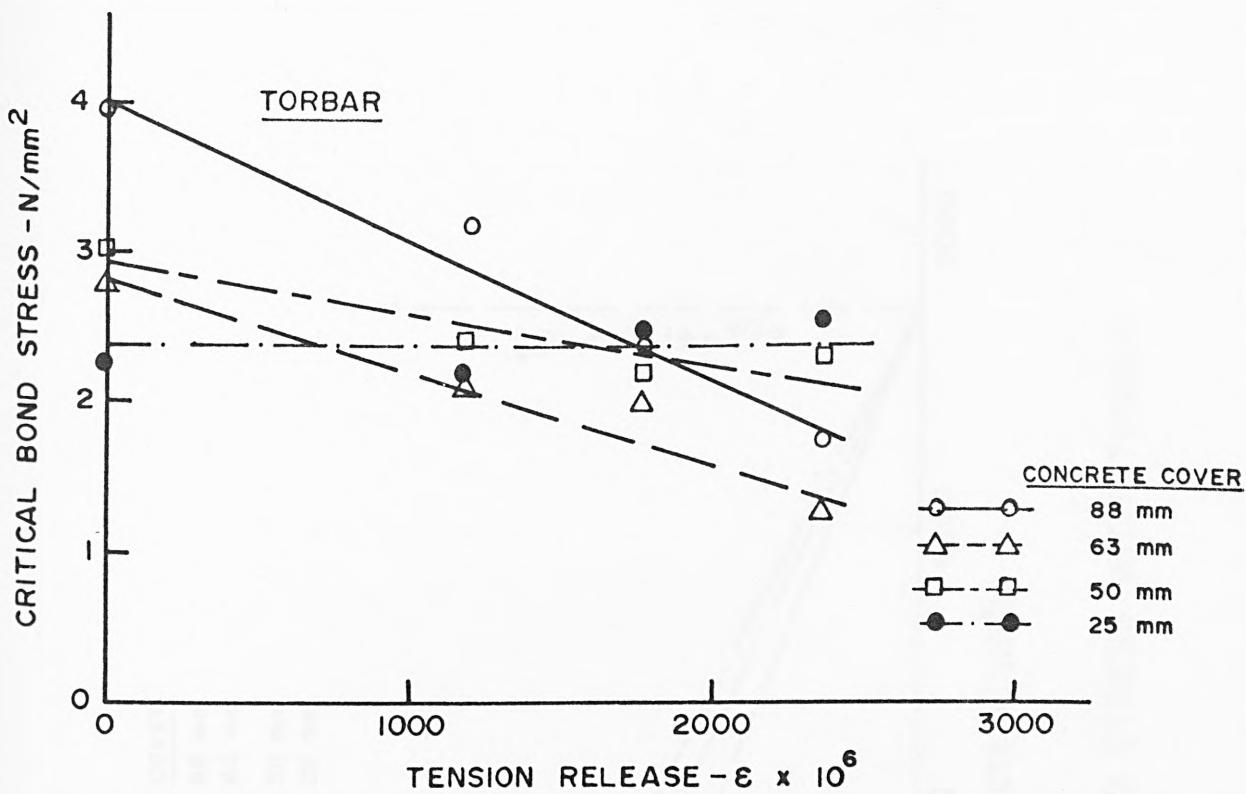


FIG. 6.11 VARIATION OF CRITICAL BOND STRESS WITH TENSION RELEASE - TORBAR



FIG. 6.12 VARIATION OF CRITICAL BOND STRESS WITH TENSION RELEASE - SQUARE-TWISTED BAR

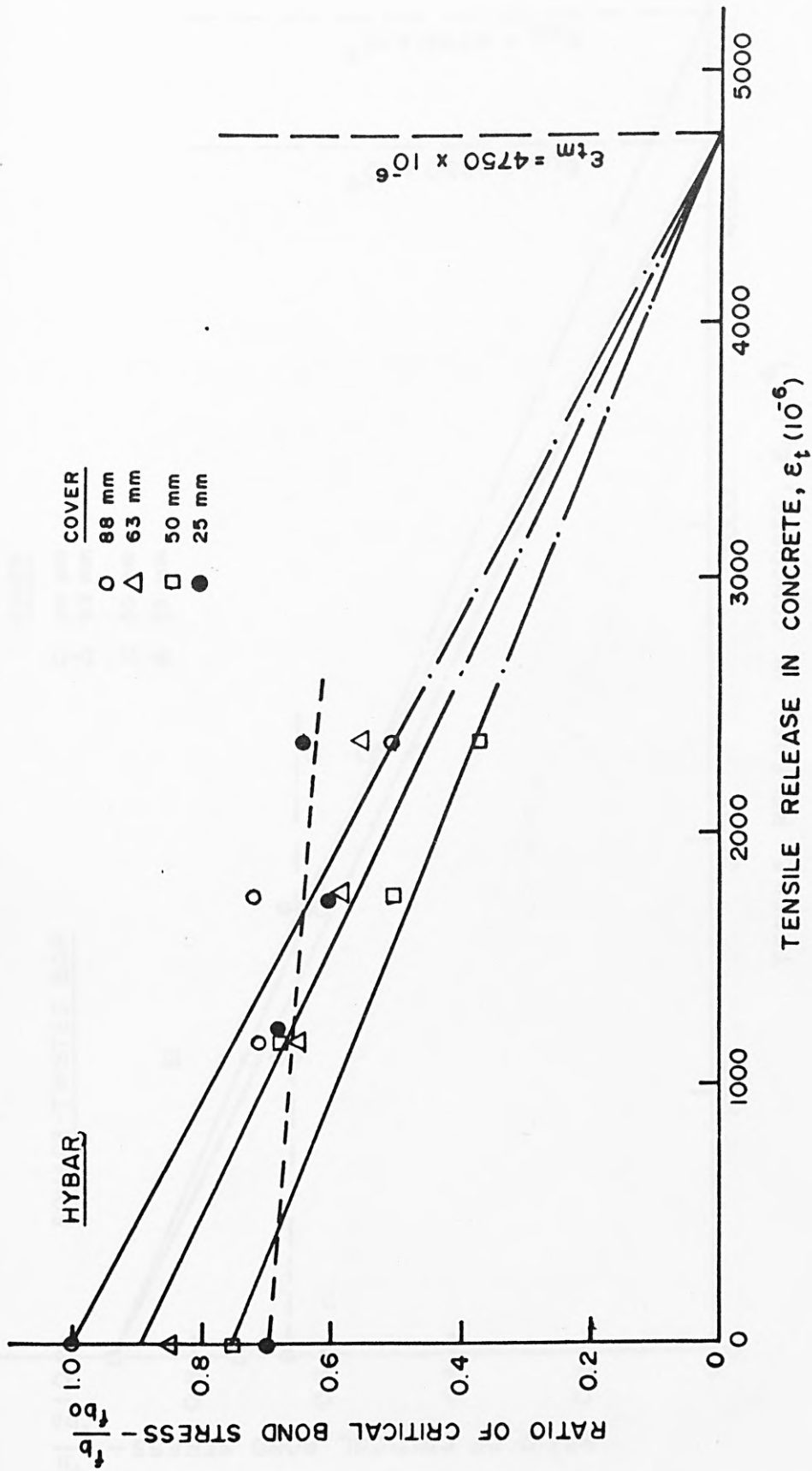


FIG. 6.13 VARIATION OF RATIO OF CRITICAL BOND STRESS WITH TENSILE RELEASE IN CONCRETE - HYBAR

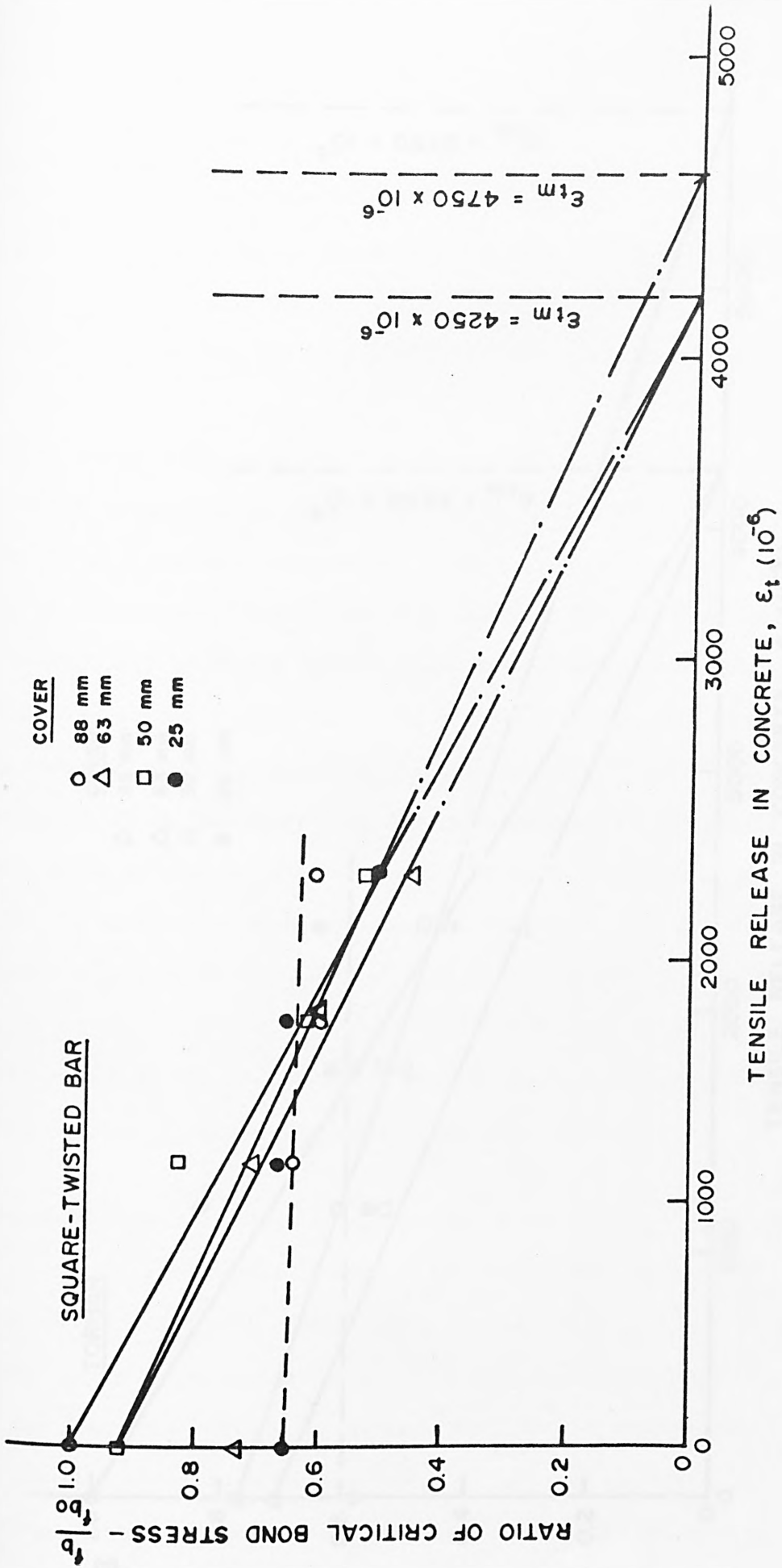


FIG. 6.14 VARIATION OF RATIO OF CRITICAL BOND STRESS WITH TENSILE RELEASE IN CONCRETE - SQUARE-TWISTED BAR

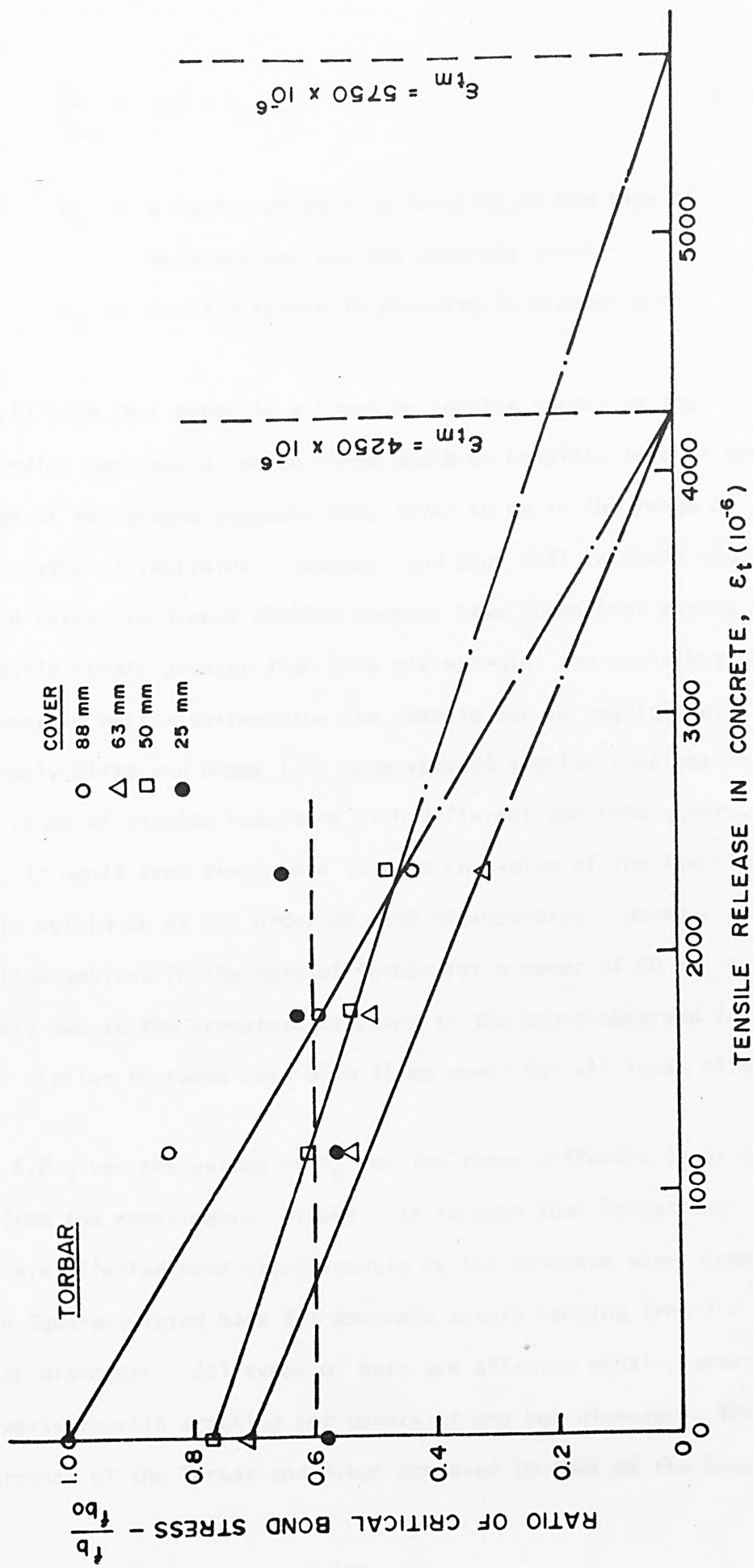


FIG. 6.15 VARIATION OF RATIO OF CRITICAL BOND STRESS WITH TENSILE RELEASE IN CONCRETE - TORBAR

$$\frac{f_b}{f_{bo}} = 1.0 - K_b \cdot \epsilon_t \quad \dots \quad (6.1)$$

where K_b = a factor which is a function of the type of deformed bar and the concrete cover.

ϵ_t = tensile strain in concrete in microstrains.

It would seem that there is a limiting tensile strain in the surrounding concrete at which there would be complete loss of bond. A study of the graphs suggests this level to be in the range of 4250 to 4750 microstrains. Somayaji and Shah (61) in their studies of bond stress in direct tension members have shown that beyond values of tensile strain greater than 4200 microstrain, the contribution of the concrete matrix surrounding the tensile bar is negligible. Previously Mirza and Houde (36) demonstrated similar findings in their study of tension specimens with different concrete covers. Hence, it would seem reasonable to take the value of the limiting tensile strain as of the order of 4250 microstrains. However, the variation noticed in the case of Torbar for a cover of 50 mm is probably due to the premature cracking in the cover observed in the tests, similar to those seen with 25 mm cover for all types of bars.

Table 6.8 gives the values of K_b for the three different types of bars from the experimental graphs. It is seen that Torbar and Hybar are affected more significantly by the concrete cover compared to the Square-twisted bars for concrete covers ranging from 2.0 to 3.5 bar diameters. All types of bars are affected equally under transverse tensile cracking for covers of one bar diameter. The performance of the Torbar and Hybar compared to that of the Square-

Type of Bar	Ratio of concrete cover/bar diameter		
	3.5	2.5	2.0
Torbar	235	165	134
Hybar	211	188	158
Square-twisted	235	216	194

TABLE 6.8 : VALUES OF K_b IN EQUATION (6.1)

twisted bar may be explained in terms of the increased ring tension produced by these bars and the restraint provided by the available concrete cover to cracking due to this ring tension.

In order to obtain a global relationship between the variation in bond resistance with different values of tension release (cracking) and concrete covers, the data is presented in a non-dimensional form as shown in Fig. 6.16 using the ratio of the tension release to the limiting tensile strain of 4250 microstrains. It is observed that the experimental results are lower bound by characteristics of the form given by

$$\frac{f_b}{f_{bo}} = K_c \left[1 - \frac{\epsilon_t}{\epsilon_{tm}} \right] \quad \dots \quad (6.2)$$

where ϵ_{tm} = limiting tensile strain of 4250 microstrains

K_c = a constant which is a function of cover

K_c is seen to vary between 1.0 and 0.7 for concrete covers varying between 3.5 to 2 bar diameters.

6.3.2 Interaction between concrete cover and tension release

Figs. 6.4, 6.5 and 6.6 also show the interactive behaviour of varying concrete cover and tension release on the critical bond stress for the three types of reinforcement bars. The general shape of the interactive surfaces for the three bars looks alike although the profiles of the curves with increasing concrete cover for Hybar and Torbar are steeper than those for Square-twisted bars.

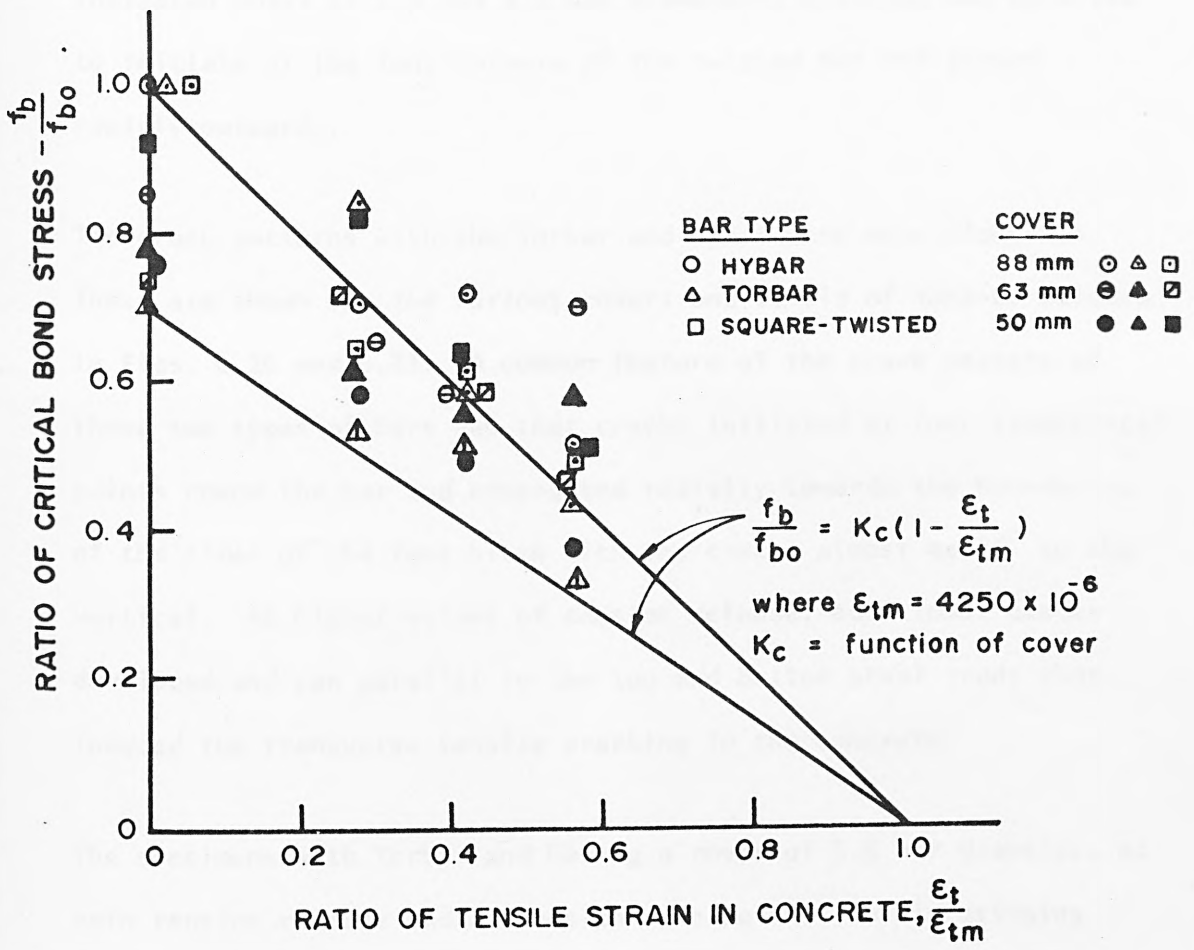


FIG. 6.16 VARIATION OF RATIO OF CRITICAL BOND STRESS WITH RATIO OF TENSILE STRAIN IN CONCRETE

6.4 Modes of ultimate failure

The photographs in Figs. 6.17, 6.18 and 6.19 show the modes of failure of the specimens representative of the three types of reinforcement bars used in the study. In the case of the Square-twisted bars, they pulled out without much cracking when the cover was small, namely with covers of one and two bar diameters. With increased cover of 2.5 and 3.5 bar diameters, cracking was observed to initiate at the four corners of the twisted bar and spread rapidly outwards.

The crack patterns with the Torbar and Hybar were more elaborate. These are shown for the various covers and levels of tension release in Figs. 6.20 and 6.21. A common feature of the crack pattern of these two types of bars was that cracks initiated at four symmetrical points round the bar and propagated radially towards the boundaries of the sides of the test block with the cracks almost at 45° to the vertical. At higher values of tension release, additional cracks developed and ran parallel to the top and bottom steel studs that induced the transverse tensile cracking in the concrete.

The specimens with Torbar and having a cover of 3.5 bar diameter, at zero tension release and at tension release of 1180 microstrains exhibited a cone type of pull-out failure in addition to the radial cracking mentioned earlier (Fig. 6.20). The spiral longitudinal rib of the Torbar seems to be able to involve a greater zone of the concrete surrounding the bar thus causing a cone of concrete to be pulled out at ultimate failure. The specimens with lower concrete cover of one and two bar diameters exhibited side cracking in the cover in addition to the radial cracks.

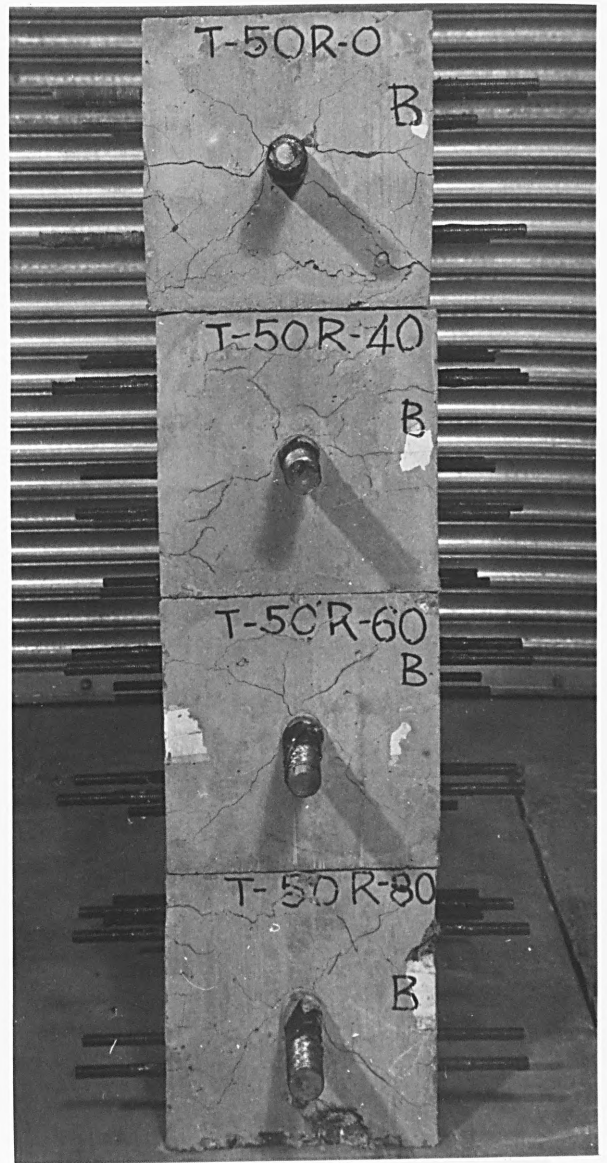
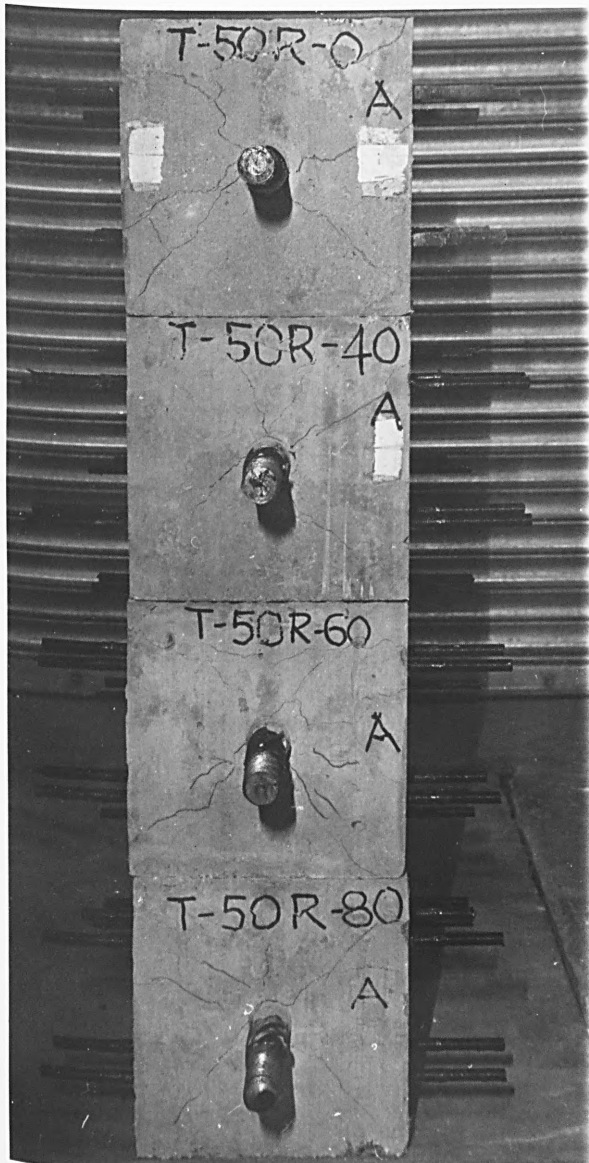
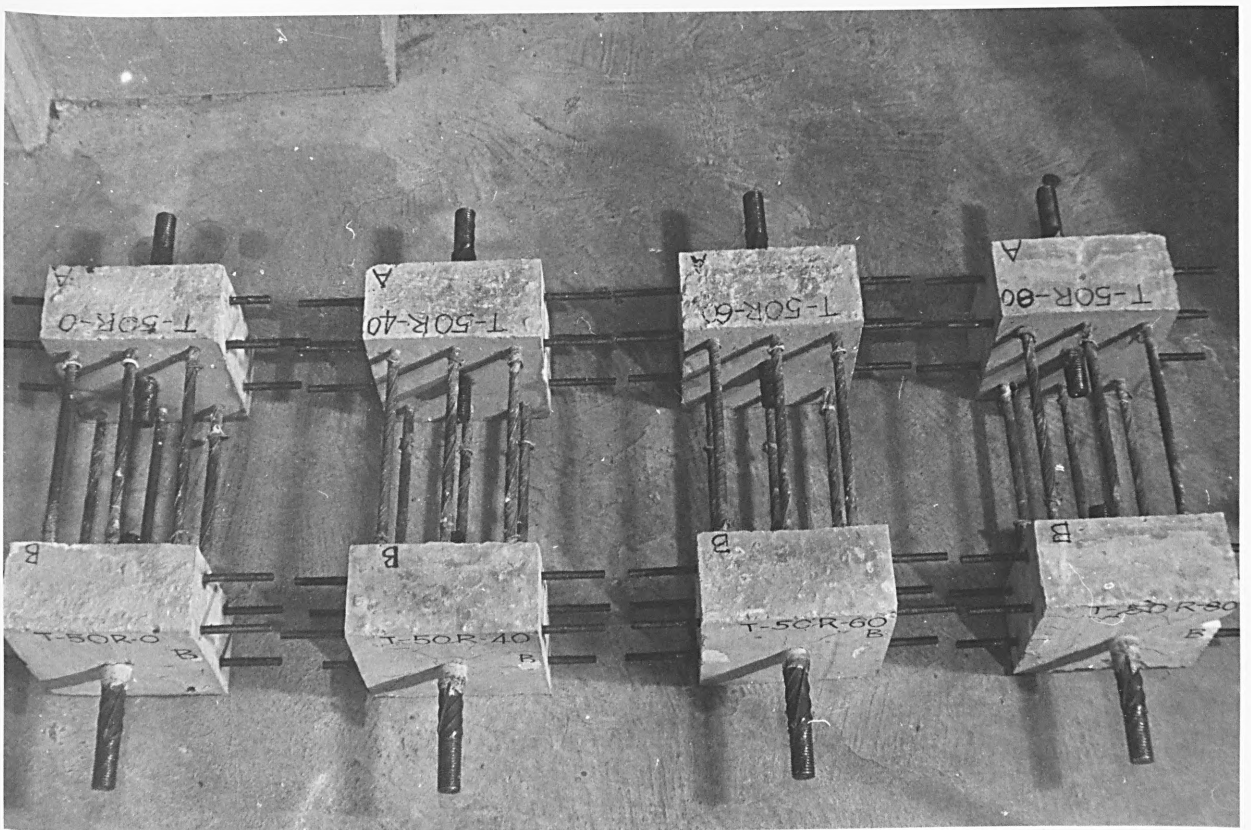


FIG. 6.17 TYPICAL FAILURE MODES UNDER TENSION RELEASE - TORBAR

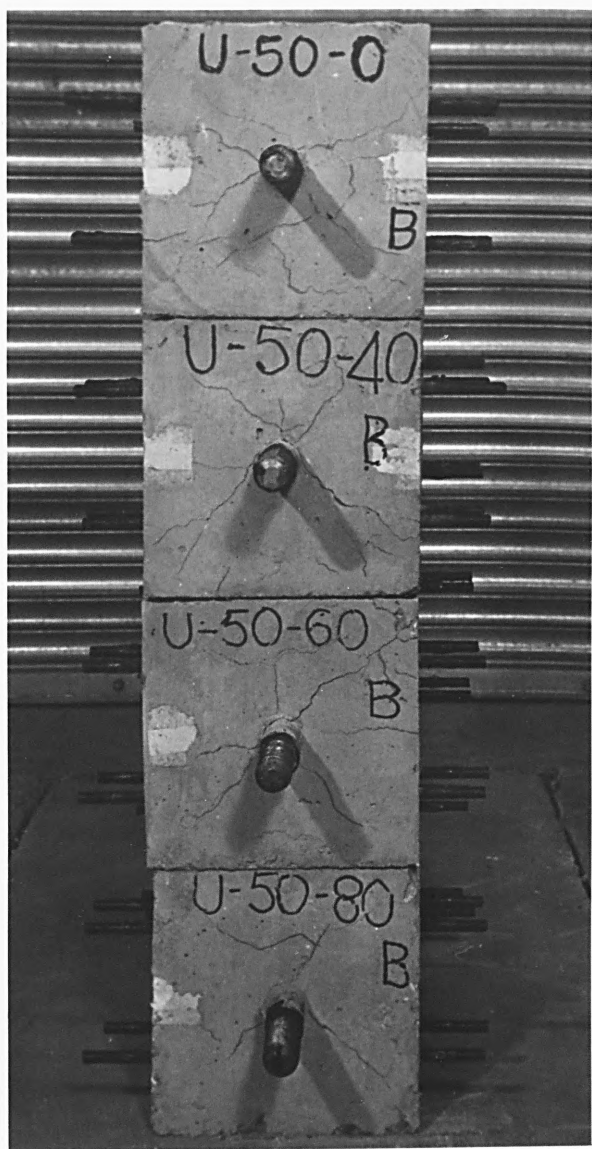
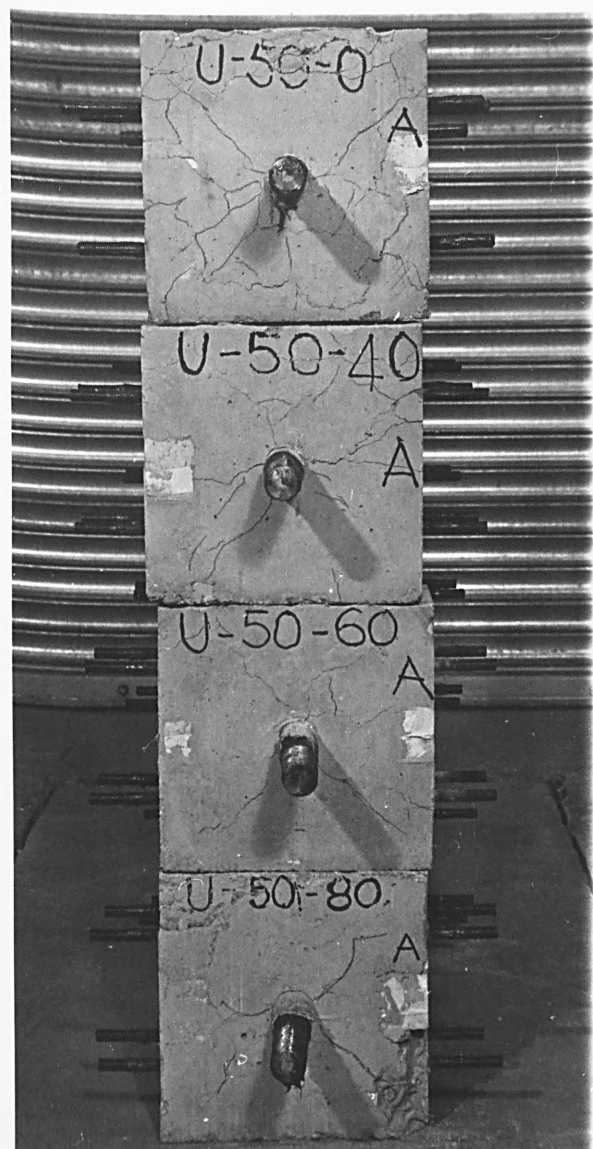
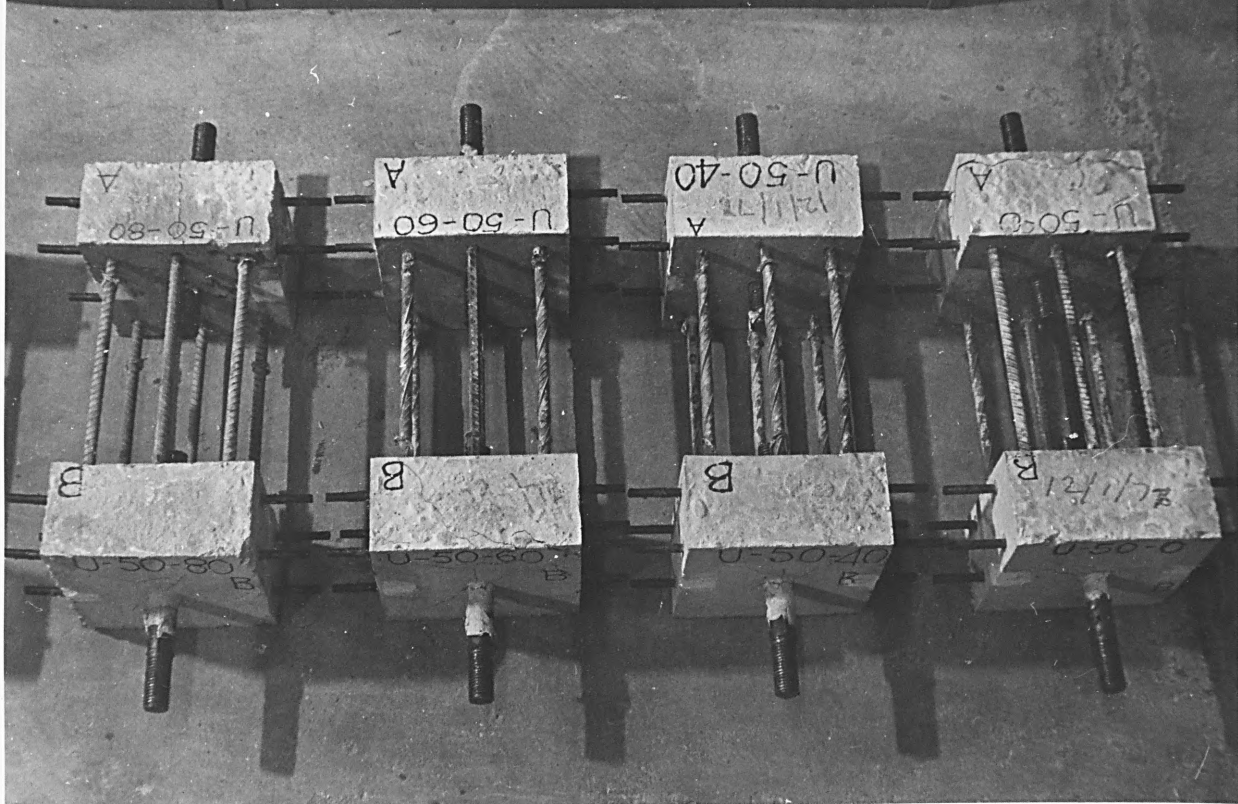


FIG. 6.18 TYPICAL FAILURE MODES UNDER TENSION RELEASE - HYBAR

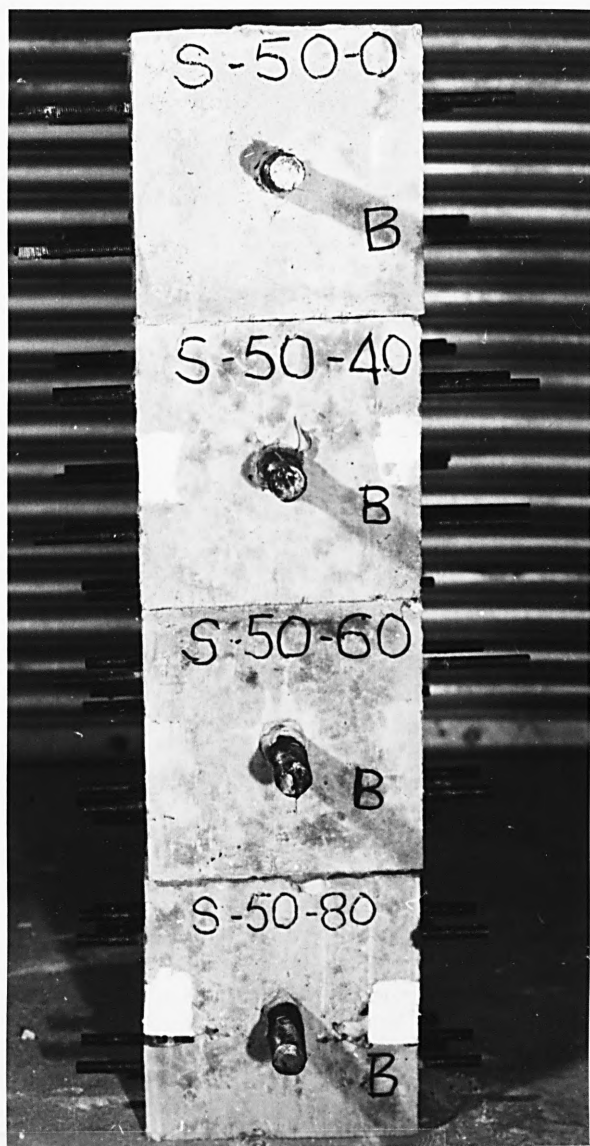


FIG. 6.19 TYPICAL FAILURE MODES UNDER TENSION RELEASE - SQUARE-TWISTED BAR

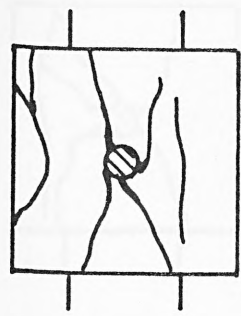
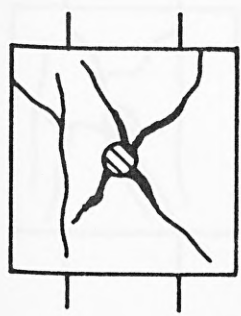
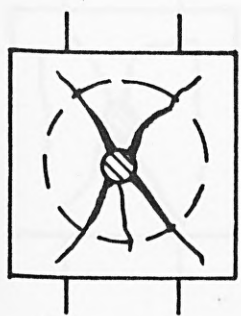
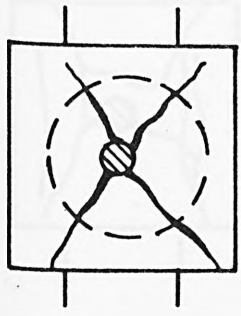
COVER (mm)

$\epsilon = 0$

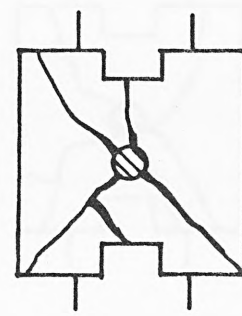
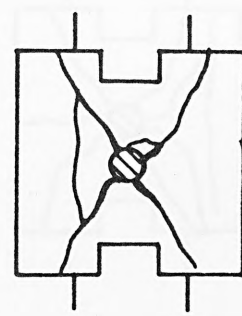
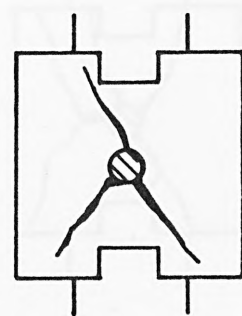
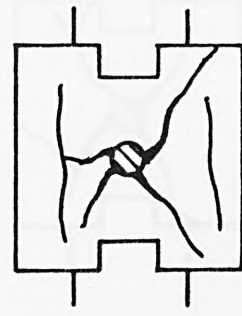
$\epsilon = 1180 \times 10^{-6}$

$\epsilon = 1770 \times 10^{-6}$

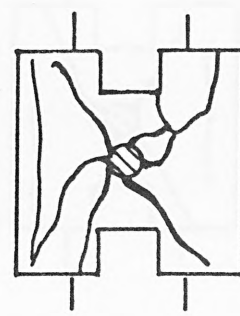
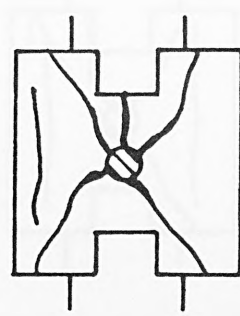
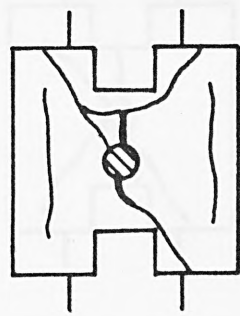
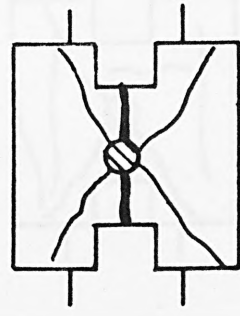
$\epsilon = 2360 \times 10^{-6}$



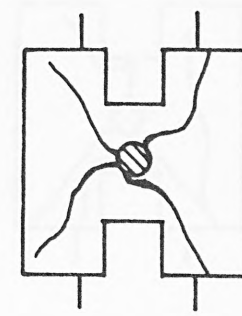
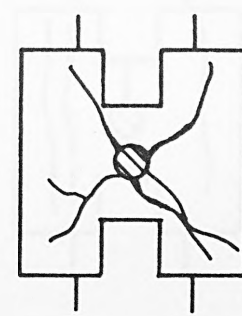
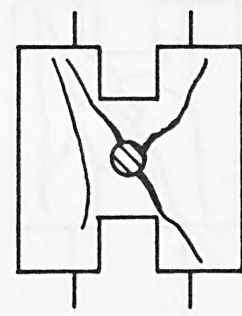
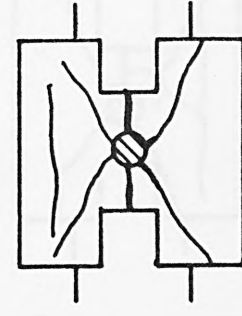
88



63



50



25

FIG. 6.20 CRACK PATTERNS AT ULTIMATE FAILURE - TORBAR

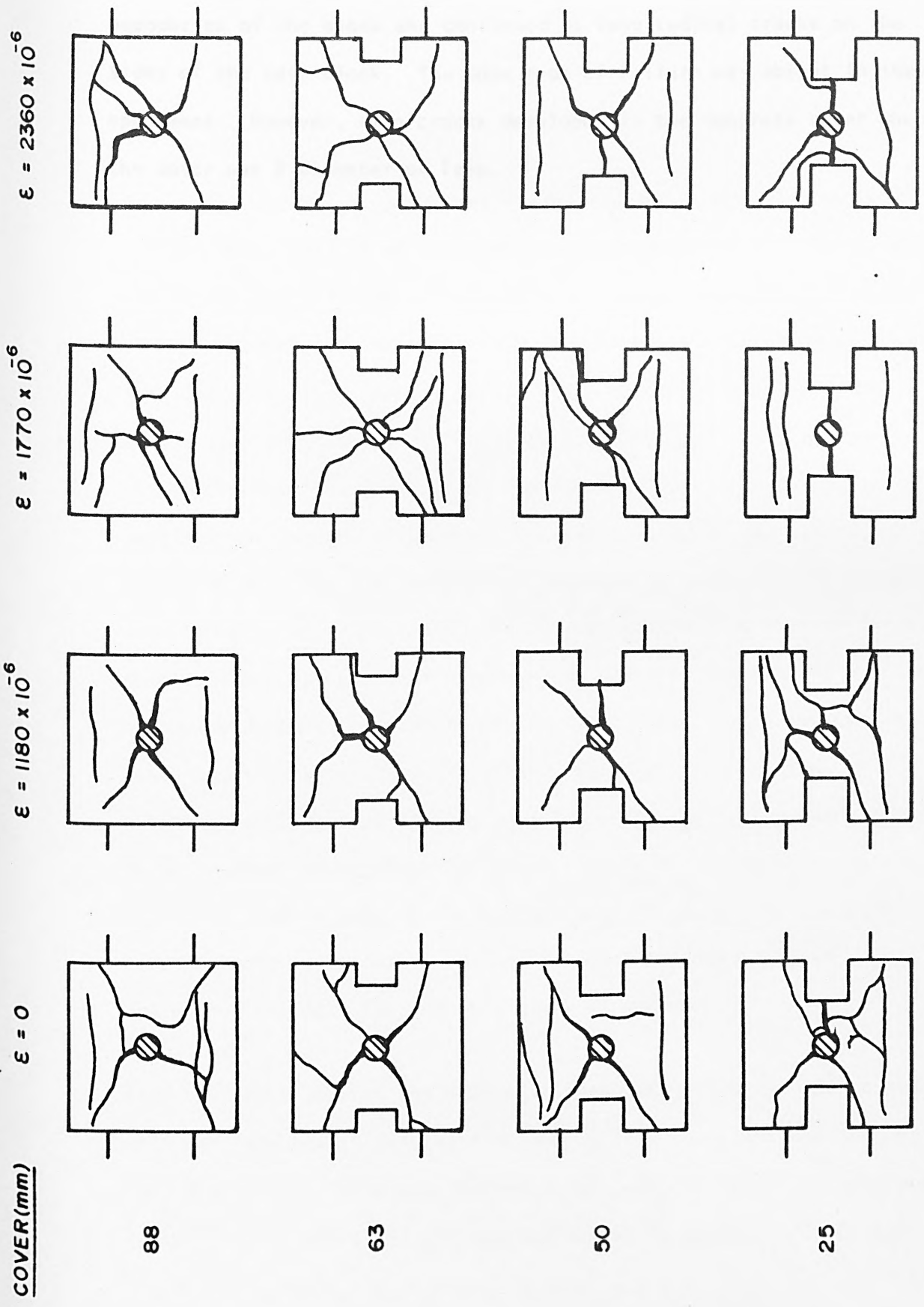


FIG. 6.21 CRACK PATTERNS AT ULTIMATE FAILURE - HYBAR

The specimens with Hybar exhibited extensive cracking with increased size of cracks (Fig. 6.21). The radial cracks propagated to the boundaries of the block and continued as longitudinal cracks on the sides of the test block. The cone type of failure was absent in these specimens. However, side cracks developed in the concrete cover when the cover was 2 diameter or less.

PRESENTATION AND DISCUSSION OF RESULTS OF EXPERIMENTS
WITH LATERAL COMPRESSION

7.1 Load-slip characteristics

As in the case of the specimens tested under tension release, no changes were observed on the dial gauges mounted against the unloaded end of the bar till the initial slip occurred. Thereafter, the slip at the unloaded end recorded increasing values with increasing load on the test bars. The load at initial slip was dependent on the position of the test bar, namely its location at the top of the block or bottom of the block during casting and the level of lateral compression applied. As loading progressed, cracks appeared on the loaded end radiating from the test bar. The first crack in most of the cases appeared as a vertical crack from the bar progressing towards the top of the block. At the same time a crack appeared immediately vertically below the bar and progressed down into the block. With increasing load, the load slip characteristics moved away from the load axis starting from the load at initial slip. With increasing load, cracking became extensive and the slip values increased causing the load-slip curves to flatten towards the horizontal. The load-slip characteristic was terminated at ultimate load after which the load dropped indicating ultimate failure of the bar in bond.

Figs. A.7 to A.30 show the load-slip characteristics for the specimens with concrete covers varying from one to four diameters and varying levels of lateral pressure for the three different types of bars used in the study. Each test yielded two load-slip curves, one for each

of the two test-bars pulled together at the same time as described earlier. The graphs for the two bars are designated 1 and 2 and the origin of the graphs for bars designated 2 are shifted by 0.2 mm on the slip axis. The loads at 0.1 mm slip are recorded in the graphs and are taken as the load at critical bond failure defined in 5.4.

The load-slip characteristics depend on the concrete cover, amount of lateral pressure applied, the type of reinforcement, and its location in the test block. Generally, for all the three types of reinforcement the slip at ultimate bond failure increased with increasing lateral pressure and decreasing concrete cover. The maximum values of slip recorded in the tests are given in Table 7.1. The values of slip recorded for top cast bars were much greater than that of bottom cast bars in a great proportion of the tests. Amongst the three types of bars, the Square-twisted bars behaved significantly differently from the other two types. The Square-twisted bars tend to reach their maximum bond resistance at slip values of 0.25 mm to 0.40 mm beyond which very little additional bond resistance is manifested. The Hybar and Torbar continue to develop bond resistance with increasing slip up to failure confirming the increased resistance that is developed due to the bearing of the transverse ribs against the concrete.

In order to study the slip movement of the two ribbed bars, it is necessary to examine the rib profiles of the Torbar and Hybar. The Hybar has transverse ribs inclined to the axis of the bar at 58° with rib face angles of 30° and 38° and rib height of 1.5 mm; the ribs are spaced at a distance of 14.7 mm. On the other hand, Torbar has transverse ribs of height 1.2 mm with rib face angles of 39° and 53°

Torbar

Cover (mm)	Lateral Pressure (N/mm ²)	Maximum slip recorded x 10 ⁻³ (mm)	
		Top Bars	Bottom Bars
100	0	1880	1057
	3.92	3442	1776
	7.84	7050	2025
	11.76	4800	1875 +
75	0	2232	379
	3.92	2870	1518
	7.84	8675	1588
	11.76	2250	775 +
50	0	688	203
	3.92	250	638
	7.84	1538	1275
	11.76	2313	1850 -
25	0	338	825
	3.92	900	375
	7.84	2963	863
	11.76	1138	875 -

Hybar

Cover (mm)	Lateral Pressure (N/mm ²)	Maximum slip recorded x 10 ⁻³ (mm)	
		Top bars	Bottom bars
100	0	375	2953
	3.92	3126	1430
	7.84	2577	577
	11.76	2857	2106 -
75	0	1198	1834
	3.92	1246	1086
	7.84	2676	686
	11.76	3308	1374 -
50	0	2309	1116
	3.92	2007	1525
	7.84	950	631
	11.76	1386	1549 -
25	0	853	1133
	3.92	2946	1737
	7.84	1494	1118
	11.76	2093	1048 -

Square-twisted

Cover (mm)	Lateral Pressure (N/mm ²)	Maximum slip recorded x 10 ⁻³ (mm)	
		Top bars	Bottom bars
100	0	2881	2898
	3.92	1650	3755
	7.84	3578	716
	11.76	1294	1314 +
75	0	1679	2293
	3.92	1309	276
	7.84	2837	1758
	11.76	836	2011 +
50	0	846	1371
	3.92	954	2414
	7.84	1129	819
	11.76	555	1416 +
25	0	1122	813
	3.92	4607	1270
	7.84	2938	1221
	11.76	2860	1983 +

TABLE 7.1 : MAXIMUM SLIP RECORDED IN TOP AND BOTTOM BARS UNDER LATERAL PRESSURE

spaced at 16.0 mm. It also has a longitudinal rib of height 3 mm twisted at about 10 bar diameters. Rehm (24, 25) and Lutz (26) have shown from their studies that rib face angles exceeding 40° produced about the same movement. Rehm further found that slip was a function of only rib height till the concrete began to crack leading eventually to the shearing of the concrete in front of the rib. Based on these studies, Hybar would be expected to perform better than the Torbar in view of the greater rib height. However, the Torbar is compensated for its lower rib height by the twisted longitudinal rib. Soretz (49) has shown in a recent study that up to 1 mm slip, the bond resistance shows no significant dependence on the pattern of the rib bars with an identical related rib area, but a reduction of the rib height would seem advantageous in order to reduce the splitting effect in the concrete. In the present tests, the greater tendency of the Hybar to cause splitting of the concrete cover was prominent compared to the Torbar and in this respect the Torbar seems to hold an advantage over the Hybar.

The increased values of slip with increased normal pressure confirms similar observations by Untrauer and Henry (7). The reduction in slip with increased cover was also observed by Chamberlin (39) who also showed that the full capacity of bond was obtained only for concrete covers exceeding three bar diameters.

7.2 Ultimate bond resistance

The ultimate pull-out force recorded for the three types of reinforcement bars together with the corresponding concrete strengths are tabulated in Tables 7.2 to 7.4. The tables also show the lateral forces ranging from 0 to 6 Tons applied in steps of 2 Tons to induce

Cover (mm)	Location of Bar	Lateral Force/Lateral Pressure - N/mm ²			
		0	2 Ton	4 Ton	6 Ton
		0	3.92	7.84	11.76
100 (113)*	Top	31.78;32.67	40.89;45.89	43.05;43.74	32.12;43.23
	Bottom	34.64;40.35	41.25;48.57	49.66;51.05	52.78;54.52
	Av. Top	32.23	43.39	43.40	37.68
	Av. Bottom	37.50	44.91	50.36	53.65
	Ratio Top: Bottom	0.86	0.97	0.86	0.70
75 (88)	Top	34.82;37.50	38.21;39.64	39.06;40.80	34.72;43.40
	Bottom	33.92;35.71	45.35;50.89	54.68;57.29	52.08;65.97
	Av. Top	36.16	38.93	39.93	39.06
	Av. Bottom	34.82	48.12	55.99	59.03
	Ratio Top: Bottom	1.04	0.81	0.71	0.66
50 (63)	Top	23.96;23.96	29.17;28.65	28.12;38.19	31.60;34.72
	Bottom	37.33;37.33	39.07;42.54	36.46;52.77	48.96;52.95
	Av. Top	23.96	28.91	33.16	33.16
	Av. Bottom	37.33	40.81	44.62	50.96
	Ratio Top: Bottom	0.64	0.71	0.74	0.65
25 (37)	Top	20.84;22.05	22.57;24.48	22.57;25.69	25.17;28.64
	Bottom	27.78;29.17	30.21;35.07	27.26;38.19	32.98;37.84
	Av. Top	21.45	23.53	24.13	26.91
	Av. Bottom	28.48	32.64	32.73	35.41
	Ratio Top: Bottom	0.75	0.72	0.74	0.76

(a) Ultimate Pull-Out Force - kN

* Values in parenthesis indicate measurement to centre of bar.

Cover (mm)	Lateral Pressure - N/mm ²			
	0	3.92	7.84	11.76
100	34.37	34.37	33.69	33.69
75	33.70	33.70	32.64	32.64
50	32.02	32.02	34.81	34.81
25	30.10	30.10	34.21	34.21

(b) Concrete Strength - N/mm²

TABLE 7.2 : ULTIMATE PULL-OUT FORCE AND CONCRETE STRENGTHS - TORBAR

Cover (mm)	Location of Bar	Lateral Force/Lateral Pressure - N/mm ²			
		0	2 Ton	4 Ton	6 Ton
		0	3.92	7.84	11.76
100 (113)*	Top	27.68;32.14	42.85;44.10	40.71;44.28	46.78;51.24
	Bottom	35.17;42.49	44.99;49.64	58.92;62.14	51.42;62.14
	Av. Top	29.91	43.48	42.50	49.01
	Av. Bottom	38.83	47.32	60.53	56.78
	Ratio Top: Bottom	0.77	0.92	0.70	0.86
75 (88)	Top	35.71;36.06	35.71;44.64	43.39;43.39	46.07;54.99
	Bottom	34.28;35.71	48.92;50.35	51.24;57.31	55.35;56.42
	Av. Top	35.89	40.18	43.39	50.53
	Av. Bottom	35.00	49.64	54.28	55.89
	Ratio Top: Bottom	1.03	0.81	0.80	0.90
50 (63)	Top	27.85;30.35	41.07;45.17	32.50;40.35	32.50;37.14
	Bottom	32.14;34.46	38.39;42.49	32.31;42.85	28.21;39.82
	Av. Top	29.10	43.12	36.43	34.82
	Av. Bottom	33.30	40.44	37.58	34.02
	Ratio Top: Bottom	0.87	1.07	0.97	1.02
25 (37)	Top	32.14;26.78	26.42;29.46	24.10;24.82	23.39;26.07
	Bottom	29.82;30.35	32.32 38.21	24.46;33.92	33.21;37.85
	Av. Top	29.46	27.94	24.46	24.68
	Av. Bottom	30.08	35.26	29.19	35.53
	Ratio Top: Bottom	0.98	0.79	0.84	0.69

(a) Ultimate Pull-Out Force - kN

* Values in parenthesis indicate measurement to centre of bar.

Cover (mm)	Lateral Pressure - N/mm ²			
	0	3.92	7.84	11.76
100	34.77	36.43	36.43	34.77
75	35.21	34.93	34.93	35.21
50	36.88	33.17	33.17	36.88
25	34.66	34.66	32.93	32.93

(b) Concrete Strengths - N/mm²

TABLE 7.3 : ULTIMATE PULL-OUT FORCE AND CONCRETE STRENGTHS - HYBAR

Cover (mm)	Location of Bar	Lateral Force/Lateral Pressure - N/mm ²			
		0	2 Ton	4 Ton	6 Ton
		0	3.92	7.84	11.76
100 (113)*	Top	10.00;10.00	11.61;17.86	18.57;26.78	14.28;15.36
	Bottom	22.85;29.46	33.92;35.71	37.14;46.78	40.17;44.28
	Av. Top	10.00	14.74	22.68	14.82
	Av. Bottom	29.16	34.82	41.96	42.23
	Ratio Top: Bottom	0.38	0.42	0.54	0.35
75 (88)	Top	8.39;16.61	19.64;19.64	21.60;28.21	20.00;22.32
	Bottom	30.35;31.60	27.50;32.67	33.92;54.98 [@]	37.50;40.35
	Av. Top	12.50	19.64	24.91	21.16
	Av. Bottom	30.98	30.09	33.92	38.93
	Ratio Top: Bottom	0.40	0.65	0.73	0.54
50 (63)	Top	16.96;19.64	16.07;20.18	25.89;25.53	15.18;20.00
	Bottom	23.21;28.75	28.57;36.60	38.39;41.96	31.42;45.35
	Av. Top	18.30	18.22	25.71	17.59
	Av. Bottom	25.98	32.59	40.18	38.39
	Ratio Top: Bottom	0.70	0.56	0.64	0.46
25 (37)	Top	14.11;17.68	19.64;28.21	15.00;19.64	13.57;16.61
	Bottom	28.75;29.46	27.85;32.67	18.39;25.00	22.14;30.89
	Av. Top	15.90	23.93	17.32	15.09
	Av. Bottom	29.11	30.26	21.70	26.52
	Ratio Top: Bottom	0.55	0.79	0.80	0.57

(a) Ultimate Pull-Out Force - kN

* Values in parenthesis indicate measurement to centre of bar

@ Deleted as high value due to jamming of bar against test bracket

Cover (mm)	Lateral Pressure - N/mm ²			
	0	3.92	7.84	11.76
100	34.40	34.40	36.94	36.94
75	35.45	35.45	35.72	35.72
50	35.34	35.34	38.09	38.09
25	34.60	34.60	37.91	37.91

(b) Concrete Strengths - N/mm²

TABLE 7.4 : ULTIMATE PULL-OUT FORCE AND CONCRETE STRENGTHS - SQUARE TWISTED BAR

lateral pressure varying from 0 to 11.76 N/mm^2 in the concrete surrounding the test bar. Two results for each cover and lateral pressure, for both top cast and bottom cast bars are given in the tables. The averages of the two individual results are used to obtain the ratio of the pull-out forces of the top and bottom cast bars.

Table 7.5 presents the values of the average pull-out force for bottom cast bars that have been corrected for the concrete strength of 35 N/mm^2 in the ratio of the square-roots of the compressive strengths. Ultimate bond stress values derived from the corrected pull-out forces are also given in the same table.

7.2.1 Effect of location of bars

The variation in bond performance of bars cast near the top of a lift of concrete has been attributed to the settlement of concrete and water gain effect by Welch and Patten (44). As soon as concrete is cast into the formwork, it begins to settle towards the bottom due to gravity and the removal of entrapped air. Concrete below the rigidly positioned test bars will settle away from them leaving some cavitation underneath. When a pull is applied on the bar, the pores and cavities thus formed by the air and water bubbles permit the bar to slip more readily as they are weaker and more compressible than concrete. On the other hand, the concrete on top of bottom cast bars exert a hydrostatic pressure thus enabling a better compaction of the concrete surrounding the bar which resists any pull applied on the bar more efficiently. The maximum values of slip recorded at the ultimate pull-out of the top cast and bottom cast bars are given in Table 7.1.

Torbar

Cover (mm)	Pull-out force (corrected) -kN				Ultimate bond stress - N/mm ²			
	p=0	p=3.92	p=7.84	p=11.76	p=0	p=3.92	p=7.84	p=11.76
100	37.86	45.34	51.33	54.69	4.79	5.73	6.49	6.78
75	35.30	49.04	57.98	61.13	4.46	6.20	7.33	7.46
50	39.03	42.66	44.74	51.10	4.93	5.39	5.66	6.46
25	30.71	35.20	33.11	35.82	3.88	4.45	4.19	4.53

Hybar

Cover (mm)	Pull-out force (corrected) -kN				Ultimate bond stress - N/mm ²			
	p=0	p=3.92	p=7.84	p=11.76	p=0	p=3.92	p=7.84	p=11.76
100	38.96	46.07	58.93	56.96	4.92	5.82	7.45	7.20
75	34.89	49.69	54.34	55.72	4.41	6.28	6.87	7.04
50	32.44	41.54	38.61	33.14	4.10	5.25	4.88	4.19
25	30.22	35.43	30.10	36.63	3.82	4.48	3.80	4.63

Square-twisted

Cover (mm)	Pull-out force (corrected) -kN				Ultimate bond stress - N/mm ²			
	p=0	p=3.92	p=7.84	p=11.76	p=0	p=3.92	p=7.84	p=11.76
100	26.39	35.12	40.84	41.10	3.18	4.24	4.93	4.96
75	30.78	29.90	33.57	38.53	3.71	3.61	4.05	4.65
50	25.85	32.43	38.51	36.80	3.12	3.91	4.64	4.44
25	29.28	30.44	20.85	25.48	3.53	3.67	2.51	3.07

Note: p in units of N/mm²

TABLE 7.5 : ULTIMATE BOND STRESS UNDER LATERAL PRESSURE
(BOTTOM CAST BARS)

It is seen that generally the top bars exhibited higher values of slip than bottom bars although in some cases the reverse may be true. The latter behaviour is attributed to possible locking-in of bigger size aggregate particles between the test bar and the transverse stirrups.

The relative bond resistance of top and bottom cast bars is demonstrated in the values of the ratio of the average ultimate pull-out force of top and bottom cast bars tabulated in Tables 7.2 to 7.4 for the three types of reinforcement bars. While for the ribbed bars, namely Torbar and Hybar, the average reductions of about 25 percent and 13 percent respectively are observed, the Square-twisted bars perform rather poorly with the reduction as much as an average of 43 percent. The better performance of the Hybar is attributed to its greater rib height compared to the Torbar. Clark (16) observed a reduction of around 30 percent in his tests, with Brettle (45, 46) recording a similar reduction. The 1977 Building Code of the American Concrete Institute (62) requires 40 percent increase in the development length for top cast bars whereas the German Code (63) specifies a reduction of 50 percent in bond resistance of top cast bars. It seems appropriate to allow a reduction of about 30 percent for ribbed bars and a greater reduction for Square-twisted bars, about 50 percent, in line with the German specifications.

7.2.2 Effect of cover

Earlier studies by Chamberlin (39), Ferguson (21, 22) and the Dutch investigation (38) have all shown that increased cover enhanced the ultimate bond resistance of the bar. The increased resistance was manifested in the ability of increased cover to resist splitting

cracking due to the ring tension developed in the bond mechanism. At ultimate load conditions, the ring tension is resisted by the cover of concrete and transverse reinforcement in the form of stirrups. However, observations made by Chung (64) have shown that the strains in stirrups decreased for the same load when the concrete cover was increased. The behaviour of stirrups is discussed more fully in 7.2.4. In the present tests, the secondary reinforcement in the form of stirrups was kept constant and hence any improvement in ultimate bond resistance with increased concrete cover has to be attributed to the concrete cover.

The variation of ultimate bond stress with concrete cover is shown in Figs. 7.1 to 7.3 for the three different types of bars. It is observed that the ultimate bond stress increases progressively with increase in concrete cover and in the case of the Torbar and Square-twisted bars the curves flatten beyond a cover of 3 to 3.5 bar diameters. This confirms the findings of Chamberlin (39) who concluded that the full capacity of the bond resistance is obtained only for a concrete cover greater than 3 bar diameters. The results also confirm with the study of McClure (56) who showed that the splitting stress in the area surrounding an internally pressurised cylinder becomes small as the cover to diameter ratio exceeds 3.5.

It may seem at first glance that the bond resistance of Torbars shows a tendency to drop for covers greater than 3.5 whereas the resistance holds in the case of the Hybar. The drooping characteristic is only an indication of the differences in the mode of failure of the two types of bars at greater concrete covers. The Torbar tended to plough through at failure when the concrete cover was large compared to the Hybar which continued to increasingly crack the concrete cover.

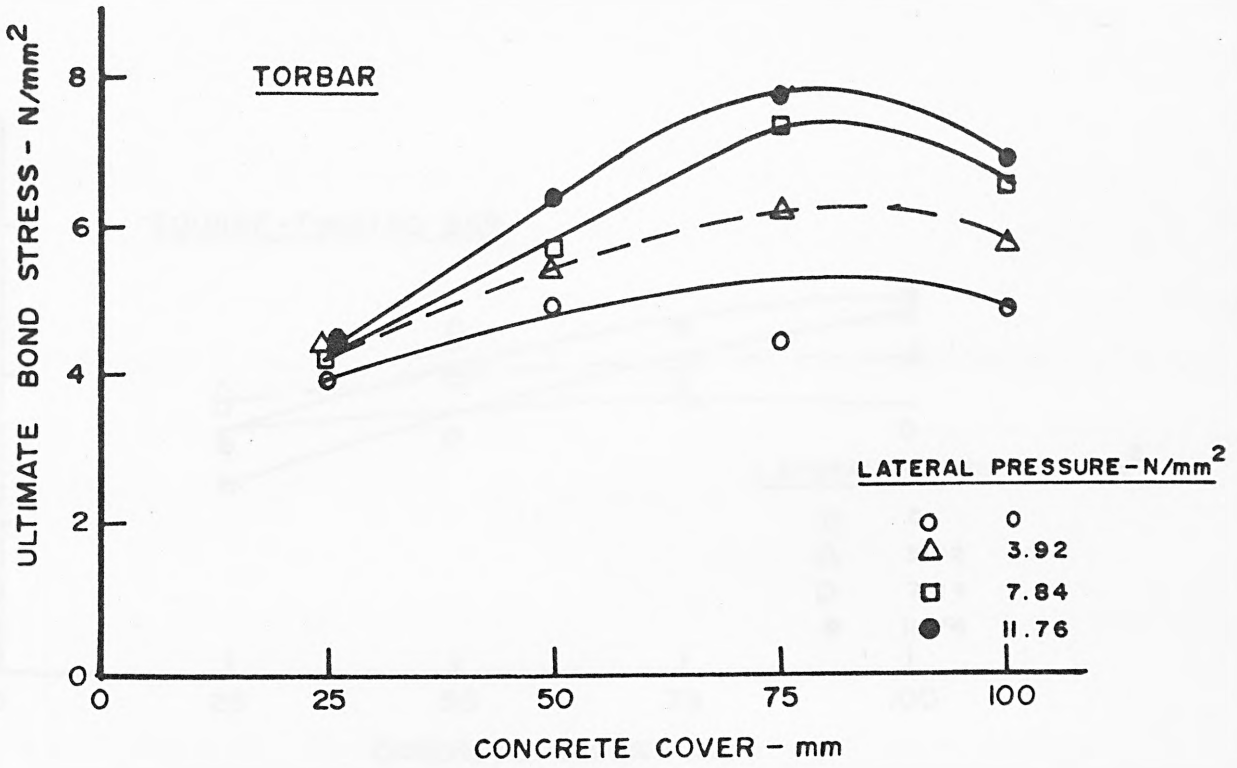


FIG. 7.1 VARIATION OF ULTIMATE BOND STRESS WITH CONCRETE COVER - TORBAR

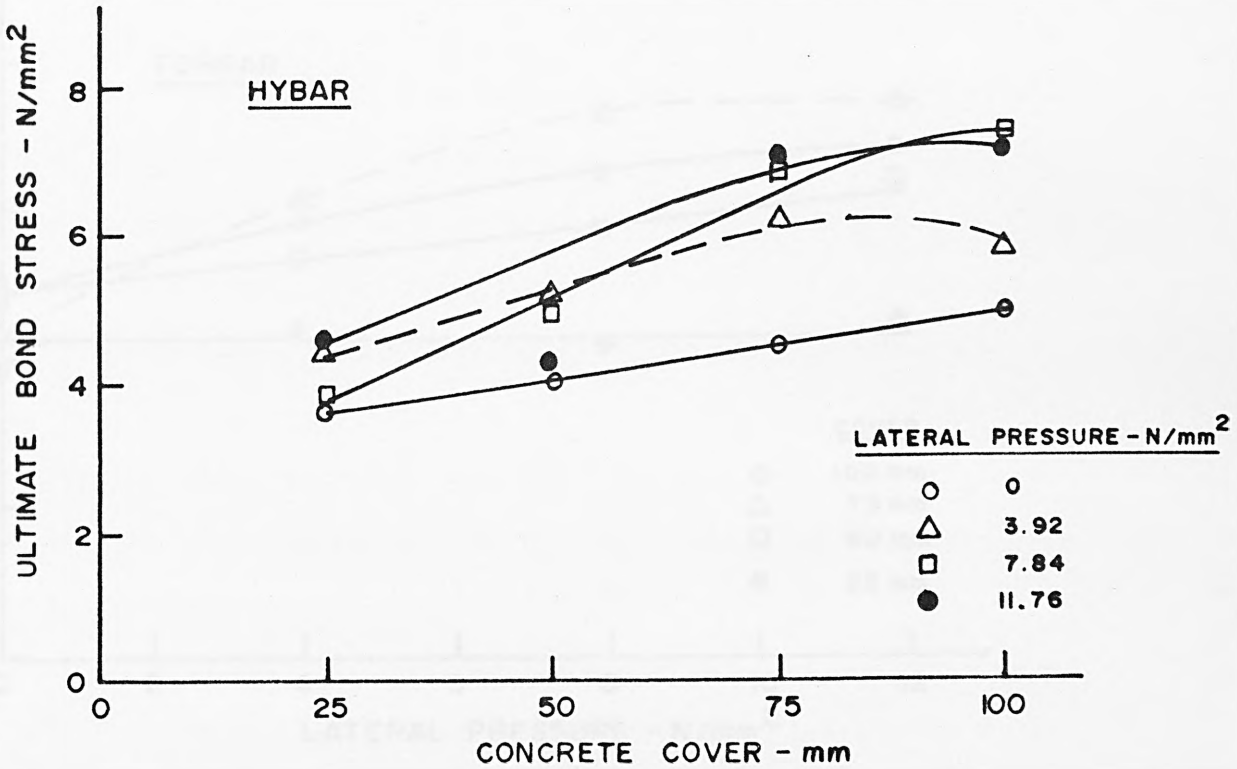


FIG. 7.2 VARIATION OF ULTIMATE BOND STRESS WITH CONCRETE COVER - HYBAR

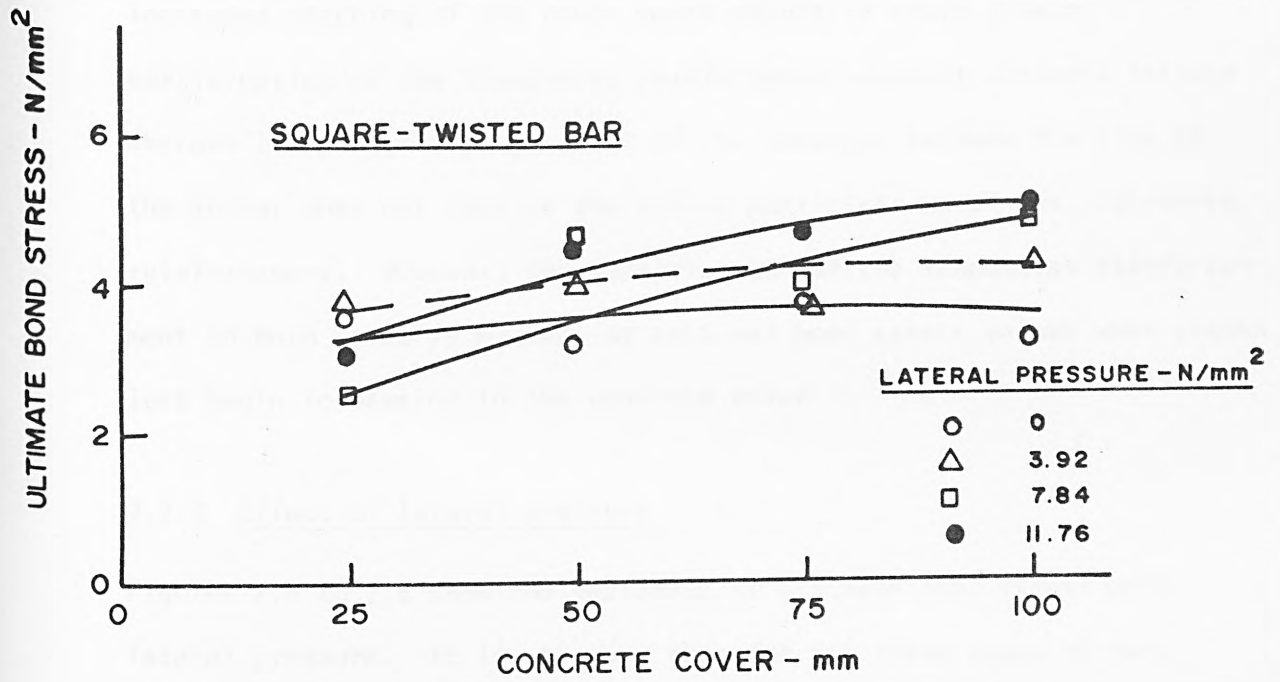


FIG. 7.3 VARIATION OF ULTIMATE BOND STRESS WITH CONCRETE COVER - SQUARE-TWISTED BAR

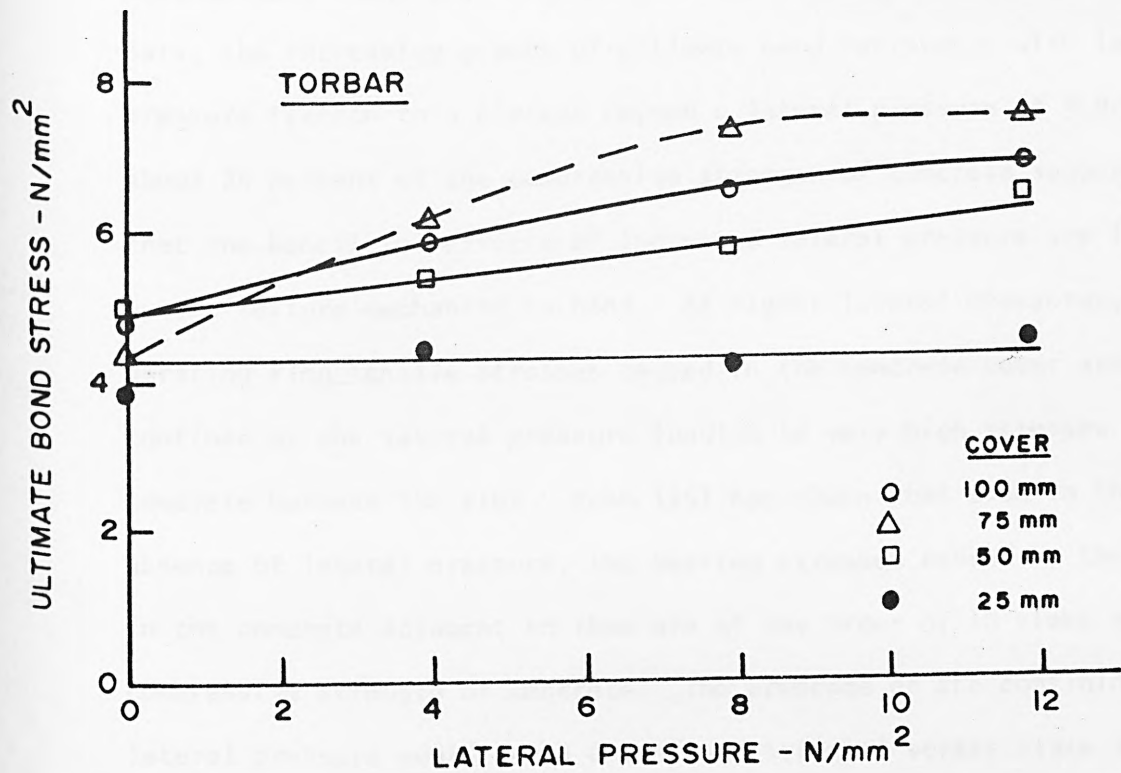


FIG. 7.4 VARIATION OF ULTIMATE BOND STRESS WITH LATERAL PRESSURE - TORBAR

Increased cracking of the cover would naturally cause greater participation of the transverse reinforcement against ultimate failure whereas the plough-through shear of the concrete between the ribs of the Torbar does not involve the active participation of the transverse reinforcement. However, the participation of the transverse reinforcement in both cases is minimal at critical bond stress values when cracks just begin to develop in the concrete cover.

7.2.3 Effect of lateral pressure

Figures 7.4 to 7.6 show the variation of ultimate bond stress with lateral pressure. It is observed that for all three types of bars lateral pressure enhances the ultimate bond stress. The maximum increase in ultimate bond resistance is about 67 and 60 percent for the Torbar and Hybar respectively and about 56 percent for the Square-twisted bar. However, it is observed that for all the three types of bars, the increasing graphs of ultimate bond resistance with lateral pressure flatten to a plateau beyond a lateral pressure of 9 N/mm^2 or about 25 percent of the compressive strength of concrete suggesting that the beneficial effects of increased lateral pressure are limited by the failure mechanism in bond. At higher lateral pressures, the bursting ring tensile stresses caused in the concrete cover are confined by the lateral pressure leading to very high stresses in the concrete between the ribs. Rehm (25) has shown that even in the absence of lateral pressure, the bearing stresses caused by the ribs in the concrete adjacent to them are of the order of 10 times the compressive strength of concrete. The presence of the confining lateral pressure would cause a confined triaxial stress state in the concrete with very high stresses that would eventually lead to a 'plastic yielding' of the concrete as in Fressyinet concrete hinges

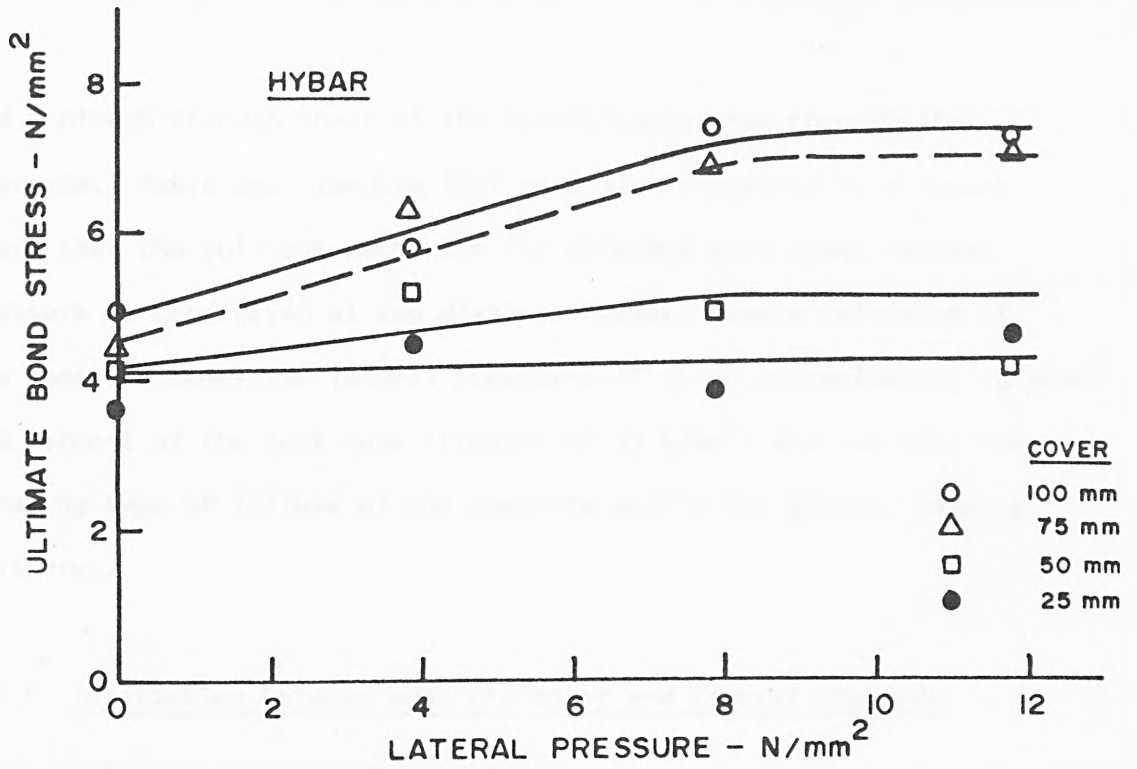


FIG. 7.5 VARIATION OF ULTIMATE BOND STRESS WITH LATERAL PRESSURE - HYBAR

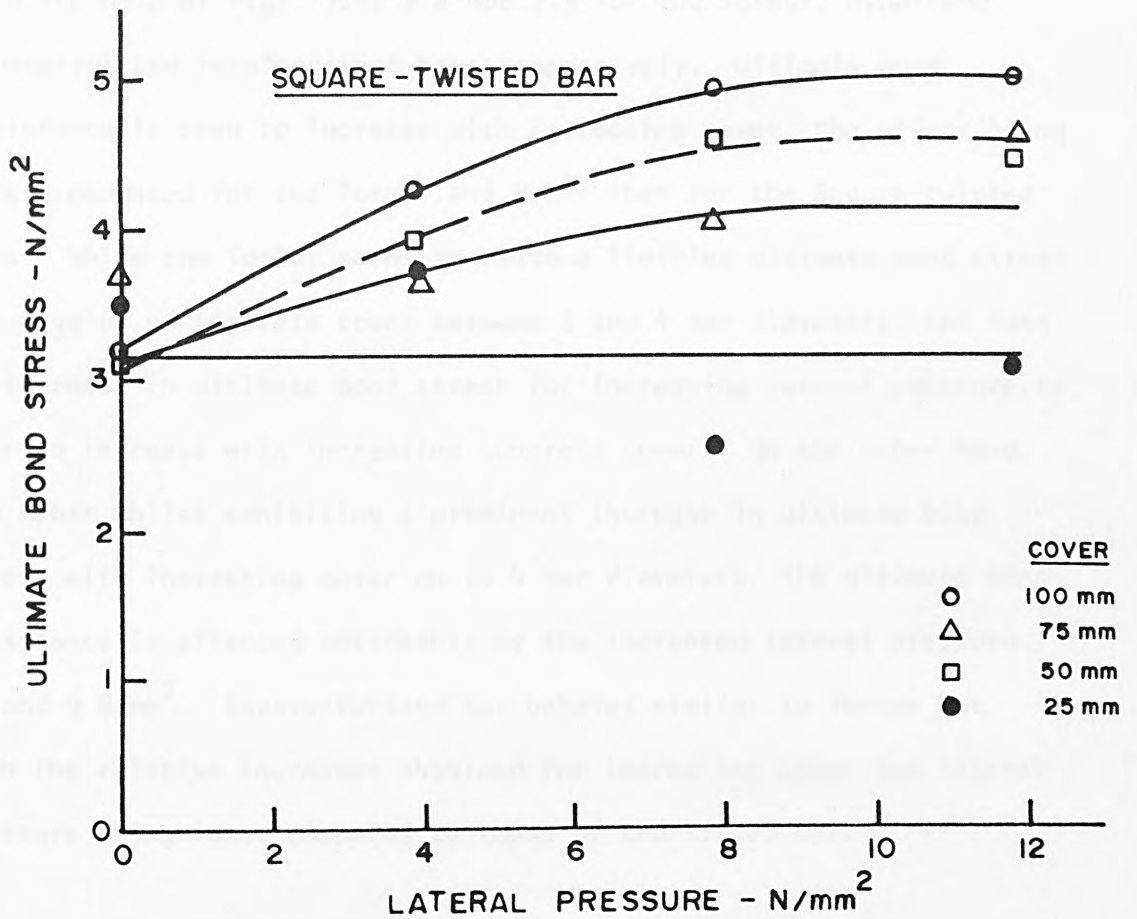


FIG. 7.6 VARIATION OF ULTIMATE BOND STRESS WITH LATERAL PRESSURE - SQUARE - TWISTED BAR

and a plough-through shear of the reinforcement bar through the concrete. Robin and Standish (65) have also suggested in a recent study that the pull-out mechanism for deformed bars under lateral pressure be considered at two distinct stages, namely splitting of the concrete cover for lateral pressures of up to approximately 10 N/mm^2 (30 percent of the test cube strength of 33 N/mm^2) and secondly the shearing type of failure of the concrete matrix for greater lateral pressures.

7.2.4 Interaction between concrete cover and lateral pressure

A study of the combined effects of varying the concrete cover and the intensity of the lateral compression on ultimate bond stress is made with the help of Figs. 7.7, 7.8 and 7.9 for the Torbar, Hybar and Square-twisted reinforcement bars respectively. Ultimate bond resistance is seen to increase with increasing cover, the effect being more pronounced for the Torbar and Hybar than for the Square-twisted bars. While the Torbar seems to reach a limiting ultimate bond stress for a value of concrete cover between 3 and 4 bar diameters, the rate of increase in ultimate bond stress for increasing lateral pressure is seen to increase with increasing concrete cover. On the other hand, the Hybar whilst exhibiting a prominent increase in ultimate bond stress with increasing cover up to 4 bar diameters, the ultimate bond resistance is affected noticeably by the increased lateral pressure beyond 9 N/mm^2 . Square-twisted bar behaves similar to Torbar but with the relative increases obtained for increasing cover and lateral pressure being lower compared to those of the ribbed bar.

The interaction surfaces suggest that, of the two variables, the concrete cover has a more marked effect on ultimate bond stress

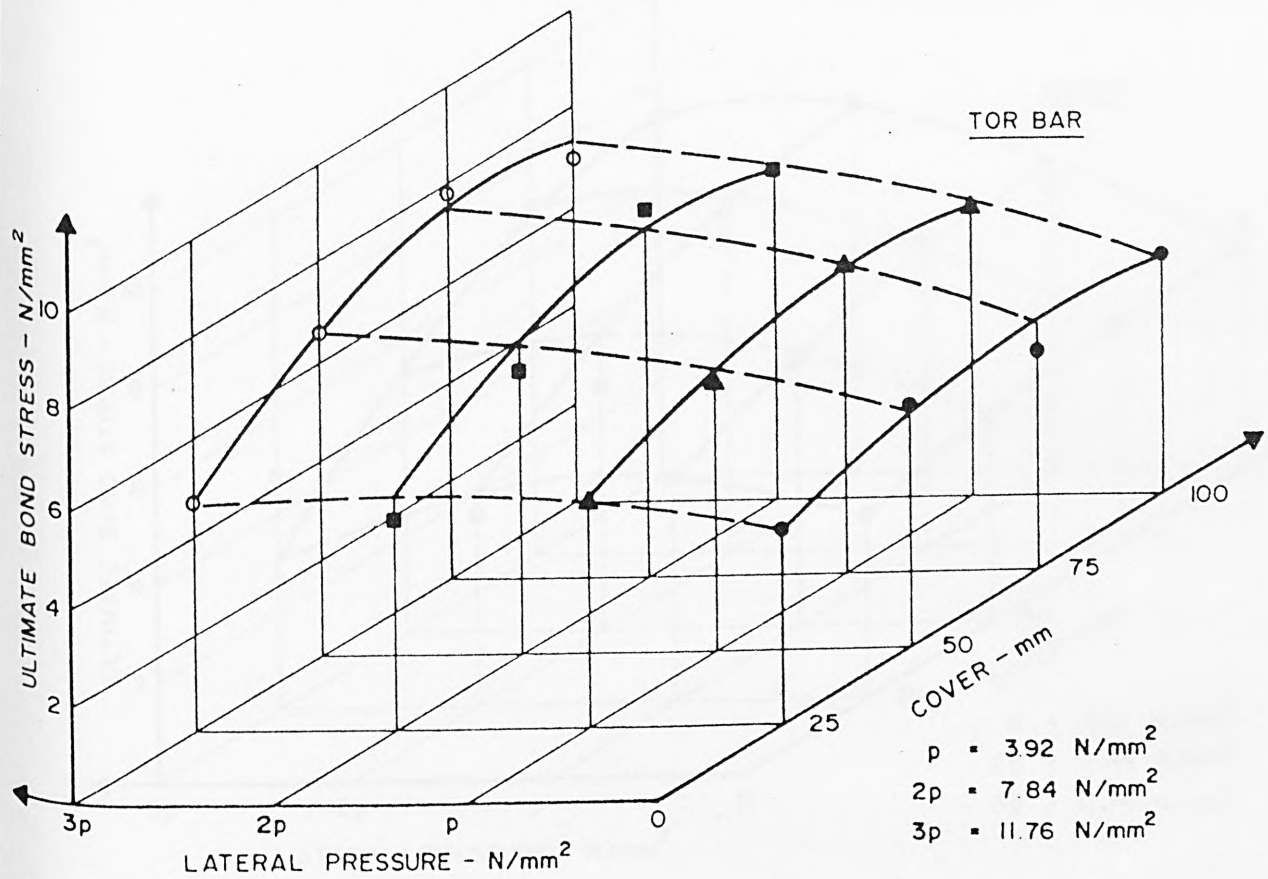
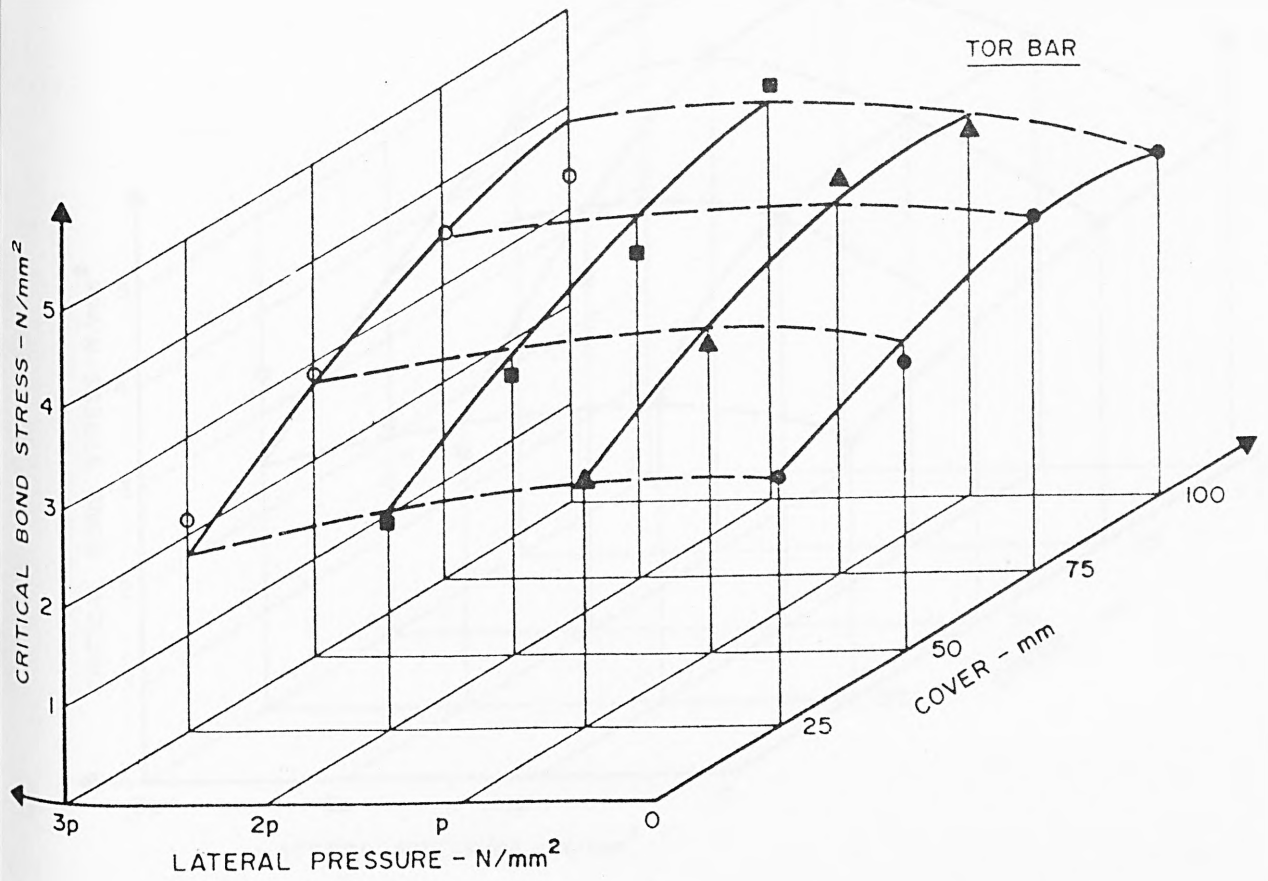


FIG. 7.7 VARIATION OF BOND STRESS WITH COVER AND LATERAL PRESSURE (Top) CRITICAL BOND STRESS, (Bottom) ULTIMATE BOND STRESS.

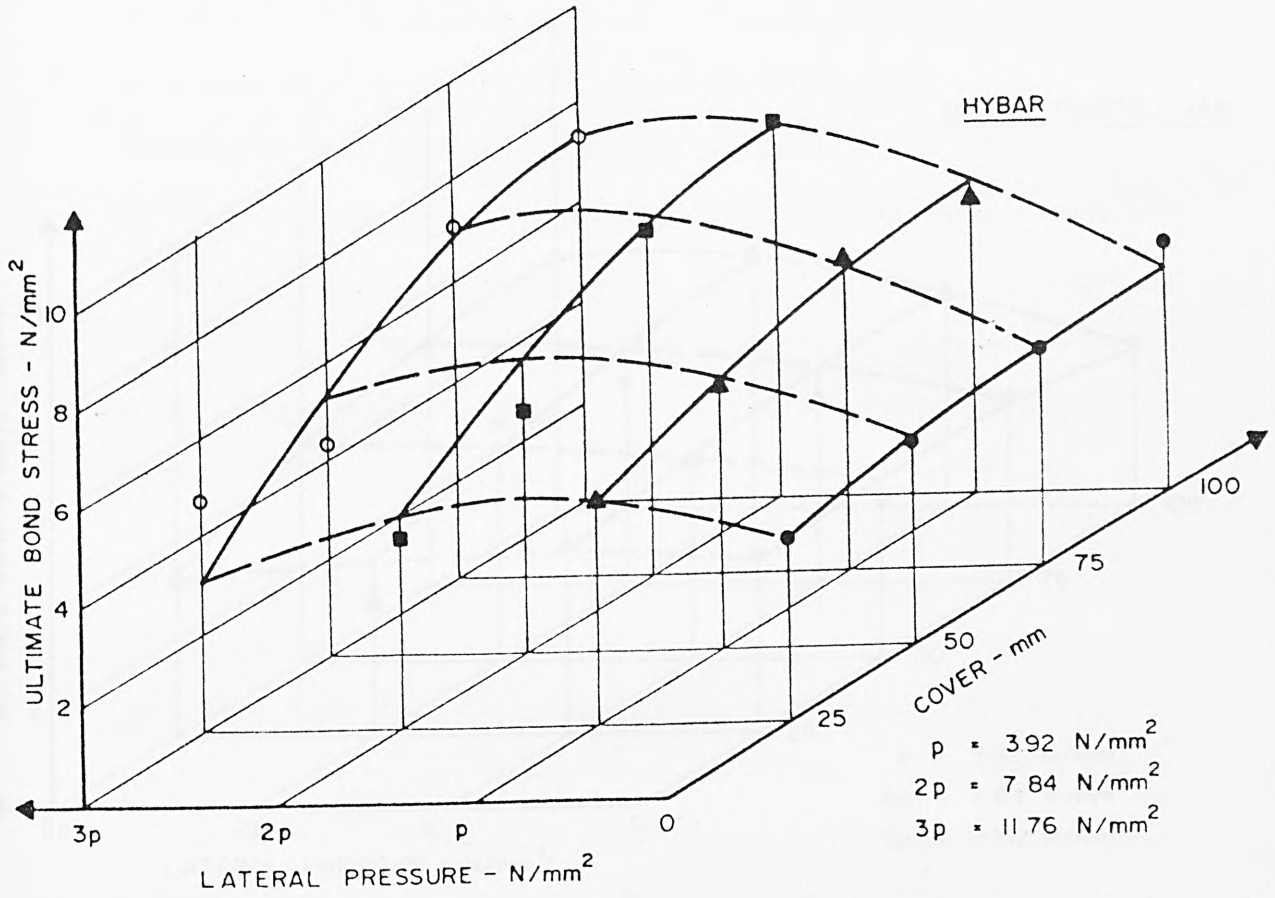
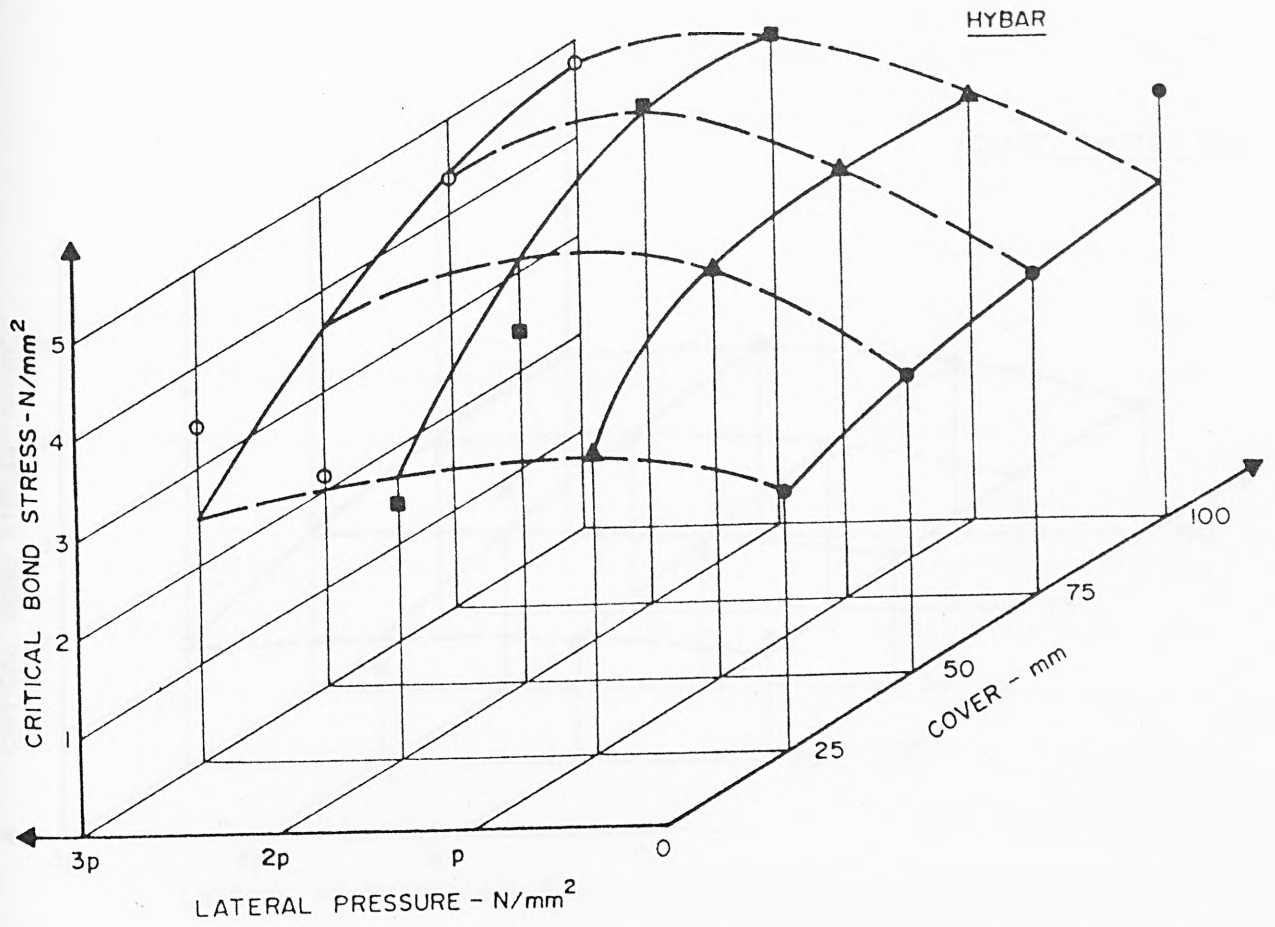
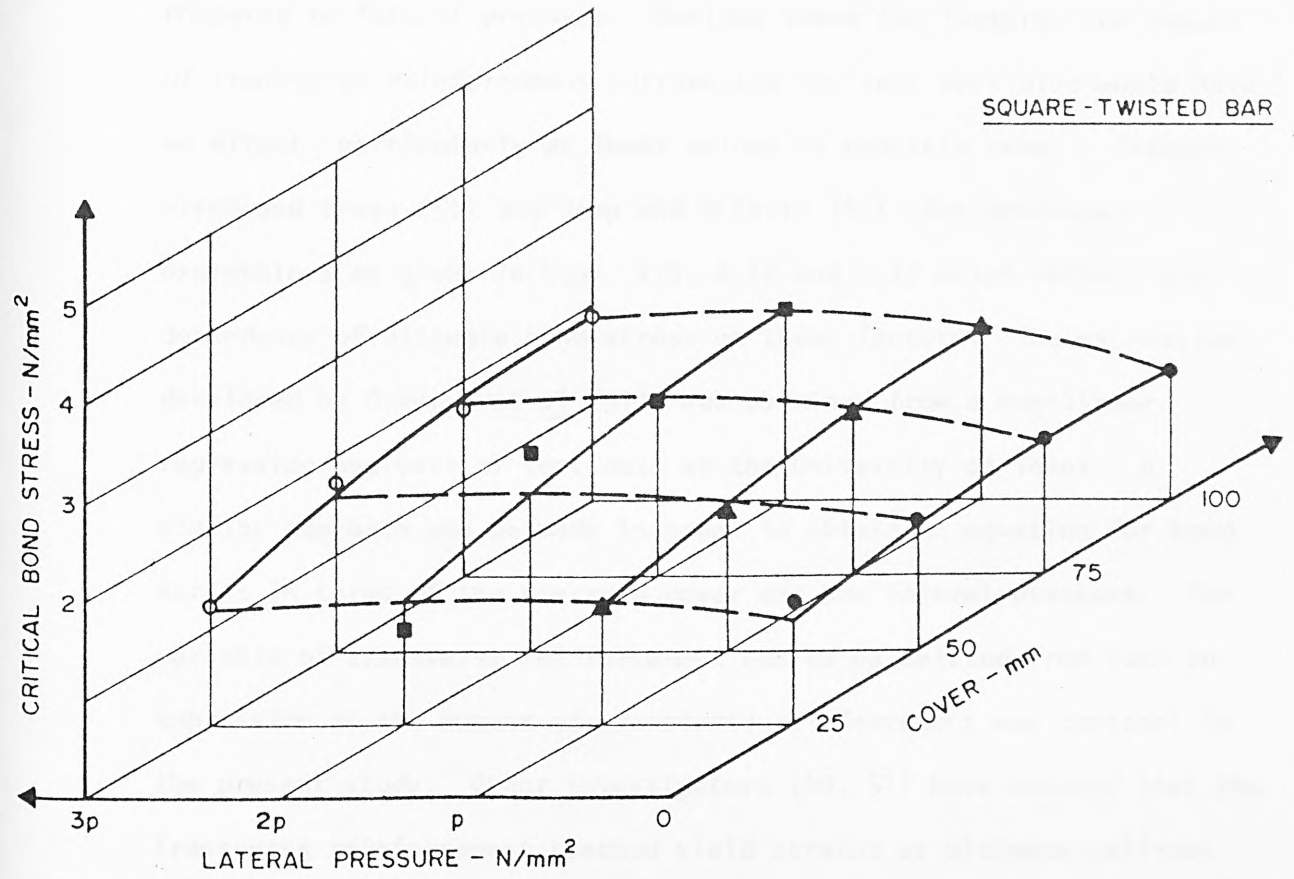


FIG. 78 VARIATION OF BOND STRESS WITH COVER AND LATERAL PRESSURE (Top) CRITICAL BOND STRESS, (Bottom) ULTIMATE BOND STRESS

SQUARE - TWISTED BAR



SQUARE - TWISTED BAR

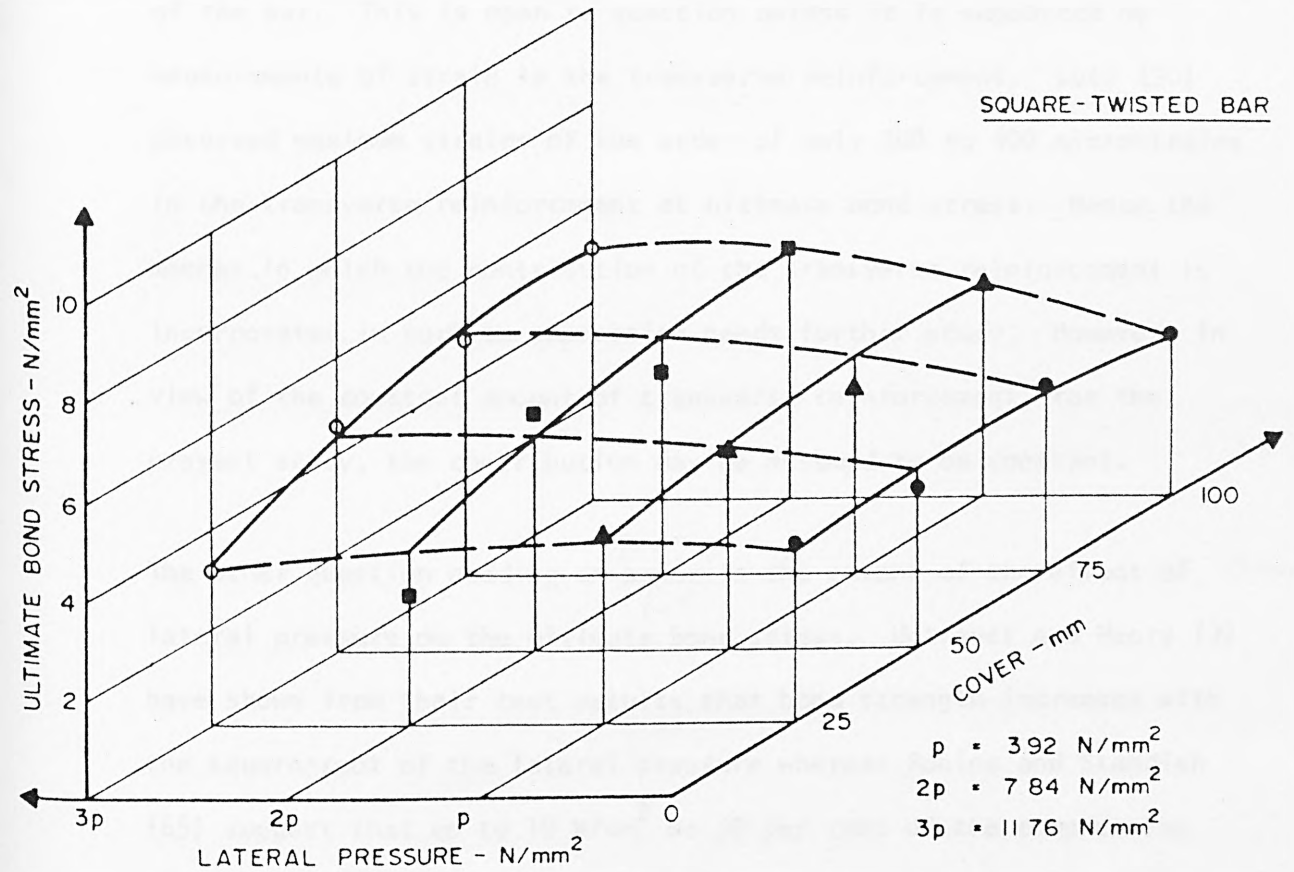


FIG 7.9 VARIATION OF BOND STRESS WITH COVER AND LATERAL PRESSURE (Top) CRITICAL BOND STRESS, (Bottom) ULTIMATE BOND STRESS

compared to lateral pressure. Besides these two factors, the amount of transverse reinforcement surrounding the test bars also would have an effect particularly at lower values of concrete cover. Orangun, Jirsa and Breen (51) and Kemp and Wilhelm (40) have developed expressions as given in Eqns. 2.9, 2.12 and 2.15 which reflect the dependence of ultimate bond stress on these factors. The expression developed by Orangun et al (51) was obtained from a non-linear regression analysis of test data at the University of Texas. A similar approach may be made in order to obtain an equation for bond stress in terms of the concrete cover and the lateral pressure. The variable of transverse reinforcement has to be deleted from such an expression as the amount of transverse reinforcement was constant in the present study. Other investigators (40, 51) have assumed that the transverse reinforcement reached yield strains at ultimate pull-out of the bar. This is open to question unless it is supported by measurements of strain in the transverse reinforcement. Lutz (50) observed maximum strains of the order of only 300 to 400 microstrains in the transverse reinforcement at ultimate bond stress. Hence the manner in which the contribution of the transverse reinforcement is incorporated in such an expression needs further study. However, in view of the constant amount of transverse reinforcement, for the present study, the contribution may be assumed to be constant.

The other question needing an ~~answer~~ answer is the extent of the effect of lateral pressure on the ultimate bond stress. Untrauer and Henry (7) have shown from their test results that bond strength increases with the square-root of the lateral pressure whereas Robins and Standish (65) suggest that up to 10 N/mm^2 or 30 per cent of the compressive strength of concrete, the bond strength increases directly with the

lateral pressure. The test results obtained in the present study were tested for both forms of variation of lateral pressure using a multiple linear regression equation and the results gave a better fit for the square-root of normal pressure criteria. However, it must be mentioned that the quantum of increase due to lateral pressure was not sufficient to favour either of the criteria very strongly. The equation may therefore be given in the form :

$$\frac{f_{bu}}{f_t} = X_1 + X_2 \cdot \frac{C}{D} + X_3 \sqrt{p} \quad \dots \quad (7.1)$$

where X_1, X_2, X_3 = experimental constants

f_{bu} = ultimate bond stress, N/mm^2

f_t = splitting tensile strength of concrete, N/mm^2

C = concrete cover, mm

D = diameter of test bar, mm

p = lateral pressure applied, N/mm^2

Based on the observations made in 7.2.2 of this study, equation (7.1) in fact has to be limited to concrete covers up to 3.5 bar diameters, but in the absence of experimental results with cover of 3.5 bar diameters, the equation would be extended to results of 4 bar diameters cover.

The ratios of the ultimate bond stress to splitting tensile stress values are given in Table 7.6. The values obtained for X_1, X_2 and X_3 by a multiple linear regression analysis for the three types of reinforcement are tabulated in Table 7.7 together with the values of the correlation coefficient. The value of the correlation coefficient is a measure of the compatibility between the experimental data and the

Torbar

Cover (mm)	Lateral pressure - N/mm ²			
	0	3.92	7.84	11.76
100	1.72	2.05	2.33	2.48
75	1.60	2.22	2.63	2.77
50	1.77	1.93	2.03	2.32
25	1.39	1.60	1.50	1.62

Hybar

Cover (mm)	Lateral pressure - N/mm ²			
	0	3.92	7.84	11.76
100	1.76	2.09	2.67	2.58
75	1.58	2.25	2.46	2.52
50	1.47	1.88	1.75	1.50
25	1.31	1.61	1.36	1.66

Square-twisted

Cover (mm)	Lateral pressure - N/mm ²			
	0	3.92	7.84	11.76
100	1.14	1.52	1.77	1.78
75	1.33	1.29	1.45	1.67
50	1.12	1.40	1.66	1.59
25	1.27	1.32	0.90	1.10

TABLE 7.6 : RATIO OF $\frac{\text{ULTIMATE BOND STRESS}}{\text{SPLITTING TENSILE STRESS}}$

Type of bar	X_1	X_2	X_3	Multiple Correlation Coefficient
Torbar	1.06610	0.21450	0.19252	0.84010
Hybar	0.83356	0.29225	0.16513	0.87487
Square-twisted	0.90781	0.12075	0.08998	0.71238

TABLE 7.7 : CORRELATION OF EXPERIMENTAL VALUES OF ULTIMATE BOND STRESS

prediction. The values obtained seem satisfactory in view of the wide scatter of data obtained in reinforced concrete in general and bond studies in particular. Kemp and Wilhelm (40) justified a correlation coefficient of 0.772 for the same reasons. Here again, the Square-twisted bar has more values falling away from the regression line than the other two bars.

The values of the coefficients X_2 and X_3 suggest that Hybar depends more than the Torbar on the concrete cover in deriving its bond resistance whereas the Torbar seems to be able to develop greater bond resistance under lateral pressure than Hybar. The pronounced effect of cover on Hybar is expected in view of its tendency to crack the concrete cover due to its heavier ribs compared to those on Torbar.

An overall view of the effects of cover and lateral pressure by comparing the bond resistance values at various concrete covers and lateral pressures to a base value of bond resistance is useful. This base value is taken as the bond resistance that would be manifested at the maximum concrete cover used in the tests, namely 4 bar diameters. Literature and the present study have shown that concrete covers exceeding 3.5 bar diameters do not influence the ultimate bond resistance. The ratios of the ultimate bond stress f_{bu} to the ultimate bond stress at cover of 4 bar diameters and zero lateral pressure are tabulated in Table 7.8 (b) for the three types of bars.

The Torbar and Hybar develop about 45 to 60 per cent more resistance with increased lateral pressure where the cover is more than 3 bar diameters but the increase drops to lesser values with 2 bar diameters. The Square-twisted bars record improved bond resistance with increased lateral pressure for concrete covers of 2 bar diameters and above

Type of bar	Pressure N/mm ²		0	3.92	7.84	11.76
	Cover (mm)					
Torbar	100		1.00	1.04	1.16	0.91
	75		1.02	1.12	0.91	0.98
	50		0.81	0.86	0.78	0.78
	25		0.70	0.69	0.58	0.59
Hybar	100		1.00	0.99	1.14	1.08
	75		0.75	1.00	1.16	1.00
	50		0.67	0.94	0.81	0.48
	25		0.58	0.69	0.59	0.77
Square- twisted	100		1.00	1.31	1.48	1.44
	75		1.09	1.27	1.35	1.32
	50		1.02	1.09	1.56	1.33
	25		0.96	0.90	0.73	0.94

(a) Ratio of $\frac{f_b}{f_{bo}}$

Type of bar	Pressure N/mm ²		0	3.92	7.84	11.76
	Cover (mm)					
Torbar	100		1.00	1.20	1.36	1.44
	75		0.93	1.30	1.53	1.61
	50		1.03	1.13	1.18	1.35
	25		0.81	1.74	0.87	0.95
Hybar	100		1.00	1.18	1.51	1.46
	75		0.90	1.28	1.39	1.43
	50		0.83	1.07	0.99	0.85
	25		0.74	0.91	0.77	0.85
Square- twisted	100		1.00	1.33	1.55	1.56
	75		1.17	1.13	1.27	1.46
	50		0.98	1.23	1.46	1.39
	25		1.10	1.15	0.79	0.97

(b) Ratio of $\frac{f_{ub}}{f_{ubo}}$

TABLE 7.8 : RATIOS OF BOND STRESSES WITH DIFFERENT COVERS AND LATERAL PRESSURES

ranging from 40 to 55 per cent. It is also noticed that Torbar and Square-twisted bars perform satisfactorily in ultimate bond provided the concrete cover is at least 2 bar diameters. The Hybar seems to perform less efficiently at 2 bar diameters compared to the other two.

7.3 Critical Bond Stress

As already stated, bond failure has been defined as occurring at a free-end slip of 0.1 mm. The bar force at 0.1 mm free-end slip as obtained from load-slip curves for the three types of bars are tabulated in Tables 7.9 to 7.11. Each specimen yielded two results and these were averaged and normalised for the concrete strength of 35 N/mm^2 . The normalised bar forces and the corresponding critical bond stress values are given in Table 7.12.

7.3.1 Effect of location of bars

Tables 7.9 to 7.11 give the ratio of the average bar forces at 0.1 mm slip in top and bottom cast bars for the various concrete covers and lateral pressures for the three types of reinforcement bars. The reductions observed for the top cast bars were about 19 and 23 per cent for the Torbar and Hybar respectively whereas Square-twisted bars show a reduction of about 33 per cent. Considering these together with the reductions observed for the three types of bars at ultimate bond stress, it may be concluded that the ribbed bars perform better than the Square-twisted bars in bond when placed at the top of a structural member.

7.3.2 Effect of cover

Figures 7.10 to 7.12 show the variation of critical bond stress with increasing cover from one bar diameter to 4 bar diameters. It is seen

Cover (mm)	Location of Bar	Lateral Pressure - N/mm ²			
		0	3.92	7.84	11.76
100	Top	23.0;30.5	19.0;28.0	18.0;19.0	14.0;20.0
	Bottom	27.0;30.0	29.0;30.0	29.6;36.0	24.5;27.0
	Av. Top	26.75	23.5	18.5	17.0
	Av. Bottom	28.50	29.5	32.75	25.75
	Ratio Top: Bottom	0.94	0.80	0.56	0.66
75	Top	33.0;33.0	23.8;29.2	13.5;17.5	12.0;17.5
	Bottom	28.5;29.0	28.0;35.0	24.5;26.0	24.5;29.7
	Av. Top	33.0	26.5	15.5	14.75
	Av. Bottom	28.75	31.5	25.25	27.1
	Ratio Top: Bottom	1.15	0.84	0.61	0.54
50	Top	16.5;19.0	16.5;19.0	20.7;21.0	18.5;22.0
	Bottom	20.0;24.5	22.0;25.5	20.0;25.0	20.0;25.0
	Av. Top	17.75	17.75	20.85	20.25
	Av. Bottom	22.25	23.75	22.5	22.5
	Ratio Top: Bottom	0.80	0.75	0.93	0.90
25	Top	15.0;17.5	16.0;17.5	13.5;15.0	13.2;15.8
	Bottom	18.25;19.0	18.0;19.0	15.5;17.7	16.2;17.5
	Av. Top	16.25	16.75	14.25	14.50
	Av. Bottom	18.63	18.5	16.6	16.85
	Ratio Top: Bottom	0.87	0.91	0.86	0.86

TABLE 7.9 : BAR FORCE AT 0.1 MM SLIP - TORBAR - KN

Cover (mm)	Location of Bar	Lateral Pressure - N/mm ²			
		0	3.92	7.84	11.76
100	Top	25.0;27.0	25.2;25.6	15.0;23.8	22.0;26.2
	Bottom	32.2;37.0	28.5;42.0	37.0;44.5	32.5;45.5
	Av. Top	26.0	25.4	19.4	24.1
	Av. Bottom	34.6	35.25	40.75	37.5
	Ratio Top: Bottom	0.75	0.72	0.48	0.64
75	Top	23.5;32.8	16.5;25.2	10.5;19.5	26.5;28.5
	Bottom	26.0;26.0	30.0;39.5	40.0;40.2	30.0;39.5
	Av. Top	28.15	20.35	15.0	27.5
	Av. Bottom	25.0	34.75	40.1	34.75
	Ratio Top: Bottom	1.08	0.59	0.37	0.79
50	Top	23.5;25.6	23.0;27.5	23.0;23.2	14.4;18.0
	Bottom	20.5;27.0	31.5;32.0	22.0;32.5	15.0;19.5
	Av. Top	24.55	25.25	23.1	16.2
	Av. Bottom	23.75	31.75	27.25	17.25
	Ratio Top: Bottom	1.03	0.80	0.85	0.94
25	Top	25.0;24.5	24.50;24.20	9.5;12.5	12.0;12.5
	Bottom	21.6;18.6	25.0; 22.5	17.0;22.5	24.5;27.5
	Av. Top	24.75	24.35	11.0	12.25
	Av. Bottom	20.10	23.75	19.75	26.0
	Ratio Top: Bottom	1.23	1.03	0.56	0.47

TABLE 7.10 : BAR FORCE AT 0.1 MM SLIP - HYBAR - kN

Cover (mm)	Location of Bar	Lateral Pressure - N/mm ²			
		0	3.92	7.84	11.76
100	Top	7.5; 9.5	11.0;15.0	13.5;19.0	13.0;19.2
	Bottom	17.0;24.5	26.5;28.0	31.0;32.5	39.5;32.5
	Av. Top	8.5	13.0	16.25	16.1
	Av. Bottom	20.75	27.25	31.75	31.0
	Ratio Top:				
	Bottom	0.41	0.48	0.51	0.52
75	Top	11.0;16.0	19.0;19.0	19.0;19.5	18.5;19.5
	Bottom	22.5;23.5	26.0;27.5	22.0;35.0	26.2;29.5
	Av. Top	13.50	19.0	19.25	19.0
	Av. Bottom	23.0	26.75	28.5	27.85
	Ratio Top:				
	Bottom	0.59	0.71	0.68	0.68
50	Top	16.0;19.0	16.0;20.0	25.5;25.8	14.5;20.0
	Bottom	19.2;23.5	18.5;27.2	33.5;34.5	25.0;33.2
	Av. Top	17.5	18.0	25.65	17.25
	Av. Bottom	21.35	22.85	34.0	29.1
	Ratio Top:				
	Bottom	0.82	0.79	0.75	0.59
25	Top	10.0;13.0	11.5;15.5	11.5;13.0	5.5; 9.8
	Bottom	20.0;20.0	17.4;20.0	12.8;18.8	15.5;25.5
	Av. Top	11.5	13.5	12.25	7.65
	Av. Bottom	20.0	18.7	15.8	20.5
	Ratio Top:				
	Bottom	0.58	0.72	0.78	0.37

TABLE 7.11 : BAR FORCE AT 0.1 MM SLIP - SQUARE TWISTED BAR-KN

Torbar

Cover (mm)	Force at 0.1mm slip(corrected)-kN				Critical bond stress - N/mm ²			
	p=0	p=3.92	p=7.84	p=11.76	p=0	p=3.92	p=7.84	p=11.76
100	28.77	29.78	33.38	26.27	3.64	3.76	4.21	3.32
75	29.30	32.10	26.15	28.06	3.70	4.06	3.31	3.55
50	23.26	24.83	22.56	22.56	2.94	3.14	2.85	2.85
25	20.09	19.95	16.76	17.04	2.54	2.52	2.12	2.15

Hybar

Cover (mm)	Force at 0.1mm slip(corrected)-kN				Critical bond stress - N/mm ²			
	p=0	p=3.92	p=7.84	p=11.76	p=0	p=3.92	p=7.84	p=11.76
100	34.71	34.32	39.67	37.62	4.39	4.34	5.01	4.76
75	25.92	34.79	40.14	34.65	3.28	4.40	5.07	4.38
50	23.30	32.62	27.99	16.80	2.95	4.12	3.54	2.12
25	20.20	23.87	20.36	26.81	2.55	3.02	2.57	3.39

Square-twisted

Cover (mm)	Force at 0.1mm slip(corrected)-kN				Critical bond stress - N/mm ²			
	p=0	p=3.92	p=7.84	p=11.76	p=0	p=3.92	p=7.84	p=11.76
100	20.93	27.49	30.90	30.17	2.52	3.32	3.73	3.64
75	22.85	26.58	28.21	27.57	2.76	3.21	3.40	3.32
50	21.25	22.74	32.59	27.89	2.56	2.74	3.93	3.36
25	20.12	18.81	15.18	19.70	2.43	2.27	1.83	2.38

Note: p in units of N/mm²

TABLE 7.12 : CRITICAL BOND STRESS UNDER LATERAL PRESSURE
(BOTTOM CAST BARS)

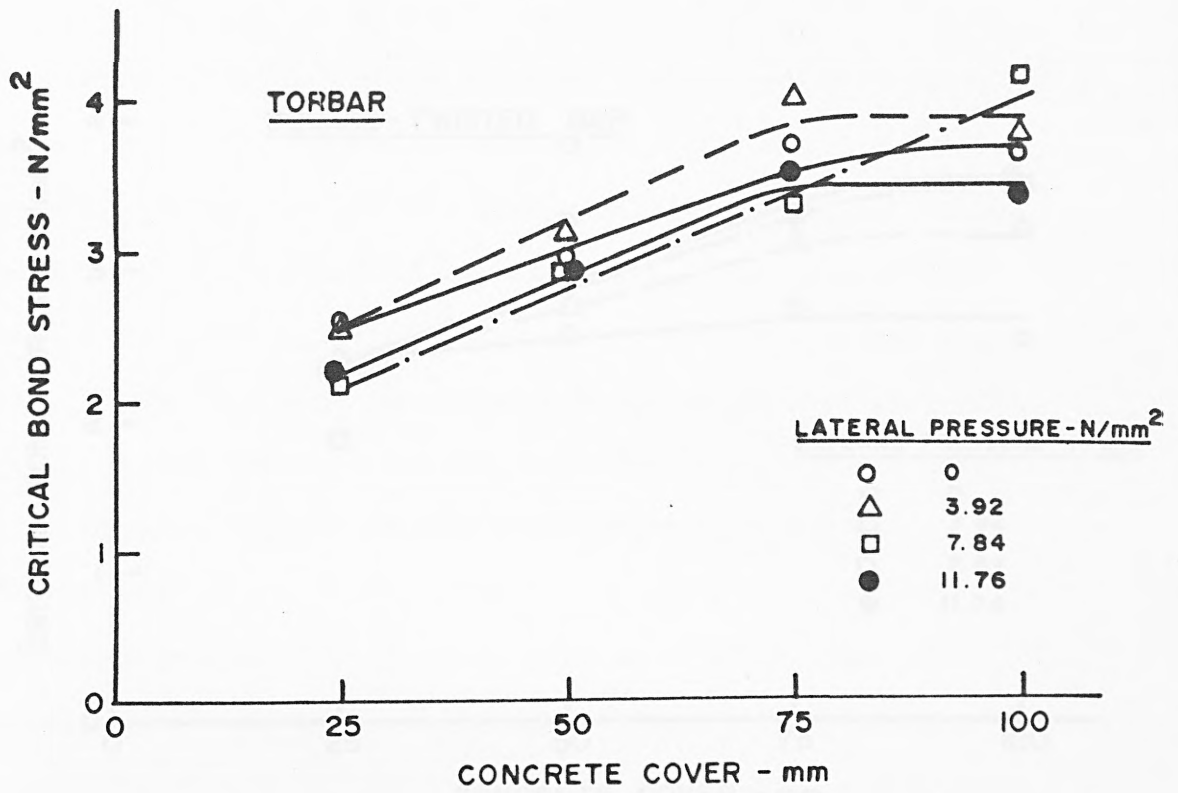


FIG. 7.10 VARIATION OF CRITICAL BOND STRESS WITH CONCRETE COVER - TORBAR

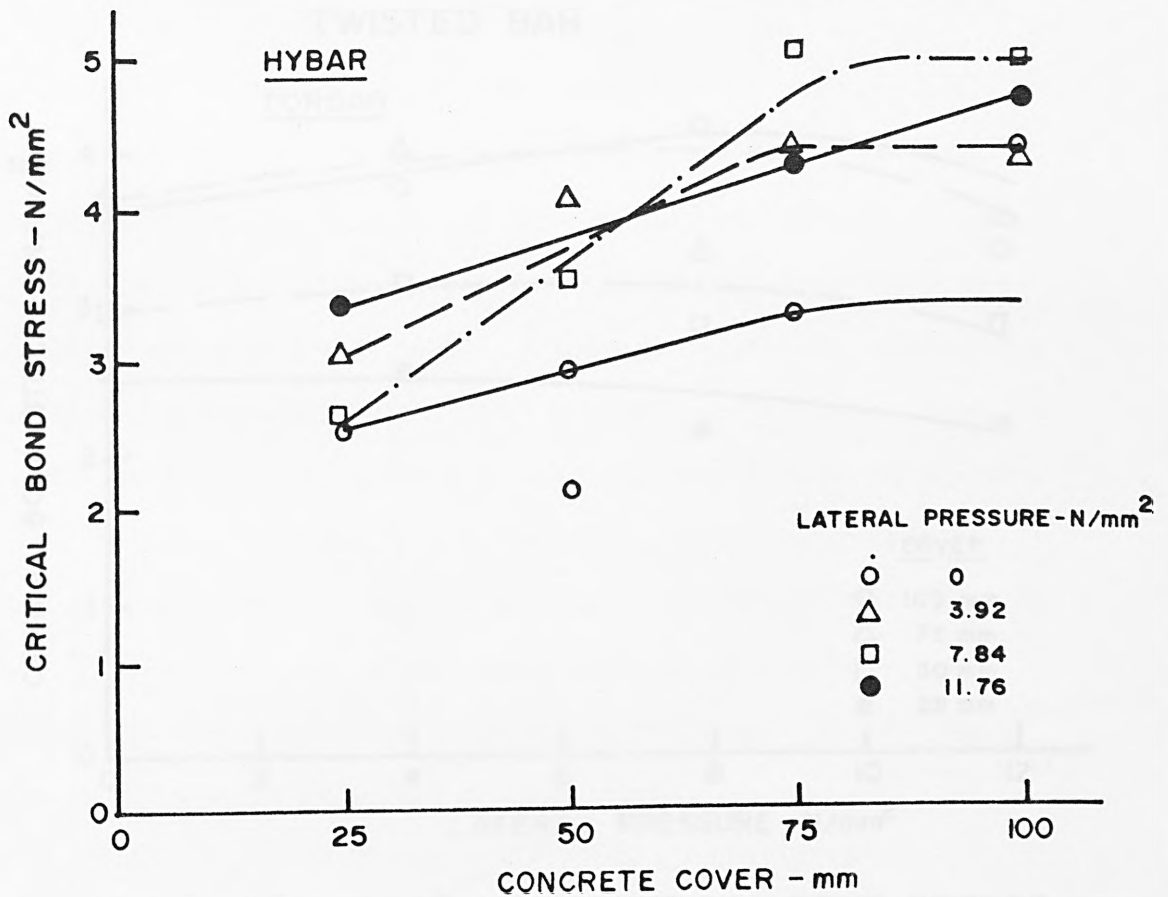


FIG. 7.11 VARIATION OF CRITICAL BOND STRESS WITH CONCRETE COVER - HYBAR

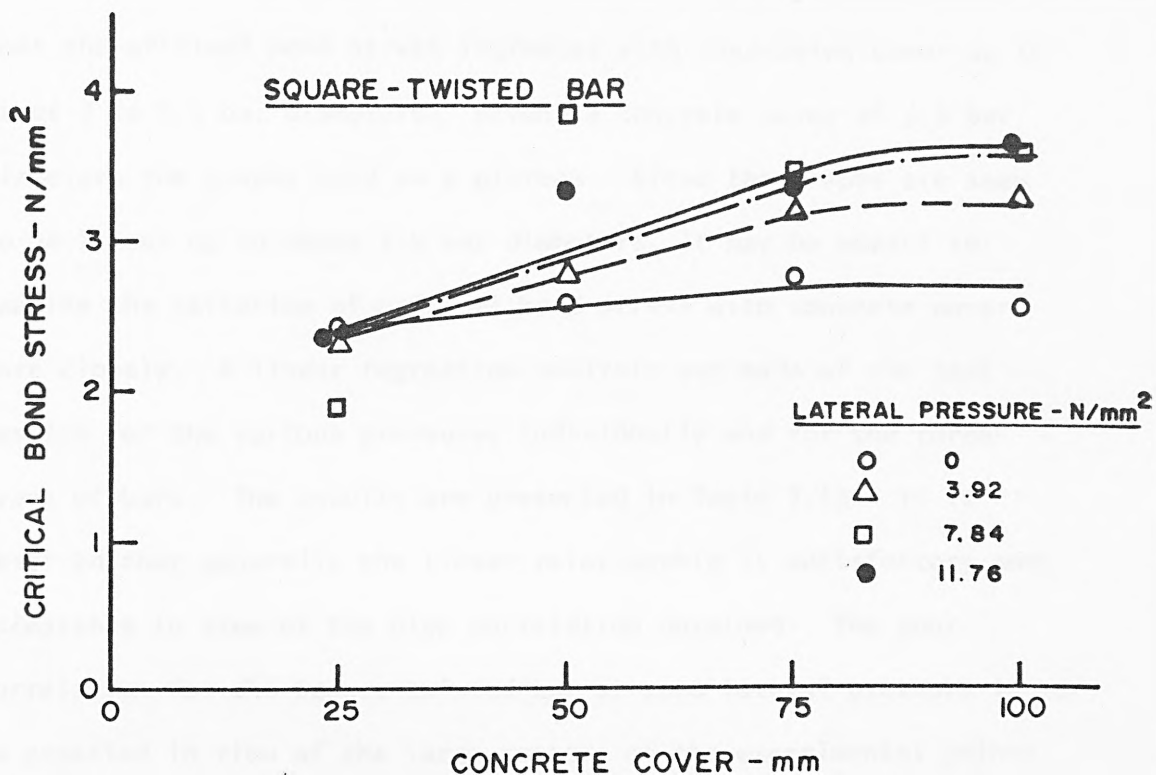


FIG. 7.12 VARIATION OF CRITICAL BOND STRESS WITH CONCRETE COVER - SQUARE-TWISTED BAR

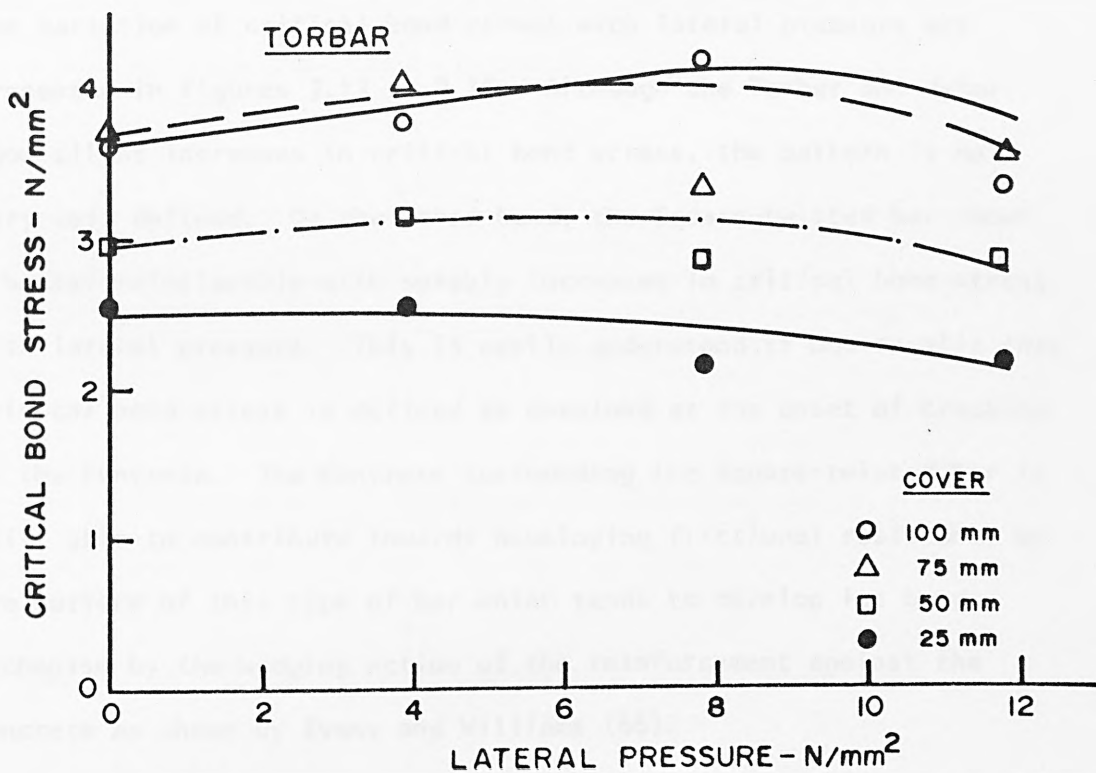


FIG. 7.13 VARIATION OF CRITICAL BOND STRESS WITH LATERAL PRESSURE - TORBAR

that the critical bond stress increases with increasing cover up to about 3 to 3.5 bar diameters. Beyond a concrete cover of 3.5 bar diameters the graphs tend to a plateau. Since the graphs are seen to be linear up to about 3.5 bar diameters, it may be useful to examine the variation of critical bond stress with concrete cover more closely. A linear regression analysis was made of the test results for the various pressures individually and for the three types of bars. The results are presented in Table 7.13. It is observed that generally the linear relationship is satisfactory and acceptable in view of the high correlation obtained. The poor correlation for the Square-twisted bar at zero lateral pressure is to be expected in view of the large scatter of the experimental points in this case.

7.3.3 Effect of lateral pressure

The variation of critical bond stress with lateral pressure are presented in Figures 7.13 to 7.15. Although the Torbar and Hybar show slight increases in critical bond stress, the pattern is not very well defined. On the other hand, the Square-twisted bar shows a better relationship with notable increases in critical bond stress with lateral pressure. This is easily understood if one recalls that critical bond stress is defined as obtained at the onset of cracking in the concrete. The concrete surrounding the Square-twisted bar is still able to contribute towards developing frictional resistance on the surface of this type of bar which tends to develop its bond mechanism by the wedging action of the reinforcement against the concrete as shown by Evans and Williams (66).

Tobar

Pressure (N/mm ²)	Constant Term	Regression Coefficient	Correlation Coefficient
0	0.785	0.145	0.9265
3.92	0.790	0.168	0.8743
7.84	0.515	0.242	0.9936
11.76	0.685	0.151	0.8816

Hybar

Pressure (N/mm ²)	Constant Term	Regression Coefficient	Correlation Coefficient
0	0.655	0.210	0.9597
3.92	1.04	0.154	0.8495
7.84	0.655	0.319	0.9426
11.76	0.745	0.228	0.6950

Square-twisted

Pressure (N/mm ²)	Constant Term	Regression Coefficient	Correlation Coefficient
0	0.880	0.016	0.4051
3.92	0.705	0.131	0.9717
7.84	0.695	0.185	0.7008
11.76	0.795	0.137	0.8878

TABLE 7.13 : VARIATION OF CRITICAL BOND STRESS WITH COVER

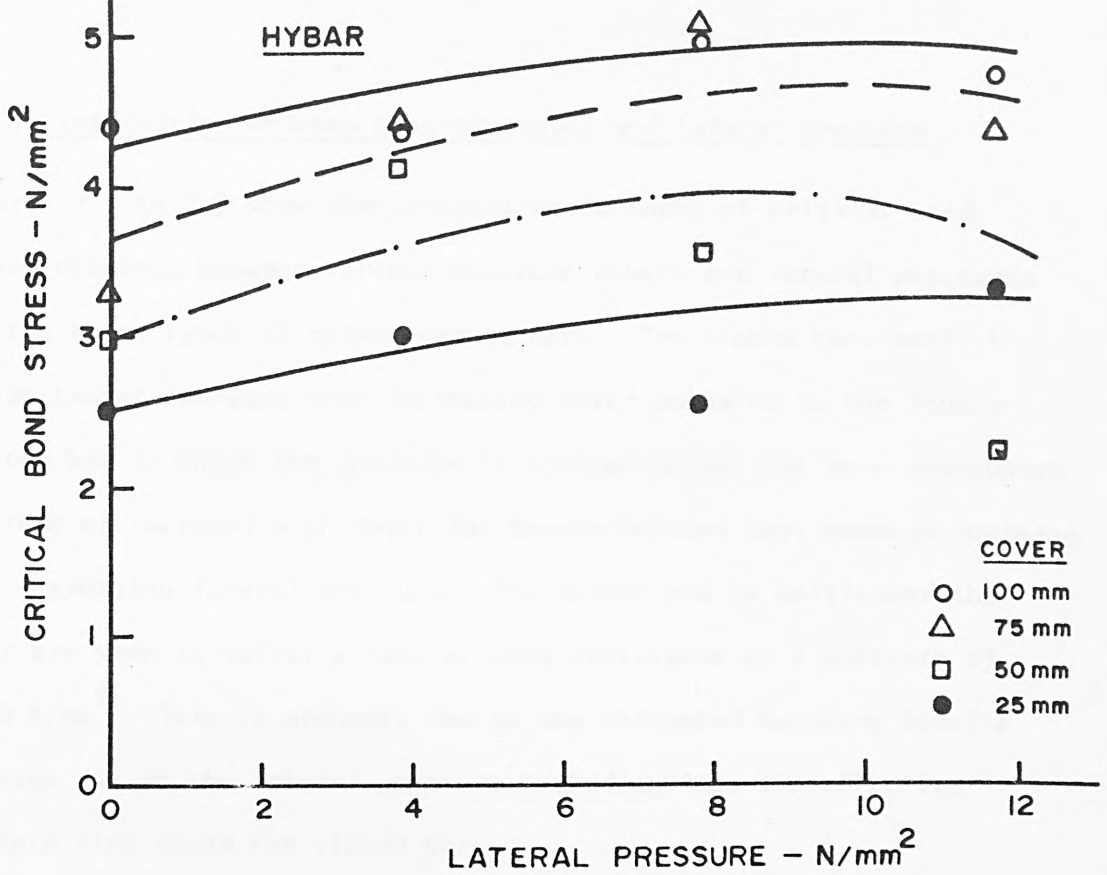


FIG. 7.14 VARIATION OF CRITICAL BOND STRESS WITH LATERAL PRESSURE - HYBAR

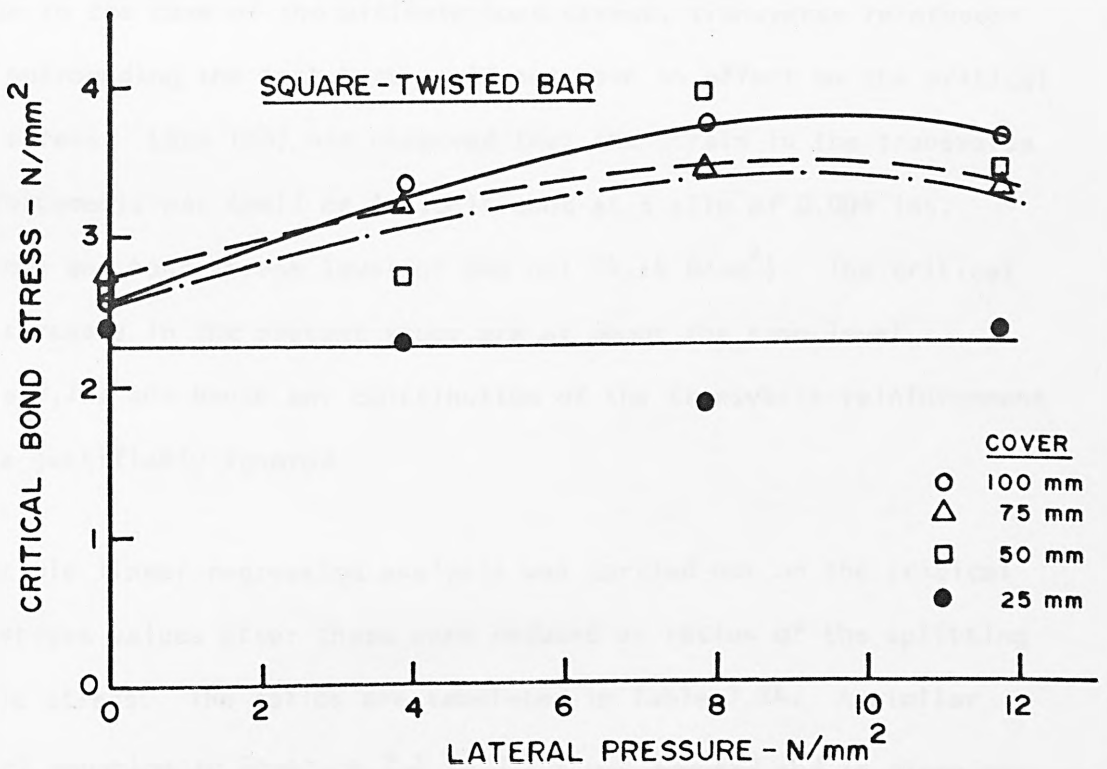


FIG. 7.15 VARIATION OF CRITICAL BOND STRESS WITH LATERAL PRESSURE - SQUARE-TWISTED BAR

7.3.4 Interaction between concrete cover and lateral pressure

Figures 7.7 to 7.9 show the interaction surfaces of critical bond stress obtained between various concrete covers and lateral pressures for the three types of reinforcement bars. The ribbed bars exhibit a significant increase with increasing cover compared to the Square-twisted bar in which the increase is noticeable but not very pronounced. The rate of increase with cover for Square-twisted bars seems to increase with increasing lateral pressure. The Torbar and in particular the Hybar are seen to suffer a loss of bond resistance at a pressure of 11.76 N/mm^2 . This is probably due to the increased bursting tensile stresses due to the lateral pressure extending into the effective concrete ring round the ribbed bars.

The interaction surfaces again suggest that of the two variables, the concrete cover affects more significantly the critical bond stress. Unlike in the case of the ultimate bond stress, transverse reinforcement surrounding the test bars would not have an effect on the critical bond stress. Lutz (50) has observed that the strain in the transverse reinforcements was small or insignificant at a slip of 0.004 ins. (0.1 mm) and bond stress level of 600 psi (4.14 N/mm^2). The critical bond stresses in the present study are at about the same level (Table 7.12) and hence any contribution of the transverse reinforcement can be justifiably ignored.

A multiple linear regression analysis was carried out on the critical bond stress values after these were reduced as ratios of the splitting tensile stress. The ratios are tabulated in Table 7.14. A similar form of equation to Equation 7.1 in 7.2.4 was adopted and is given as:

Tobar

Cover (mm)	Lateral pressure - N/mm ²			
	0	3.92	7.84	11.76
100	1.30	1.35	1.51	1.19
75	1.33	1.46	1.19	1.27
50	1.05	1.13	1.02	1.02
25	0.91	0.90	0.76	0.77

Hybar

Cover (mm)	Lateral pressure - N/mm ²			
	0	3.92	7.84	11.76
100	1.57	1.56	1.80	1.71
75	1.18	1.58	1.82	1.57
50	1.06	1.48	1.27	0.76
25	0.91	1.08	0.92	1.22

Square-twisted

Cover (mm)	Lateral pressure - N/mm ²			
	0	3.92	7.84	11.76
100	0.90	1.19	1.34	1.31
75	0.99	1.15	1.22	1.19
50	0.92	0.98	1.41	1.20
25	0.87	0.81	0.66	0.85

TABLE 7.14 : RATIO OF CRITICAL BOND STRESS/SPLITTING TENSILE STRESS

$$\frac{f_b}{f_t} = X_4 + X_5 \frac{C}{D} + X_6 \sqrt{p} \quad \dots \quad (7.2)$$

where X_4, X_5, X_6 = experimental constants

f_b = critical bond stress, N/mm^2

The values obtained from $X_4, X_5,$ and X_6 for the three types of reinforcement are tabulated in Table 7.15. Torbar and Hybar show better correlation compared to the Square-twisted bar. It is observed that X_6 has a negative value for Torbar suggesting that the lateral pressure was not beneficial. However, a reference to the interactive surface shows that the negative value may be caused by the results of the higher lateral pressures. Hence, an analysis was carried out excluding the results of the $11.76 N/mm^2$ pressure for all the three types of bars. The correlation obtained was better as shown by the values in parenthesis in Table 7.15. However, the coefficient X_6 for Torbar still remains negative though a much smaller value suggesting that the benefit derived from lateral pressure at critical bond stress is minimal although it is seen from the value of X_3 for Torbar in 7.2.4 that lateral pressure increases ultimate bond stress substantially compared to the other types of bars. A more detailed study needs to be carried out with Torbar in order to assess the quantitative contribution of lateral pressure to critical bond stress in view of the positive contribution from lateral pressure at ultimate limit state conditions.

The critical bond resistance developed by each type of bar at maximum concrete cover of 4 bar diameters and zero pressure was again adopted

Type of bar	X_4	X_5	X_6	Multiple Correlation Coefficient
Torbar	0.73747 (0.70813)*	0.17650 (0.18500)	-0.0213 (-0.00218)	0.89361 (0.90952)
Hybar	0.65938 (0.62049)	0.22775 (0.22767)	0.05572 (0.10220)	0.81208 (0.90667)
Square-twisted	0.62453 (0.63309)	0.11725 (0.11067)	0.07027 (0.07965)	0.75710 (0.71818)

* Values in parenthesis are after excluding results with pressure of 11.76 N/mm².

TABLE 7.15 : CORRELATION OF EXPERIMENTAL VALUES OF CRITICAL BOND STRESS

as the base value to compare the performance of the different bars with varying cover and lateral pressure. The ratios of critical bond stress to the base value are given in Table 7.8 (a). It is clearly seen from these values that Torbar and Hybar derived marginal benefit from increased lateral pressure only when the cover was 3 bar diameters or more and for values of lateral pressure below 9 N/mm^2 . The Square-twisted bars derived substantial benefit as much as about 48 per cent, and showed beneficial effects from a cover of 2 bar diameters to larger covers.

7.4 Comparison of experimental results with theory

An empirical theory has been proposed in 5.2.4 in order to help in the understanding of the bond behaviour of reinforcement bars under lateral compression. It has been suggested that the force developed in the reinforcement bar at bond failure i.e. at 0.1 mm slip is given by F of the form :

$$F = F_{cr} + F_{fr} \quad \dots \quad (7.3)$$

where F_{cr} = the force causing tensile cracking in the concrete surrounding the bar due to ring tension.

and F_{fr} = the frictional force resisting the slip of the bar from the concrete surrounding it.

The frictional component F_{fr} may be obtained by multiplying the radial force acting on the perimetral surface of the bar over the bonded length of 100 mm by the coefficient of friction between the surface of the bar and the concrete surrounding it. A value of 0.50 is used for the coefficient of friction between steel and concrete and the perimetral surface is taken based on the effective diameter of the

reinforcement bar which is obtained from its weight per unit length. It has been shown in 5.2.4 that the average radial pressure acting over the perimeter of the bar is half the lateral pressure applied in a diametral direction.

$$\text{i.e. } p_{av} = p/2$$

Therefore, the friction component of the force is given by

$$\begin{aligned} F_{fr} &= b_{fr} \times p_{av} \cdot \pi D \cdot L. \\ &= 0.5 \times p/2 \cdot \pi D \cdot L. \end{aligned} \quad \dots \quad (7.4)$$

In the present study, $L = 100 \text{ mm}$

$$\begin{aligned} \text{Hence } F_{fr} &= 0.5 \times p/2 \times \frac{\pi D \times 100}{1000} \text{ kN} \\ &= \frac{p \cdot \pi D}{40} \text{ kN} \end{aligned} \quad \dots \quad (7.5)$$

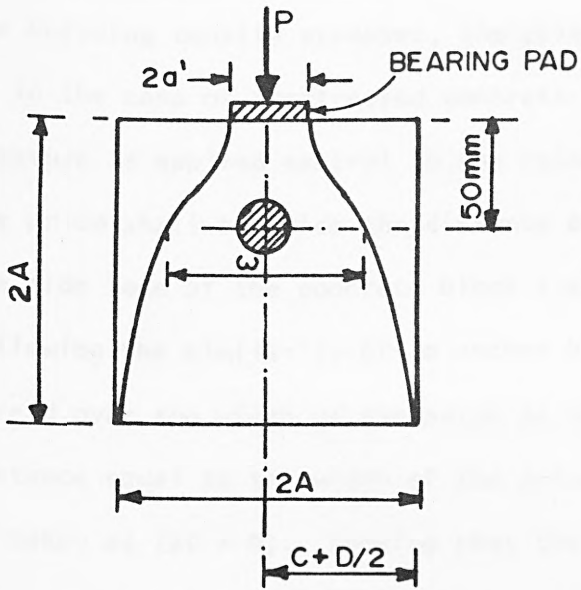
The contribution of the force required to cause tensile cracking depends on the tensile strength f_t of the concrete in the absence of lateral compression. However, when lateral compression is applied in one direction, this compression causes bursting tensile stresses to develop in a direction at right angles to the pressure as in anchor blocks in prestressed concrete. These tensile stresses cause cracking to develop in the concrete by reducing the effective tensile capacity of the concrete. The magnitude of these tensile bursting stresses have been interpolated from the curves given by Yettram and Robins in Reference 59 and are tabulated in Table 7.16. The pressure applied at the top of the concrete test block fans out over a wider breadth than the width of the bearing pad as shown in Fig. 7.16 and hence the pressure at the level of the bar depends on the width of dispersion of the vertical pressure lines. Work by Iyengar (59) and Yettram and

Cover (mm)	Width of prism (mm)	Width of bearing (mm)	Col.3 Col.2	Average σ_y/σ_x at 50 mm from top	Bursting tensile stress σ_{y2} due to vertical load -N/mm ²		
					19.6 kN	39.2 kN	58.8 kN
100	225	50	0.22	0.30	0.260	0.520	0.781
75	175	50	0.28	0.26	0.290	0.579	0.869
50	125	50	0.40	0.26	0.404	0.809	1.213
25	75	50	0.68	0.10	0.265	0.530	0.795

TABLE 7.16 : BURSTING TENSILE STRESSES AT LEVEL OF BAR

Cover (mm)	Distance to centre of bar (mm)	Width of prism (mm)	Effective width 'w' (mm)	Pressure due to vertical load at 50 mm depth - N/mm ²		
				2 ^T =19.6kN	4 ^T =39.2kN	6 ^T =58.8kN
100	113	225	119	1.65	3.29	4.94
75	88	175	111	1.77	3.53	5.30
50	63	125	98	2.0	4.0	6.0
25	37	75	72	2.72	5.44	8.17

TABLE 7.17 : PRESSURE AT LEVEL OF BAR DUE TO VERTICAL LOAD



- $A = C + D/2.$
- $\omega =$ EFFECTIVE WIDTH AT LEVEL OF BAR.
- $2a' =$ WIDTH OF BEARING PAD.
- $L =$ LENGTH OF BEARING PAD.
- $=$ EMBEDMENT LENGTH OF BAR.

FIG. 7.16 BURSTING STRESS DUE TO CONCENTRATED LOAD IN AN ANCHOR BLOCK



FIG. 7.17 LONGITUDINAL SECTIONAL PROFILE OF SQUARE-TWISTED BAR

Robins (60) have shown that these pressure lines follow a parabolic path. Based on the width of dispersion so obtained, the "effective pressure" at the level of the bar is calculated. In order to obtain the bursting tensile stresses, the prism of concrete must be defined as in the case of prestressed concrete anchor blocks. As the lateral pressure is applied central to the reinforcement bar, the width of the prism shall be twice the distance of the centre of the bar from the side face of the concrete block i.e. $2(C + D/2)$ or $(2C + D)$. Following the similarity of an anchor block, the curved pressure lines spread over the width of the prism as uniform vertical pressure at a distance equal to the width of the prism, i.e. the height of the prism is taken as $(2C + D)$. Knowing that the curved parabolic pressure lines originating from the bearing pad on which the load is applied becomes vertical pressure at a distance of $(2C + D)$ from their origins, the equation to these curved lines may be defined and subsequently the width of dispersion obtained. These are given in Table 7.17 together with the effective pressure at the level of the bar. Detailed sample calculations are given in Appendix D.

These values of effective pressure would be substituted for p in Equation 7.5 to obtain the frictional component F_{fr} .

Having obtained the bursting tensile stress, σ_y , the bond stress at cracking may be obtained from Equation (5.13) by substitution for f_t with the expression $(f_t - \sigma_y)$

Hence equation (5.13) becomes

$$f_b = (f_t - \sigma_y) \frac{(C + D/2)}{1.664D} \quad \dots \quad (7.6)$$

The force causing tensile cracking in the concrete surrounding the bar due to ring tension, F_{cr} is given by

$$F_{cr} = \pi D \cdot L \cdot (f_t - \sigma_y) \frac{(C + D/2)}{1.664D} \quad \dots \quad (7.7)$$

When $L = 100$ mm and f_t, σ_y are in N/mm^2

$$\begin{aligned} F_{cr} &= \frac{\pi D \cdot 100}{1000} (f_t - \sigma_y) \frac{(C + D/2)}{1.664D} \text{ kN} \\ &= \frac{\pi D}{10} \cdot (f_t - \sigma_y) \frac{(C + D/2)}{1.664D} \text{ kN} \quad \dots \quad (7.8) \end{aligned}$$

Therefore, the theoretical force at bond failure, F is given by

$$F = p \cdot \frac{\pi D}{40} + \frac{\pi D}{10} (f_t - \sigma_y) \frac{(C + D/2)}{1.664D} \text{ kN} \quad \dots \quad (7.9)$$

It has to be mentioned here that the effective value of $(C + D/2)$ to be taken in calculations is the dimension which gives the thinner concrete ring. For example, for the specimens with cover 25 mm, the distance of the centre of the bar from the side of the concrete block is 37 mm but 50 mm from the top of the block. Hence the dimension 37 mm governs and is taken as the external radius of the concrete ring. For all the other values of concrete cover, the distances of the centre of the bar are greater than the distance from the top of the block, and hence this dimension, namely 50 mm governs. The concrete ring in those cases is taken as having an external radius of 50 mm.

The values of F for the three types of reinforcement have been calculated and are compared with the values obtained at critical bond stress in the experiments. These are presented in Tables 7.18 to 7.20.

Cover (mm)	External Pressure (N/mm ²)	Calculated Bar Force - kN			Plough through Pull-out Force (kN)	Experimental Bar Force (kN)	Ratio of Col.7 ÷ Col.5
		Cracking Component F _{cr}	Friction Component F _{fr}	Total F			
100 (113)*	0	26.30	-	26.30	43.35	28.77	1.09
	3.92	23.84	3.24	27.08		29.78	1.10
	7.84	21.38	6.48	27.86		33.38	1.20
	11.76	18.92	9.72	28.64		26.27	0.92
75 (88)	0	26.30	-	26.30		29.30	1.11
	3.92	23.56	3.48	27.04		32.10	1.19
	7.84	20.81	6.95	27.76		26.15	0.94
	11.76	18.08	10.43	28.51		28.06	0.98
50 (63)	0	26.30	-	26.30		23.26	0.88
	3.92	22.48	3.94	26.42		24.83	0.94
	7.84	18.65	7.87	26.52		22.56	0.85
	11.76	14.83	11.81	26.64		22.56	0.85
25 (37)	0	19.72	-	19.72	20.09	1.02	
	3.92	17.85	5.35	23.20	19.95	0.86	
	7.84	15.96	10.71	26.67	16.76	0.63	
	11.76	14.08	16.08	30.16	17.04	0.57	

* Figures in parenthesis indicate measurement to centre of reinforcement bar. Average : 0.95

TABLE 7.18 : COMPARISON OF BAR FORCE AT CRITICAL BOND STRESS - TORBAR

1 2 3 4 5 6 7 8

Cover (mm)	External Pressure (N/mm ²)	Calculated Bar Force - kN			Plough through Pull-out Force (kN)	Experimental Bar Force (kN)	Ratio of Col.7 ÷ Col.5
		Cracking Component F _{Cr}	Friction Component F _{Fr}	Total F			
100 (113)*	0	26.79	-	26.79	51.50	34.71	1.30
	3.92	24.29	3.30	27.59		34.32	1.24
	7.84	21.78	6.60	28.38		39.67	1.40
	11.76	19.28	9.90	29.18		37.62	1.29
75 (88)	0	26.79	-	26.79	51.50	25.92	0.97
	3.92	24.75	3.36	28.11		34.79	1.24
	7.84	21.20	7.08	28.28		40.14	1.42
	11.76	18.42	10.63	29.05		34.65	1.19
50 (63)	0	26.79	-	26.79	51.50	23.30	0.87
	3.92	22.90	4.01	26.91		32.62	1.21
	7.84	19.00	8.02	27.02		27.99	1.04
	11.76	15.11	12.03	27.14		16.80	0.62
25 (37)	0	20.09	-	20.09	51.50	20.20	1.01
	3.92	18.19	5.45	23.64		23.87	1.01
	7.84	16.26	10.91	27.17		20.36	0.76
	11.76	14.34	16.38	30.72		26.81	0.87

Average : 1.09

* Figures in parenthesis indicate measurement to centre of reinforcement bar

TABLE 7.19 : COMPARISON OF BAR FORCE AT CRITICAL BOND STRESS - HYBAR

Cover (mm)	External Pressure (N/mm ²)	Calculated Bar Force - kN			Plough through Pull-out Force (kN)	Experimental Bar Force (kN)	Ratio of Col.7 ÷ Col.5
		Cracking Component F _{Cr}	Friction Component F _{Fr}	Total F			
100 (113)*	0	27.70	-	27.70	44.17	20.93	1.32
	3.92	25.11	3.41	28.52		27.49	0.96
	7.84	22.52	6.83	29.35		30.90	1.05
75 (88)	11.76	19.93	10.24	30.17		22.85	1.00
	0	27.70	-	27.70		26.58	0.82
	3.92	24.82	3.67	28.49		28.21	0.93
50 (63)	7.84	21.92	7.32	29.24		27.57	0.97
	11.76	19.04	10.99	30.03		21.25	0.92
	0	27.70	-	27.70		22.74	0.77
25 (37)	3.92	23.68	4.15	27.83		32.59	0.82
	7.84	19.65	8.29	27.94		27.89	1.17
	11.76	15.62	12.44	28.06		20.12	0.99
	0	20.77	-	20.77		18.81	0.97
	3.92	18.80	5.64	24.44		15.18	0.77
	7.84	16.81	11.28	28.09		19.70	0.54
	11.76	14.83	16.94	31.77		0.62	

Average : 0.91

* Figures in parenthesis indicate measurement to centre of reinforcement bar.

TABLE 7.20 : COMPARISON OF BAR FORCE AT CRITICAL BOND STRESS - SQUARE-TWISTED BAR

The ratios of the experimental to the theoretical values are also tabulated together with the overall average for each type of bar. They show that the theory proposed fits the experimental results within ± 10 per cent and this may be taken as satisfactory for all practical design purposes. However, it is observed that the Hybar develops more resistance than that obtained by theory whereas resistances of the Torbar and Square-twisted bars fall below the theoretical values. The averages would improve if the values for 25 mm cover and particularly those when the lateral pressures are high are omitted, as in such cases the cracking in the cover would be extensive and the required frictional forces would not be fully mobilised. In such cases, the experimental values are quite close to those obtained for F_{cr} , the cracking component specially for the Square-twisted bar which derives a part of its bond resistance on the wedging of the surface in the concrete.

The differences between the force given by the theory and the tests may be attributed to lack of complete mobilisation of the frictional component when the concrete cover suffers cracking. This view is supported by the better correlation obtained for all the bars when the cover was 4 bar diameters or the lateral compression was less than 9 N/mm^2 . It is suggested that the higher compressive pressure of 11.76 N/mm^2 causes increased bursting stresses resulting in reduced contribution from the frictional component.

7.5 Modes of ultimate failure

The modes of failure for all three types of bar depend on the concrete side cover to the reinforcement bar and the intensity of lateral pressure applied. In practically all cases, for the specimens with the least concrete cover, namely a cover of one bar diameter, side cover cracks developed at ultimate failure and the bar pulled out.

When the cover was increased, the failure pattern changed to that of vertical cracks above and below the bar. The vertical cracks above the bar were to be expected. This follows from the discussion in Section 5.2 that cracking in the concrete cover would occur first at the thinnest part of the concrete ring surrounding the reinforcement bar. The dimension of 50 mm from the centre of the bar to the top of the test block gives the thinnest cover for all specimens except those with a side cover of 25 mm. Side cover cracks were absent in these cases. The vertical cracks below the bar demonstrate that the bursting tensile stresses due to the lateral compression were cracking the concrete and support the theory developed in the study. It was also observed that the extent of propagation of the vertical crack below the bar was dependent on the intensity of the pressure, the length of propagation increasing with the lateral pressure. At higher values of concrete cover, the Hybar and Torbar pulled out with a cone of concrete being pulled out proud of the surface of the concrete as a conical wedge. This behaviour was more prominent with Torbar than with Hybar. The specimens with the latter exhibited more extensive cracking.

At this stage, it is appropriate to discuss the failure mechanism of Square-twisted bars. The Square-twisted bars, though considered as having a similar action to ribbed bars, develop comparatively reduced bursting forces. The shape of the longitudinal cross-section of a Square-twisted bar is shown in Fig. 7.17. It consists of a series of equal arcs, the spacing of which depends on the pitch of the twist. Evans and Williams (66) have explained that the bond mechanism of Square-twisted bars is caused by the wedging action of the reinforcement against the concrete and the maximum bond values occur at the bursting strength of the concrete. Any restraint, either with increased cover or restraining lateral reinforcement like

stirrups would assist in the wedging action to proceed until the maximum bond stress is reached. Roberts (67) has shown that provided the concrete cover does not burst and fall away from the bar, continued slip under load causes plough-through shear of well twisted bars (pitch of twist around 6 diameter or less).

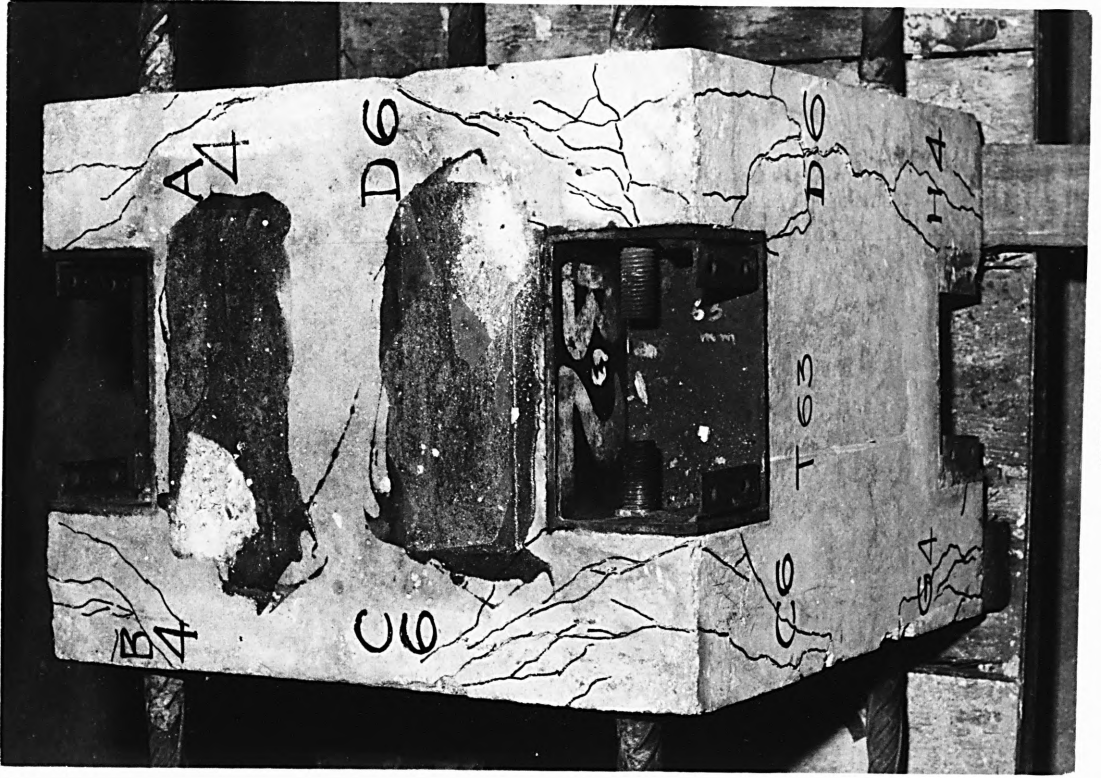
However Roberts (67) demonstrated using a reflecting mirror that a special phenomenon of unscrewing attends the pull out of twisted square bars with a pitch of twist (as supplied commercially) around 10-12 diameters pitch. The bars used in the present study have a pitch of twist of approximately 11 diameters. The wedging action on the lateral form and tapering faces results in a twisting moment in the direction of the twist which causes the unscrewing of the bar from the surrounding concrete. Once this commences at the free end, the rest of the bar will untwist itself, the resistance being only that due to the plastic torsion of the bar and the sliding friction between the bar surface and the surrounding concrete. In such circumstances, any tension cracking in the concrete due to bursting tensile stresses caused by lateral pressure would adversely affect the ultimate resistance of this type of bar.

The modes of failure with Torbar, as described earlier, depended on the concrete cover and the intensity of the lateral pressure. At concrete cover of one bar diameter and at low values of lateral pressure, the mode of failure was due to a crack in the side cover. However, as the intensity was increased to 7.84 N/mm^2 , together with the side crack, a vertical crack above the bar extending to the top surface of the concrete block was observed. With further increase of pressure to 11.76 N/mm^2 , there was no visible side crack, but in addition to the vertical crack above the bar, a vertical crack below the bar appeared. As the cover was increased to 2 and 3 bar diameters,

the appearance of vertical cracks above and below the bar became a consistent behaviour. The cracks above the bar extended into the top surface whereas the crack below extended into the concrete block below distances varying from 130 mm at a pressure of 3.92 N/mm^2 to 200 mm at 11.76 N/mm^2 . At the maximum cover of 4 bar diameters, whilst vertical cracks developed both above and below the bar at all pressures, at low pressures the bars pulled out in a plough-through type of failure. Typical failures are shown in Figs. 7.18 and 7.19.

Hybar demonstrated similar cracking pattern to that of Torbar. With the lowest cover of the bar diameter and without any pressure as well as at a low pressure of 3.92 N/mm^2 , side cracks developed. However as the pressure was increased to 7.84 N/mm^2 and 11.76 N/mm^2 , vertical cracks developed, both above the bar and below the bar, the latter extending to 170 mm and 200 mm respectively. Similarly with 2 and 3 bar diameter as concrete cover, no side crack was observed but the vertical cracks extended further into the concrete below to distances of up to 250 mm for the maximum lateral pressure. The behaviour of cracking both above the bar and below the bar was continued into all the specimens with concrete cover of 4 bar diameters. Typical failures are shown in Figs. 7.20 to 7.22.

It was interesting to observe that the Square-twisted bar had crack patterns similar to the ribbed bars though the extent of cracking was very much subdued. No side crack was observed on all the specimens except in those two with the minimum concrete cover of one bar diameter, the one under low lateral pressure of 3.92 N/mm^2 and the other without lateral pressure. All other specimens exhibited the phenomenon of vertical cracking above and below the bar. However, the crack below the bar did not propagate very far into the concrete below. Typical failures are shown in Figs. 7.23 and 7.24.

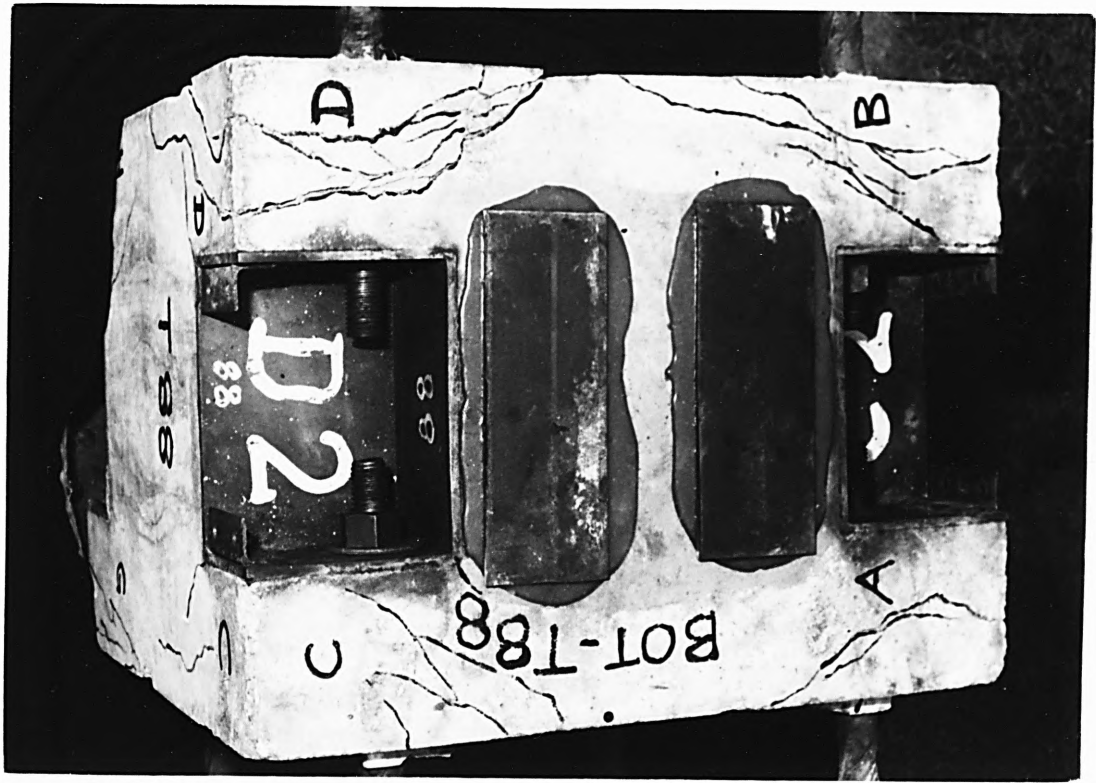


TOP VIEW

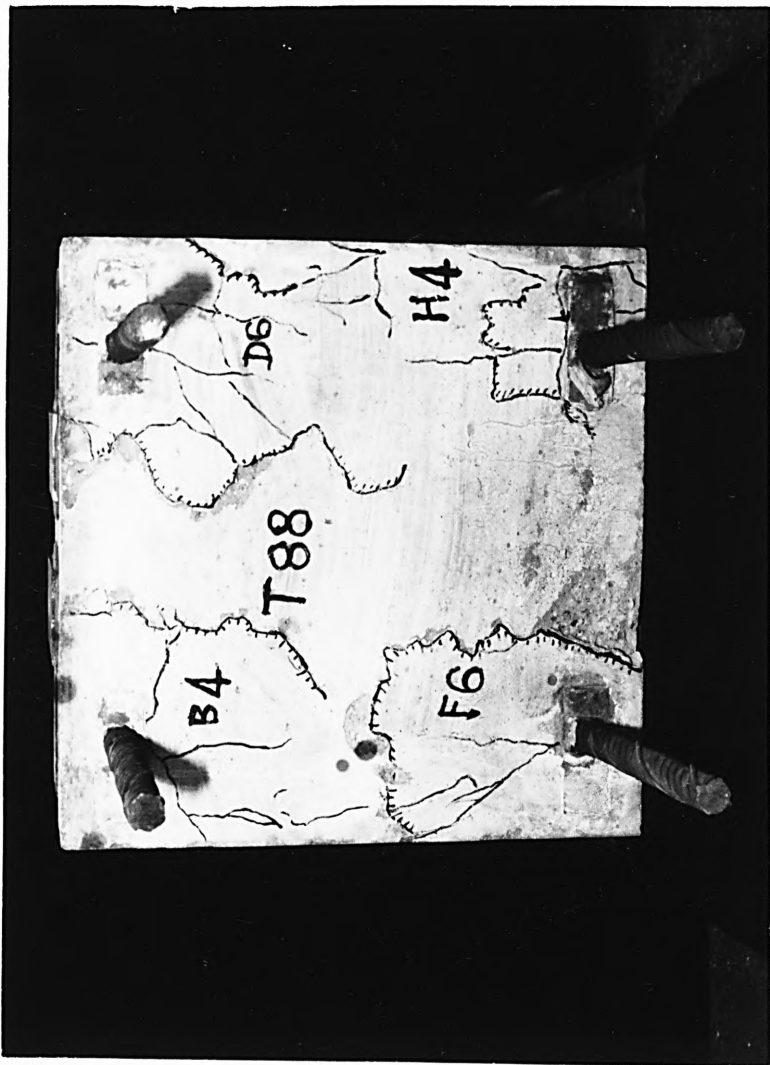


END VIEW

FIG. 7.18 TYPICAL FAILURE MODES - TORBAR - PLATE 1

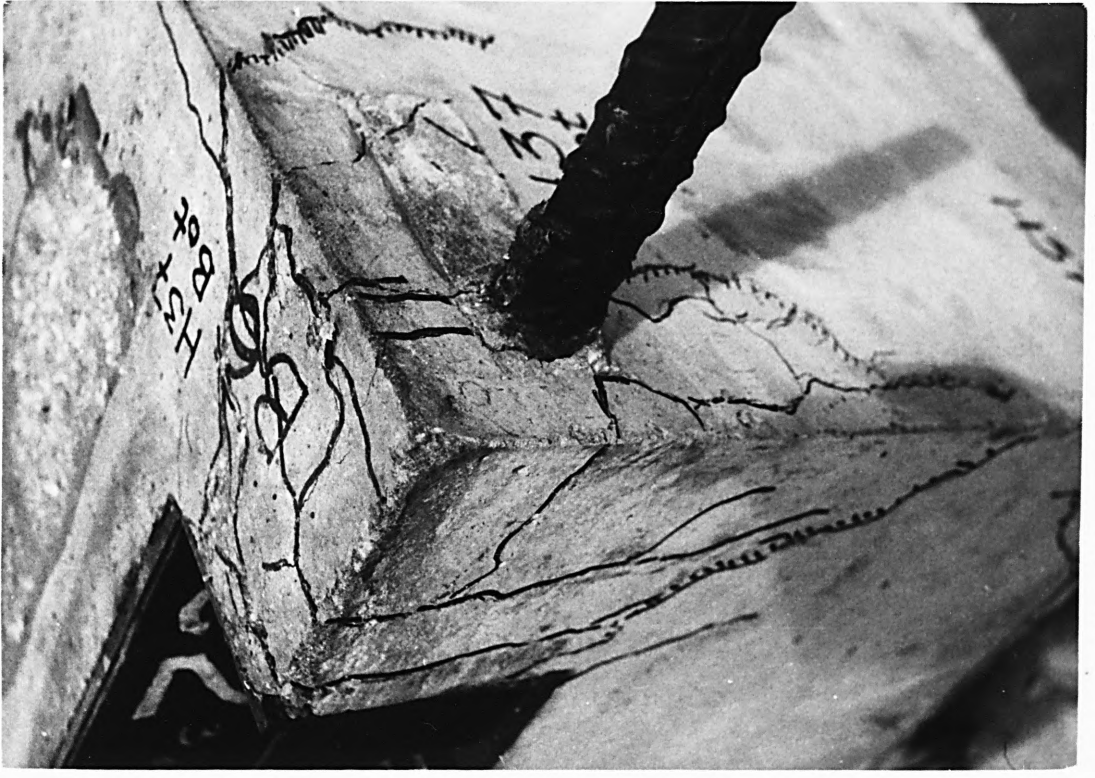


TOP VIEW



END VIEW

FIG. 7.19 TYPICAL FAILURE MODES - TORBAR - PLATE 2

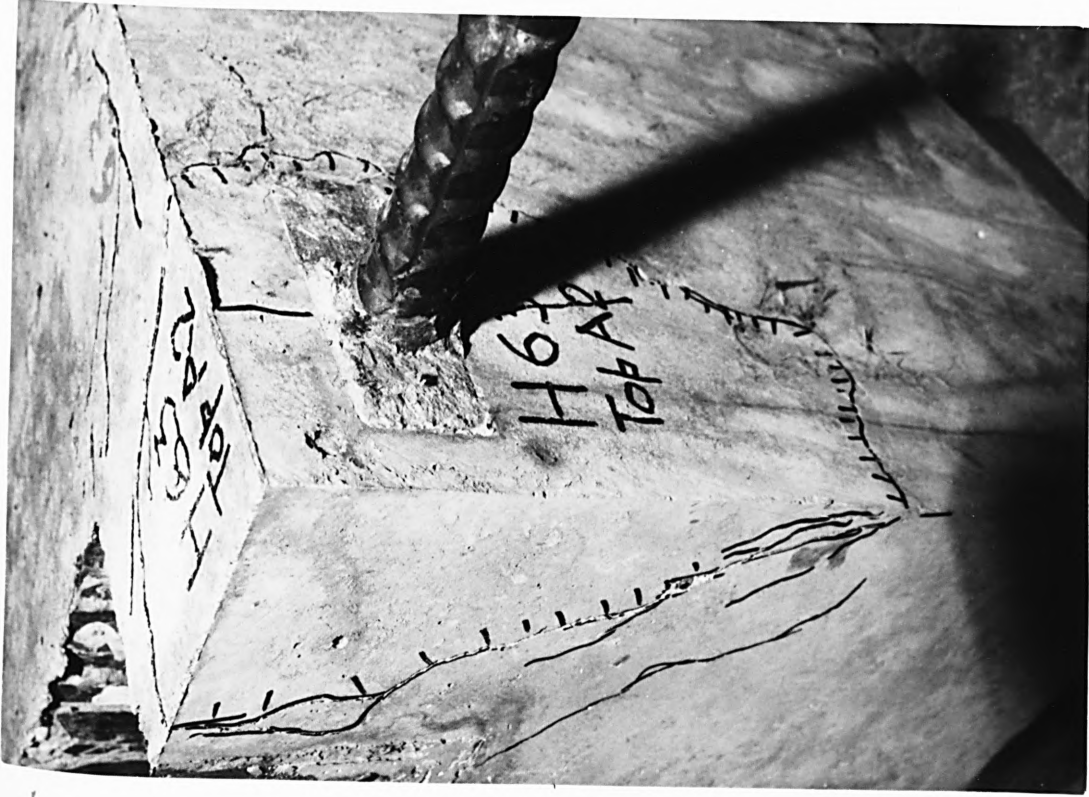


COVER 25 mm - PRESSURE 11.76 N/mm²



COVER 25 mm - PRESSURE ZERO

FIG. 7.20 TYPICAL FAILURE MODES - HYBAR - PLATE 1



COVER 50 mm - PRESSURE 3.92 N/mm²



COVER 75 mm - PRESSURE 7.84 N/mm²

FIG. 7.21 TYPICAL FAILURE MODES - HYBAR - PLATE 2



COVER 100 mm - PRESSURE 3.92 N/mm²



COVER 100 mm - PRESSURE 7.84 N/mm²

FIG. 7.22 TYPICAL FAILURE MODES - HYBAR - PLATE 3



COVER 50 mm - PRESSURE 7.84 N/mm²



COVER 25 mm - PRESSURE 11.76 N/mm²

FIG. 7.23 TYPICAL FAILURE MODES - SQUARE-TWISTED BAR - PLATE 1



COVER 75 mm - PRESSURE 11.76 N/mm²



COVER 75 mm - PRESSURE 7.84 N/mm²

FIG. 7.24 TYPICAL FAILURE MODES - SQUARE-TWISTED BAR - PLATE 2

The modes of failure support the theory proposed that the bursting tensile stress due to the lateral pressure plays an important role in the failure mechanism of reinforcement bars under lateral pressure.

CHAPTER 8

COMPARISON OF RESULTS WITH DESIGN CODE PROVISIONS IN

C.P. 110

A designer is always concerned about the factor of safety available in the structures designed by him according to the provisions of prevailing Codes of Practice. Hence it is of interest to study the results obtained in this investigation in comparison with the bond stresses permissible in design in the current Code of Practice for Structural Concrete namely the C.P. 110: 1972 (Amended 1979), (68).

In order to compare the bond stresses, it is necessary to decide on the type of permissible bond stress that is to form the basis in the study since the Code provides both the ultimate local bond stress and the ultimate anchorage bond stresses. In the investigation, the bond stresses are obtained over a finite embedment length, though a short one and is an average bond stress value over the embedded length. Hence, it is more appropriate to use the ultimate anchorage bond stress values given in the Code. These are also average stresses to be used to determine the anchorage length. The effective factor of safety is thus determined as a ratio of the experimentally obtained bond stress values either at critical bond stress state or ultimate bond stress state divided by the ultimate anchorage bond stress permitted in the Code for the specified grade of concrete, namely of characteristic strength 35 N/mm^2 .

The provisions in the Code are specified for different types of bars and either in tension or compression. The Code also allows deformed

bars to be classified under Type 1 and Type 2 with the additional observation that the value of bond stresses for deformed bars of Type 2 may be increased by 30 per cent. Amongst the bars used in the study, Square-twisted bars are generally classified as of Type 1 and the Torbar and Hybar as Type 2 bars. The factors of safety calculated are therefore based on enhanced permissible bond stresses for Torbar and Hybar.

8.1 Factor of safety under lateral tension release

The values of factor of safety calculated both at the critical bond stress state and ultimate bond stress state are tabulated in Table 8.1 for the three-types of bars.

It is observed that at ultimate bond stress, with no tension release in the concrete, the factors of safety are above 1.0 for all the types of bars, and for all concrete covers with the values for the Torbar and Hybar substantially higher than 1.0. There is a drop in the values with increased tension release and the Square-twisted bar performs very poorly at the high levels of tension release of 1770 and 2360 microstrains. The factors of safety improve with increased cover as expected. In this respect, the Hybar yields higher factors of safety than the Torbar at a concrete cover of 25 mm or equal to one bar diameter. The effects of cover and tension release are compounded in the case of the Square-twisted bars resulting in very low factors of safety.

While the factors of safety at ultimate bond stress indicate that there is no risk of failure of the bars in bond at the ultimate limit state, if it is accepted that the critical bond stress is

Torbar : Permissible anchorage bond stress (C.P.110)
 $= 1.3 \times 2.4 = 3.12 \text{ N/mm}^2$

Cover (mm)	At critical bond stress				At ultimate bond stress			
	$\epsilon = 0$	$\epsilon = 1180$	$\epsilon = 1770$	$\epsilon = 2360$	$\epsilon = 0$	$\epsilon = 1180$	$\epsilon = 1770$	$\epsilon = 2360$
88	1.27	1.08	0.76	0.56	2.19	2.07	2.31	1.96
63	0.90	0.67	0.65	0.41	2.28	2.27	2.12	2.04
50	0.98	0.78	0.71	0.74	2.21	2.34	2.05	2.00
25	0.74	0.71	0.79	0.83	1.48	1.56	1.83	1.79

Hybar : Permissible anchorage bond stress (C.P.110)
 $= 1.3 \times 2.4 = 3.12 \text{ N/mm}^2$

Cover (mm)	At critical bond stress				At ultimate bond stress			
	$\epsilon = 0$	$\epsilon = 1180$	$\epsilon = 1770$	$\epsilon = 2360$	$\epsilon = 0$	$\epsilon = 1180$	$\epsilon = 1770$	$\epsilon = 2360$
88	1.46	1.04	1.06	0.74	2.39	2.48	2.20	2.20
63	1.24	0.95	0.87	0.81	2.32	2.38	2.24	2.46
50	1.10	1.00	0.74	0.54	2.15	2.33	2.13	1.84
25	1.03	0.99	0.88	0.94	2.12	1.91	2.00	1.88

Square-twisted bar : Permissible anchorage bond stress (C.P.110)
 $= 2.4 \text{ N/mm}^2$

Cover (mm)	At critical bond stress				At ultimate bond stress			
	$\epsilon = 0$	$\epsilon = 1180$	$\epsilon = 1770$	$\epsilon = 2360$	$\epsilon = 0$	$\epsilon = 1180$	$\epsilon = 1770$	$\epsilon = 2360$
88	1.17	0.89	0.84	0.70	1.32	1.02	1.02	0.90
63	1.01	0.99	0.82	0.62	1.50	1.24	1.15	1.01
50	1.27	1.15	0.85	0.71	1.49	1.21	1.07	0.80
25	0.90	1.03	0.92	0.85	1.00	1.04	0.93	0.88

Tension release ϵ is in microstrains

TABLE 8.1 : SAFETY FACTORS ON ALLOWABLE STRESSES - TENSION RELEASE

representative of serviceability limit states of cracking and also deflection, the factors of safety seem to drop alarmingly low with increasing tensile release at serviceability conditions. However, the factors of safety are satisfactory and above 1.0 for the various concrete covers with no tension release except in the case of the Torbar, the behaviour of which is rather unexpected. It may seem that the Square-twisted bar yields factors higher than the Torbar at critical bond stress state for all levels of tension release, but this has to be seen in the light of the enhanced permissible anchorage bond stress value used in the computations for the factor of safety for Torbar. It would thus seem prudent to use anchorage bond stress values without the 30 per cent enhancement in order that serviceability requirements may be satisfied.

8.2 Factor of safety under lateral compression

Table 8.2 gives the factors of safety calculated both at critical bond stress and ultimate bond stress for the three types of bars. The factors of safety at ultimate bond stress are all above 1.0 for all types of bars and increase with increasing lateral pressure. The Torbar and Hybar have slightly higher values than Square-twisted bars even with the 30 per cent enhanced allowable bond stress. It would be safe to conclude that all the three types of bars would be safe at ultimate limit state of bond.

At critical bond state, which may be considered the criteria of a serviceability limit state of bond, the Square-twisted bar is safe with covers exceeding one bar diameter. Whereas the factors of safety of the Hybar are higher than those of the Torbar, both the types of bars are safe at critical bond state only with covers

Torbar : Permissible anchorage bond stress (C.P.110)
 $= 1.3 \times 2.4 = 3.12 \text{ N/mm}^2$

Cover (mm)	At critical bond stress				At ultimate bond stress			
	p=0	p=3.92	p=7.84	p=11.76	p=0	p=3.92	p=7.84	p=11.76
100	1.17	1.21	1.35	1.06	1.54	1.84	2.08	2.17
75	1.19	1.30	1.06	1.14	1.43	1.99	2.35	2.39
50	0.94	1.01	0.91	0.91	1.58	1.73	1.81	2.07
25	0.81	0.81	0.68	0.69	1.24	1.43	1.34	1.45

Hybar : Permissible anchorage bond stress (C.P.110)
 $= 1.3 \times 2.4 = 3.12 \text{ N/mm}^2$

Cover (mm)	At critical bond stress				At ultimate bond stress			
	p=0	p=3.92	p=7.84	p=11.76	p=0	p=3.92	p=7.84	p=11.76
100	1.41	1.39	1.61	1.53	1.58	1.87	2.39	2.31
75	1.05	1.41	1.63	1.40	1.41	2.01	2.20	2.26
50	0.95	1.32	1.13	0.68	1.31	1.68	1.56	1.34
25	0.82	0.97	0.82	1.09	1.22	1.44	1.22	1.48

Square-twisted bar : Permissible anchorage bond stress (C.P.110)
 $= 2.4 \text{ N/mm}^2$

Cover (mm)	At critical bond stress				At ultimate bond stress			
	p=0	p=3.92	p=7.84	p=11.76	p=0	p=3.92	p=7.84	p=11.76
100	1.05	1.38	1.55	1.52	1.33	1.77	2.05	2.07
75	1.15	1.34	1.42	1.38	1.55	1.50	1.69	1.94
50	1.07	1.14	1.64	1.40	1.30	1.63	1.93	1.85
25	1.01	0.95	0.76	0.99	1.47	1.53	1.05	1.28

Lateral pressure 'p' in N/mm^2 units

TABLE 8.2 : SAFETY FACTORS ON ALLOWABLE STRESSES - LATERAL PRESSURE

exceeding 2 bar diameters.

8.3 Outlook for design

It would seem that till more detailed studies have been carried out on the effects of lateral pressure particularly at serviceability limit state conditions, the beneficial effects of lateral pressure shall not be taken into account for design purposes. Furthermore, in regions where there is increased pressure caused by compression forces such as in beams at beam column joints, sufficient side cover shall be provided to reinforcement bars in order that the bond resistance is fully mobilised. In situations where there is a lateral tension release, it seems prudent to use the basic bond stress values provided in the Code irrespective of the classification of the particular deformed bar.

CHAPTER 9

CONCLUSIONS

The purpose of this study was to obtain fundamental information on the bond of deformed reinforcing bars under lateral restraint, both under tension release and lateral compression. The two aspects were investigated experimentally. Although some findings are common to both, it is preferable, at the risk of repetition, to summarise the findings separately in order to avoid confusion.

9.1 Main conclusions relating to lateral tension release

- (i) The shape of the bond characteristics depends on the type of reinforcement bar, namely the profile of the bar, and the level of tension release in the concrete (6.1).
- (ii) Ribbed bars continue to offer bond resistance even with high levels of tension release due to their ability to lock into the concrete 'teeth' caused by cracking under tension release (6.1.1; 6.2.1).
- (iii) Increased concrete cover offers increased bond resistance, but a limiting cover of 3.5 bar diameters offers the maximum resistance (6.2.1; 6.3.1).
- (iv) A complete loss of bond is to be expected at a tension release value of about 4250 microstrains. Based on this limiting tensile strain, the critical bond stress may be obtained from a relationship of the form given by Equation 6.2. This could form the basis of a design equation for bond resistance under tension release (6.3.1).

- (v) Hybar with its heavier ribs develops higher bond resistance but causes greater cracking, whereas the Torbar seems to be able to involve a greater zone of the concrete surrounding it accompanied by less cracking (6.4).
- (vi) It seems prudent to use in situations where tension release is present the basic anchorage bond stress values given in C.P. 110: 1972 but without the 30 per cent enhancement for Type 2 bars, in order that serviceability requirements may be satisfied (8.1).

9.2 Main conclusions relating to lateral compression

- (i) The load-slip characteristic depends on the concrete cover, amount of lateral pressure, the profile of the reinforcement bar and the location of the bar in a structural member. Slip at ultimate load failure increases with increasing lateral compression. Increased concrete cover causes a reduction in slip (7.1).
- (ii) Top cast bars are inferior in bond compared to bottom cast bars. A reduction in the bond resistance of 30 per cent is recommended for Torbar and Hybar and 50 per cent for Square-twisted bars when reinforcement bars are placed at locations where the concrete below the bar is more than 300 mm (7.2.1).
- (iii) Ultimate bond stress increases progressively with increase of concrete cover. A limiting maximum cover of 3.5 bar diameters is suggested as sufficient to develop the maximum bond strength of a reinforcement bar (7.2.2).

- (iv) Ultimate bond stress increases with increasing lateral pressure as the square-root of the lateral pressure for a concrete of constant strength up to a limiting value of lateral pressure of 25 per cent of the cube strength (7.2.3).
- (v) Critical bond stress values of ribbed bars increase only marginally with lateral pressure but Square-twisted bars show notable increase of critical bond stress with increasing lateral pressure (7.3.3).
- (vi) The concrete cover affects the ultimate bond stress more significantly than the lateral pressure (7.2.4).
- (vii) The theory proposed for the bond resistance at bond failure defined as at 0.1 mm free-end slip is satisfactory to meet the requirements of design of bond under lateral pressure (7.4).

9.3 Bond efficiency of the different types of bars

- (i) The ribbed bars, namely Torbar and Hybar, develop higher ultimate bond resistance with increasing lateral pressure than the Square-twisted bars (7.2.4).
- (ii) The tendency of the Hybar to split the concrete cover is prominent compared to the Torbar and Square-twisted bars (7.5).
- (iii) Hybar depends more than the Torbar on the concrete cover to develop its bond resistance. All bars perform efficiently at concrete covers above 2 bar diameters, with the Hybar performing less efficiently than the other two at 2 bar diameters (7.2.4).

9.4 Recommendations for further study

During the investigation, and arising from the discussion of the results, a few areas which need further investigation have been identified. These may be studied in depth in order to understand more fully the behaviour of reinforcement bars in bond under lateral restraint.

- (i) The Torbar shows very marginal beneficial effects of lateral pressure at the serviceability criteria of critical bond stress. This needs further study in relation to its rib profile and the bursting tensile stresses developed due to lateral pressure (7.3.4).
- (ii) It has been suggested in this study that the lateral pressure shall not be greater than 25 per cent of the cube strength of concrete. This needs further investigation as the stress system surrounding a bar subjected to lateral pressure is a complex three-dimensional one and the ultimate failure mechanism may need to be studied by considering failure of concrete in a state of triaxial stress (7.2.3).
- (iii) It has been mentioned, whilst developing the theory under lateral pressure, that there is a need to study with the help of a mathematical model the pattern of stress around the reinforcing bar subjected to a lateral pressure in one direction only as different from that of a bar under a uniform pressure around its perimeter. The proposed study needs to be carried out in order to fully appreciate the behaviour of reinforcing bars subjected to unidirectional compression such as those obtaining at a beam-column junction (5.2.4).

- (iv) The contribution of transverse reinforcement to the development of ultimate bond resistance needs to be studied in detail with particular attention to the strain levels in such lateral reinforcement at ultimate bond failure of the reinforcement bar (7.2.4). ✓

1. "The Effect of Transverse Reinforcement on the Bond of Reinforcement Bars in Concrete", *Journal of the American Concrete Institute*, Vol. 74, No. 1, January 1977, pp. 1-10.

2. "Effect of Transverse Reinforcement on the Bond of Reinforcement Bars in Concrete", *Journal of the American Concrete Institute*, Vol. 74, No. 1, January 1977, pp. 11-20.

3. "Effect of Transverse Reinforcement on the Bond of Reinforcement Bars in Concrete", *Journal of the American Concrete Institute*, Vol. 74, No. 1, January 1977, pp. 21-30.

4. "Tests of Bond Resistance Between Reinforcement and Concrete", *Technical Paper No. 10*, U.S. Army Corps of Engineers, 1959.

5. "Tests of Bond Resistance Between Reinforcement and Concrete", *Technical Paper No. 10*, U.S. Army Corps of Engineers, 1959.

6. "The Behavior of Reinforced Concrete Beams with Joints", *Technical Report 10-47*, U.S. Army Corps of Engineers, 1959.

7. "The Behavior of Reinforced Concrete Beams with Joints", *Technical Report 10-47*, U.S. Army Corps of Engineers, 1959.

8. "Some Detailing Problems in Concrete Frames of Buildings", *The Structural Engineer*, Vol. 24, No. 1, January 1976, pp. 10-20.

9. "Some Detailing Problems in Concrete Frames of Buildings", *The Structural Engineer*, Vol. 24, No. 1, January 1976, pp. 10-20.

10. "The Need to Consider the Influence of Lateral Reinforcement on Bond", *ACI Symposium on Bond and Trace Properties of Reinforced Concrete*, Vol. 1, December 1952, pp. 1-10.

11. "The Need to Consider the Influence of Lateral Reinforcement on Bond", *ACI Symposium on Bond and Trace Properties of Reinforced Concrete*, Vol. 1, December 1952, pp. 1-10.

REFERENCES

1. THADDEUS HYATT
"An Account of Some Experiments with Portland Cement-Concrete Combined with Iron as a Building Material with Reference to Economy of Metal in Construction and for Security Against Fire in the Making of Roofs, Floors and Walking Surfaces", London, 1877.
2. ABRAMS DUFF A.
"Tests of bond between concrete and steel", Engineering Experiment Station, University of Illinois, Urbane, 1913, Bulletin No. 71, p. 238.
3. SLATER, W.A., RICHART, F.E. AND SCOFIELD G.G.
"Tests of Bond Resistance Between Concrete and Steel", Technologic Paper No. 173, U.S. Bureau Standards, 1920.
4. TAYLOR, H.P.J.
"The Behaviour of In-situ Concrete Beam - Column Joints", Technical Report 42.492, Cement and Concrete Association, England, May 1974, 32 pp.
5. TAYLOR, H.P.J. AND CLARKE, J.C.
"Some detailing problems in concrete framed structures".
The Structural Engineer, Vol. 54, No. 1, January 1976, pp. 19-32.
6. LEONHARDT, F.
"On the need to consider the influence of lateral stresses on bond", RILEM Symposium on Bond and Crack Formation in Reinforced Concrete, Vol. 1, Stockholm, 1957 p. 29.

7. UNTRAUER, R.E. AND HENRY, R.L.
 "Influence of Normal Pressure on Bond Strength", ACI Journal,
 Proceedings, Vol. 62, May 65, pp. 577-586.
8. NAVARATNARAJAH, V.
 "Effect of Anchorage Efficiency of Lateral Reinforcement on
 the Torsional Strength of Reinforced Concrete Beams",
ACI Journal, Proc. V. 65, November 1968, pp. 965-968.
9. LEONHARDT, F. AND SCHELLING, G.
 "Torsionversuche an Stahlbetonbalken", Deutscher Ausschuss fur
 Stahlbeton, Heft 239, Berlin 1974, 122 pp.
10. BICHARA, A.
 "Etude du probleme de l'adherence dans le beton arme"
Cashiers du Centre Scientifique et Technique du Batiment, n^o 117/
 127-1951.
11. SAILLARD Y.
 "Recherches sur les aciers d'armatures de limite d'elasticite
 60 kg/mm². Determination d'un acier "TOR-60". Travaux,
 n^o 227, Septembre 1953.
12. SAILLARD, Y.
 "Mechanisme de la liaison beton-acier", Archiwum inzynierii
 ladowej, Tome VL-4, Varsovie 1960.
13. PLOWMAN, J.M.
 "The measurement of bond strength", Symposium R.I.L.E.M.,
 Scockholm, 1957.
14. DUTRON, R.
 "Adherence des armatures au beton", Revue des materiaux de
 construction et de travaux publics, Paris n^o 514 a' 517, 1958.

15. MENZEL, CARL A.
"Some Factors Influencing Results of Pull-Out Bond Tests"
ACI Journal, Proc. Vol. 35, June 1939, p. 517-544.
16. CLARK, A.P.
"Comparative Bond Efficiency of Deformed Concrete Reinforcing Bars", ACI Journal, Proc. Vol. 43, December 1946, p. 381-400.
17. CLARK, A.P.
"Bond of Concrete Reinforcing Bars", ACI Journal, Proc. V. 46, November 1949, p. 161-183.
18. WATSTEIN, DAVID
"Distribution of Bond Stress in Concrete Pull-Out Specimens",
ACI Journal, Proc. Vol. 43, May 1947 pp. 1041-1052.
19. MATHEY, R.G. AND WATSTEIN, D.
"Investigation of Bond in Beam and Pull-Out Specimens with High-Yield Strength Deformed Bars". ACI Journal, Proc. V. 57, March 1961, pp. 1071-1090.
20. MAINS, R.M.
"Measurement of the Distribution of Tensile and Bond Stresses Along Reinforcing Bars", ACI Journal, Proc. V. 48, November 1951, pp. 225-252.
21. FERGUSON, P.M., TURPIN, R.D. AND THOMPSON, J.N.
"Minimum Bar Spacing as a Function of Bond and Shear Strength",
ACI Journal, Proc. V. 50, June 1954, p. 869-887.
22. FERGUSON, P.M. AND THOMPSON, J.N.
"Development length of High Strength Reinforcement Bars in Bond", ACI Journal, Proc. Vol. 59, July 1962, pp. 887-922.

23. FERGUSON, P.M. AND THOMPSON, J.N.
"Development length for Large High Strength Reinforcement Bars"
ACI Journal, Proc. Vol. 62, January 1965, pp. 71-94.
24. REHM, G.
"The Fundamental Law of Bond", RILEM Symposium on Bond and Crack Formation in Reinforced Concrete, Vol. II, Stockholm, 1957, pp. 491
25. REHM, G.
"Über die Grundlagen des Verbundes Zwischen Stahl und Beton.
(The Basic Principles of the bond between steel and concrete)."
Deutscher Ausschuss für Stahlbeton, No. 138, 1961 pp. 59.
Translated from the German by C. Van Amerongen, London. Cement and Concrete Association, 1968 pp. 66 Library Translation No. 134.
26. LUTZ, L.A.
"Information on the Bond of Deformed Bars from Special Pull-Out Tests". ACI Journal, Proc. V. 67, November 1970, pp. 885-887.
27. LUTZ, L.A. AND GERGELY, P.
"Mechanics of bond and slip of deformed bars in concrete".
ACI Journal, Proc. V. 64, November 1967, pp. 711-721.
28. BROMS, B.B.
"Technique for Investigation of Internal Cracks in Reinforced Concrete Members". ACI Journal, Proc. V. 62, January 1965, pp. 35-44.
29. GOTO, Y.
"Cracks Formed in Concrete Around Deformed Tension Bars",
ACI Journal, Proc. V. 68, April 1971, pp. 244-251.

30. TEPFERS, R.

"A theory of bond applied to overlapped tensile reinforcement splices for deformed bars". Chalmers University of Technology, Division of Concrete Structures, Gothenberg, Publication No. 73: 2, 328 pp.

31. TEPFERS, R.

"Cracking of concrete cover along anchored deformed reinforcing bars". Magazine of Concrete Research, Vol. 31, No. 106, March 1979, pp. 3-12.

32. LOSBERG, A AND OLSSON, P.

"Bond Failure of Deformed Reinforcing Bars Based on the Longitudinal Splitting Effect of the Bars", ACI Journal, Proc. V. 76, January 1979, pp. 5-18.

33. SKOROBOGATOV, S.M. AND EDWARDS, A.D.

"The influence of the geometry of deformed steel bars on their bond strength in concrete". The Institution of Civil Engineers, Proceedings, V. 67, Part 2, June 1979, pp. 327-339.

34. CAIRNS, J.

"An analysis of the ultimate strength of lapped joints of compression reinforcement". Magazine of Concrete Research, V. 31, No. 106, March 1979, pp. 19-27.

35. MIRZA, S.M. AND HOUDE, J.

"Study of Bond Stress-Slip Relationships in Reinforced Concrete", ACI Journal, Proc. V. 76, January 1979, pp. 19-46.

36. EDWARDS, A.D. AND YANNOPOULOS, P.J.

"Local Bond-Stress to Slip Relationships for Hot Rolled Deformed Bars and Mild Steel Plain Bars", ACI Journal, Proc. V. 76, March 1979, pp. 405-413.

37. GVOZDEV, A.A.

"Quelques resultats d'essais sur l'ancrage des armatures et sur la redistribution des moments flechissants des poutres hyperstatiques produite par la fissuration", RILEM Symposium, Stockholm 1957.

38. C.U.R. REPORT NO. 23.

"Onderzoek naar de samenwerking van geprofileerd stahl mit beton" (An Investigation of the Bond of Deformed Steel Bars with Concrete) Translation No. 112, Cement and Concrete Association, 28 pp.

39. CHAMBERLIN, S.

"Spacing of Reinforcement in Beams", ACI Journal, Proc. V. 53, July 1956, pp. 113-134.

40. KEMP, E.L. AND WILHELM, W.J.

"Investigation of the Parameters Influencing Bond Cracking" ACI Journal, Proc. V. 76, January 1979, pp. 47-71.

41. JIMENEZ, R., WHITE, R.N., AND GERGELY, P.

"Bond and Dowel Capacities of Reinforced Concrete" ACI Journal, Proc. V. 76, January 1979, pp. 73-92.

42. MORITA, S. AND KAKU, T.

"Splitting Bond Failures of Large Deformed Reinforcing Bars", ACI Journal, Proc. V. 76, January 1979, pp. 93-110.

43. MENZEL, C.A.

"Effect of Settlement of Concrete on Results of Pull-Out Bond Tests", Portland Cement Association, Research Department Bulletin No. 41, November 1952.

44. WELCH, G.B. AND PATTEN, B.J.F.
"Factors affecting bond between concrete and reinforcement",
Constructional Review, Sydney, Vol. 34, No. 3, February 1961.
45. BRETTLER, H.J.
"Average Bond Stresses of Deformed Bars Embedded Horizontally
in Concrete", Constructional Review, V. 32, No. 2, February 1959,
pp. 30-34.
46. BRETTLER, H.J.
"Bond Characteristics of Cold-Twisted Square Steel Reinforcing
Bars", Constructional Review, V. 32, No. 3, March 1959,
pp. 29-32.
47. DJABRY, W.
"Contribution a l'etude de l'adherence des fers d'armature au
beton" Laboratoire Federal d'Essai des Materiaux, Zurich,
Rapport n^o 184, 1952.
48. RUSCH, H. AND REHM, G.
"Versuche mit Betonformstahlen", Deutscher Ausschuss fur
Stahlbeton, Heft 140, 160, 165, Berlin 1963, 1964.
49. SORETZ, S. AND HOLZENBEIN, H.
"Influence of Rib Dimensions of Reinforcing Bars on Bond and
Bendability", ACI Journal, Proc. Vol. 76, January 1979, pp. 111-125
50. LUTZ, L.
"The Mechanics of Bond and Slip of Deformed Reinforcing Bars in
Concrete", Thesis, Ph.D. 1966, Cornell University.
51. ORANGUN, C.O., JIRSA, J.O., AND BREEN, J.E.
"A Re-evaluation of Test Data on Development Length and Splices"
ACI Journal, Proc. Vol. 74, March 1977, pp. 114-122.

52. COMITE EUROPEEN DU BETON.
"Bibliographical Research concerning Bond and Anchorage",
Report, Committee II Steels - Bonds and Anchorage.
53. REHM, G. AND ELIGEHAUSEN, R.
"Bond of Ribbed bars under High Cycle Repeated Loads",
ACI Journal, Proc. V. 76, No. 2, February 1979, pp. 297-309.
54. KWAMINA AMONO-NEIZER.
"Optimum properties of high tensile reinforcement", M. Phil.
Thesis, 1967, The City University, Department of Civil
Engineering.
55. DASTIDAR, N.R.G.
"The bursting effect and bond development length of deformed
bars", Ph.D. Thesis, 1969, The City University, Department of
Civil Engineering.
56. McCLURE, J.
"The relationship between bond strength, bar size, bar cover
and bar spacing in reinforced concrete flexural members",
Ph.D. Thesis, 1974, The University of Alabama.
57. TILANTERA, T. AND RECHARDT, T.
"Bond of reinforcement in lightweight aggregate", Technical
Report No. 17, Division of Structural Engineering, Helsinki
University of Technology, 1977.
58. TIMOSHENKO, S. AND GOODIER, J.N.
Theory of Elasticity, (McGraw Hill).
59. IYENGAR, K.T.S.R.
"Two dimensional theories of anchorage zone stresses in post-
tensioned prestressed concrete beams", ACI Journal, Proc. V. 59,
No. 10, 1962 pp. 1443-1466.

60. YETTRAM, A.L. AND ROBBINS, K.
"Anchorage zone stressed in axially post-tensioned members of uniform rectangular section", Mag. of Conc. Research, Vol. 21, No. 67, June 1969, pp. 103-112.
61. SOMAYAJI, S. AND SHAH, S.P.
"Bond Stress versus Slip Relationship and Cracking Response of Tension Members", ACI Journal, Proc. V. 78, No. 3, May-June 1981, pp. 217-225.
62. AMERICAN CONCRETE INSTITUTE.
"Building Code Requirements for Reinforced Concrete, ACI 318-77.
63. DEUTSCHEN AUSSCHUSSES FÜR STAHLBETON.
DIN 1045 - Beton-und Stahlbeton bau, Bemessung und Ausführung, 1972.
64. CHUNG TAI HO, RAYMOND.
"Bond performance and failure mechanism of tensile lapped joints of deformed bars in concrete beams", Ph.D. Thesis, 1971, The City University, Department of Civil Engineering.
65. ROBINS, P.J. AND STANDISH, I.G.
"Effect of lateral pressure on bond reinforcing bars in concrete", Proceedings of International Conference on Bond in Concrete, Paisley, 1982, Applied Science, Publishers, London, pp. 262-272.
66. EVANS, R.H. AND WILLIAMS, A.
"Bond stress and crack width in beams reinforced with Square-grip reinforcement", Symposium on Bond and Crack Formation in Reinforced Concrete, Stockholm, 1957, Vol. 1, pp. 105-116.

67. ROBERTS, N.P.

"Limit state theory of anchorage bond in reinforced concrete",
Ph.D. Thesis, 1969, University of London.

68. BRITISH STANDARDS INSTITUTION.

Code of Practice for Structural Concrete, C.P. 110: 1972
(Amended 1979).



APPENDIX A

LOAD-SLIP CHARACTERISTICS

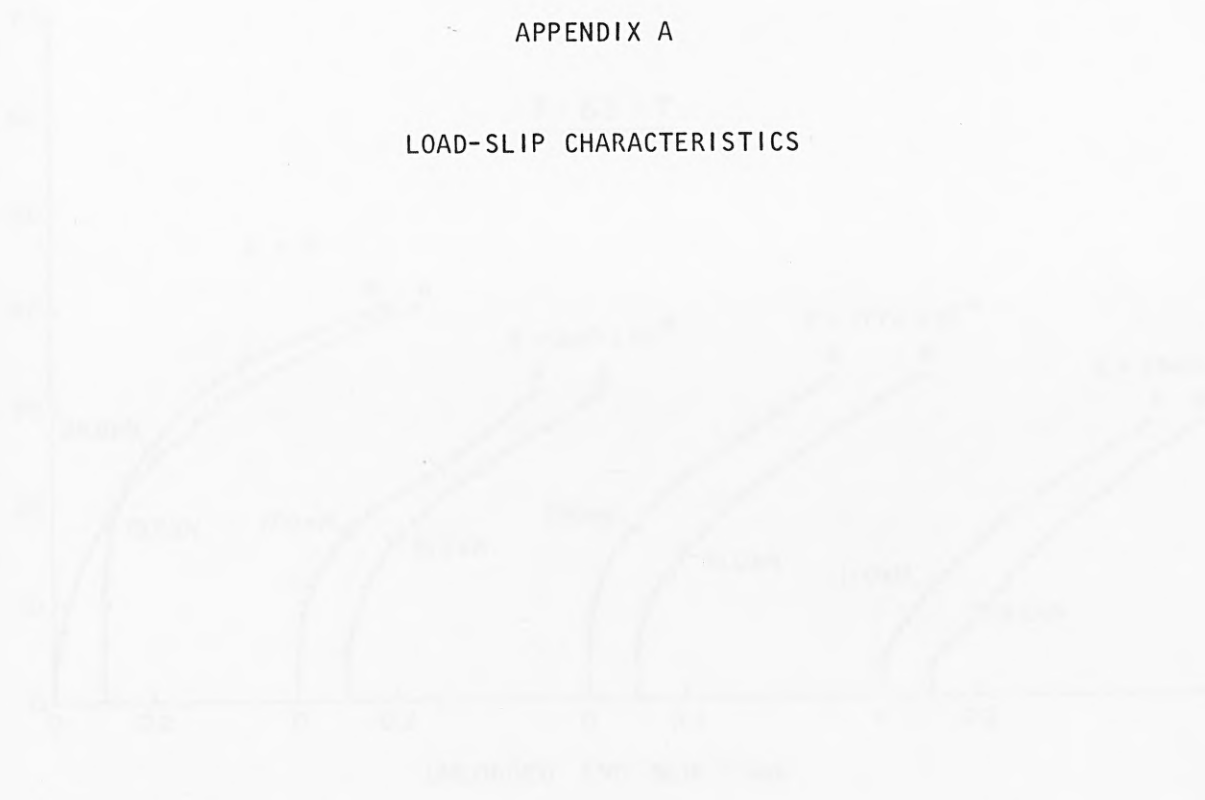


FIG. 21. LOAD-SLIP CHARACTERISTICS AT UNENGAGED SRC-TUBES

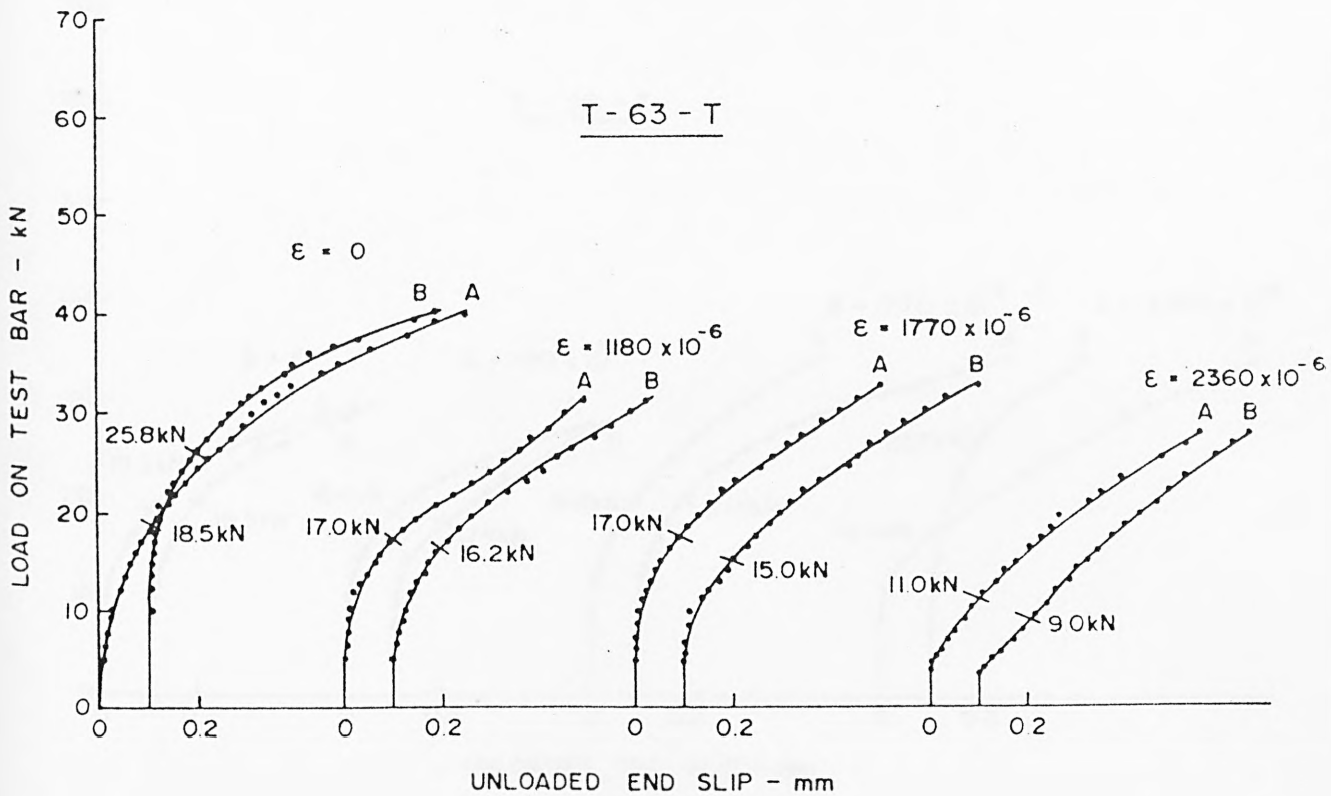
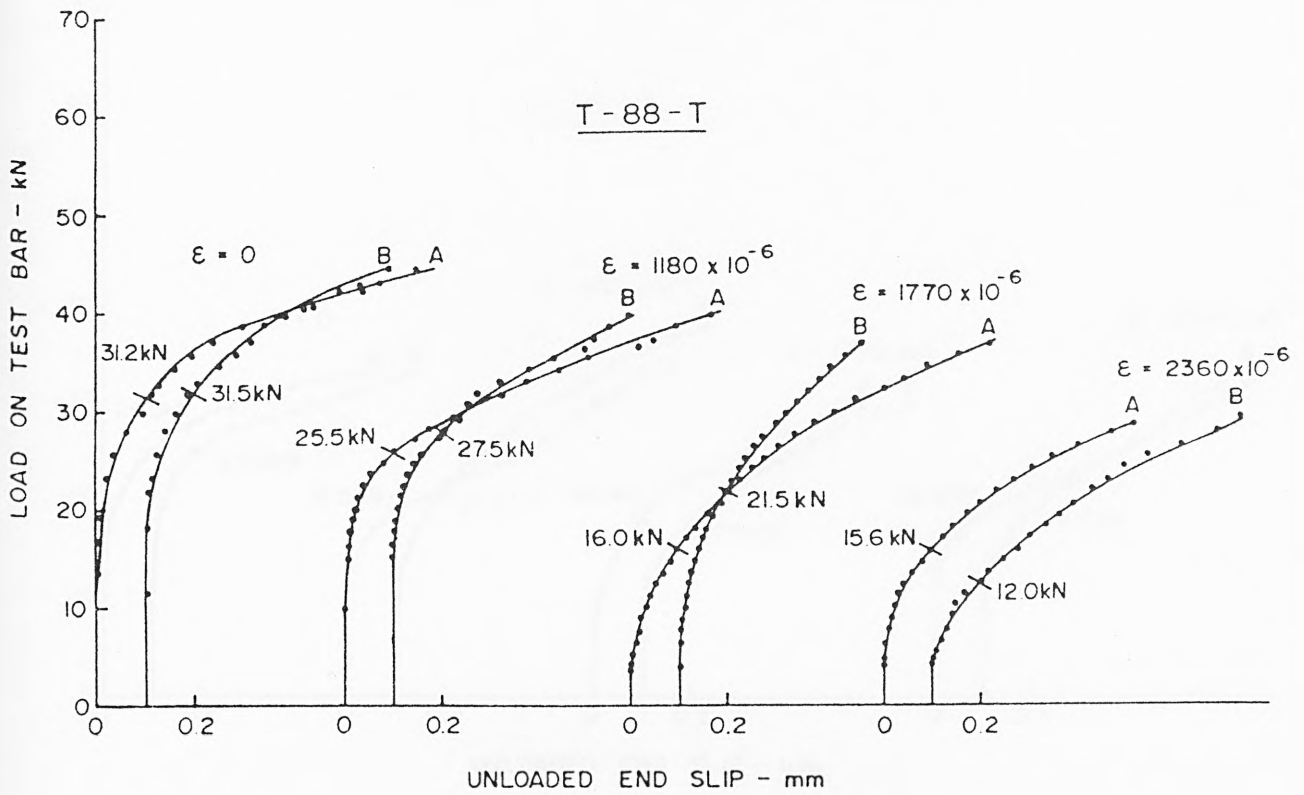


FIG. A.1 LOAD - SLIP CHARACTERISTICS AT UNLOADED END - TORBAR

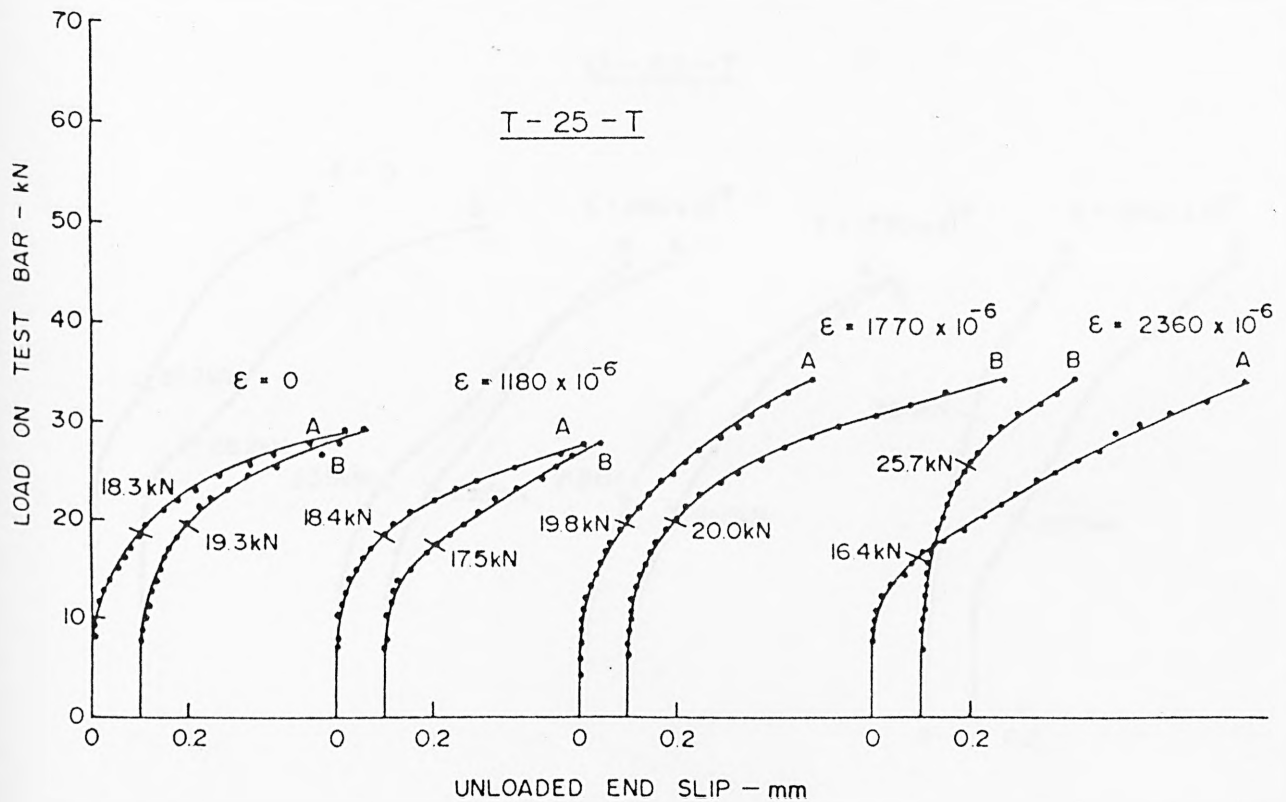
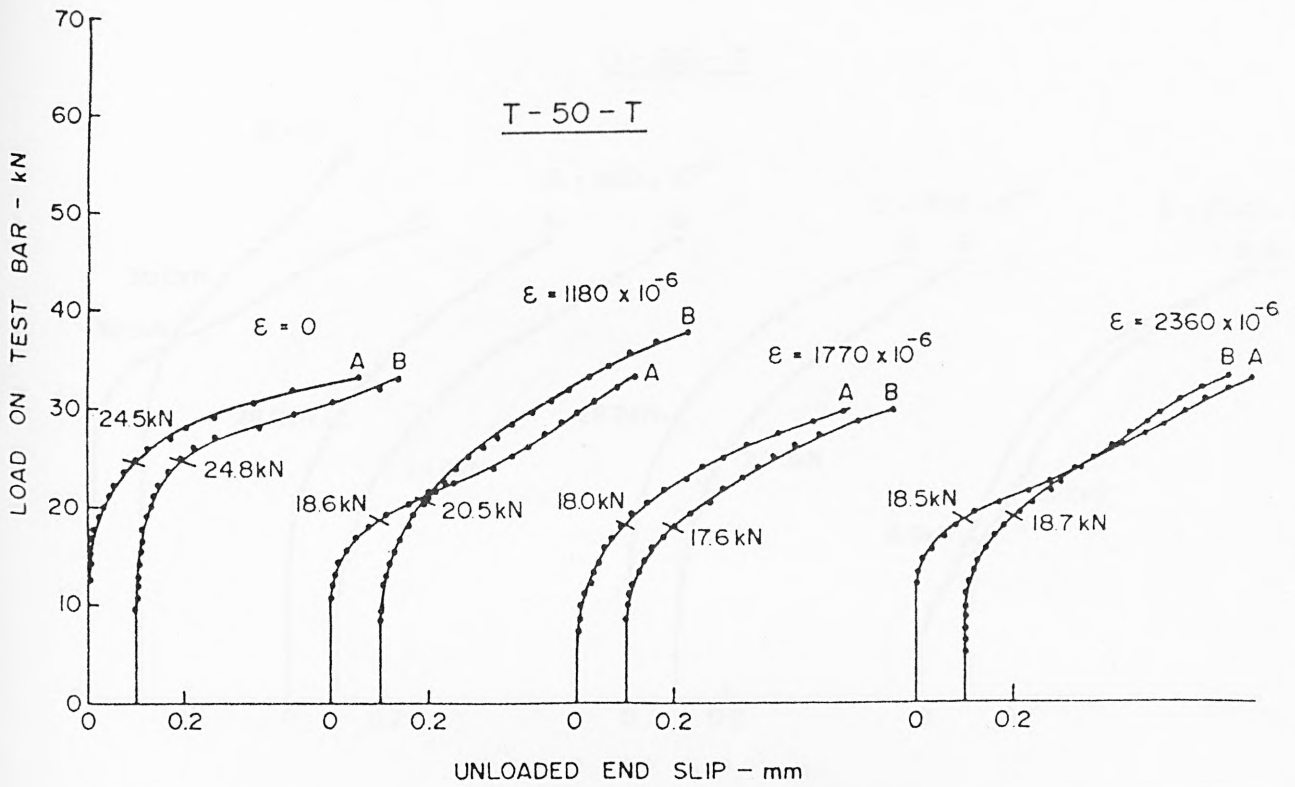


FIG. A2 LOAD-SLIP CHARACTERISTICS AT UNLOADED END - TORBAR

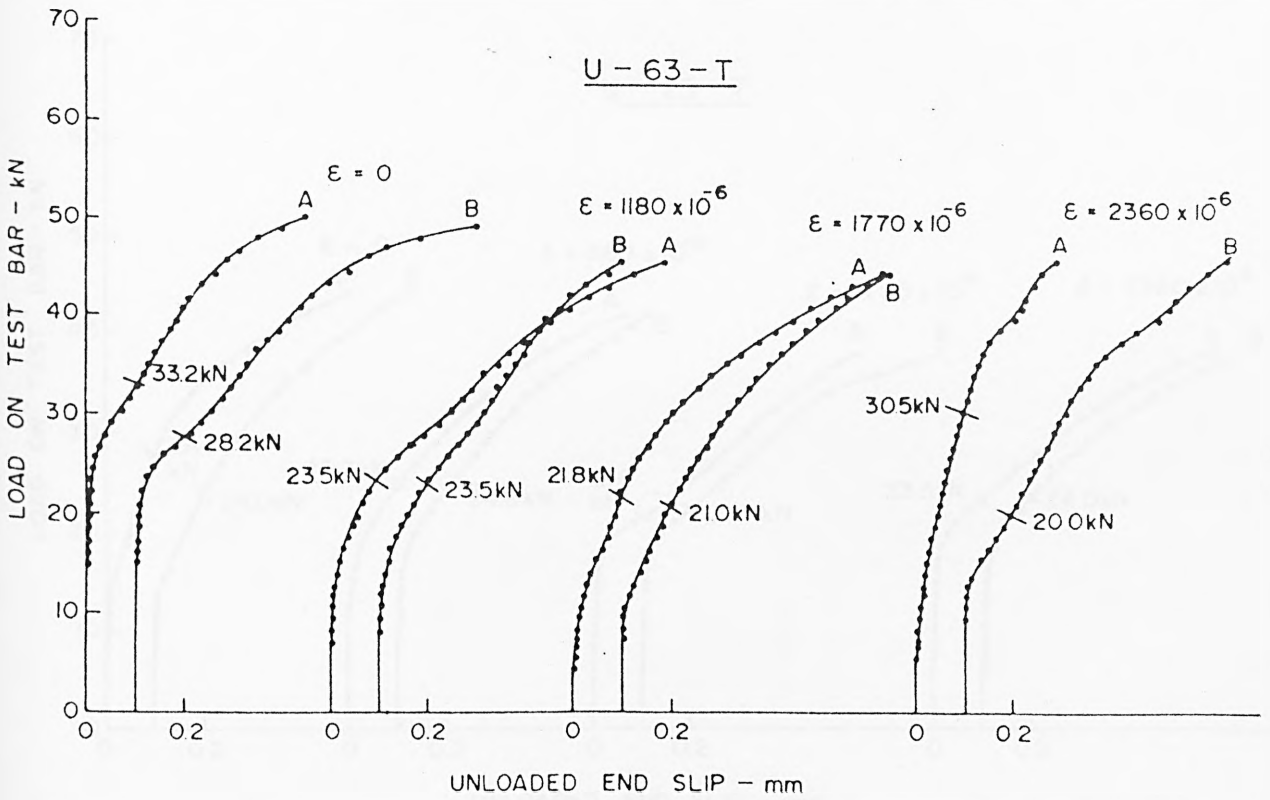
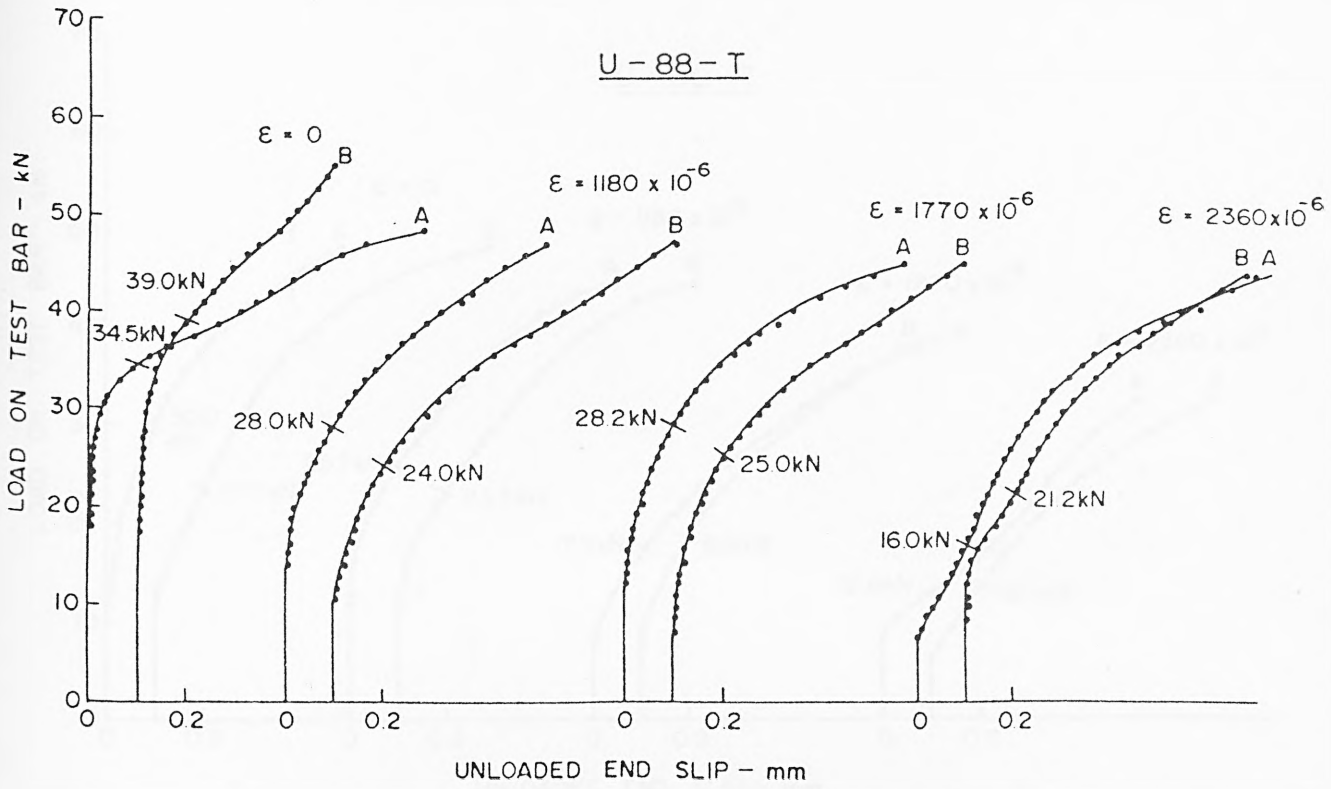


FIG A.3 LOAD-SLIP CHARACTERISTICS AT UNLOADED END - HYBAR

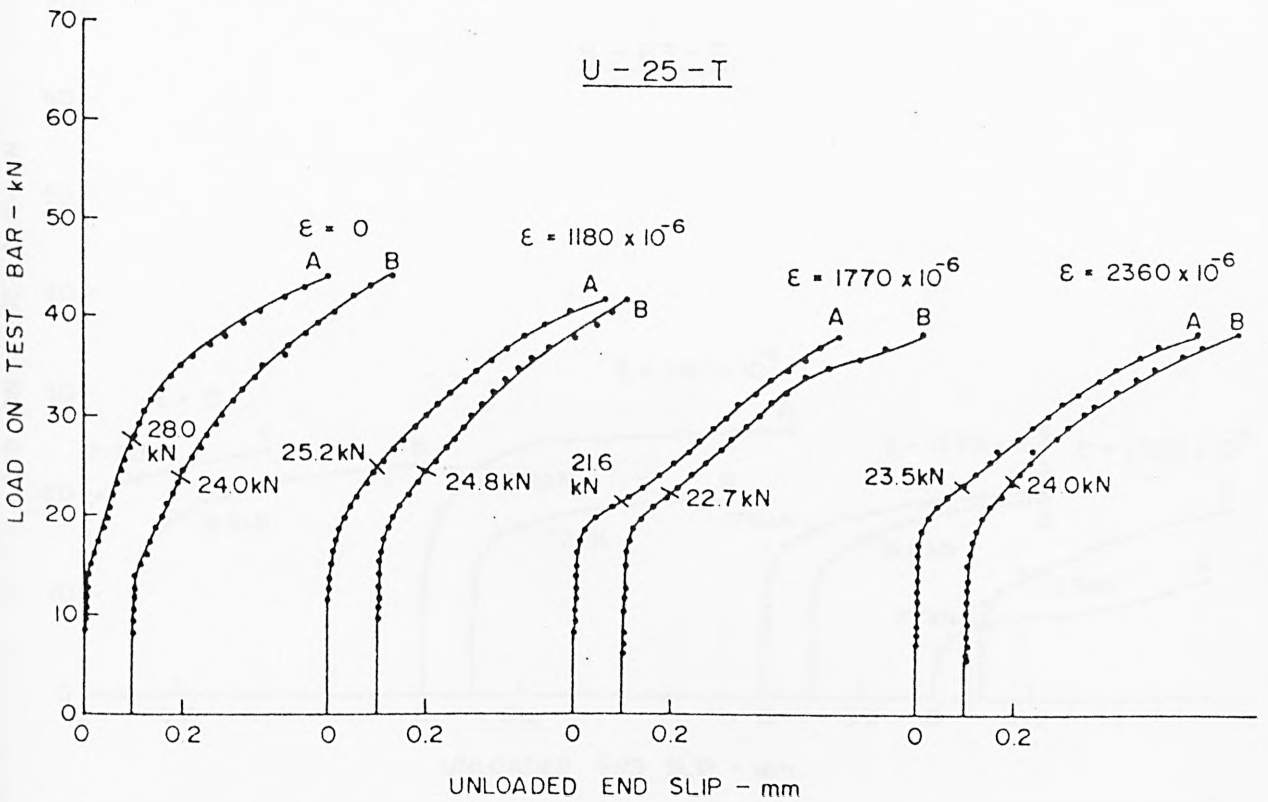
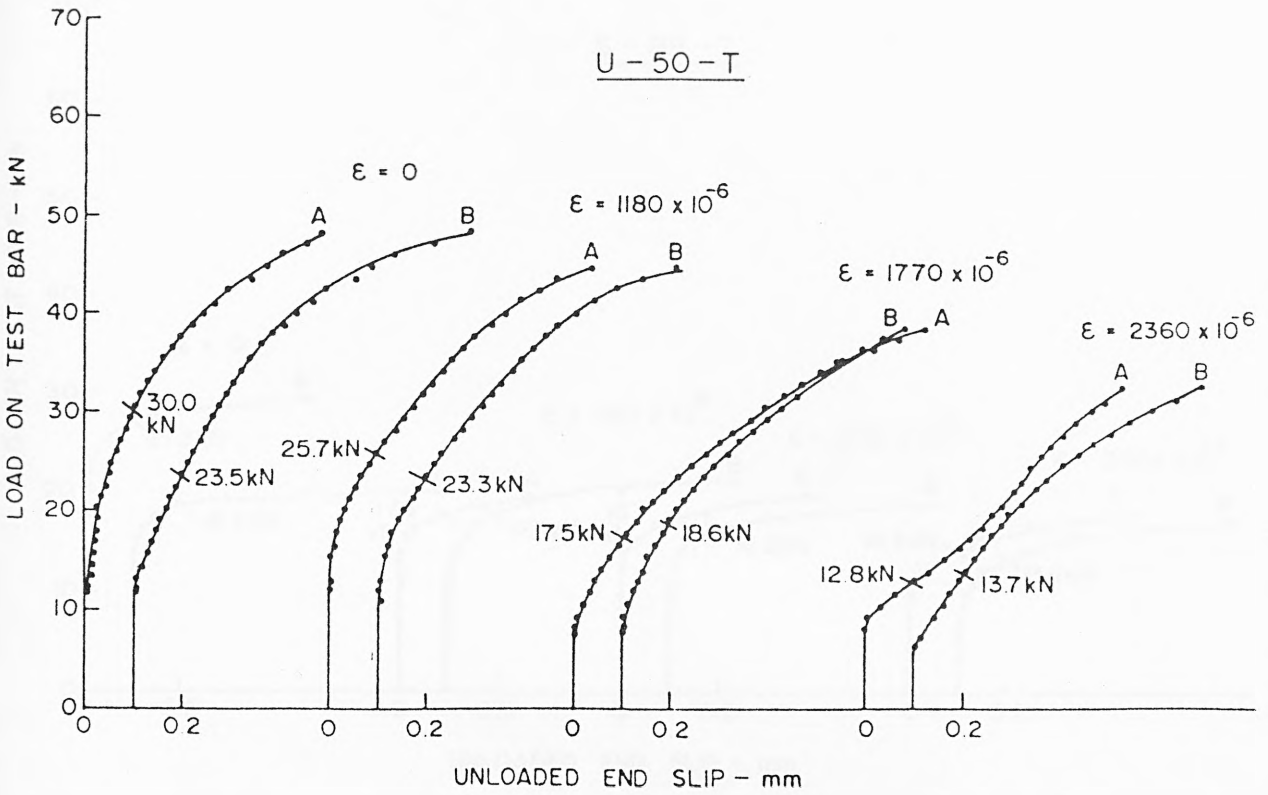
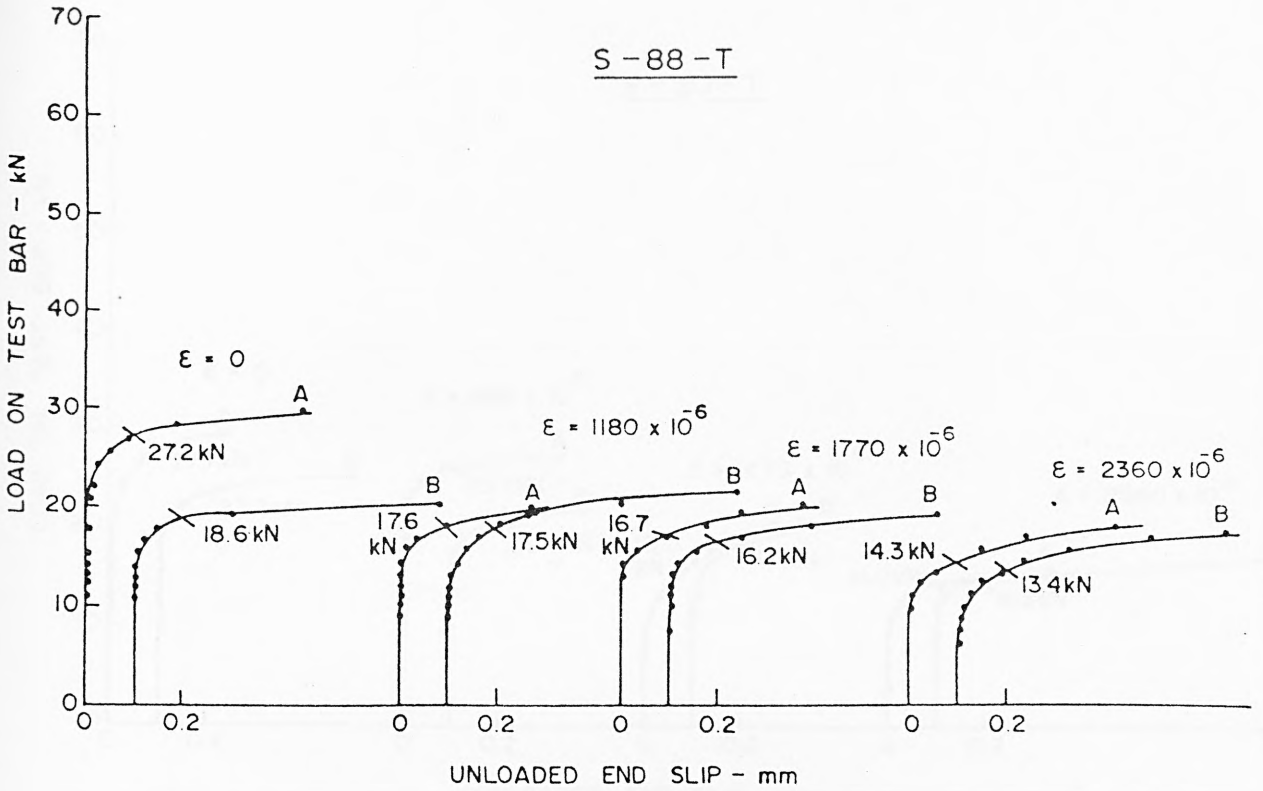


FIG A4 LOAD-SLIP CHARACTERISTICS AT UNLOADED END - HYBAR

S - 88 - T



S - 63 - T

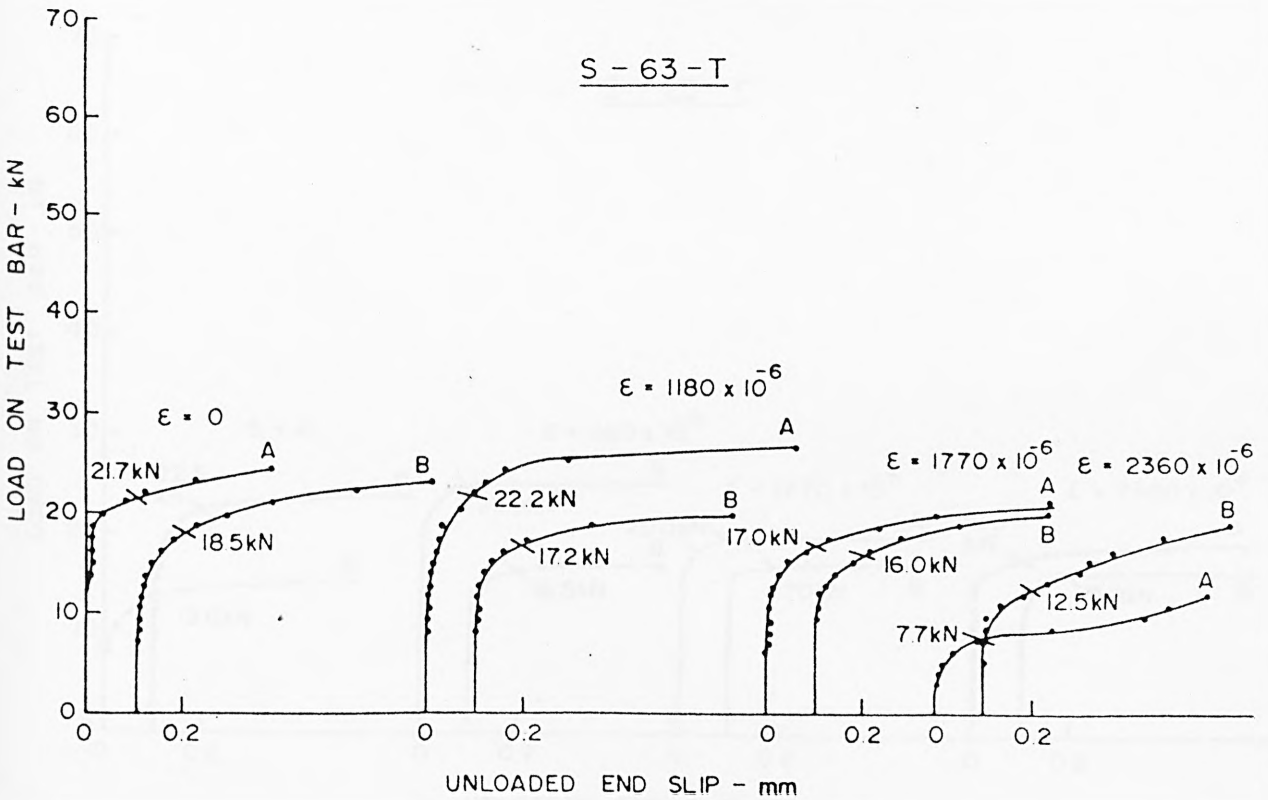


FIG A.5 LOAD-SLIP CHARACTERISTICS AT UNLOADED END - SQUARE-TWISTED BAR

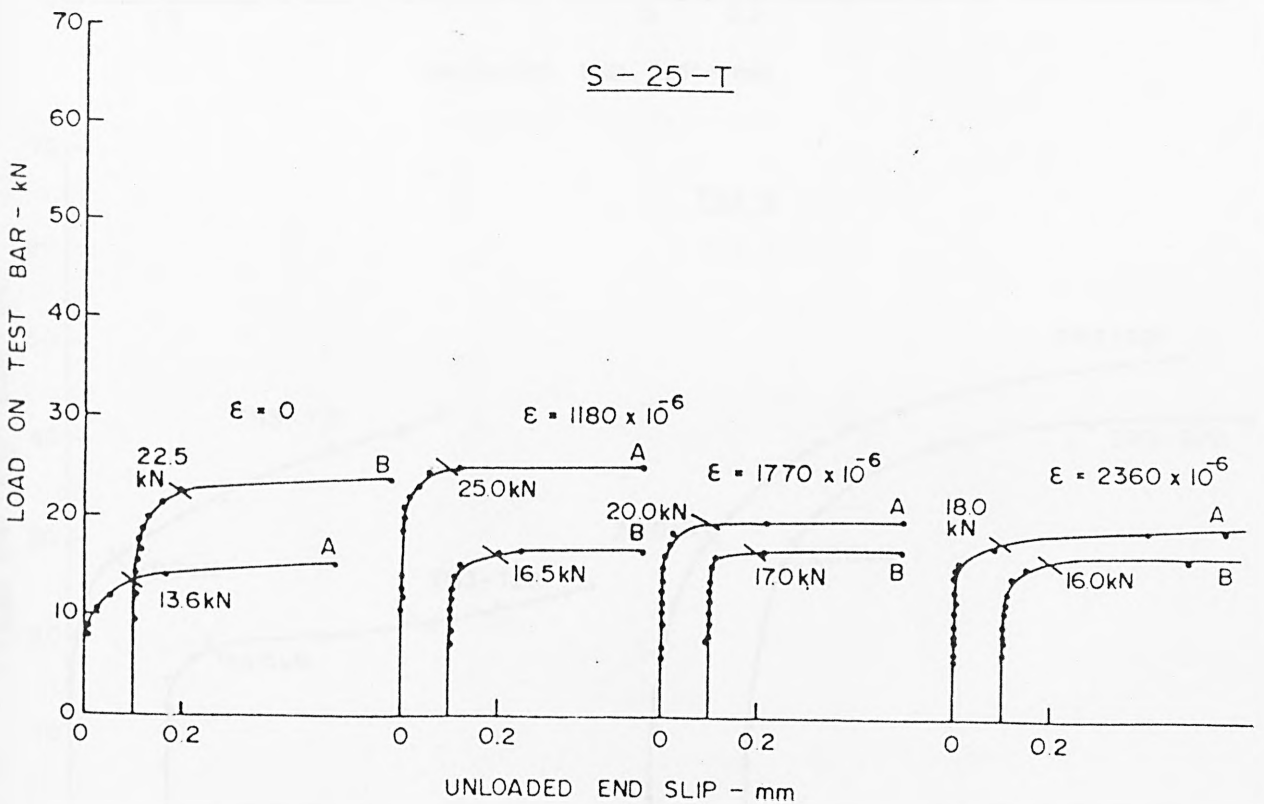
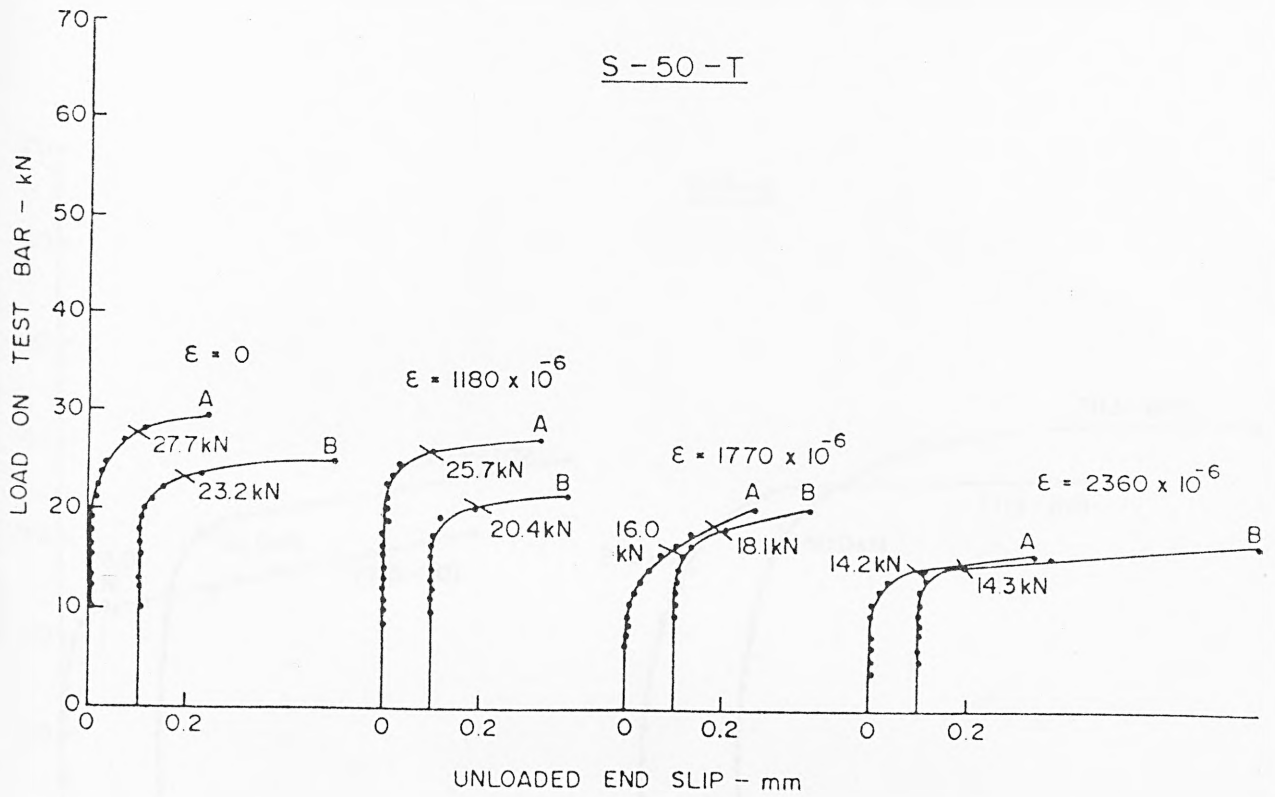


FIG A6 LOAD-SLIP CHARACTERISTICS AT UNLOADED END - SQUARE-TWISTED BAR

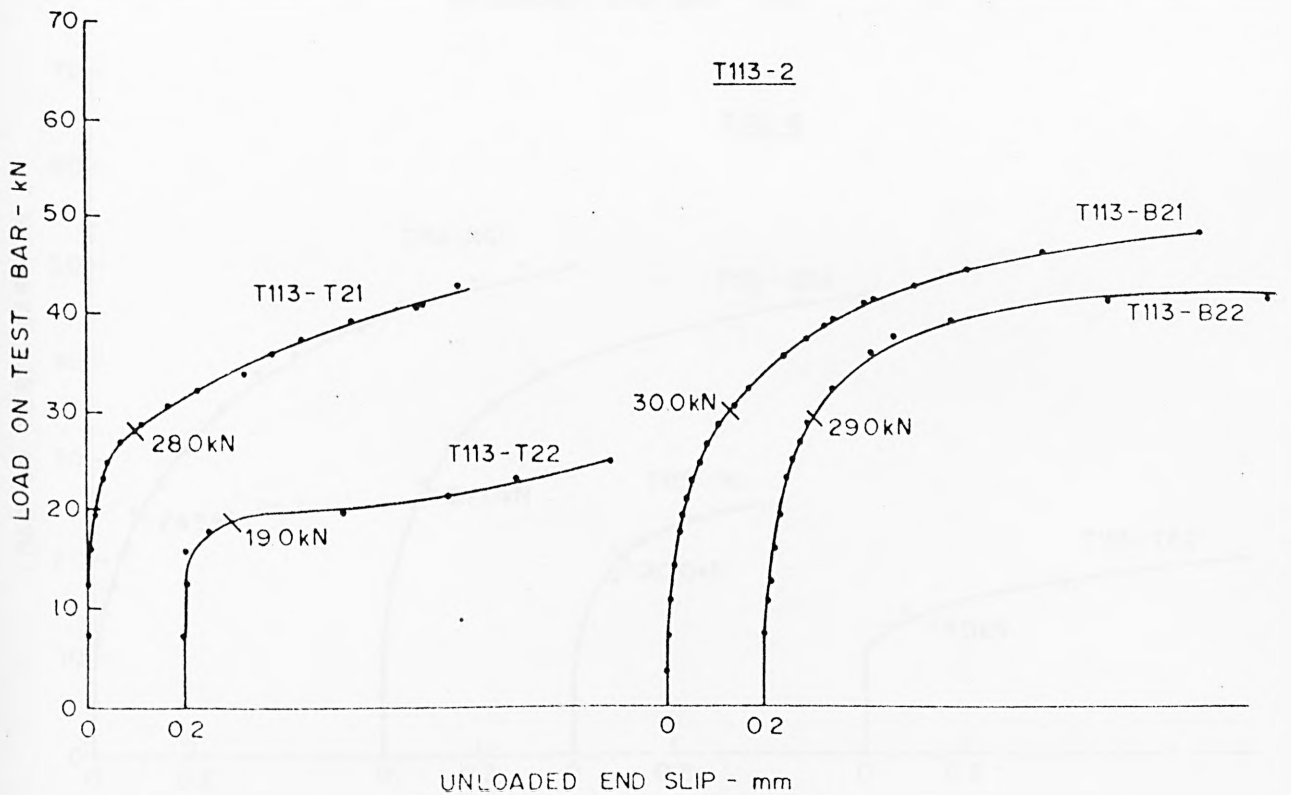
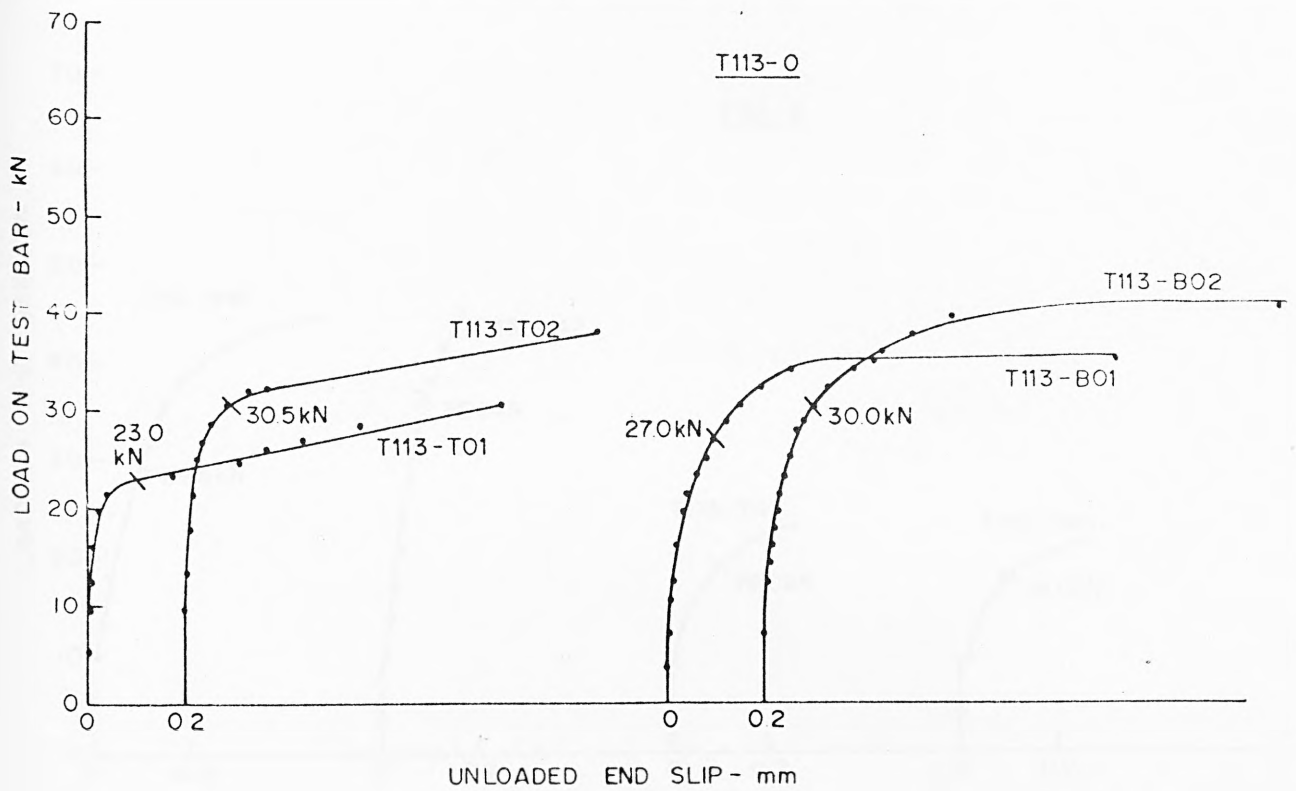


FIG A7 LOAD - SLIP CHARACTERISTICS AT UNLOADED END - TORBAR

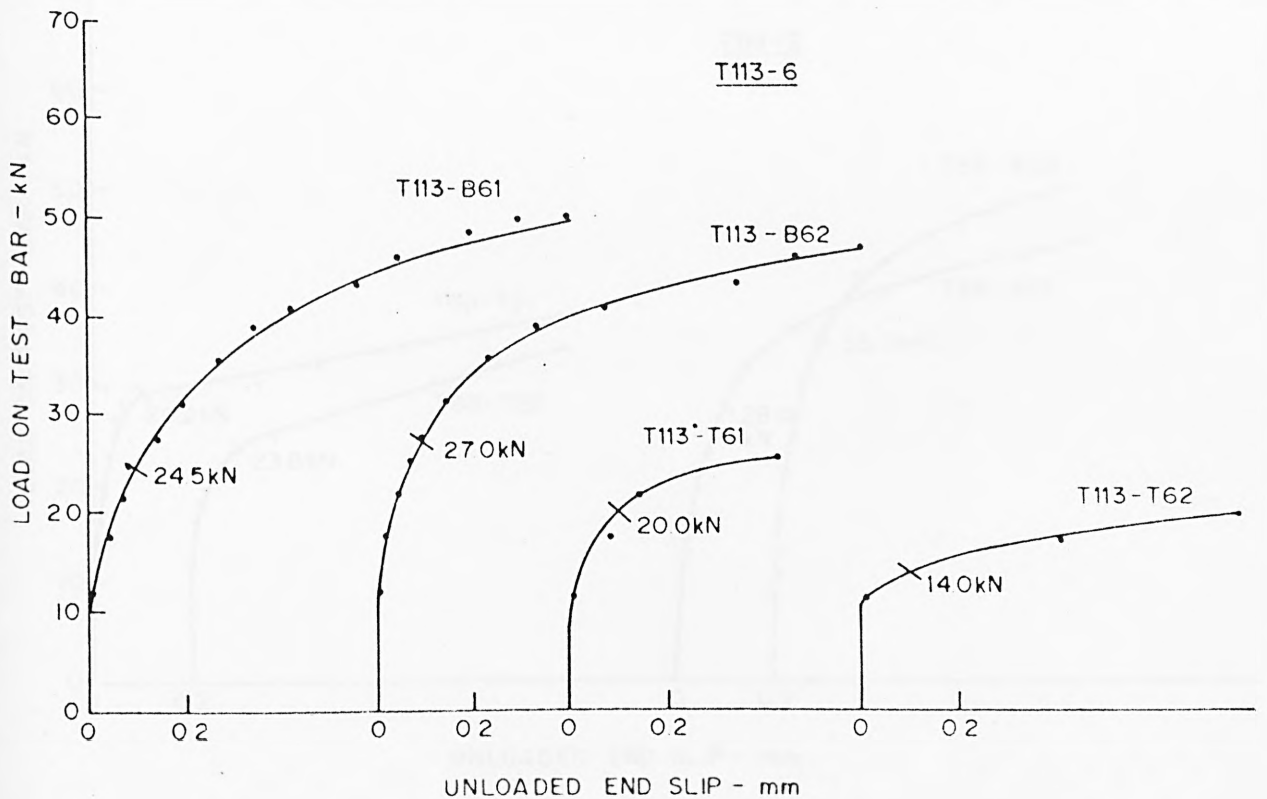
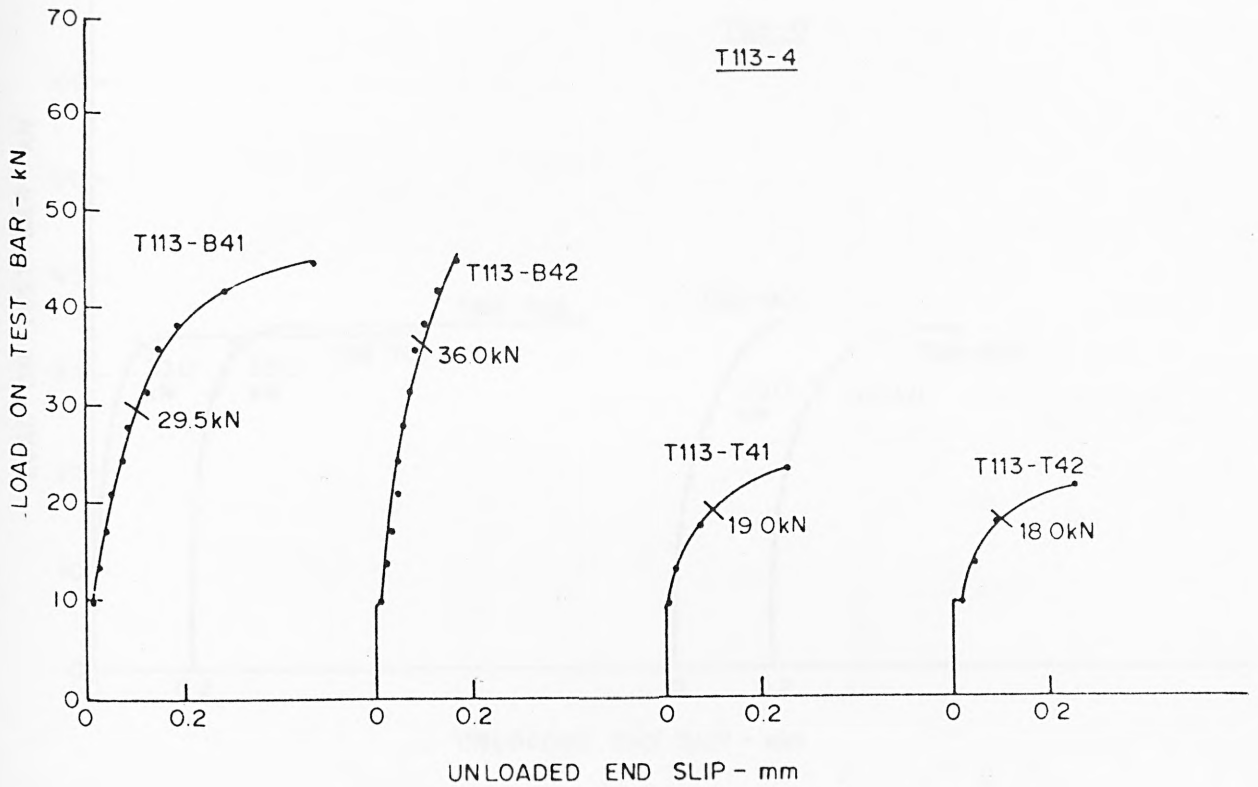


FIG A8 LOAD-SLIP CHARACTERISTICS AT UNLOADED END - TORBAR

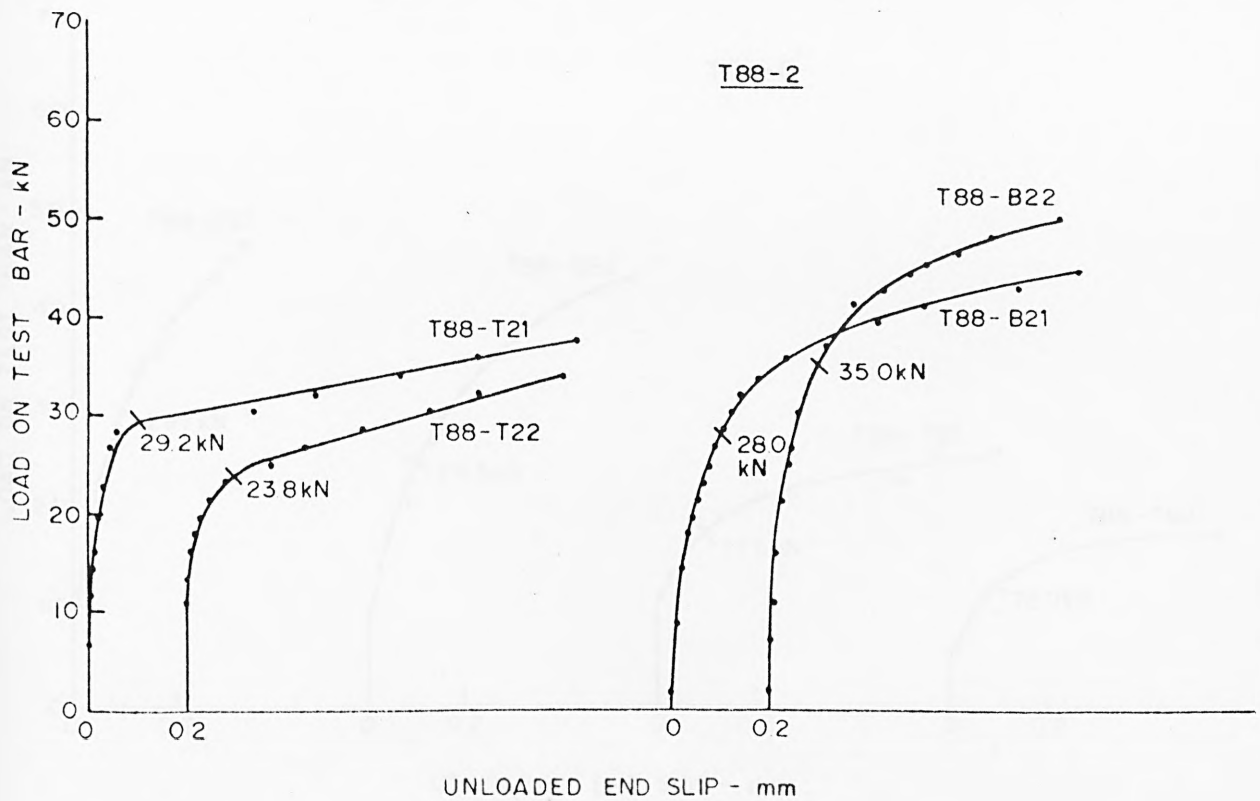
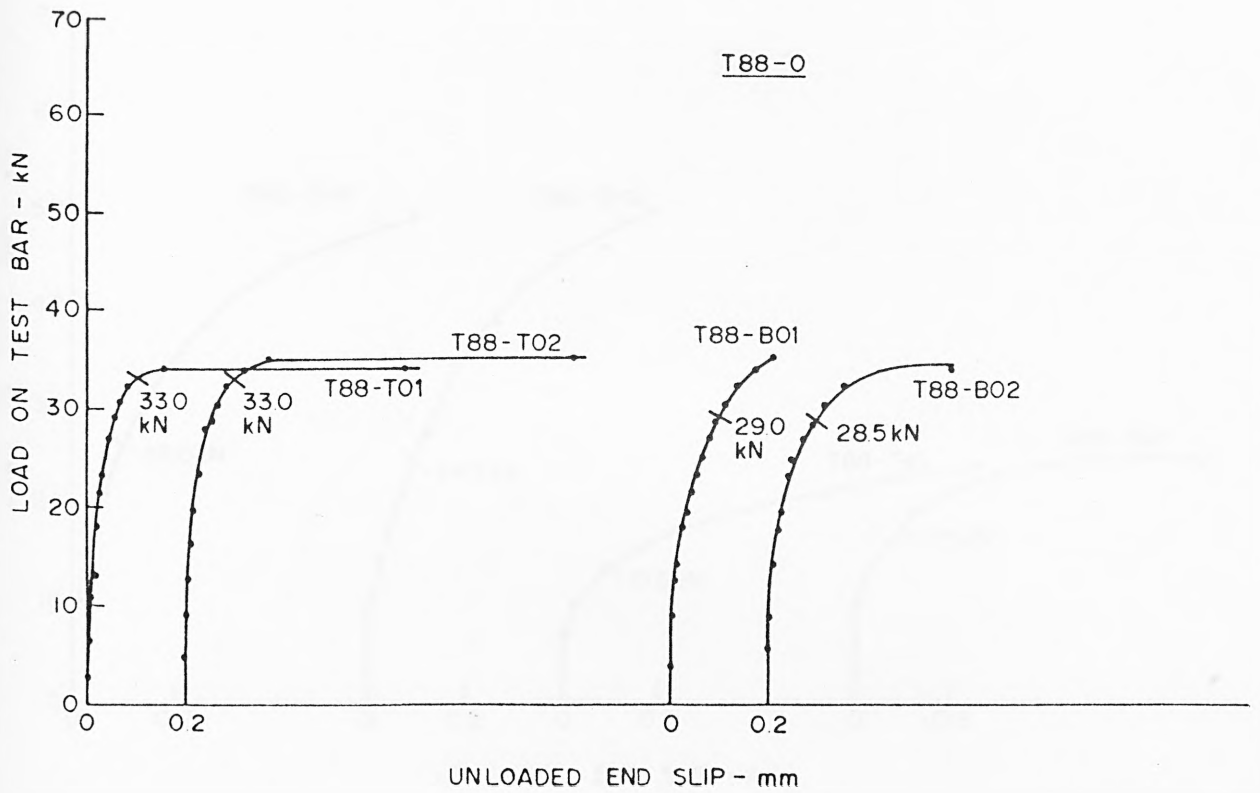


FIG. A.9 LOAD-SLIP CHARACTERISTICS AT UNLOADED END - TORBAR

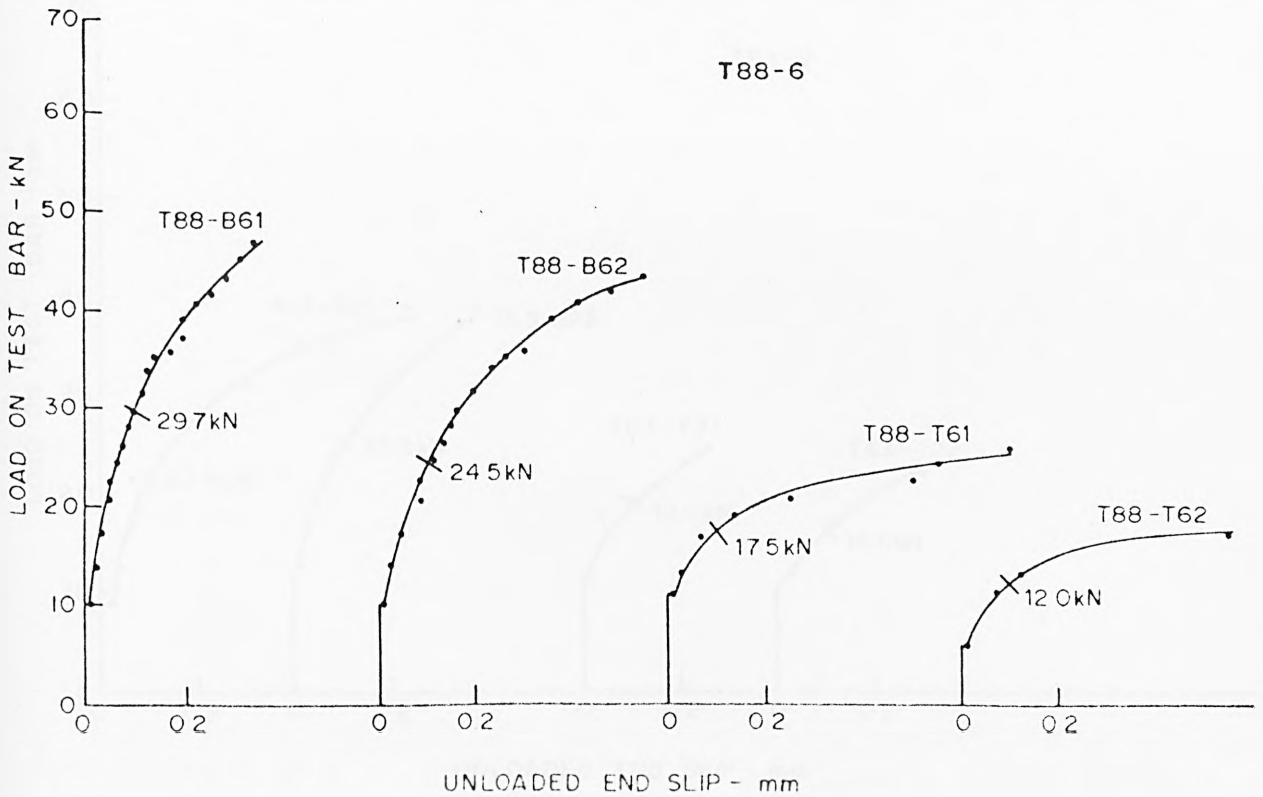
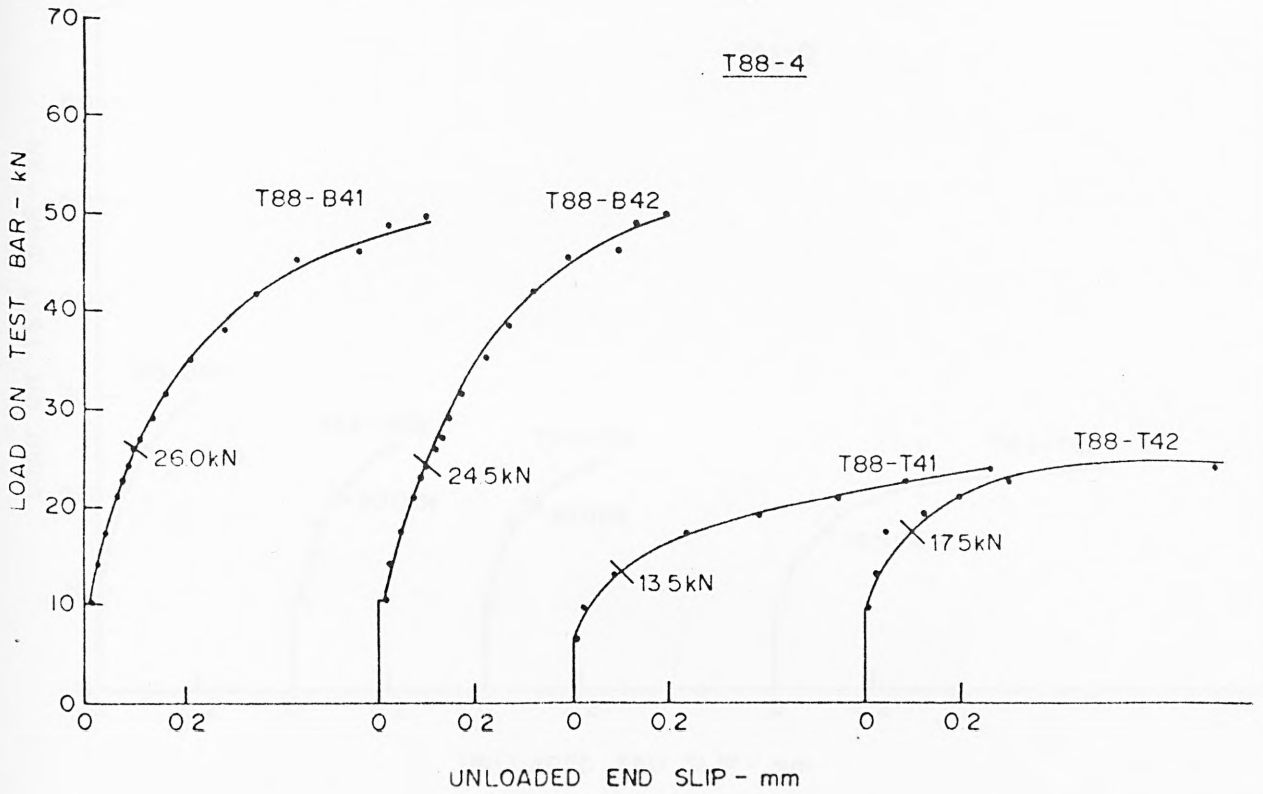


FIG A10 LOAD-SLIP CHARACTERISTICS AT UNLOADED END - TORBAR

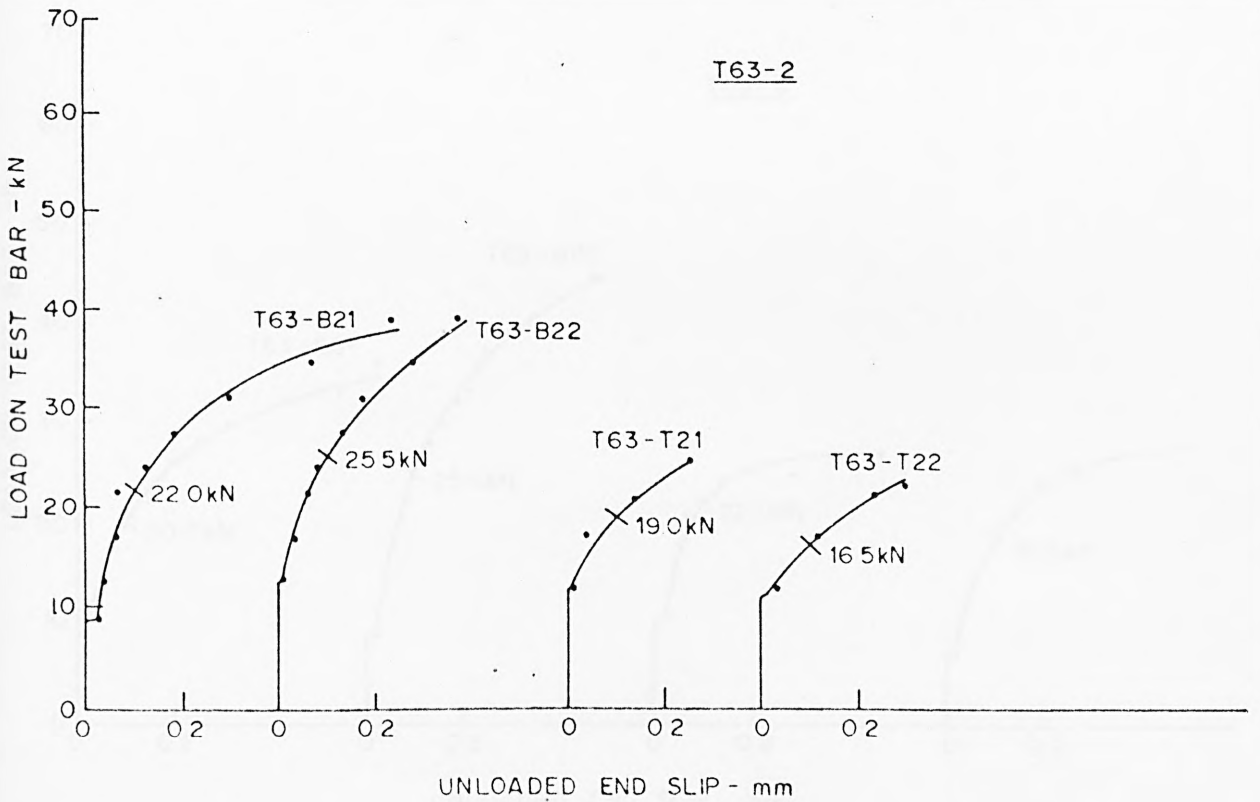
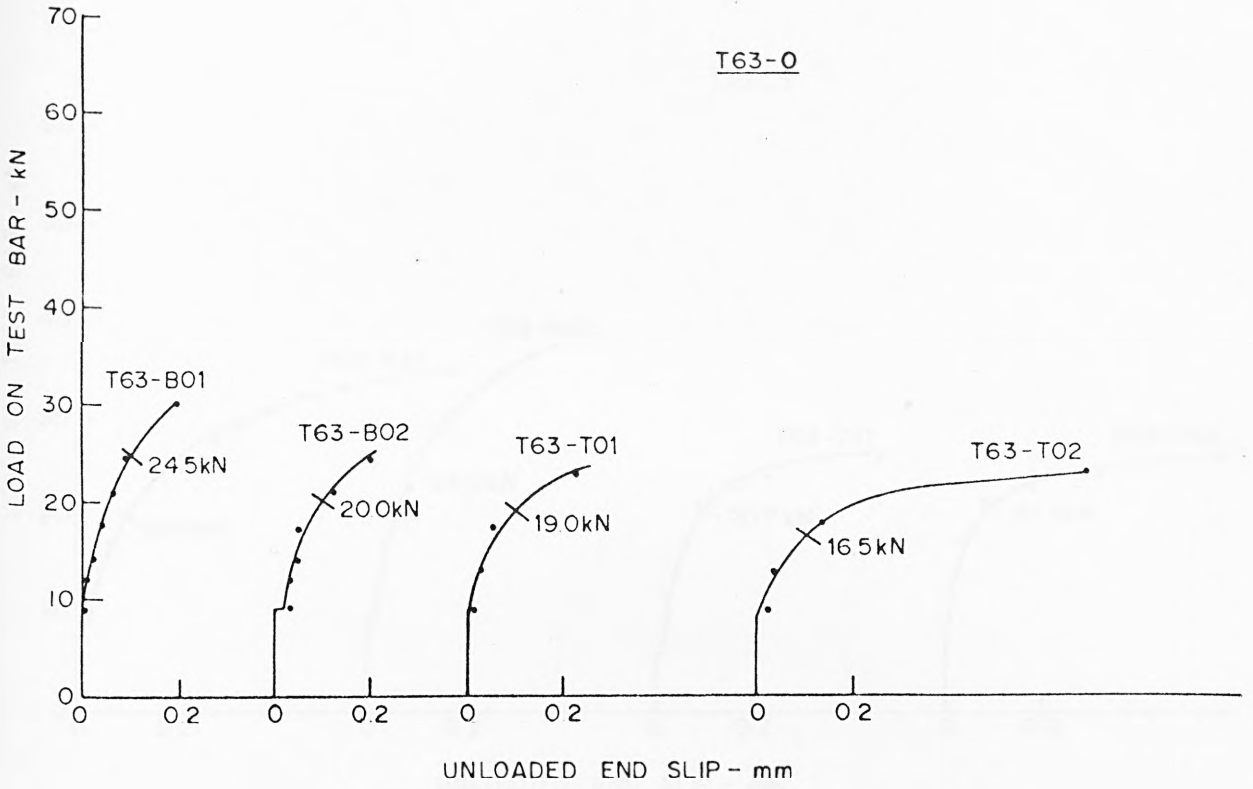


FIG A11 LOAD-SLIP CHARACTERISTICS AT UNLOADED END - TORBAR

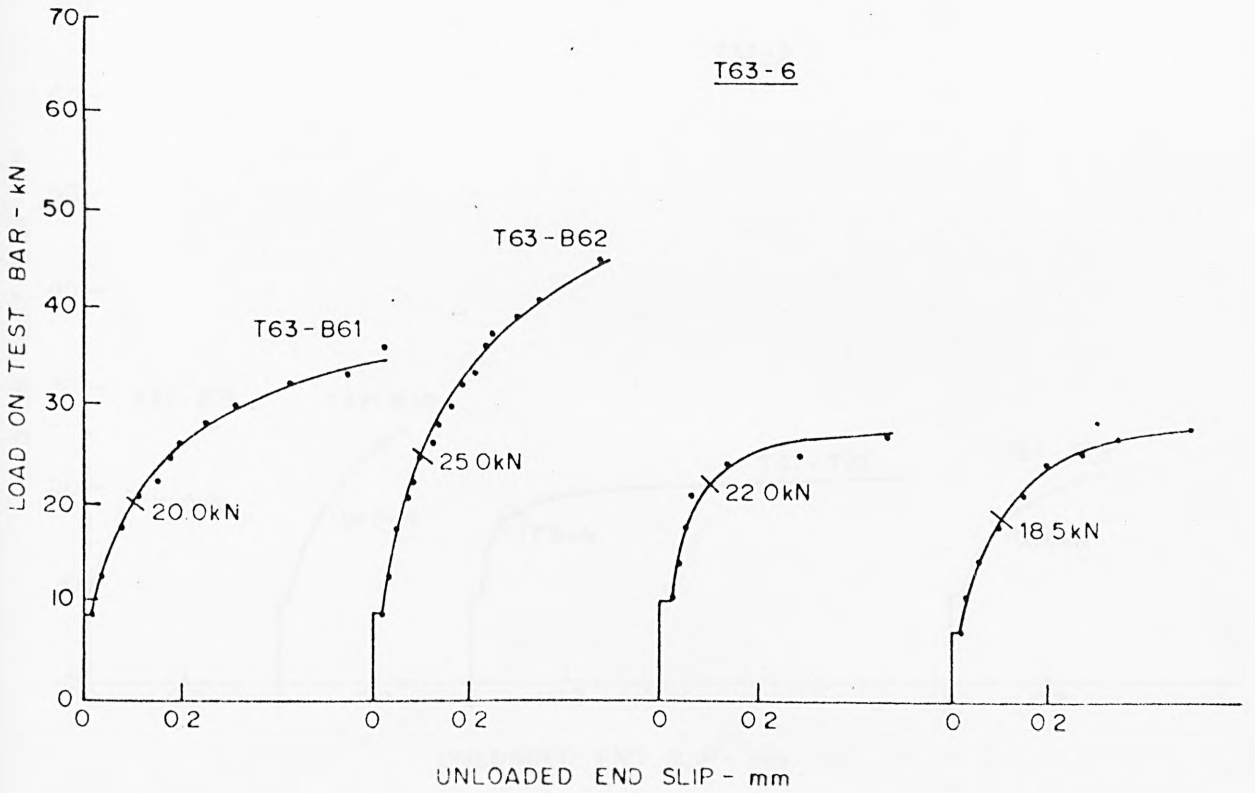
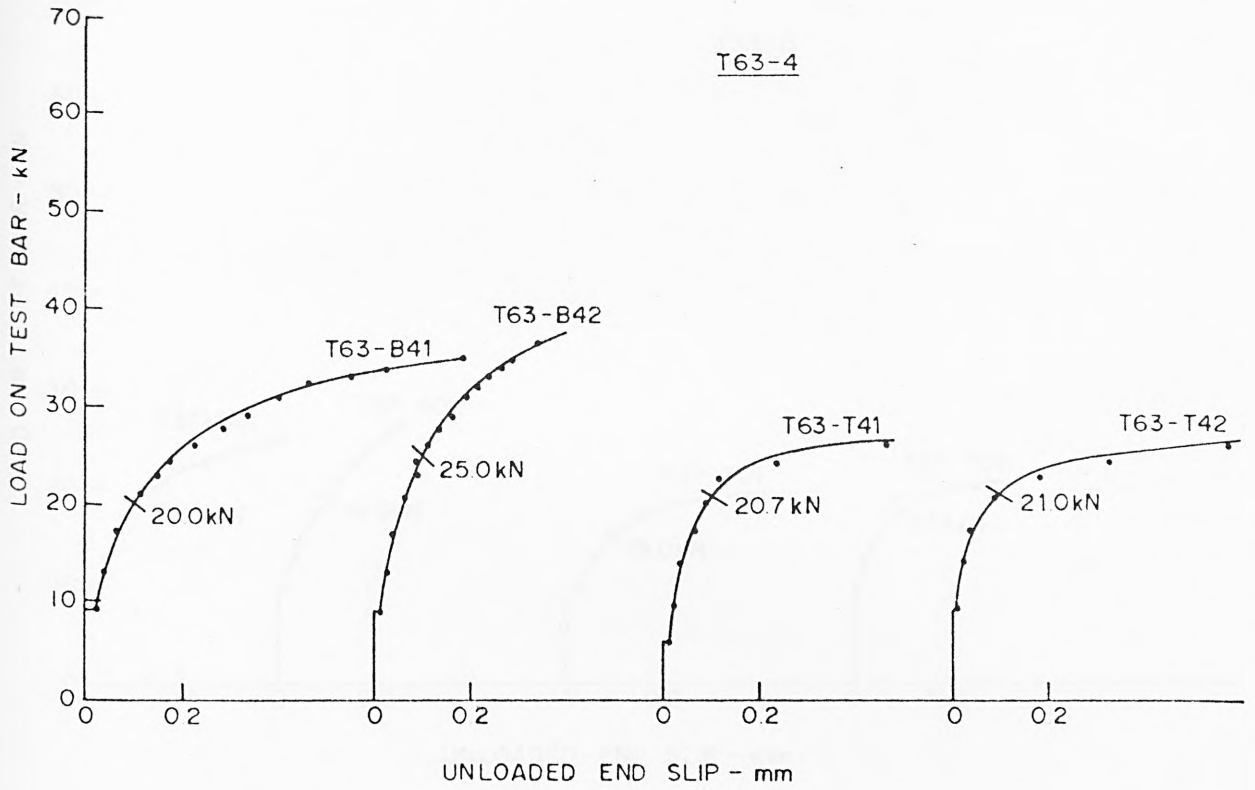


FIG A12 LOAD-SLIP CHARACTERISTICS AT UNLOADED END - TORBAR

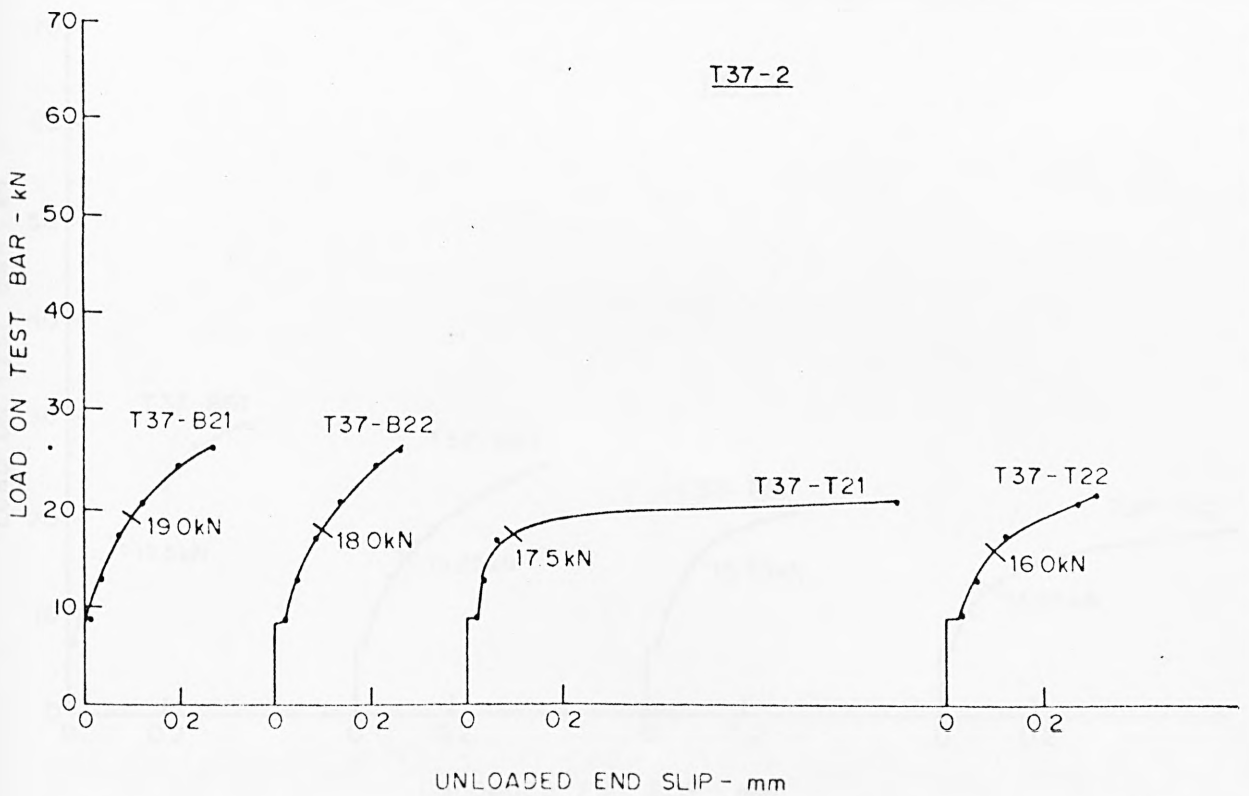
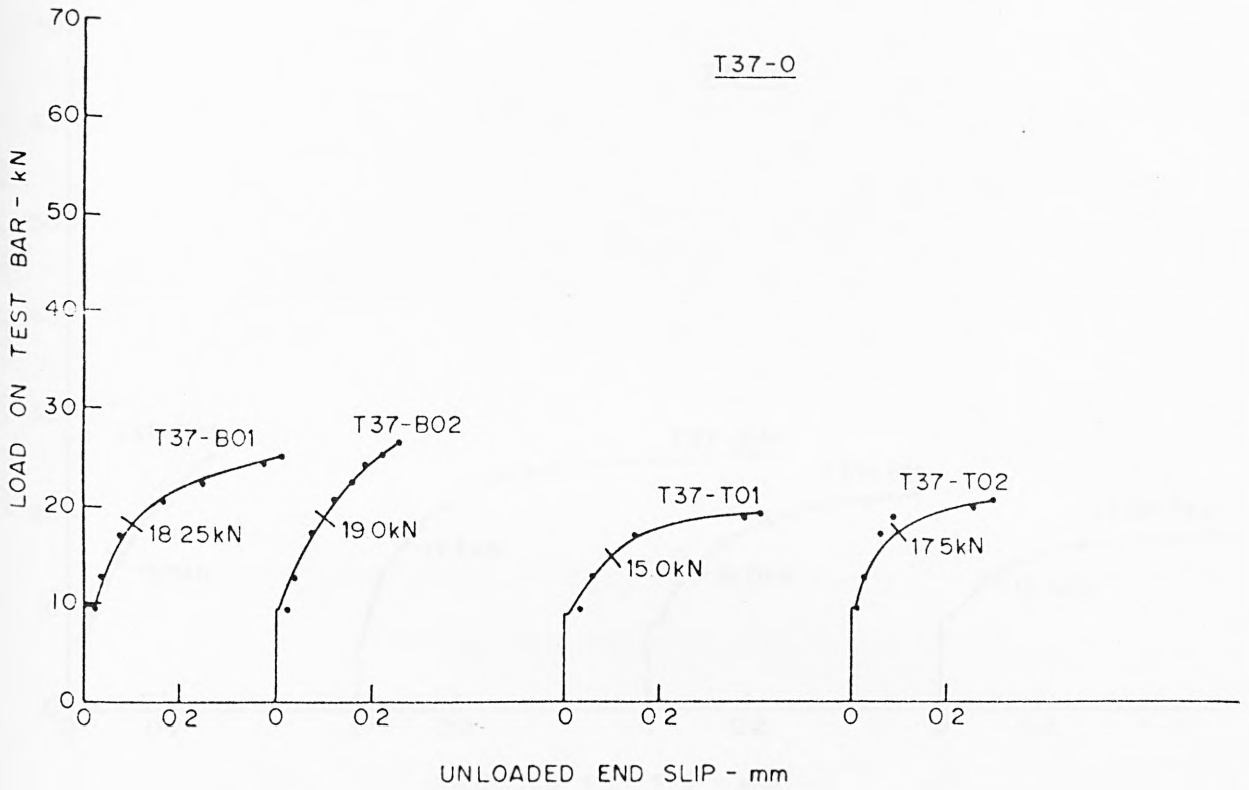


FIG A13 LOAD-SLIP CHARACTERISTICS AT UNLOADED END - TORBAR

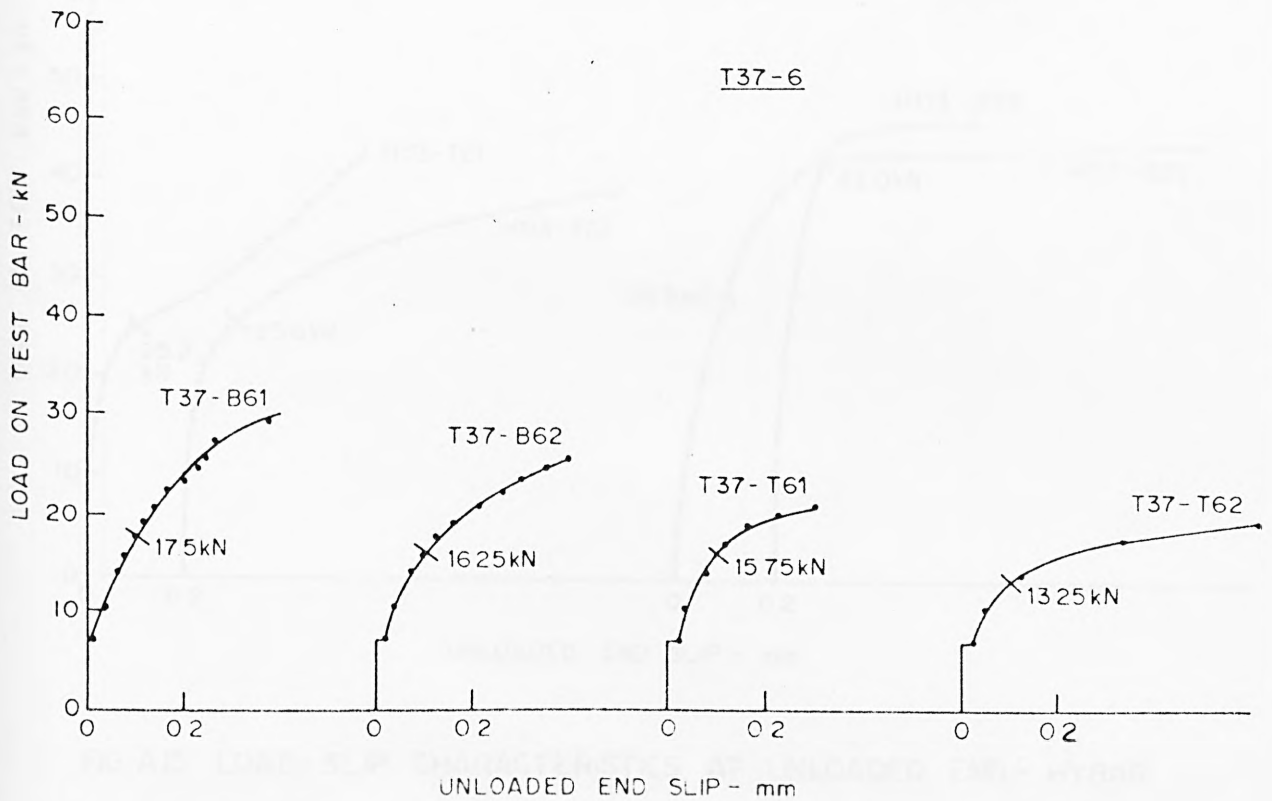
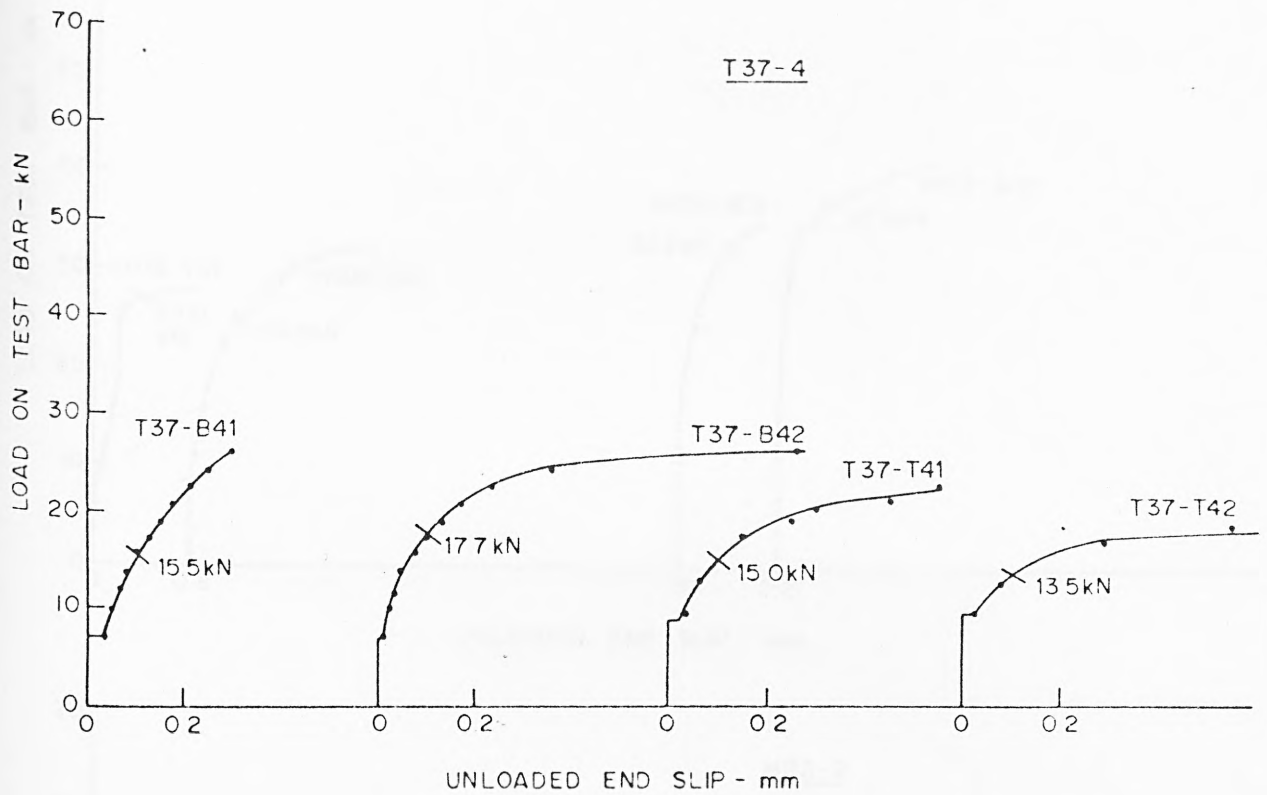


FIG A14 LOAD-SLIP CHARACTERISTICS AT UNLOADED END - TORBAR

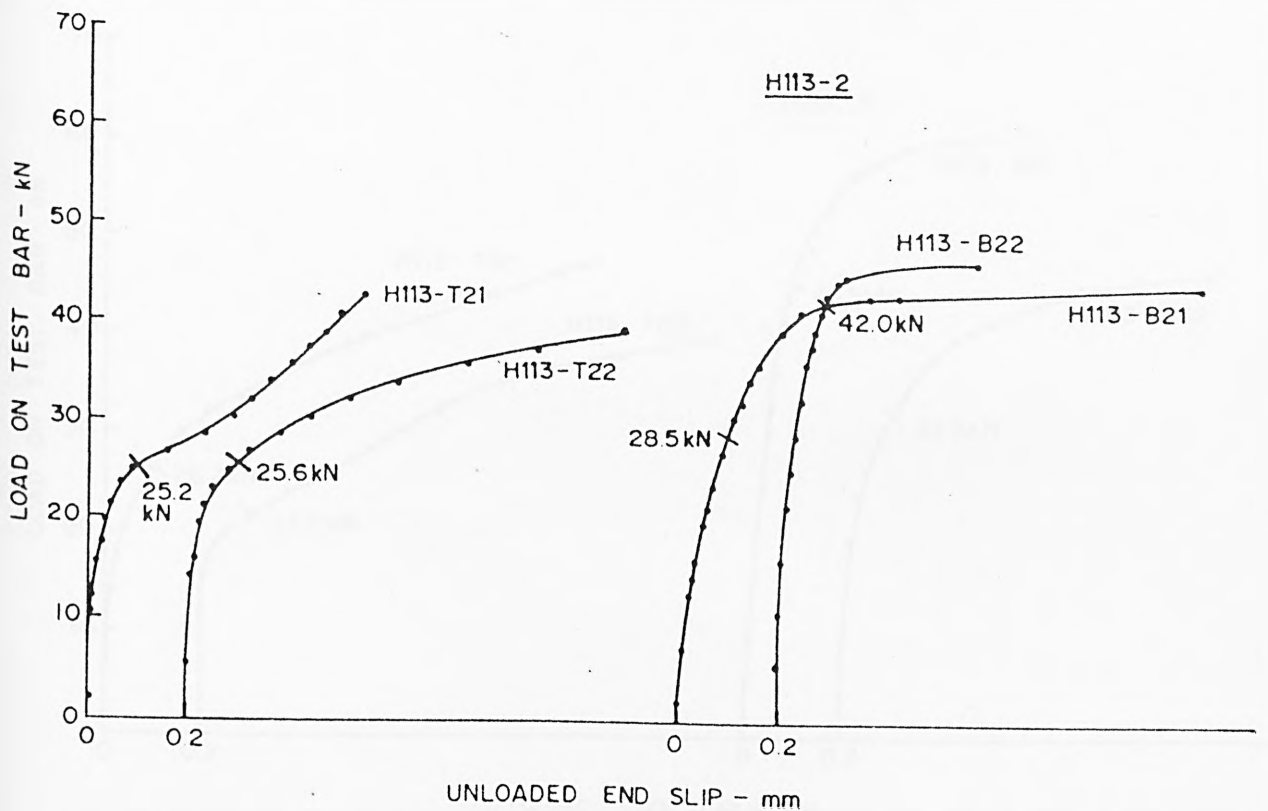
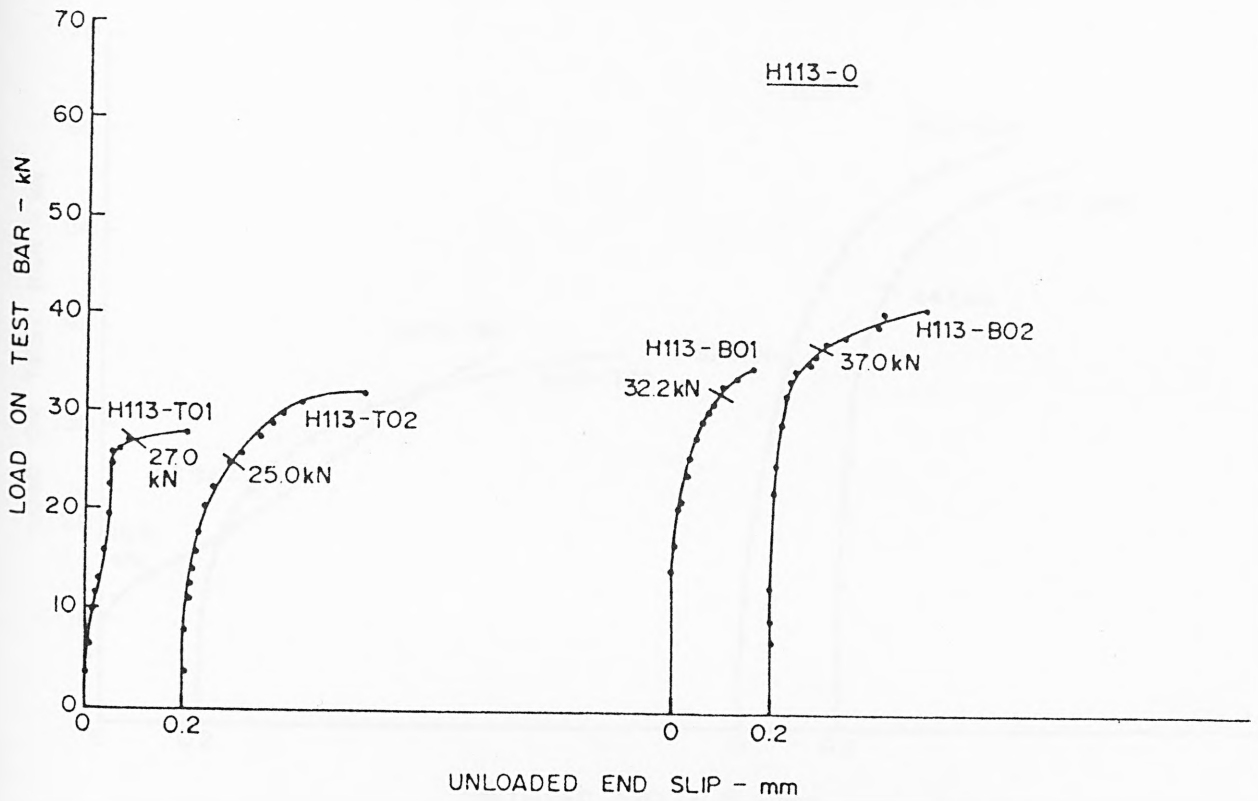


FIG. A15 LOAD-SLIP CHARACTERISTICS AT UNLOADED END - HYBAR

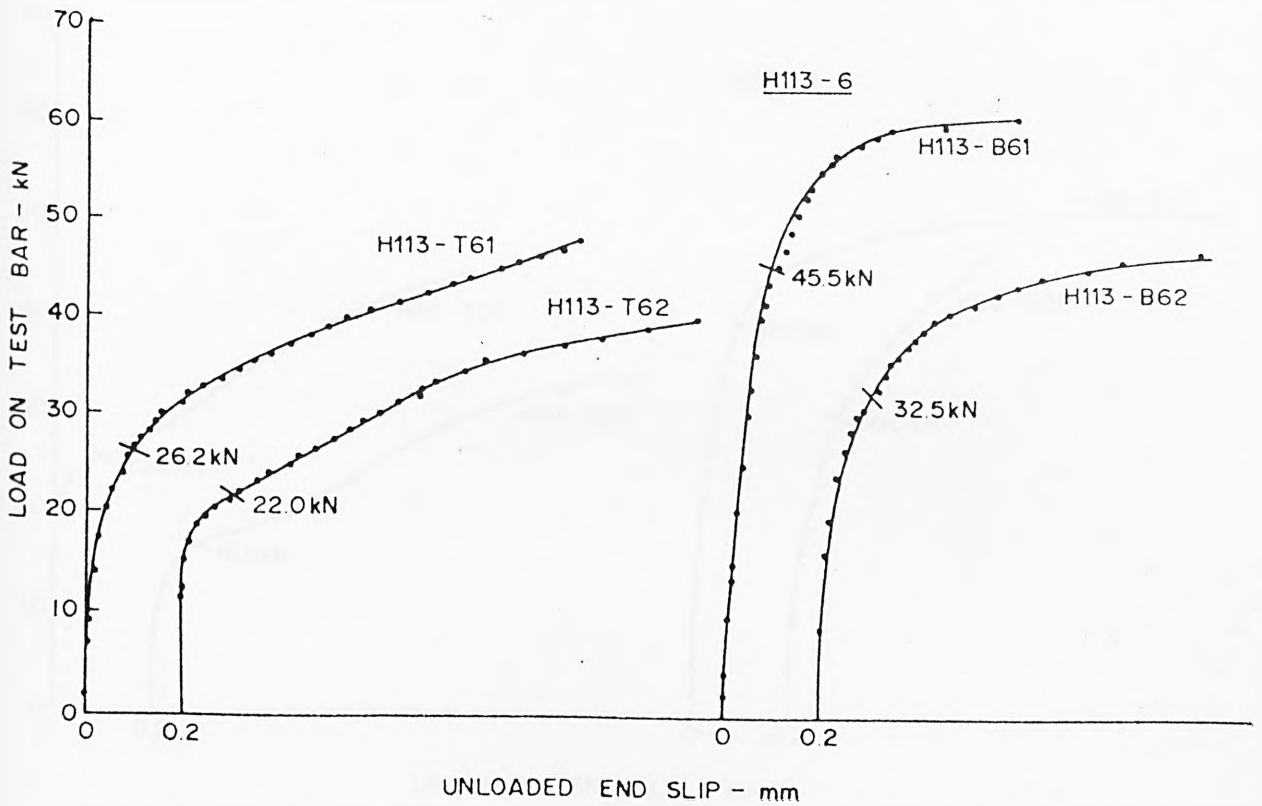
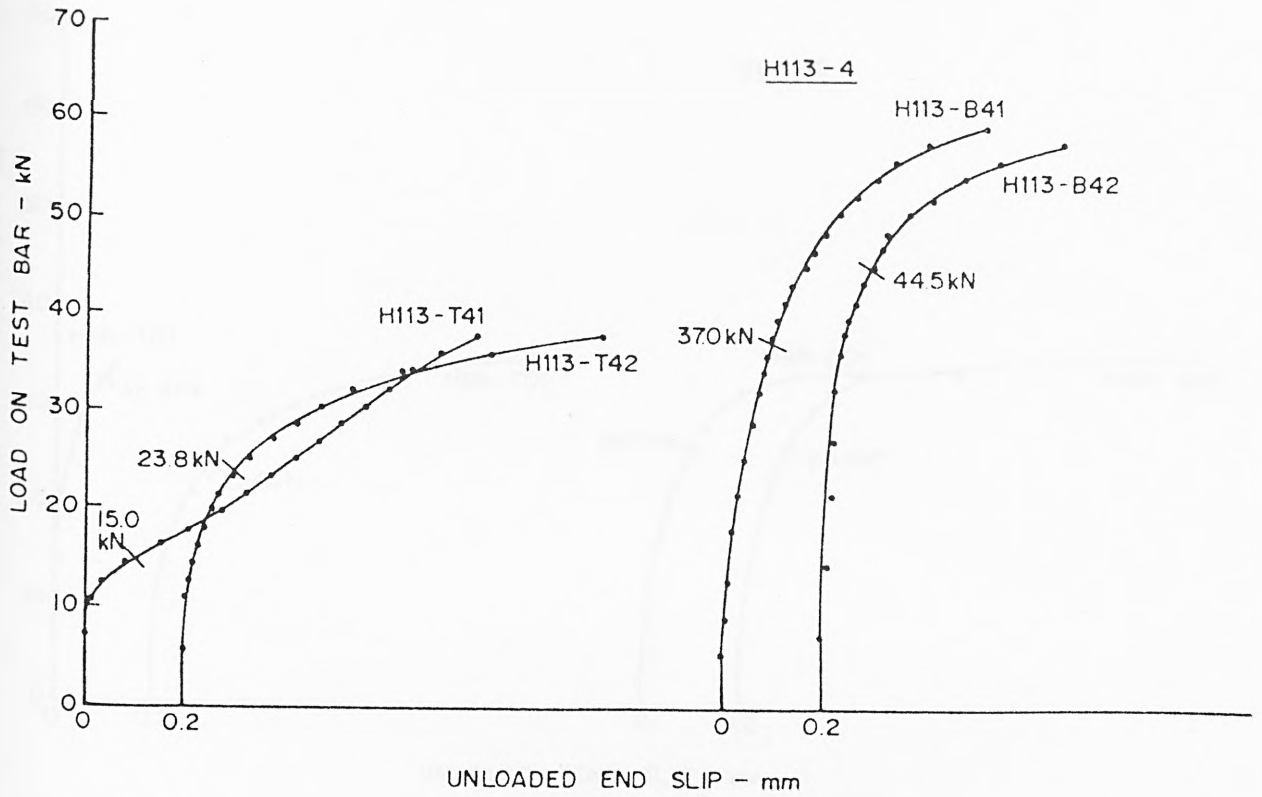


FIG. A.16 LOAD-SLIP CHARACTERISTICS AT UNLOADED END - HYBAR

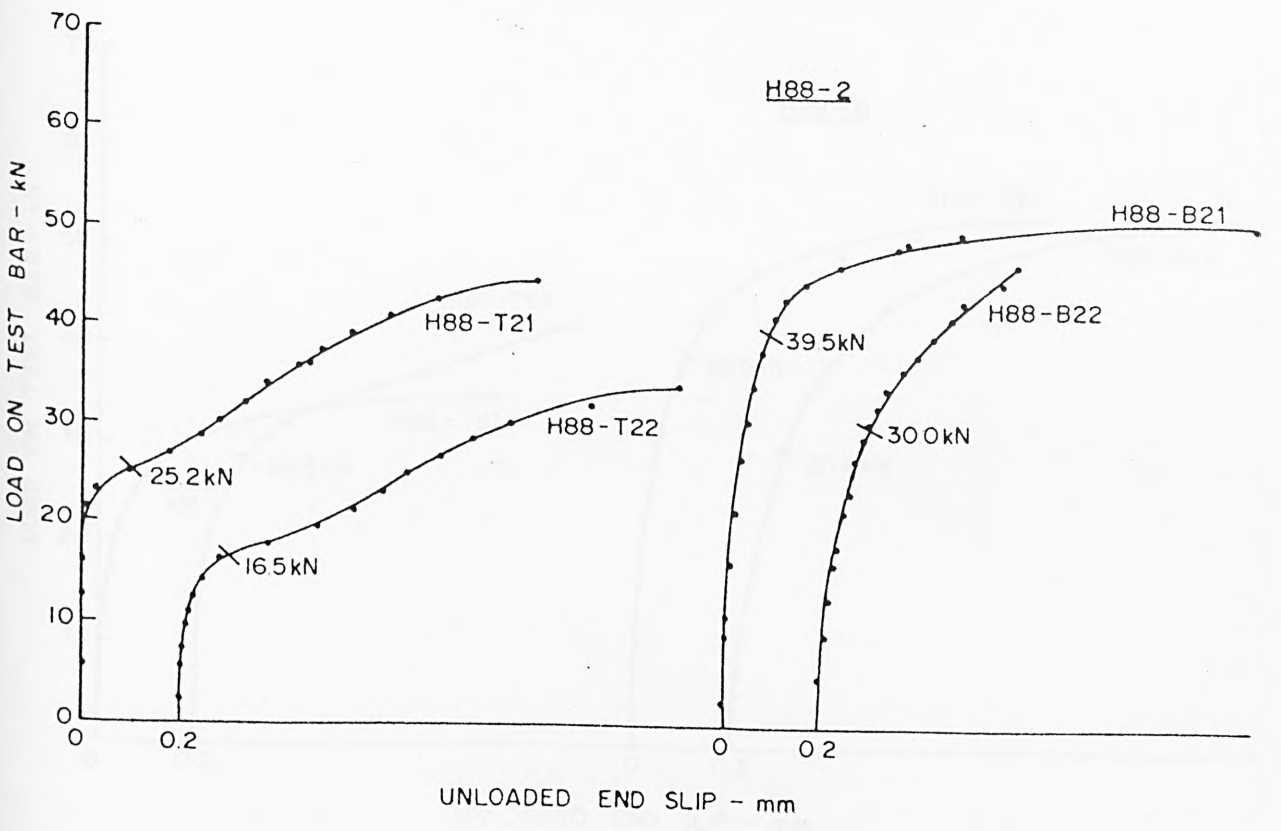
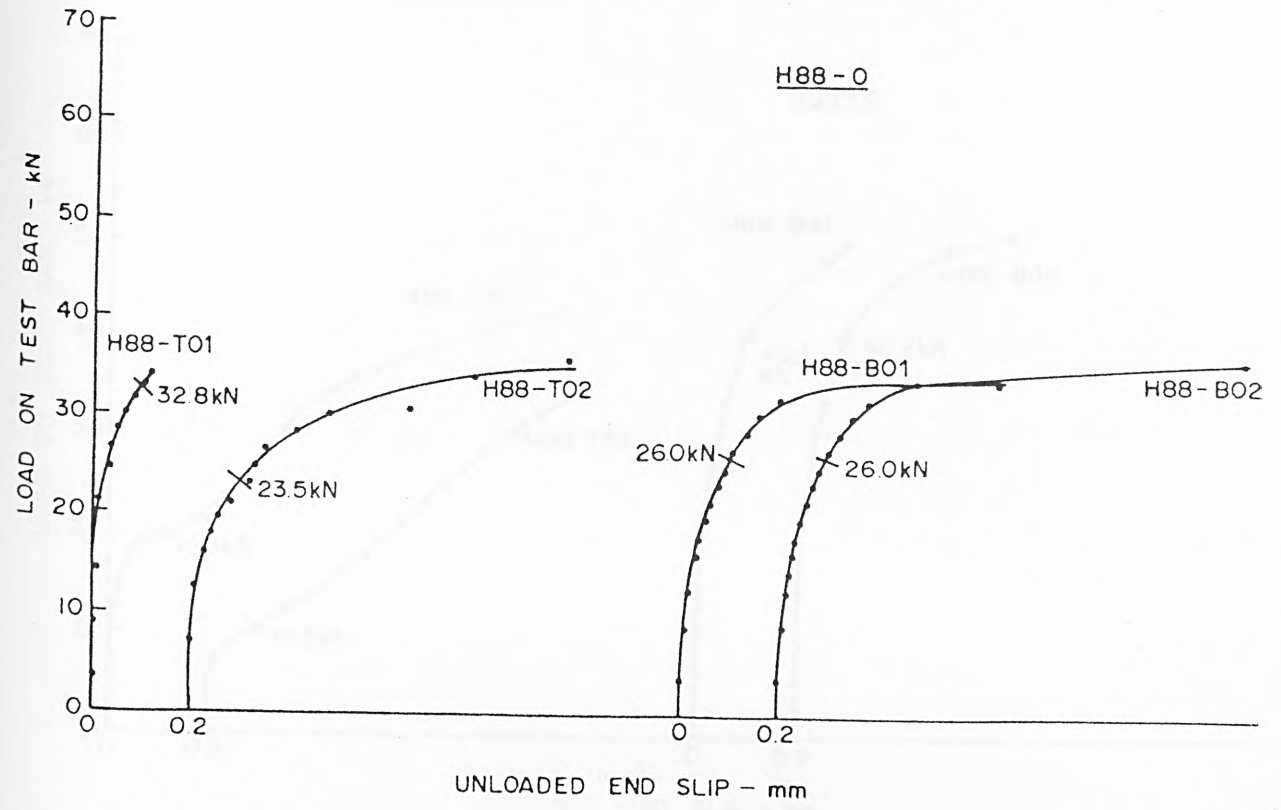


FIG A17 LOAD-SLIP CHARACTERISTICS AT UNLOADED END - HYBAR

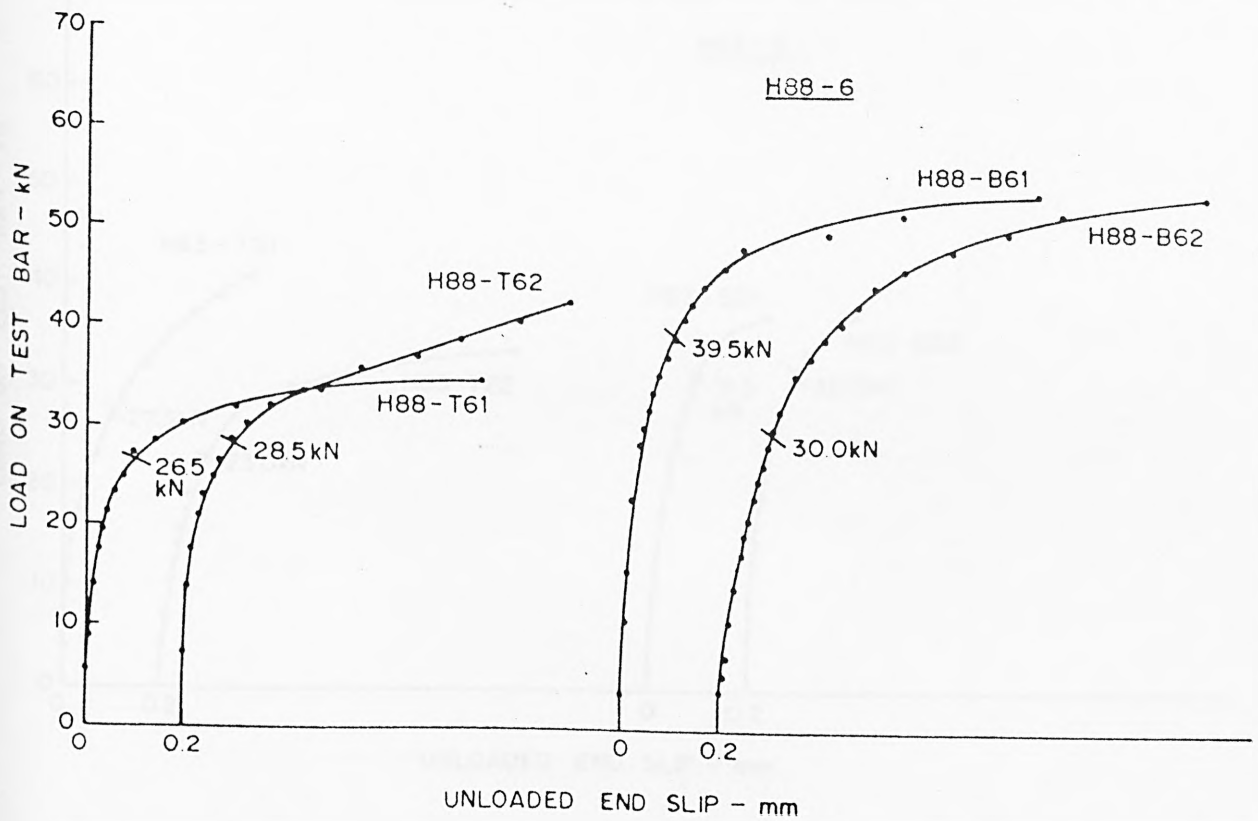
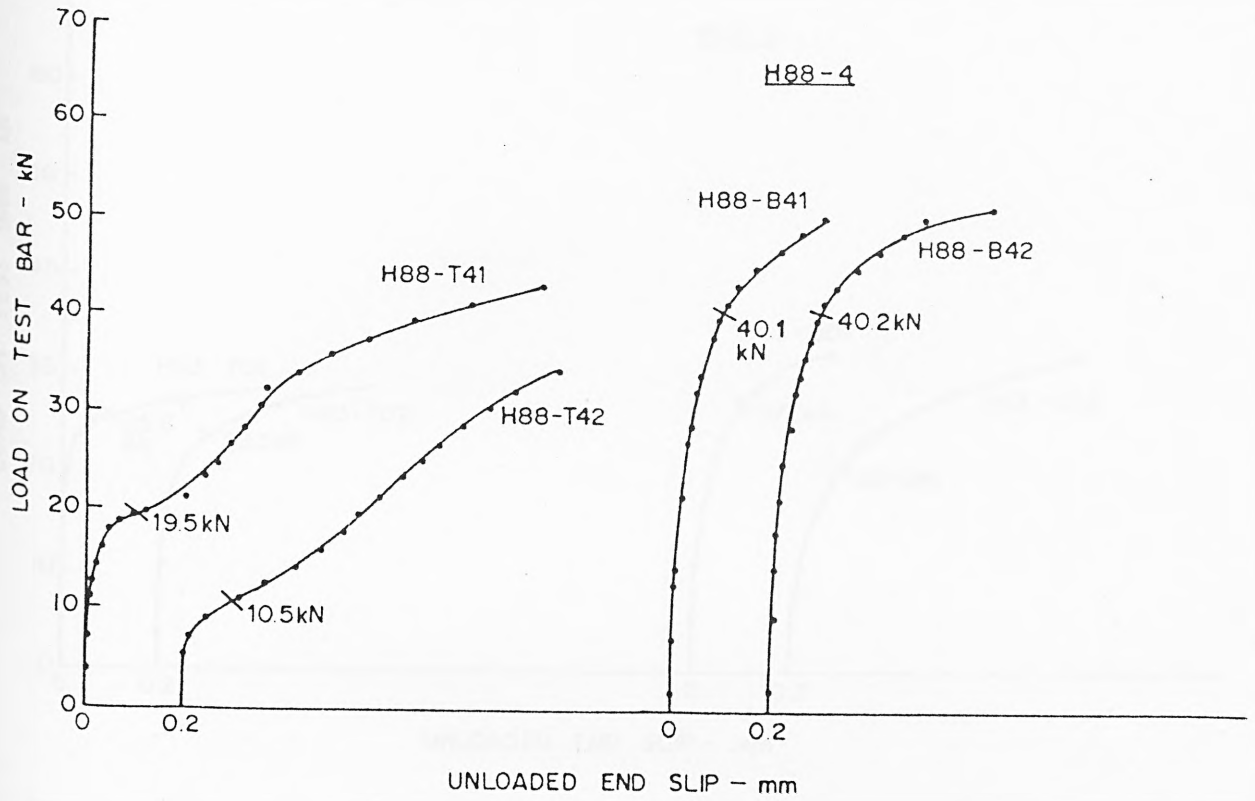


FIG A18 LOAD-SLIP CHARACTERISTICS AT UNLOADED END - HYBAR

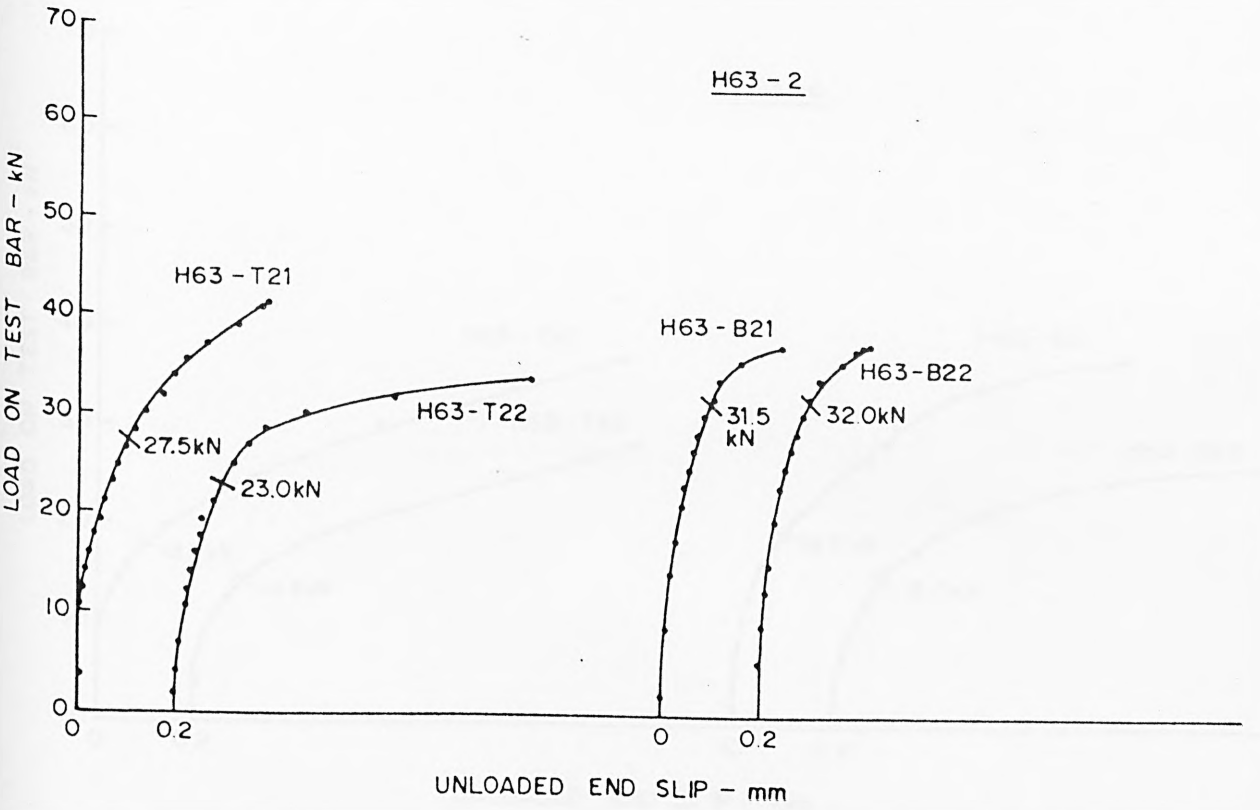
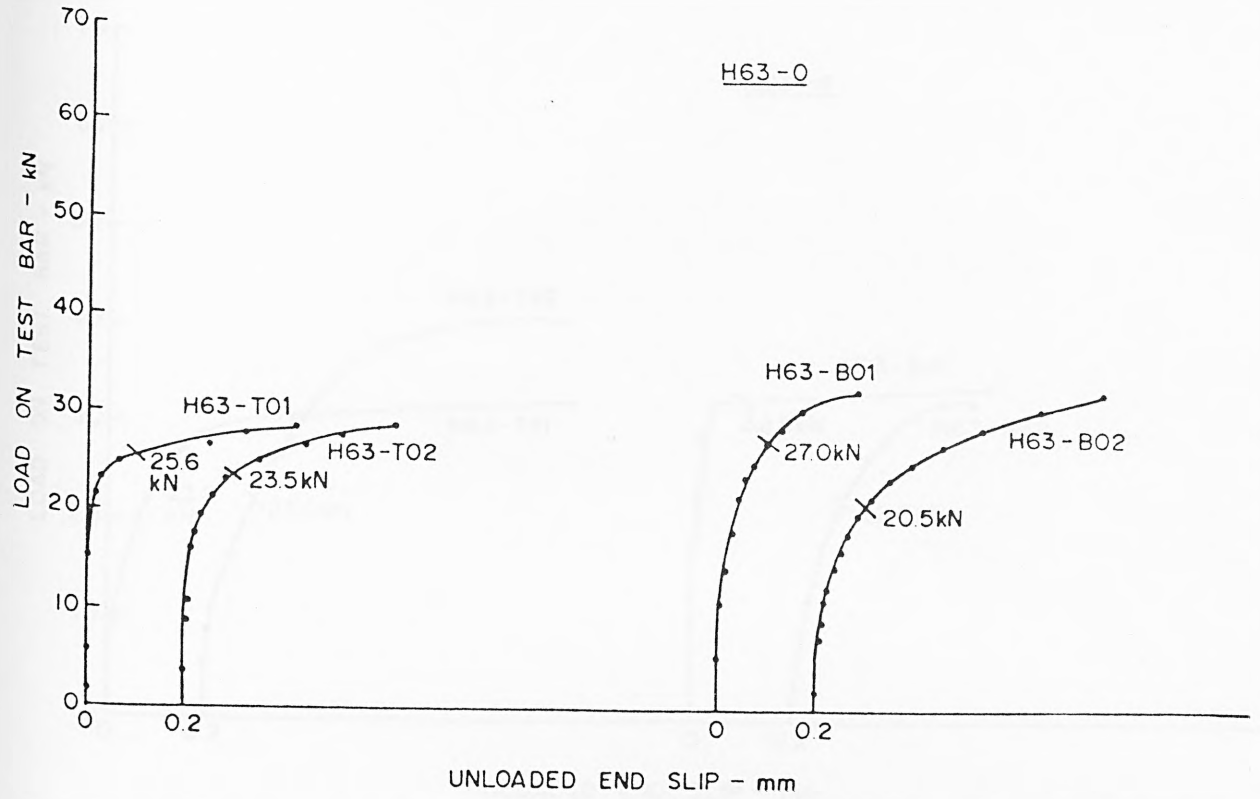


FIG. A19 LOAD-SLIP CHARACTERISTICS AT UNLOADED END - HYBAR

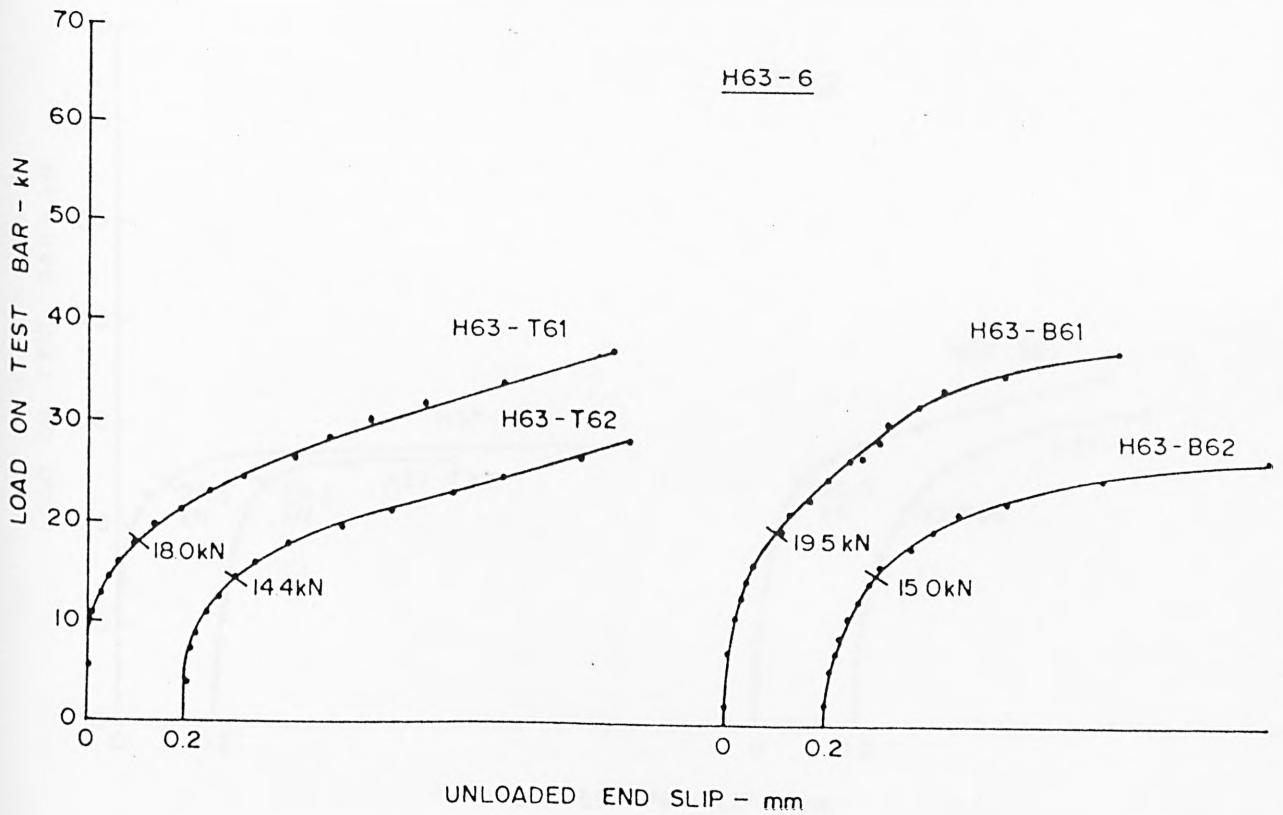
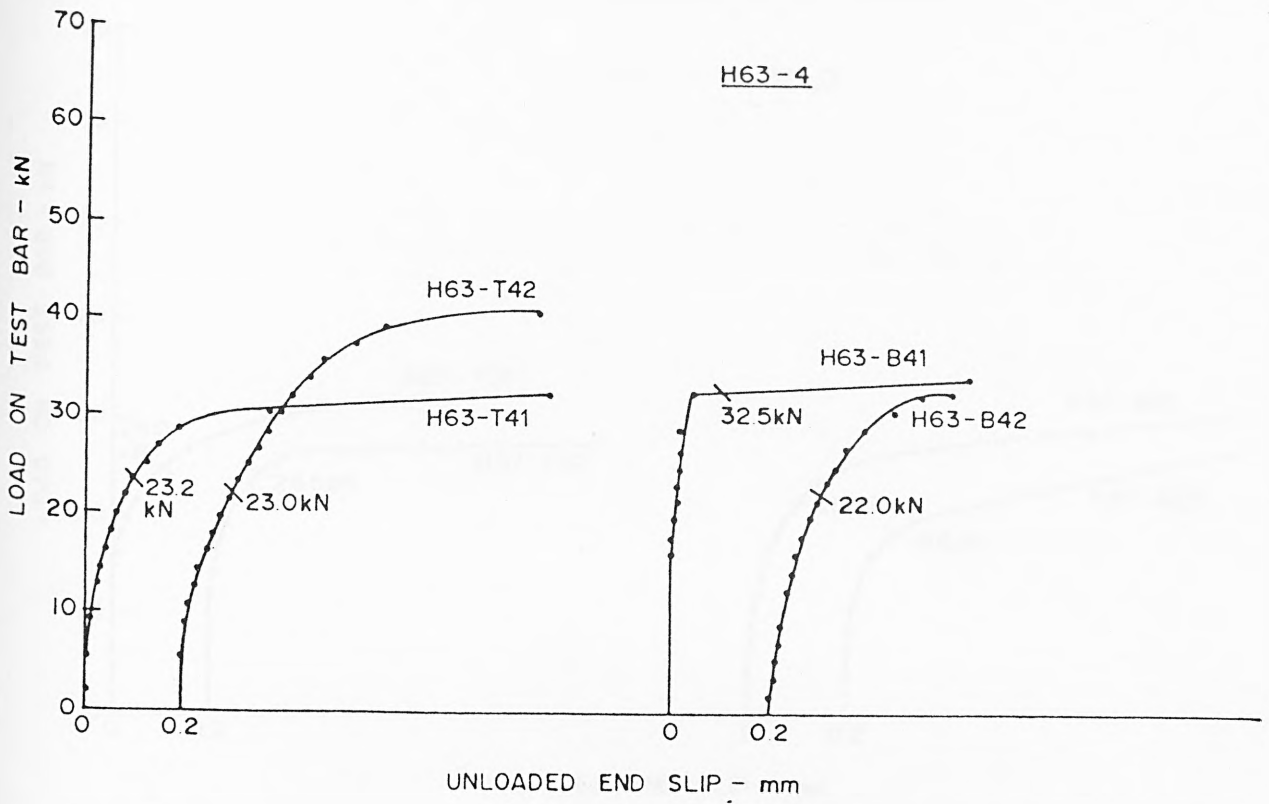


FIG A 20 LOAD-SLIP CHARACTERISTICS AT UNLOADED END-HYBAR

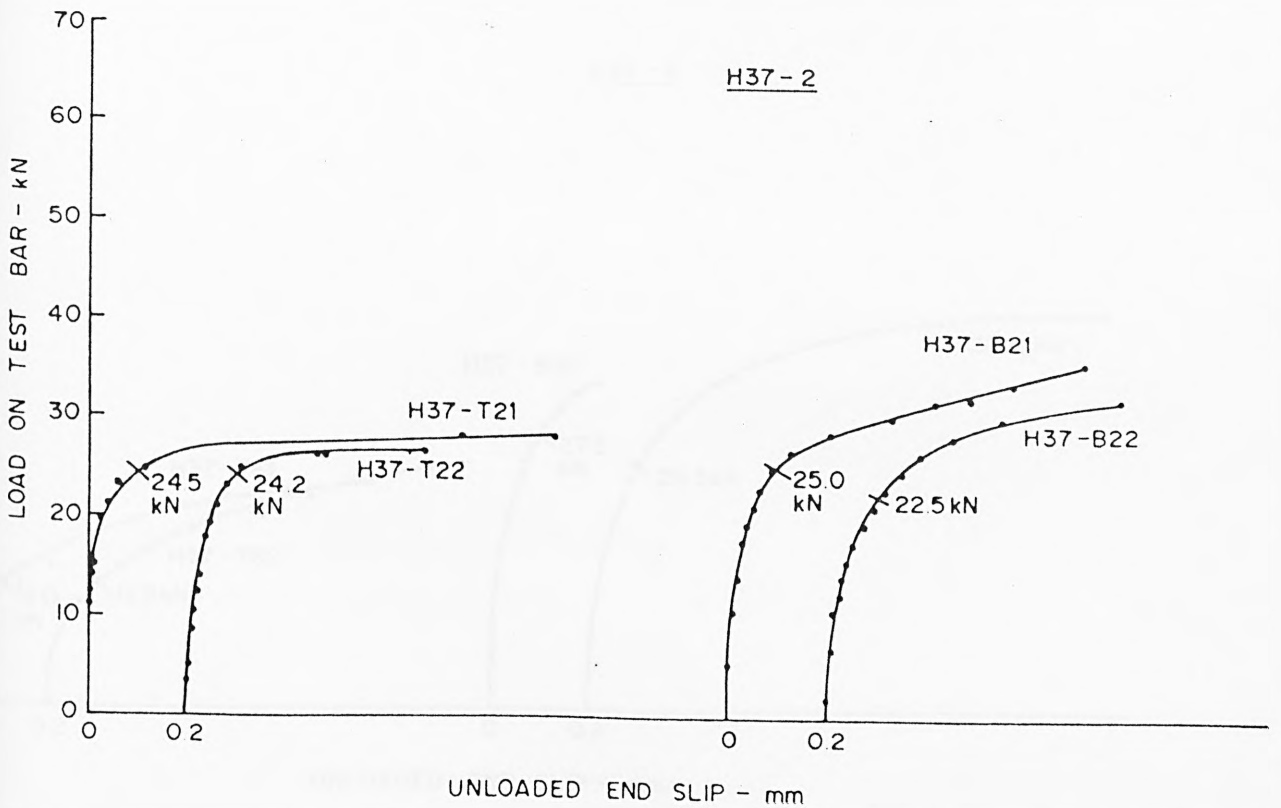
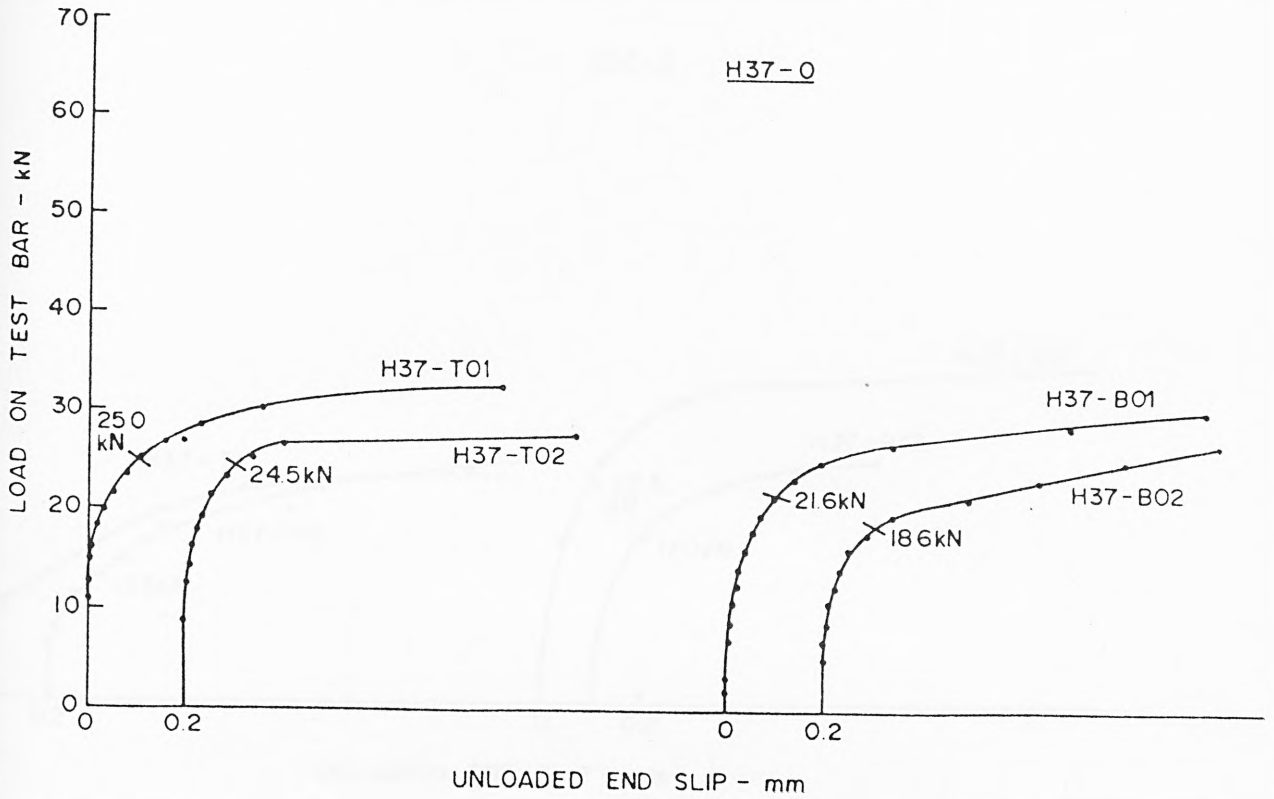


FIG A 21 LOAD-SLIP CHARACTERISTICS AT UNLOADED END-HYBAR

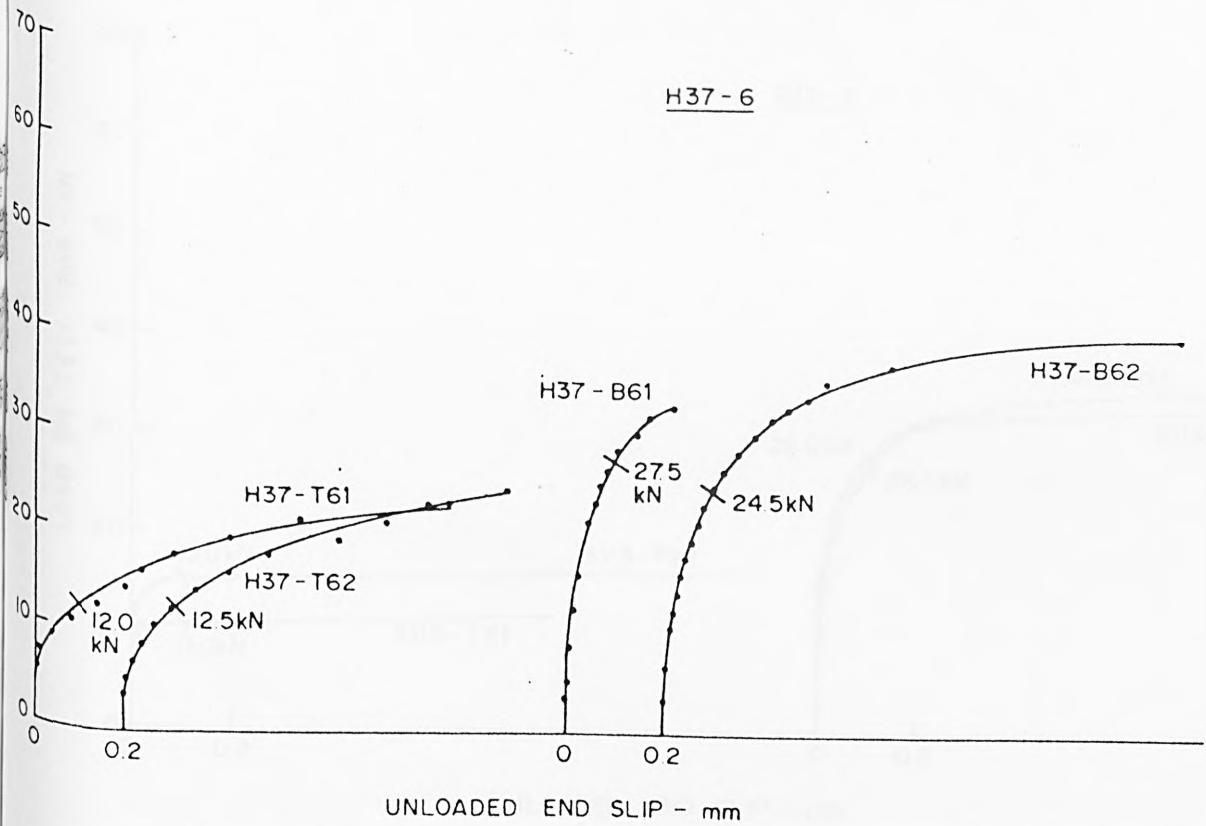
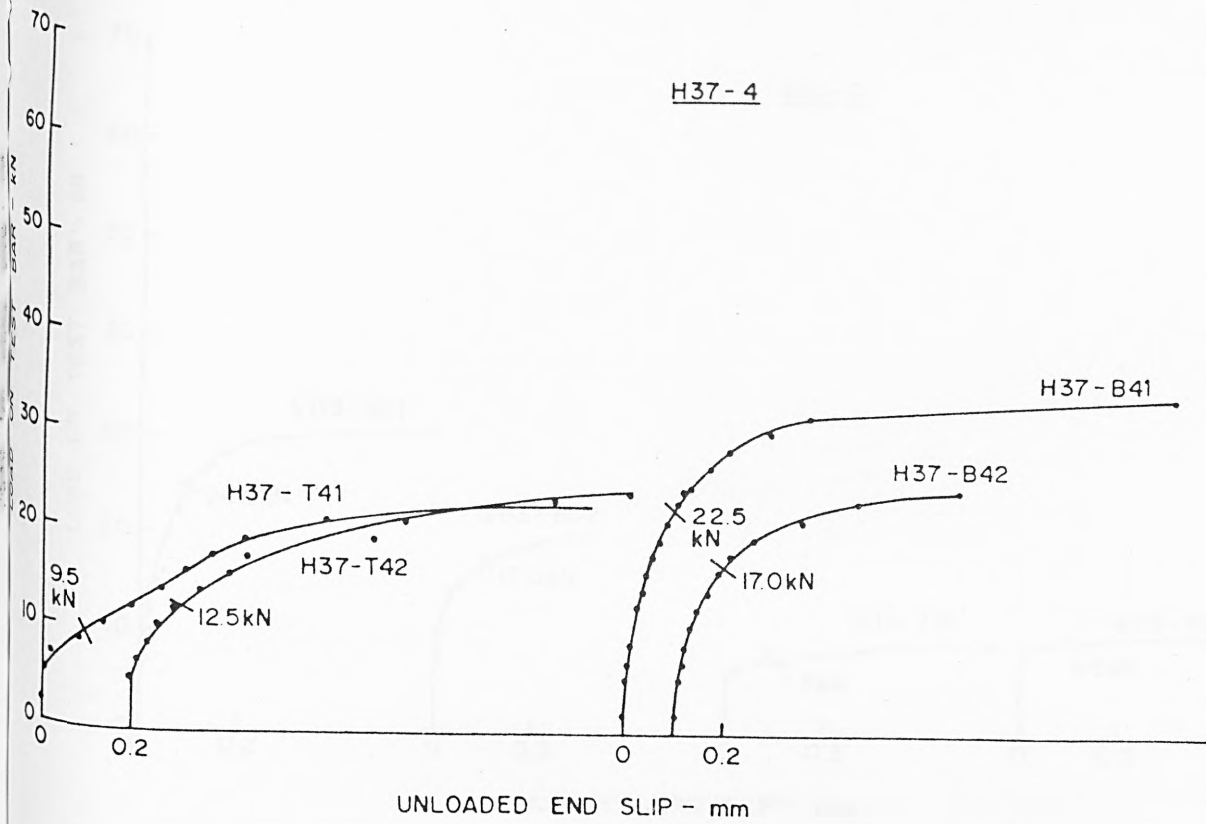


FIG A22 LOAD-SLIP CHARACTERISTICS AT UNLOADED END - HYBAR

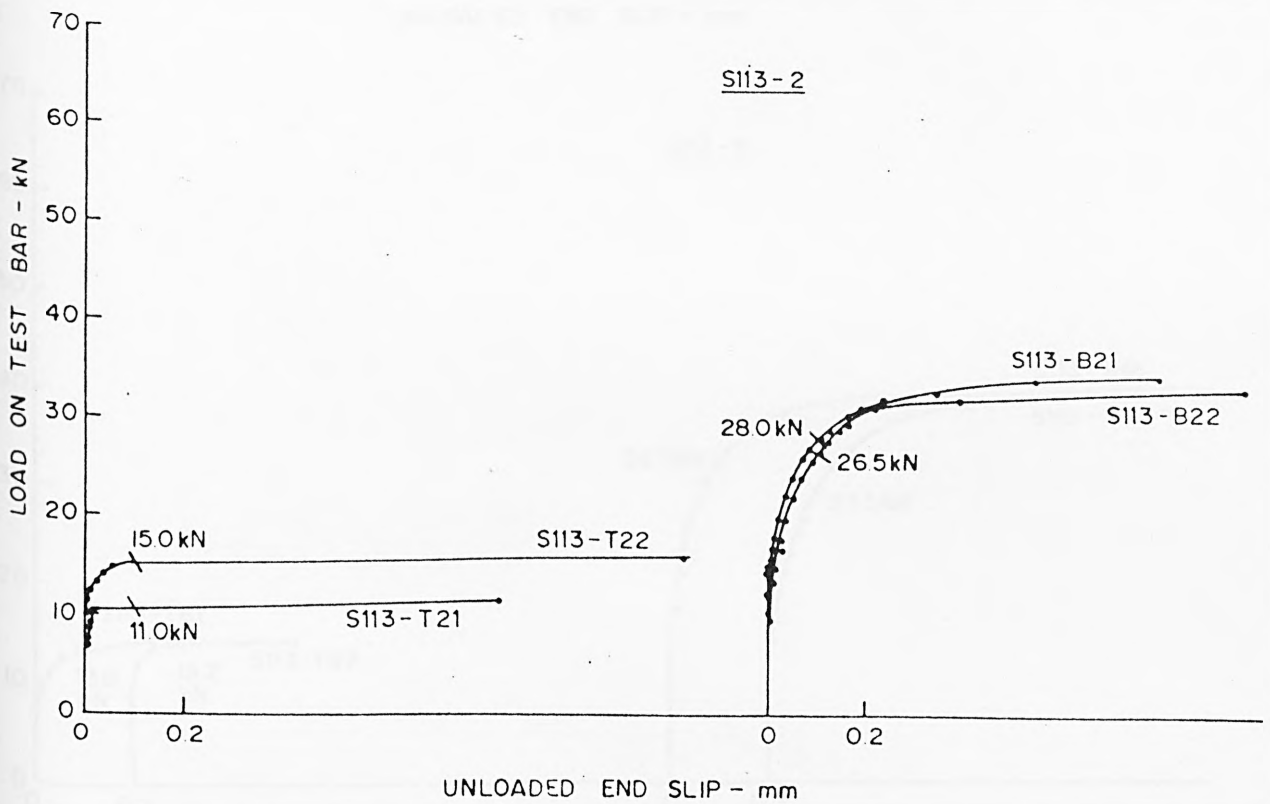
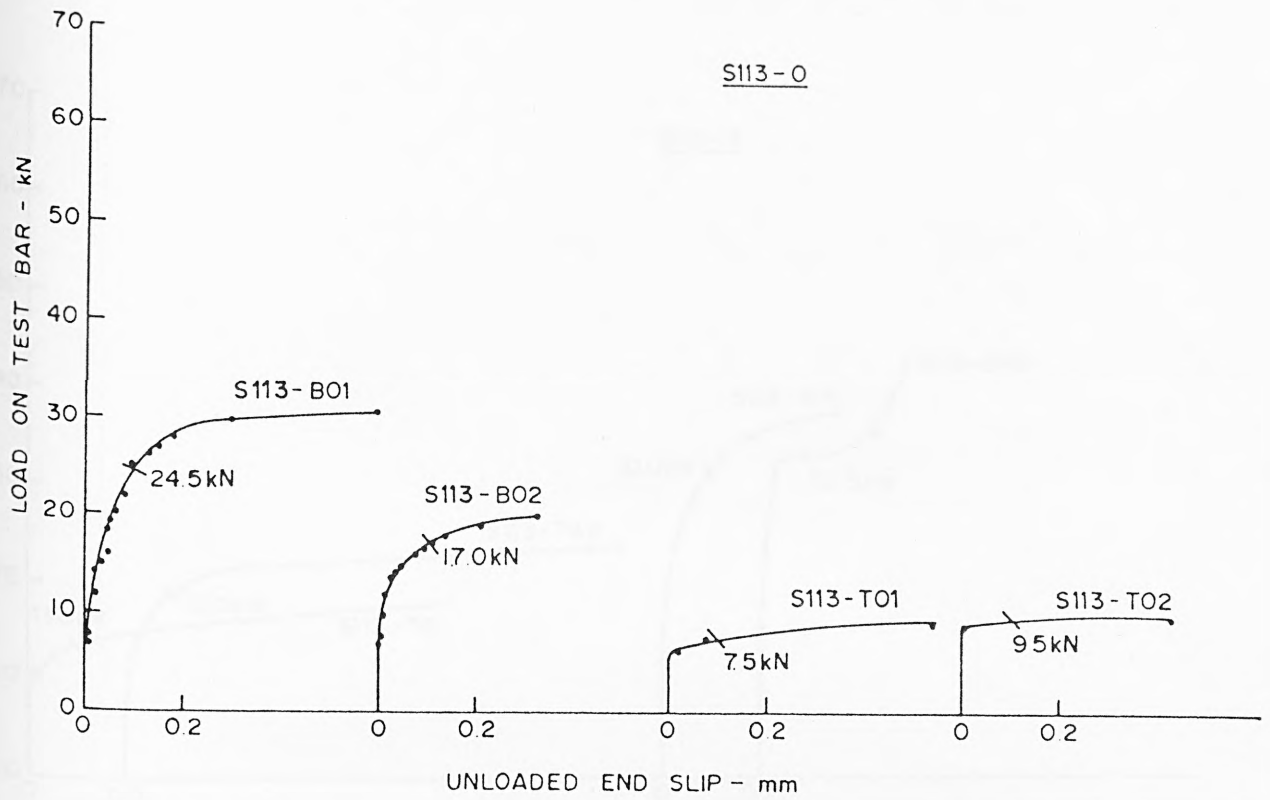


FIG A23 LOAD-SLIP CHARACTERISTICS AT UNLOADED END - SQUARE-TWISTED BAR

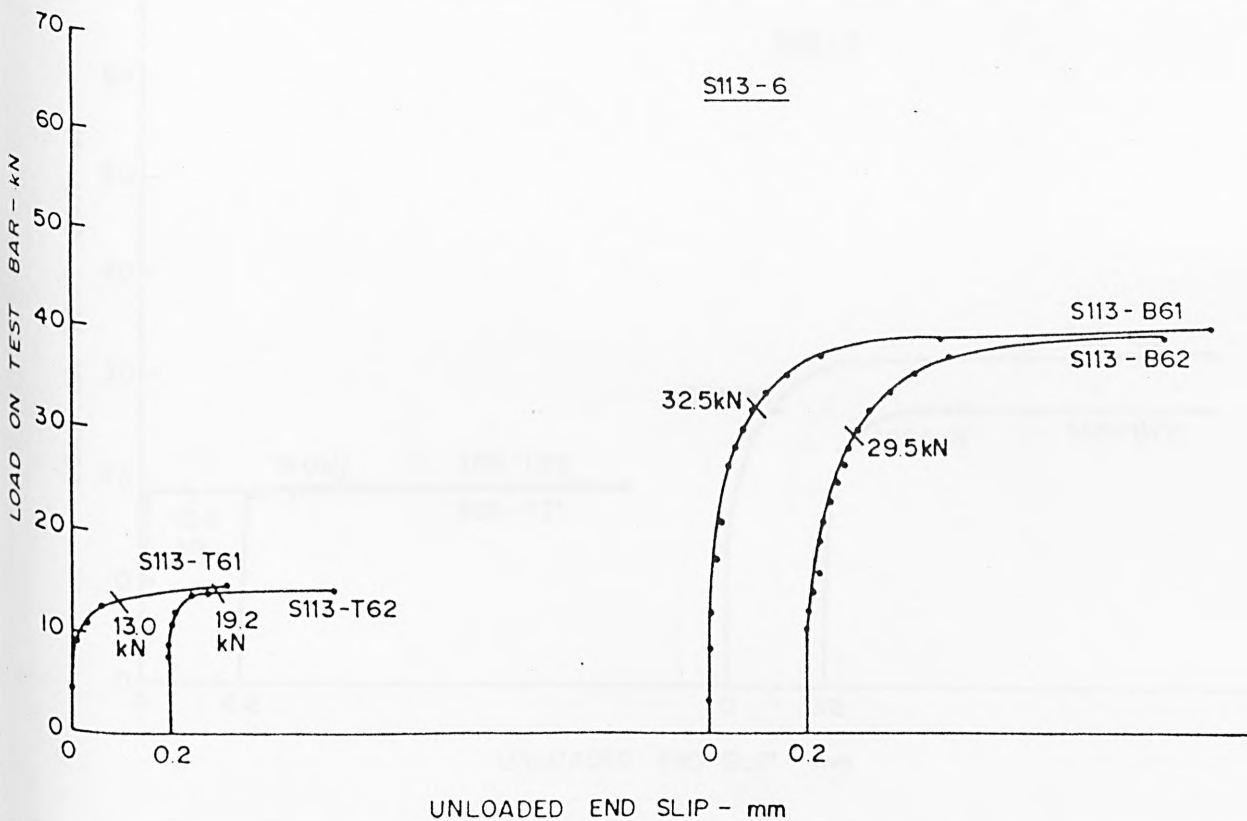
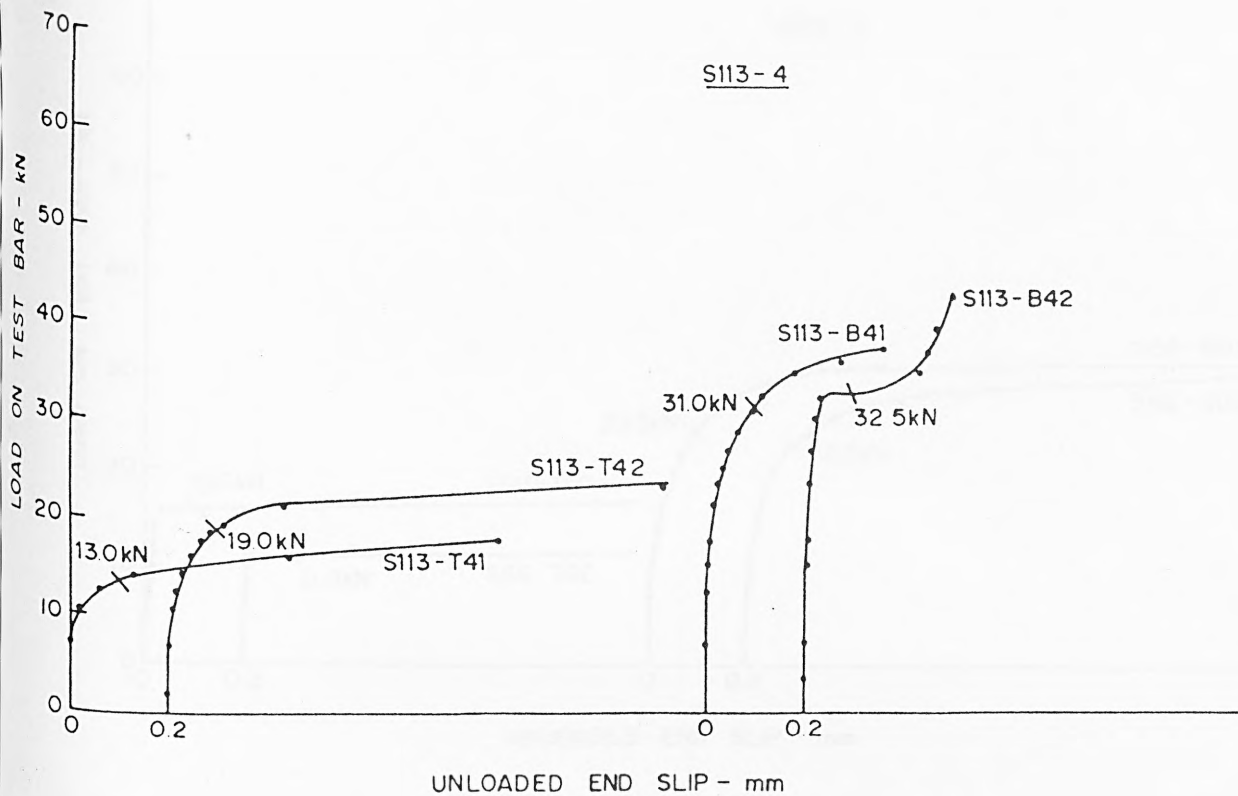


FIG A 24 LOAD-SLIP CHARACTERISTICS AT UNLOADED END - SQUARE-TWISTED BAR

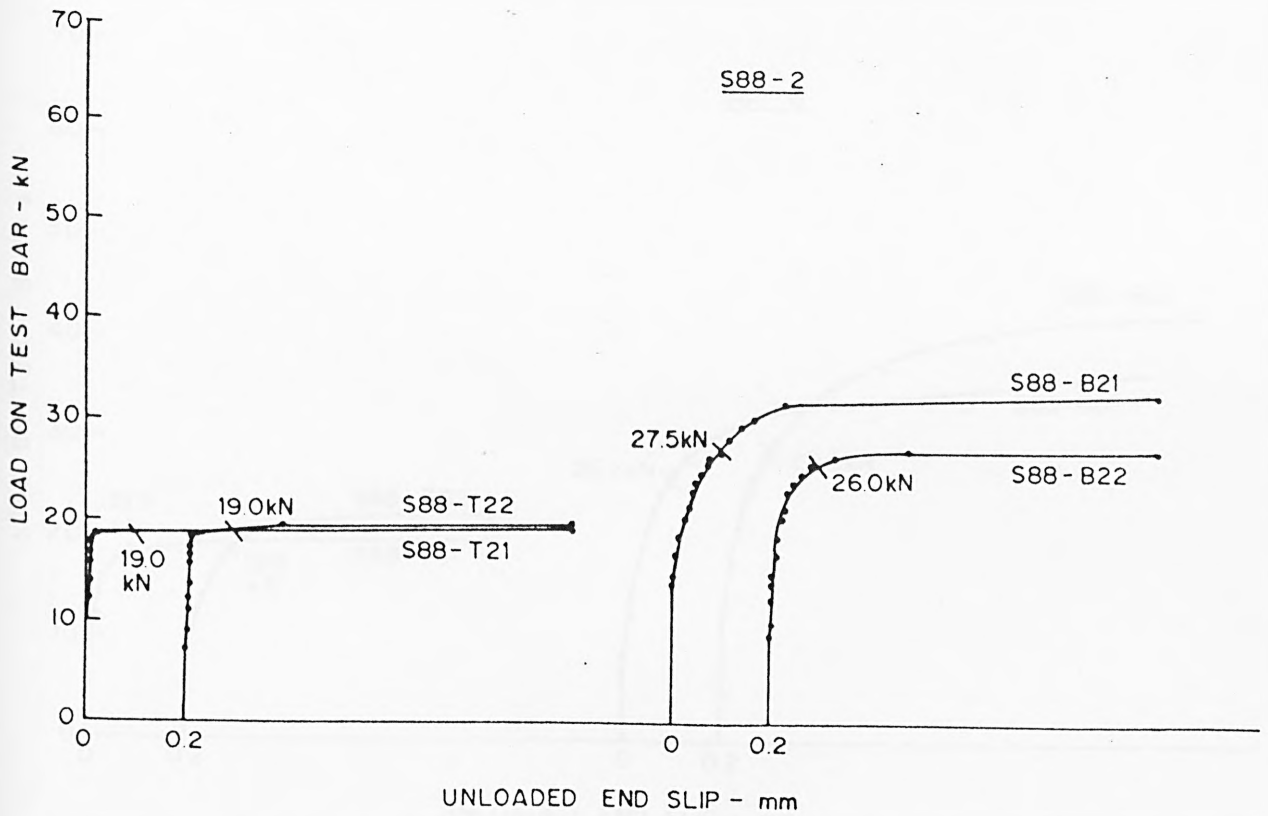
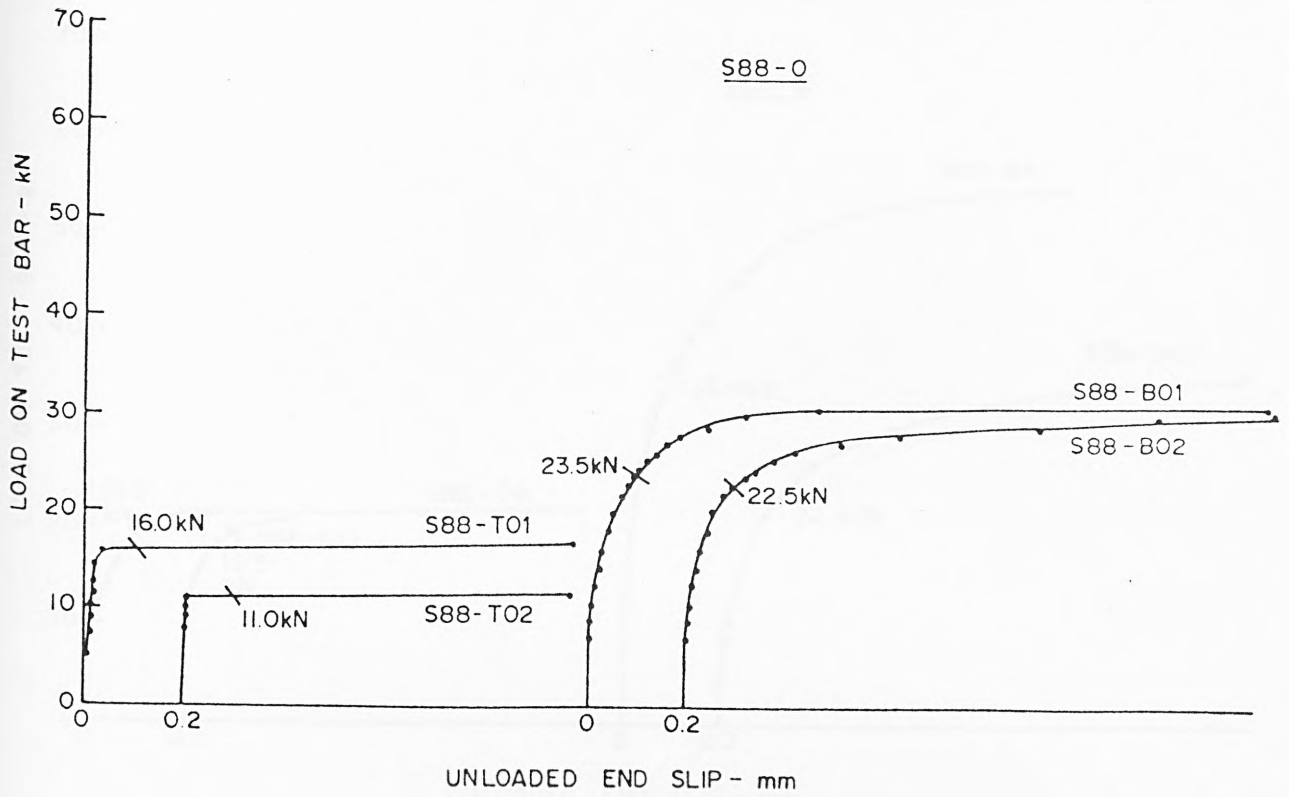


FIG A 25 LOAD-SLIP CHARACTERISTICS AT UNLOADED END - SQUARE-TWISTED BAR

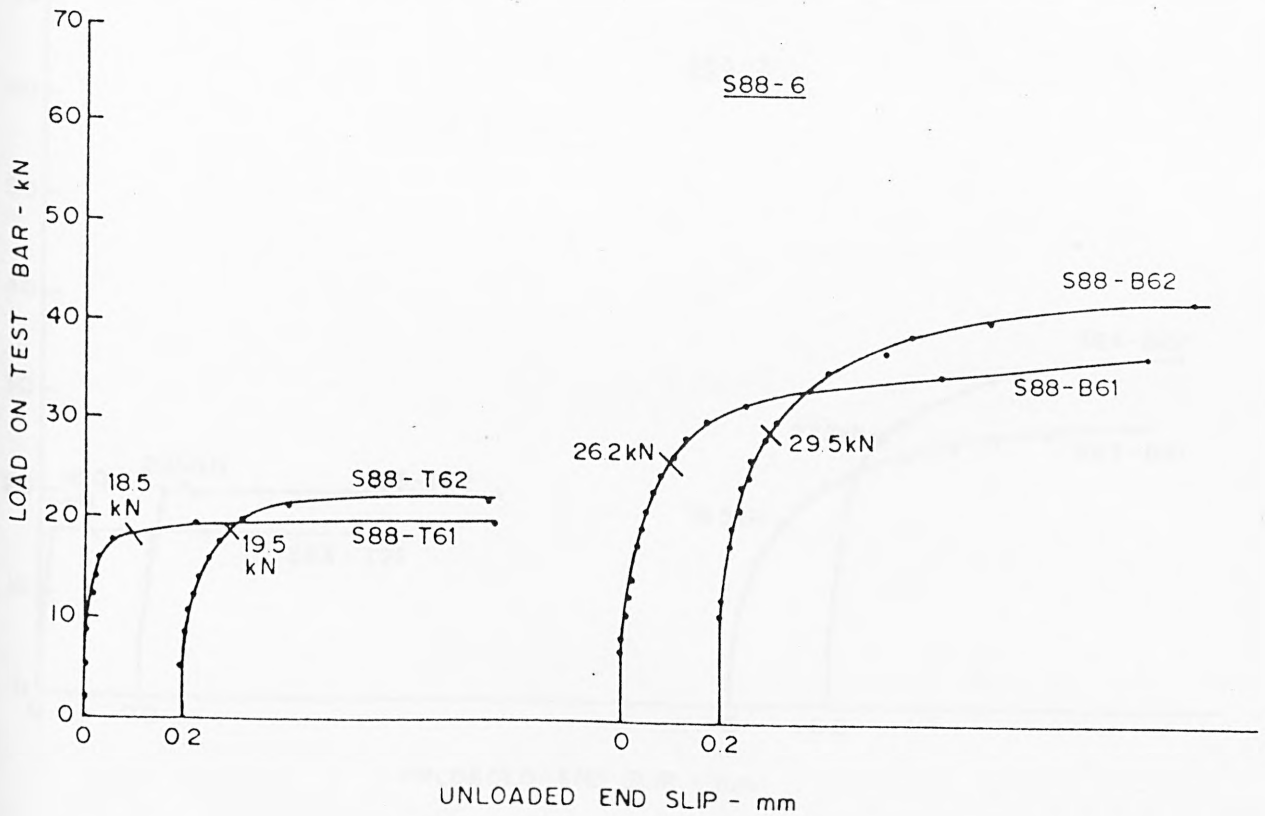
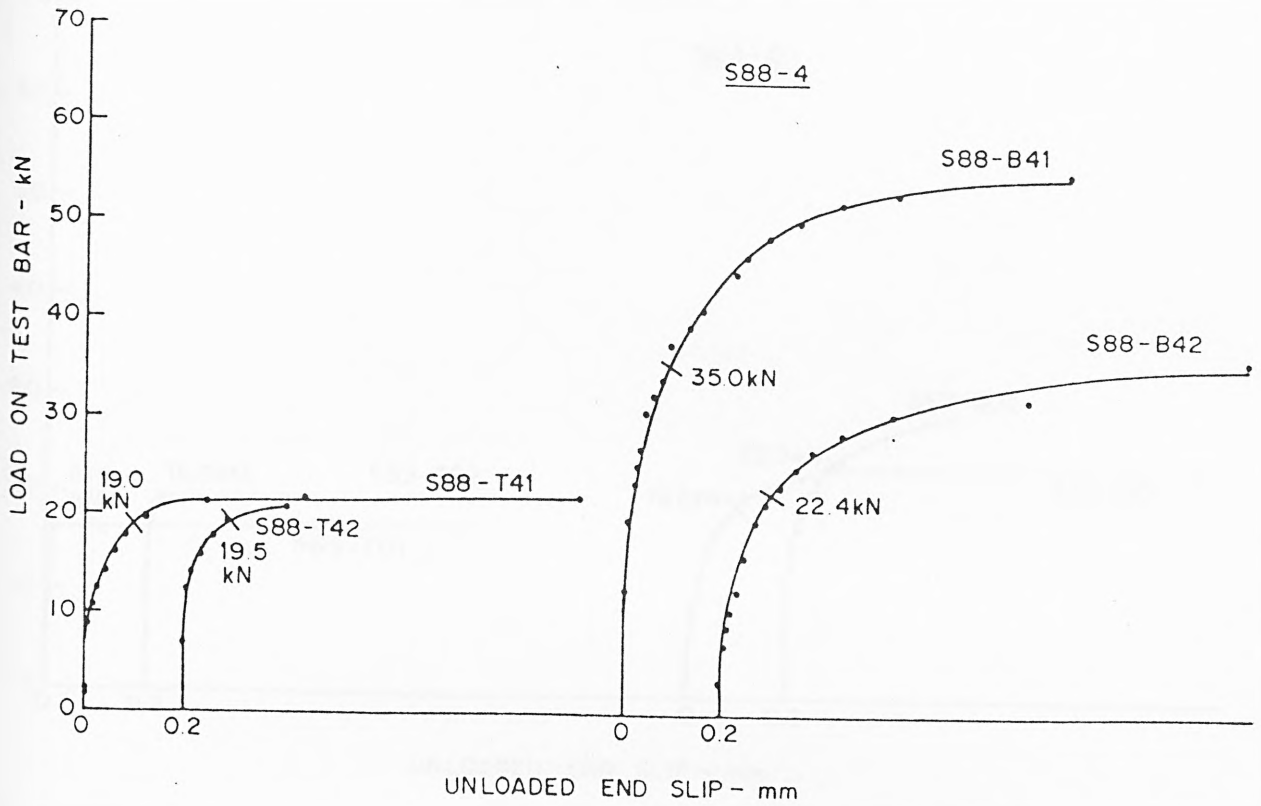


FIG A.26 LOAD-SLIP CHARACTERISTICS AT UNLOADED END - SQUARE-TWISTED BAR

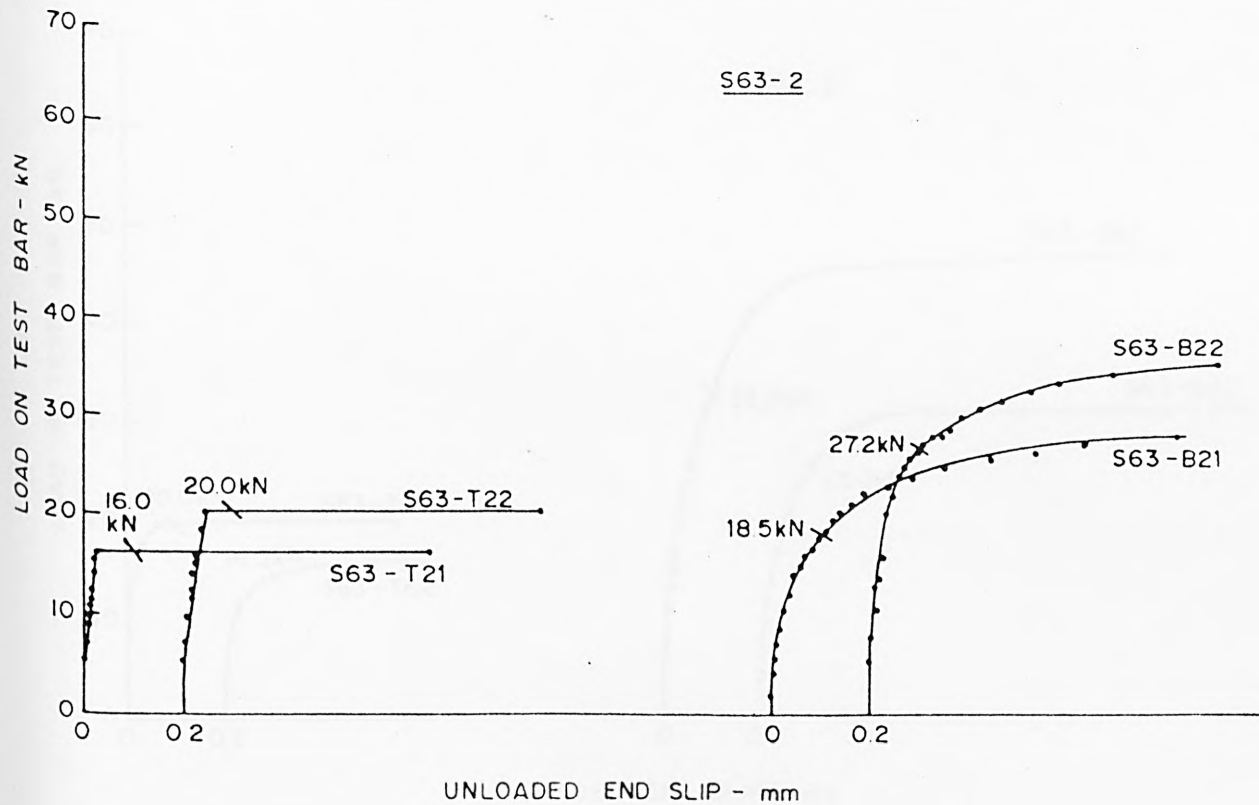
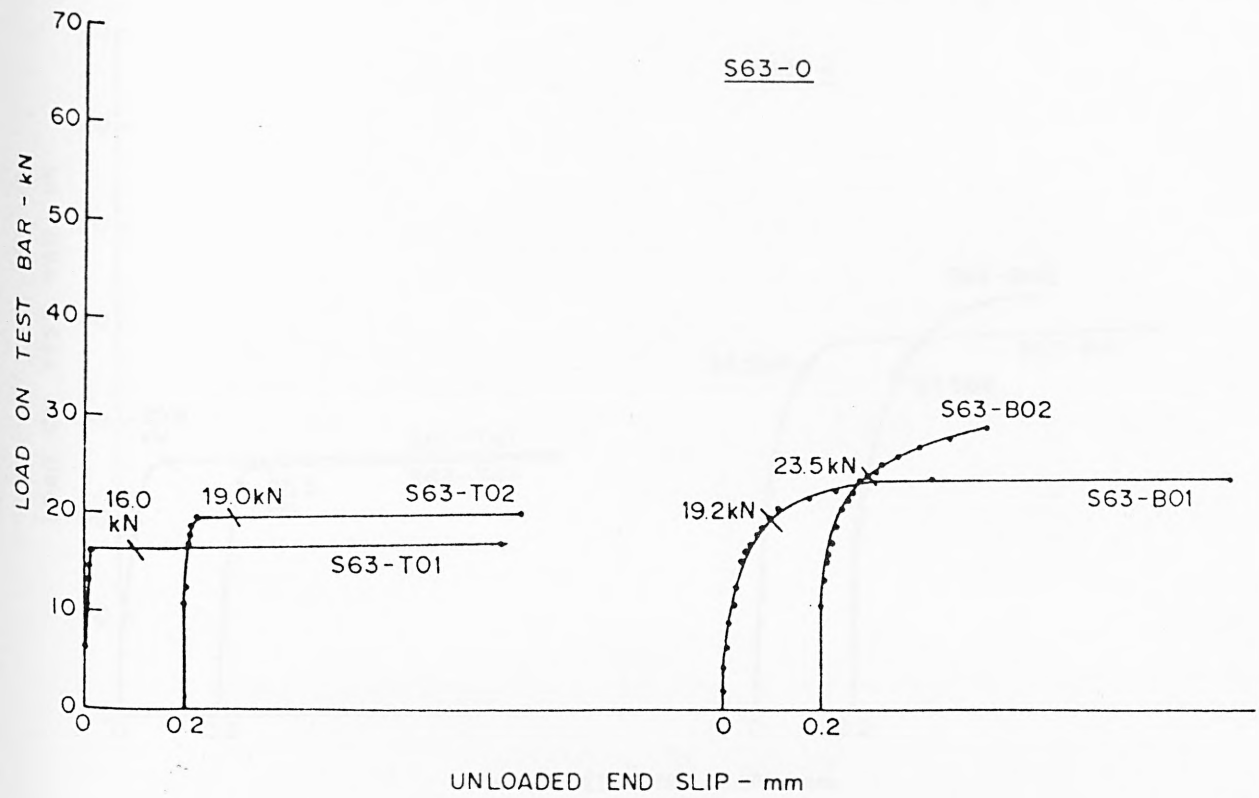


FIG A 27 LOAD-SLIP CHARACTERISTICS AT UNLOADED END - SQUARE-TWISTED BAR

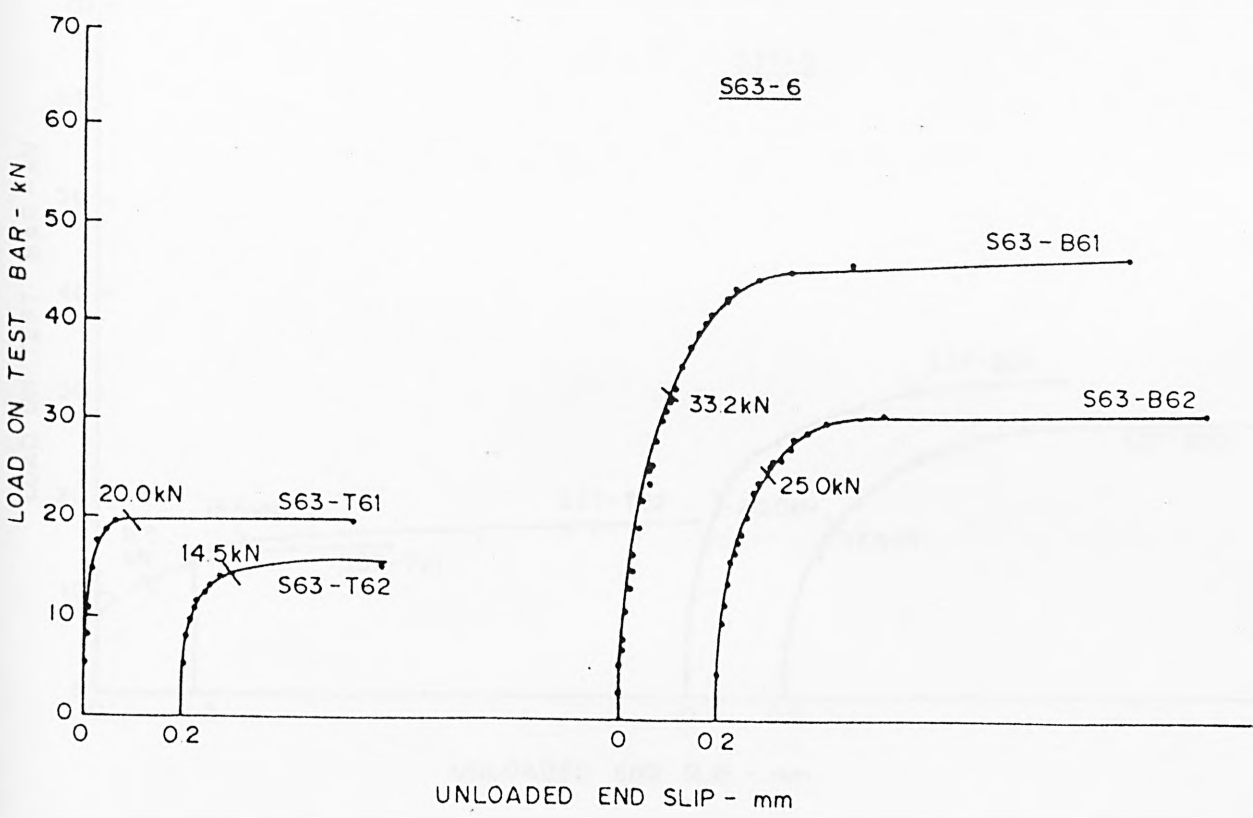
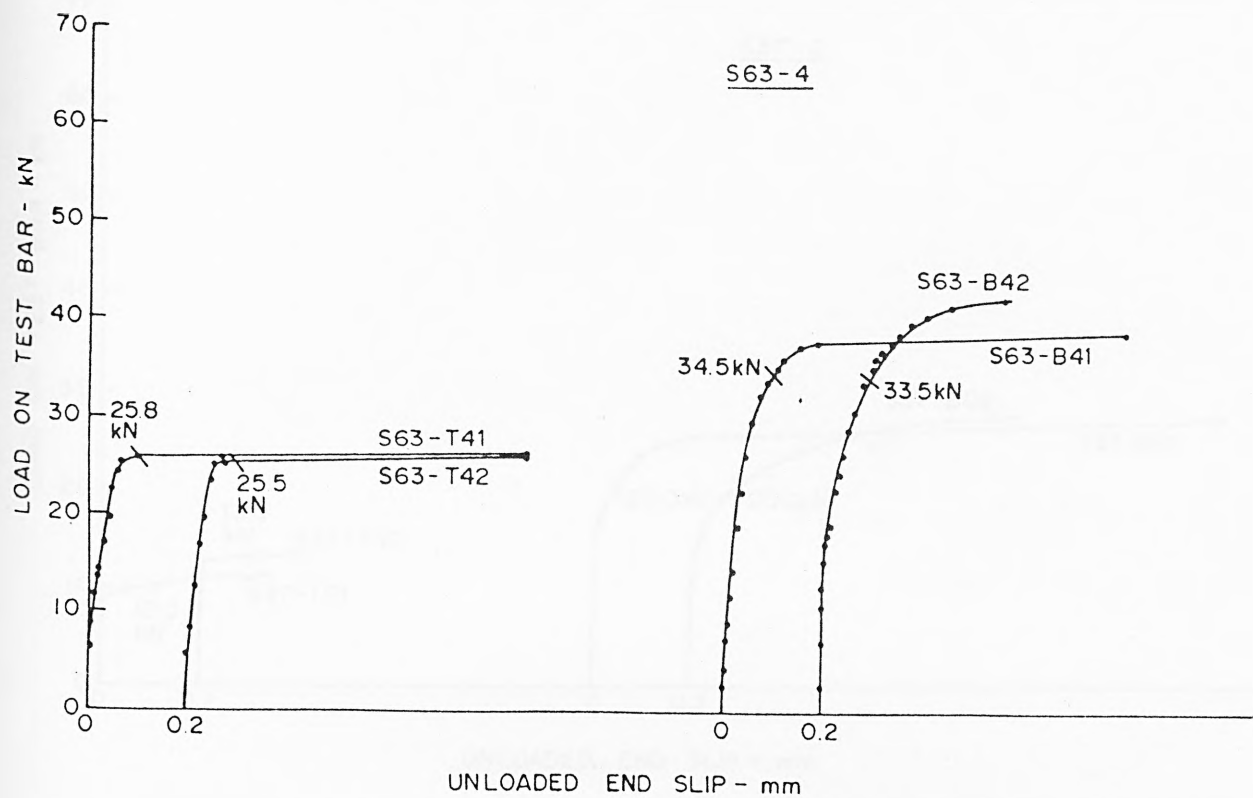


FIG A.28 LOAD-SLIP CHARACTERISTICS AT UNLOADED END - SQUARE-TWISTED BAR

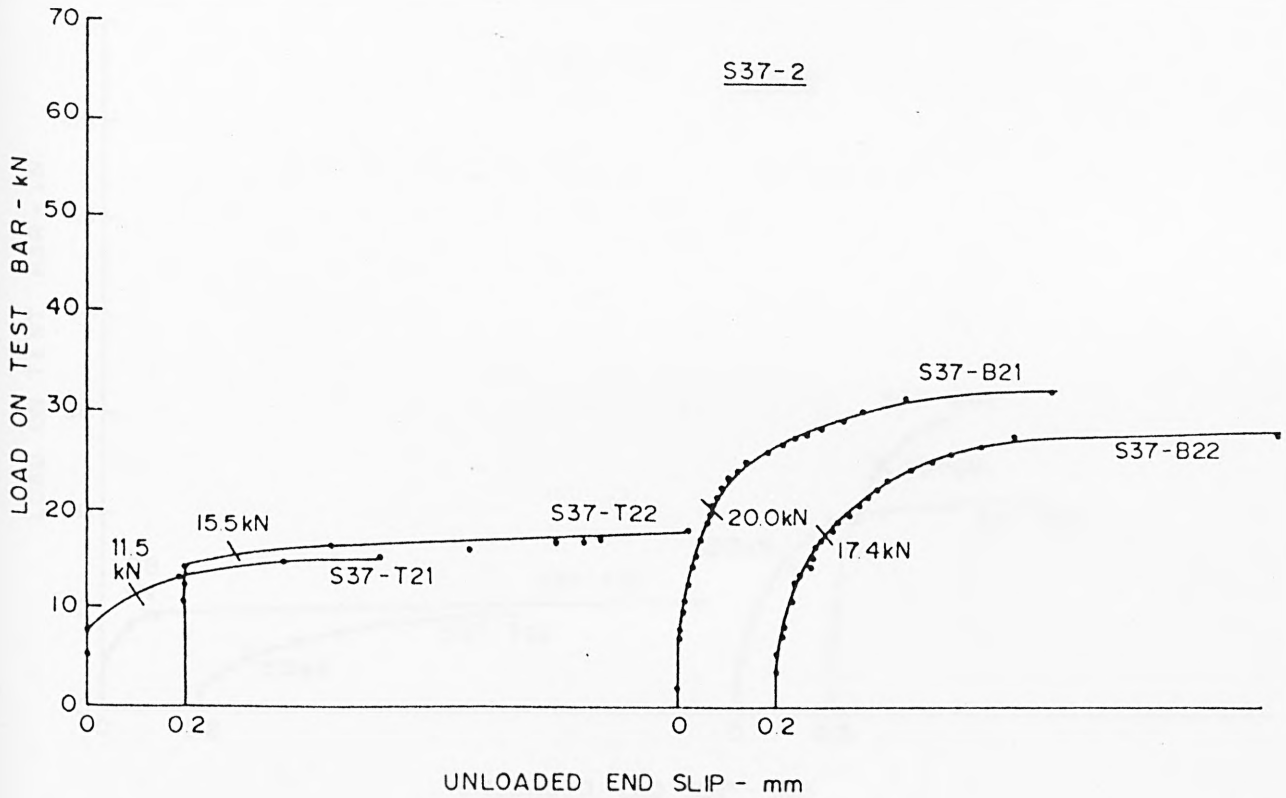
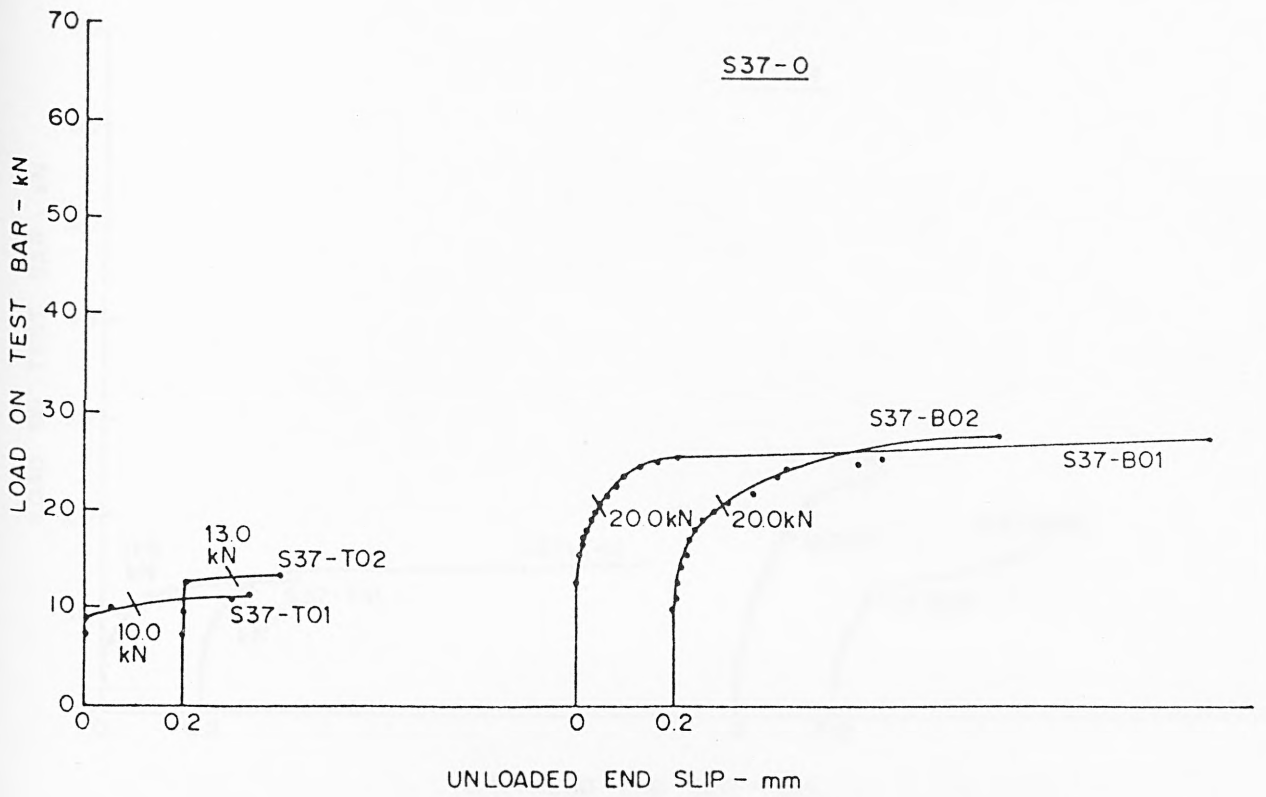


FIG. A 29 LOAD-SLIP CHARACTERISTICS AT UNLOADED END - SQUARE-TWISTED BAR

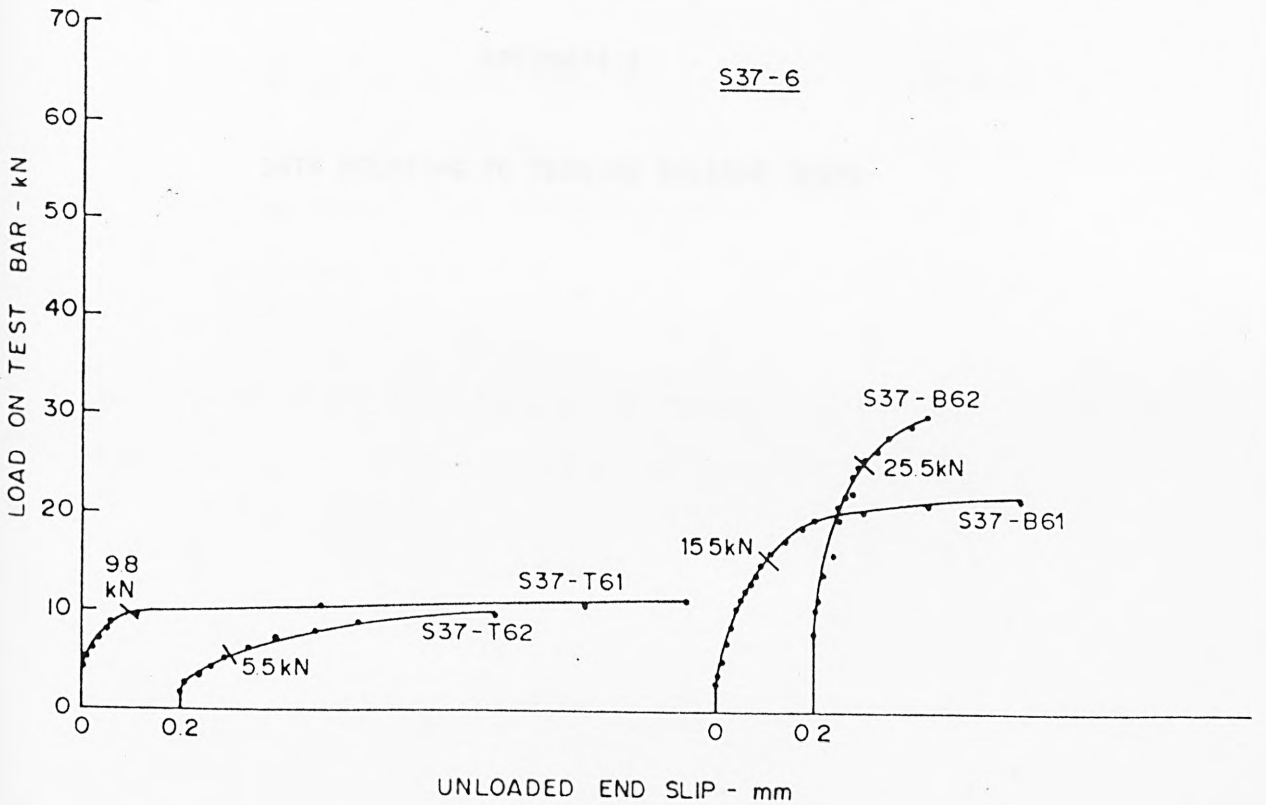
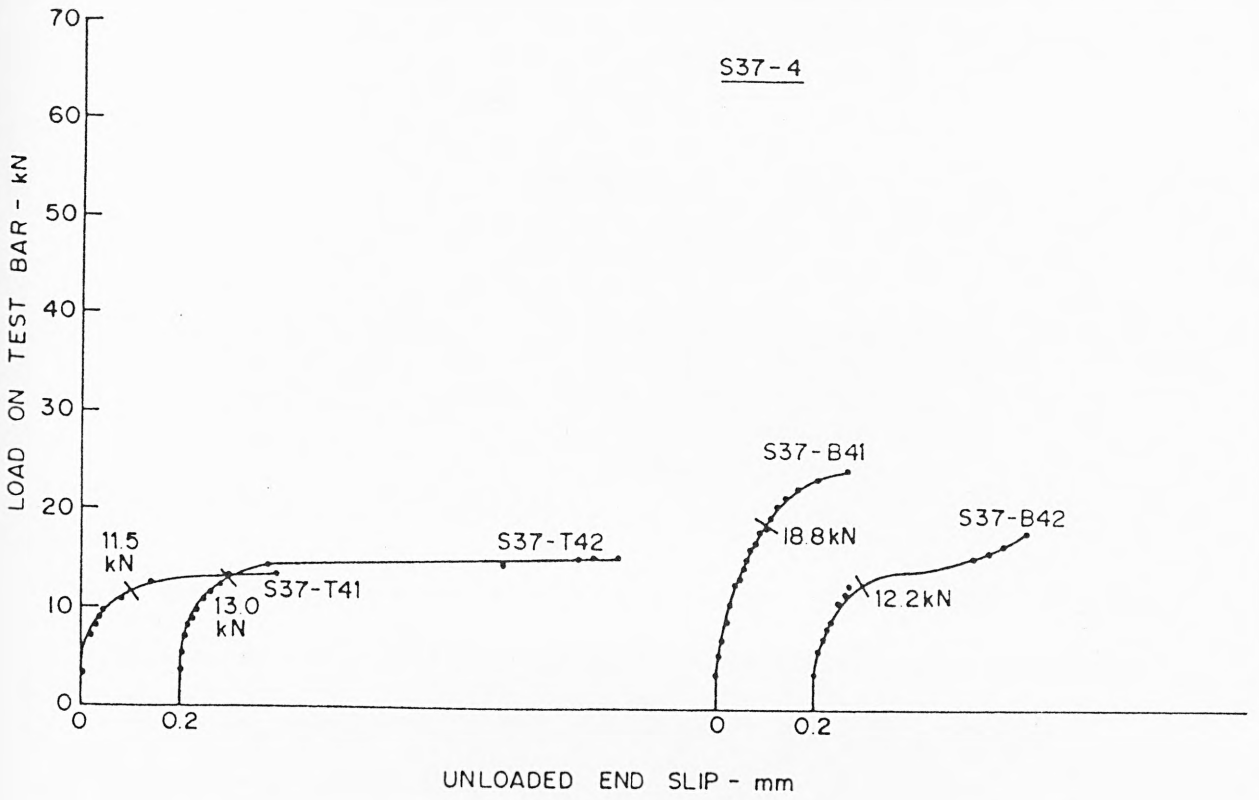


FIG A 30 LOAD-SLIP CHARACTERISTICS AT UNLOADED END - SQUARE-TWISTED BAR

APPENDIX A

4.2 Details of compression tests

The details of the compression tests used in the failure mechanism study were performed at the City University, London and shown below for 1.5mm and 2.0mm diameter of bars. The test results are given in Table A.1 for 1.5mm diameter and 2.0mm bars.

APPENDIX B

DATA RELATING TO TENSION RELEASE TESTS

Weight of steel	15.25 kg
Weight of steel	51.21 kg
Weight of steel	22.80 kg
Weight of steel	15.25 kg

The results of the steel compression strength tests are detailed in Table A.1. The results of the steel tension release tests are given in Table B.1.

APPENDIX 'B'

B.1 Details of concrete mix

The details of the concrete mix used in the lateral tension release tests performed at the City University, London are given below for 4 Nos. test specimens, 8 Nos. 100 mm cubes and 2 Nos. cylinders 150 mm diameter and 300 mm long.

Weight of cement (Blue Circle Brand)	=	28.26 kg
Weight of river sand	=	51.91 kg
Weight of river gravel (20 mm)	=	99.82 kg
Weight of water	=	14.50 kg

The results of the cube compression strength tests and splitting tensile strength of the cylinders are given in Table B.1.

Test Specimen	Date Cast	Date tested	Cube Strength (N/mm ²)	Splitting cylinder strength (N/mm ²)
T 88	18.11.76	7.12.76	34.95	2.79
T 63	23.11.76	3.12.76	34.87	2.83
T 50	20.1.77	31.1.77	36.30	2.97
T 25	1.12.76	7.12.76	35.98	2.97
U 88	6.1.77	17.1.77	36.13	2.86
U 63	10.1.77	18.1.77	35.23	2.70
U 50	12.1.77	21.1.77	34.35	2.82
U 25	17.1.77	24.1.77	36.44	2.86
S 88	3.12.76	21.12.76	34.23	2.82
S 63	9.12.76	20.12.76	35.17	2.74
S 50	20.12.76	6.1.77	35.20	2.74
S 25	22.12.76	10.1.77	35.8	2.74

TABLE B.1 : STRENGTH OF CONCRETE - TENSION RELEASE

B. 2: Calibration of Load Cells

The calibration data of the load cells used in the tension release tests are given in Table B.2 below:

LOAD CELL NO. T₃

Load-Tons	Meter Reading
0	0
1	7
2	14
3	21
4	28
5	36
6	43.5
7	51
8	58
9	65
10	73

LOAD CELL NO. T₄

Load-Tons	Meter Reading
0	0
1	7
2	14
3	21.5
4	29
5	37
6	44
7	51
8	58.5
9	66.5
10	74

LOAD CELL NO. T₅

Load-Tons	Meter Reading
0	0
1	7
2	14
3	21
4	29
5	36
6	44
7	52
8	59
9	67
10	74

LOAD CELL NO. T₆

Load-Tons	Meter Reading
0	0
1	7
2	14
3	21
4	28
5	36
6	43
7	50
8	58
9	66
10	73

LOAD CELL NO. C₁

Load-Tons	Meter-Reading
0	0
1	5
2	10
3	15
4	20
5	25
6	31
7	36
8	41
9	46
10	51

LOAD CELL NO. C₂

Load-Tons	Meter Reading
0	0
1	5
2	10
3	15
4	20
5	25.5
6	30.5
7	36
8	41
9	46
10	51

Meter Settings : Gauge Factor = 2; Attenuation Factor = 2;
Range = 0.25

Date Calibrated: 30.10.76

TABLE B.2: CALIBRATION OF LOAD CELLS

B.3 Properties and details of geometry of the test bars

The three types of reinforcement bars were mechanically tested for ultimate strength and percentage elongation. The average values of the results are given in Table B.3.

The area of cross-section of the bars was determined by weighing a known length of each bar. In the case of Torbar and Hybar, the area of cross-section with the ribs as well as the area of cross-section of the 'core' i.e. without the ribs were determined. In order to determine the 'core' area, the ribs on the bars were removed by machining. The values of the areas so determined are given in Table B.3.

The details of the ribs including the rib face angles, inclination of the ribs to the axis of the bar and centre to centre spacing of ribs were also determined. These are shown in Fig. B.1 and Table B.3.

Stress-strain properties of the high tensile steel studs

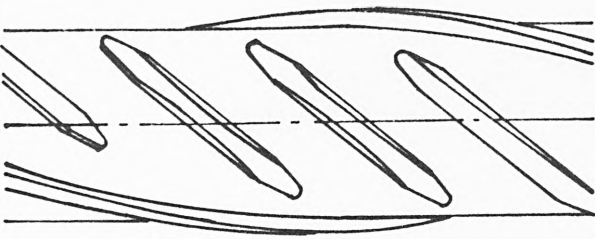
The high tensile steel studs used to obtain the tension release in the concrete were tested in tension in a Universal testing machine and the average stress-strain characteristic obtained is given in Fig. B.2. The essential details of the test are as follows :-

Gauge length	= 4 ins. (100 mm)
Diameter of stud	= 0.311 ins (7.9 mm)
1 division of extensometer	= 0.506×10^{-4} ins.
Gradient of graph	= 23.81 lbs/division (from Fig. B.2)
Area of stud	= $\frac{\pi}{4} \times 0.311^2 = 0.0759 \text{ in}^2$

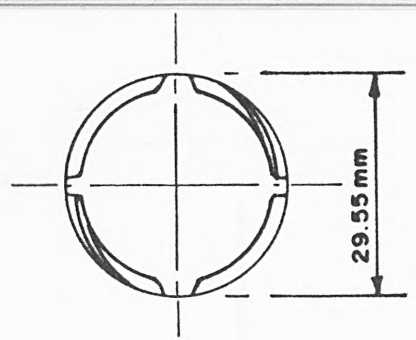
Type of bar	Area with all ribs (mm ²)	Area with longitudinal rib only (mm ²)	Area with no ribs (mm ²)	Pitch of twist of ribs (mm)	Distance centre to centre of ribs (mm)	Ultimate tensile strength (N/mm ²)	Percentage elongation
Torbar	493.09	472.45	455.38	255	16.0	559.75	16.95
Hybar	511.96	474.63	471.11	-	14.7	576.22	23.45
Square-twisted	517.46	-	-	280	-	577.67	17.50

TABLE B.3: PROPERTIES OF TEST BARS

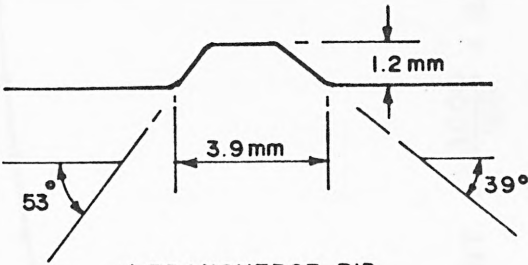
TORBAR



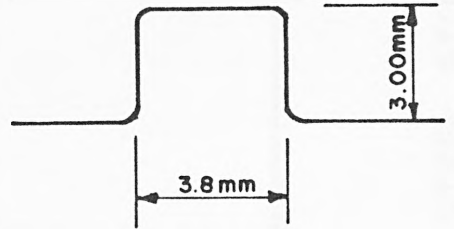
LONGITUDINAL ELEVATION



CROSS SECTION



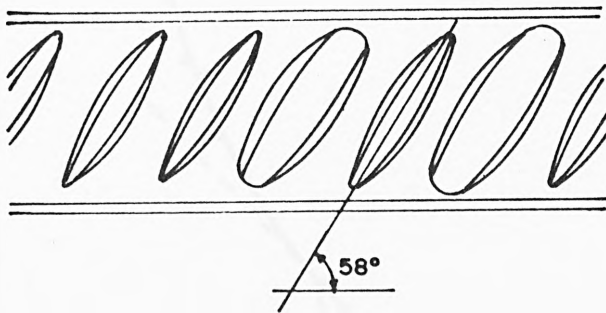
a) TRANSVERSE RIB



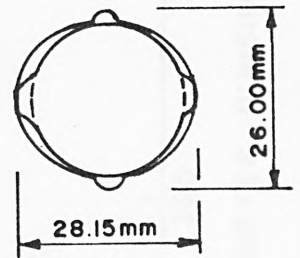
b) LONGITUDINAL RIB

RIB PROFILES

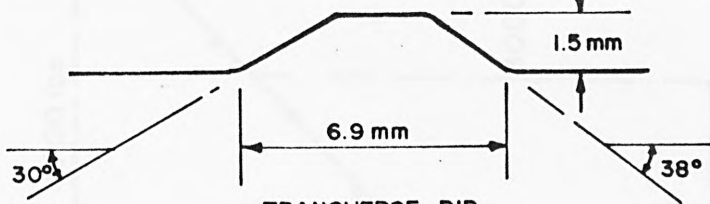
HYBAR



LONGITUDINAL ELEVATION



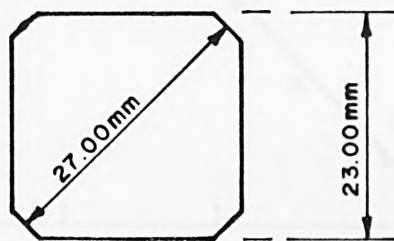
CROSS SECTION



TRANSVERSE RIB

RIB PROFILE

SQUARE-TWISTED BAR



CROSS SECTION

FIG. B1 DETAILS OF TEST BAR

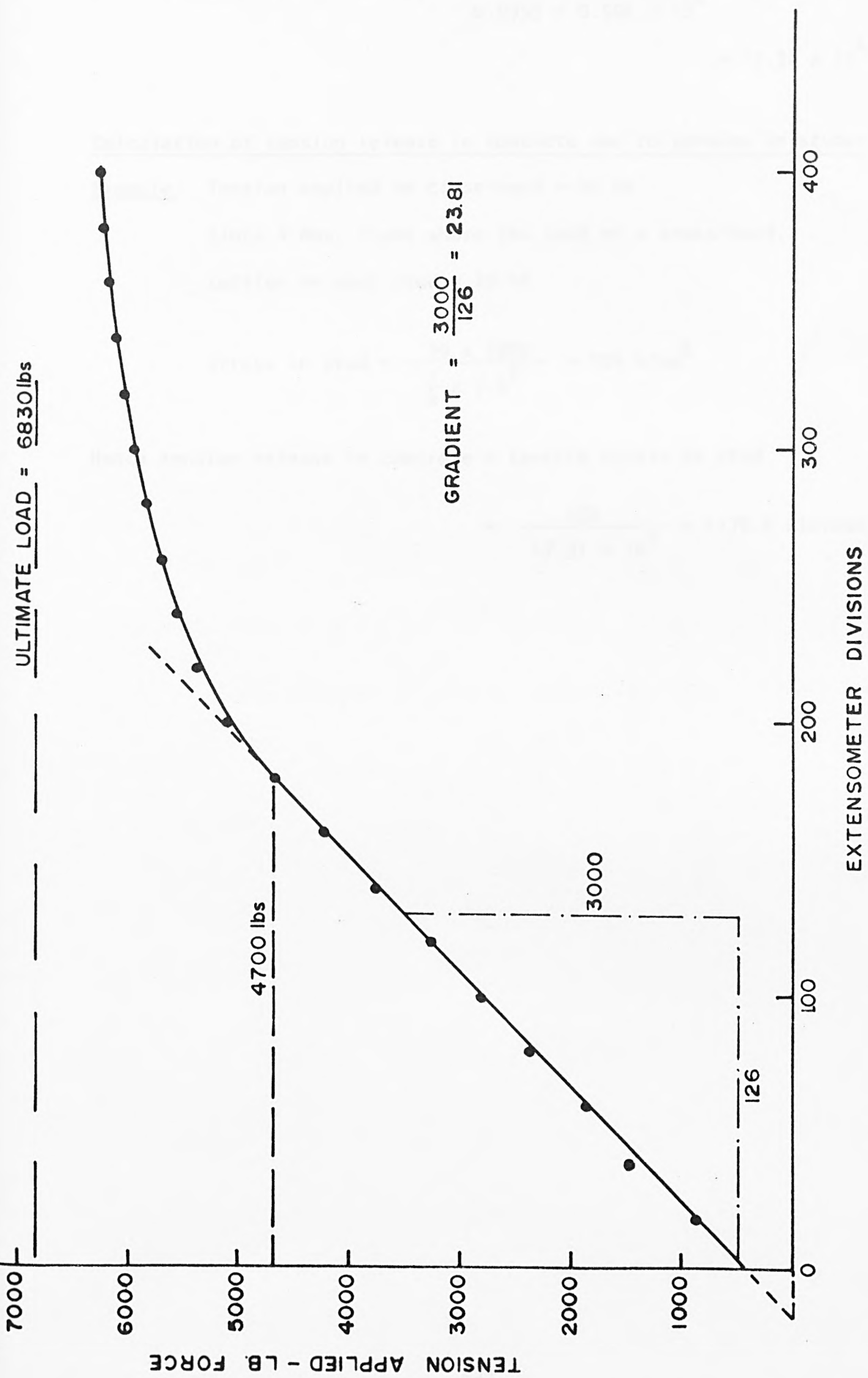


FIG. B.2 STRESS-STRAIN CHARACTERISTIC OF HIGH TENSILE STEEL STUD

$$\therefore \text{Modulus of elasticity} = \frac{23.81 \times 4}{0.0759 \times 0.506 \times 10^{-4}} = 25.1 \times 10^6 \text{ lb/in}^2$$

$$= 17.31 \times 10^4 \text{ N/mm}^2$$

Calculation of tension release in concrete due to tension in studs:

Example: Tension applied on cross-head = 40 kN

Since 4 Nos. studs share the load on a cross-head,
tension on each stud = 10 kN

$$\therefore \text{Stress in stud} = \frac{10 \times 1000}{\frac{\pi}{4} \times 7.9^2} = 204 \text{ N/mm}^2$$

p.32

Hence tension release in concrete = tensile strain in stud

$$= \frac{204}{17.31 \times 10^4} = 1178.6 \text{ microstrains.}$$

APPENDIX C

DATA RELATING TO LATERAL COMPRESSION TESTS

APPENDIX 'C'

C.1 Details of concrete mix

The details of the concrete mix used in the lateral compression tests performed at the University of Malaya, Kuala Lumpur are given below for casting one test block and accompanying 100 mm cubes (12 Nos.) and 2 Nos. 150 mm diameter x 30 mm long cylinders.

- Weight of cement (Tiger Brand) = 38.5 kg
- Weight of mining sand = 76.5 kg
- Weight of granite (20 mm) = 133.0 kg
- Weight of water = 21.0 kg

The results of the cube compression strength tests and splitting tensile strength of cylinders are given in Table C.1.

Test Specimen	Date cast	Date tested	Cube Strength (N/mm ²)	Splitting cylinder strength (N/mm ²)
T 113-0; T 113-2	10.3.81	28.3.81	34.37	2.99
T 113-4; T 113-6	8.7.75	30.7.75	33.69	2.31
T 88-0; T 88-2	22.4.81	11.5.81	33.70	2.60
T 88-4; T 88-6	12.8.75	30.8.75	32.64	2.49
T 63-0; T 63-2	24.6.75	16.7.75	32.02	2.54
T 63-4; T 63-6	26.8.75	12.9.75	34.81	2.63
T 37-0; T 37-2	30.6.75	25.7.75	30.10	2.16
T 37-4; T 37-6	15.9.75	23.9.75	34.21	2.90
H 113-0; H 113-6	23.1.80	5.2.80	34.77	2.90
H 113-2; H 113-4	7.5.80	23.5.80	36.43	2.90
H 88-0; H 88-6	24.3.80	8.4.80	35.21	3.18
H 88-2; H 88-4	11.6.80	27.6.80	34.93	2.72
H 63-0; H 63-6	1.4.80	16.4.80	36.88	2.80
H 63-2; H 63-4	23.7.80	9.8.80	33.17	2.90
H 37-0; H 37-2	10.2.82	27.2.82	34.66	2.79
H 37-4; H 37-6	7.10.80	26.10.80	32.93	2.95
S 113-0; S 113-2	8.11.77	23.11.77	34.40	2.68
S 113-4; S 113-6	7.6.79	23.6.79	36.94	2.79
S 88-0; S 88-2	10.1.78	3.2.78	35.45	2.70
S 88-4; S 88-6	17.7.79	8.8.79	35.72	3.01
S 63-0; S 63-2	31.1.78	24.2.78	35.34	2.25
S 63-4; S 63-6	3.10.79	24.10.79	38.09	2.63
S 37-0; S 37-2	16.8.78	2.9.78	34.60	2.76
S 37-4; S 37-6	27.11.79	12.12.79	37.91	3.21

TABLE C.1: STRENGTH OF CONCRETE - LATERAL PRESSURE

C.2 Calibration of load cell

The calibration data of the load cell used in measuring the load applied in the lateral compression test series is given in Table C.2 below:

Load (Tons)	Reading on Digital Bridge (Microstrains)
0	0
1	52
2	108
3	165
4	220
5	276
6	331
7	386
8	444
9	495

Calibration Constant of Load Cell

Range 0 - 6 Tons.

No. of divisions per ton = 55.17

100 divisions = 17.86 kN

TABLE C.2: CALIBRATION OF LOAD CELL

C.3 Verification of system of applying lateral pressure

The system of applying the lateral pressure to the concrete is explained in Section 4.3. It was assumed that the vertical load applied by the jack on the thrust block is distributed evenly by the thrust block over an area 100 mm x 50 mm. A simple experiment was conducted to determine the effectiveness of the system adopted.

A prism of concrete P measuring 100 mm long and cross-section 25 mm x 25 mm cut from a cube of concrete was mounted on opposite faces with

strain gauges at positions 1, 2, 3 and 4 as shown in the sketch. This strain-gauged prism was then cast in

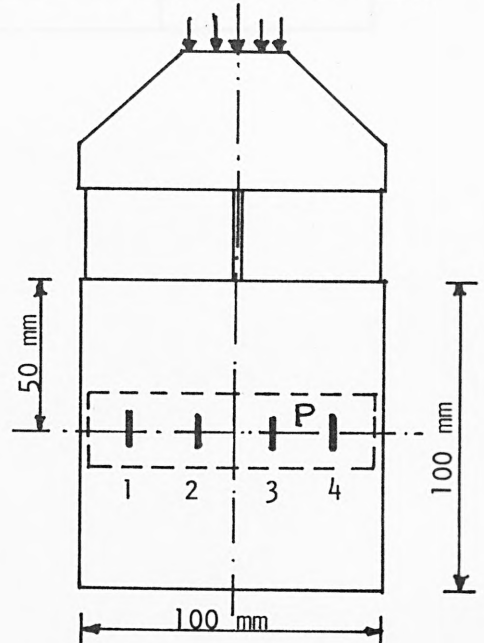
a concrete block measuring 100 mm x 100 mm x 75 mm with its centre line placed at a depth of 50 mm from the

top of the block. Load was then applied to the thrust block placed as shown on the concrete block in

a Universal testing machine and strain-gauge readings were recorded. The average strains recorded

at different load levels is given in the table below. The loading arrangement seems to offer a reasonable distribution of pressure

with a slightly greater pressure at the centre. The low reading at position 1 is considered as possibly due to a malfunctioning of one of the gauges at that position.



Load Applied (Tons)	Strain readings in microstrains			
	Position 1	Position 2	Position 3	Position 4
0	0	0	0	0
1.0	32	48	45	44
1.5	45	70	68	64
2.0	60	90	92	83
2.5	75	112	114	102

4.1. Calculated Bond in Lap of Reinforcement

Example calculation:

First condition (S1): total stress $f_s = f_{yk} = \frac{N_{Ed}}{A_s}$

Based on the procedure to determine the design stress $f_{s,Ed}$ in accordance with the existing design strength f_{yk} related to the design strength f_{yk} relation

$$f_{s,Ed} = 0.87 f_{yk}$$

$$f_{s,Ed} = 0.87 \cdot 275 = 239.25 \text{ N/mm}^2$$

APPENDIX D

Type of bar: Y12

CALCULATIONS OF BOND FORCE

1.1) Design stress $f_{s,Ed} = 1.2 \cdot 275 = 330 \text{ N/mm}^2$

1.2) Pressure $p = 0.1 \cdot f_{s,Ed} = 2.75 \text{ N/mm}^2$

$$= 2.75 \times 0.0001 \text{ m}^2 = 2.75 \times 10^{-4} \text{ m}^2$$

1.3) Effective bond length $l_{b,eff} = 30d$

$F = f_{b,Ed} \cdot l_{b,eff} \cdot A_s$ is a coefficient of bar in development length

$$= \frac{2.75 \times 12.75 \times 100}{1000} \times 12.75 \times 10$$

APPENDIX 'D'

D.1 Calculated force in bar at bond failure

Sample calculations:

From equation (5.13), bond stress $f_b = f_t \frac{(C + D/2)}{1.664 D}$

Based on the concrete strength results in Table C.1 in Appendix 'C', the splitting tensile strength is related to cube strength by the relation

$$f_t = 0.47 \sqrt{f_{cu}}$$

$$\therefore f_t = 0.47 \sqrt{35} = 2.78 \text{ N/mm}^2$$

Type of Bar: Torbar

$$\text{Perimeter} = \pi \times 25.06 = 78.72 \text{ mm}$$

1. Cover = 25 mm = 1.0 D; $C + D/2 = 37 \text{ mm}$

(i) Pressure = 0; $f_b = 2.78 \times \frac{1.5 D}{1.664 D}$

$$= 2.78 \times 0.90144 = 2.506 \text{ N/mm}^2$$

Frictional component $F_{fr} = 0$;

$\therefore F = F_{cr} = f_b \times \text{perimeter of bar} \times \text{embedment length}$

$$= \frac{2.506 \times 78.72 \times 100}{1000} \text{ kN} = \underline{19.72 \text{ kN}}$$

(ii) Pressure = 3.92 N/mm^2 (Vertical load = 19.6 kN)

From Table 7.16, $\sigma_y = 0.265 \text{ N/mm}^2$

From Table 7.17, vertical pressure at level of bar = 2.72 N/mm^2

$$f_b = (2.78 - 0.265) \times 0.90144 = 2.267 \text{ N/mm}^2$$

$$F_{cr} = \frac{2.267 \times 78.72 \times 100}{1000} = 17.85 \text{ kN}$$

$$F_{fr} = f_{br} \times p_{av} \times \text{perimeter of bar} \times \text{embedment length}$$

$$= 0.5 \times \frac{2.72}{2} \times 78.72 \times \frac{100}{1000} = 5.35 \text{ kN}$$

$$\therefore F = F_{cr} + F_{fr} = 17.85 + 5.35 = \underline{23.20 \text{ kN}}$$

(iii) Pressure = 7.84 N/mm^2 (Vertical load = 39.2 kN)

From Table 7.16, $\sigma_y = 0.530 \text{ N/mm}^2$

From Table 7.17, vertical pressure at level of bar = 5.44 N/mm^2

$$f_b = (2.78 - 0.530) \times 0.90144 = 2.028 \text{ N/mm}^2$$

$$\therefore F = \frac{2.028 \times 78.72 \times 100}{1000} + 0.5 \times \frac{5.44}{2} \times 78.72 \times \frac{100}{1000}$$

$$= \underline{26.67 \text{ kN}}$$

(iv) Pressure = 11.76 N/mm^2 (Vertical load = 58.8 kN)

From Table 7.16; $\sigma_y = 0.795 \text{ N/mm}^2$

From Table 7.17; vertical pressure at level of bar = 8.17 N/mm^2

$$f_b = (2.78 - 0.795) \times 0.90144 = 1.789 \text{ N/mm}^2$$

$$\therefore F = 1.789 \times 78.72 \times \frac{100}{1000} + 0.5 \times \frac{8.17}{2} \times 78.72 \times \frac{100}{1000}$$

$$= \underline{30.16 \text{ kN}}$$

The calculations are now repeated for the other covers. Values of σ_y are obtained from Table 7.16 and the values of vertical pressure at level of bar are from Table 7.17.

2. Cover = 50 mm = 2.0 D;

In this case, the top cover to the bar governs i.e. $C + D/2 = 50 \text{ mm}$

(i) Pressure = 0; $f_b = 2.78 \times \frac{2.0 D}{1.664 D}$

$$= 2.78 \times 1.2019 = 3.34 \text{ N/mm}^2$$

Frictional component $F_{fr} = 0$

$$\therefore F = F_{cr} = 3.34 \times 78.72 \times \frac{100}{1000} = \underline{26.30 \text{ kN}}$$

(ii) Pressure = 3.92 N/mm^2

$$\sigma_y = 0.404 \text{ N/mm}^2$$

Vertical pressure at level of bar = 2.0 N/mm^2

$$f_b = (2.78 - 0.404) \times 1.2019 = 2.855 \text{ N/mm}^2$$

$$\begin{aligned} \therefore F &= 2.855 \times 78.72 \times \frac{100}{1000} + 0.5 \times \frac{2.0}{2} \times 78.72 \times \frac{100}{1000} \\ &= \underline{26.42 \text{ kN}} \end{aligned}$$

(iii) Pressure = 7.84 N/mm^2

$$\sigma_y = 0.809 \text{ N/mm}^2$$

Vertical pressure at level of bar = 4 N/mm^2

$$f_b = (2.78 - 0.809) \times 1.2019 = 2.369 \text{ N/mm}^2$$

$$\begin{aligned} \therefore F &= 2.369 \times 78.72 \times \frac{100}{1000} + 0.5 \times \frac{4.0}{2} \times 78.72 \times \frac{100}{1000} \\ &= \underline{26.52 \text{ kN}} \end{aligned}$$

$$(iv) \text{ Pressure} = 11.76 \text{ N/mm}^2$$

$$\sigma_y = 1.213 \text{ N/mm}^2$$

$$\text{Vertical pressure at level of bar} = 6 \text{ N/mm}^2$$

$$f_b = (2.78 - 1.213) \times 1.2019 = 1.883 \text{ N/mm}^2$$

$$\begin{aligned} \therefore F &= 1.883 \times 78.72 \times \frac{100}{1000} + 0.5 \times \frac{6.0}{2} \times 78.72 \times \frac{100}{1000} \\ &= \underline{26.64 \text{ kN}} \end{aligned}$$

$$3. \text{ Cover} = 75 \text{ mm} = 3.0 D$$

In this case too, the top cover to the bar governs i.e. $C + D/2 = 50 \text{ mm}$

$$(i) \text{ Pressure} = 3.92 \text{ N/mm}^2$$

$$\sigma_y = 0.290 \text{ N/mm}^2$$

$$\text{Vertical pressure at level of bar} = 1.77 \text{ N/mm}^2$$

$$f_b = (2.78 - 0.290) \times 1.2019 = 2.993 \text{ N/mm}^2$$

$$\begin{aligned} \therefore F &= 2.993 \times 78.72 \times \frac{100}{1000} + 0.5 \times \frac{1.77}{2} \times 78.72 \times \frac{100}{1000} \\ &= \underline{27.04 \text{ kN}} \end{aligned}$$

$$(iii) \text{ Pressure} = 7.84 \text{ N/mm}^2$$

$$\sigma_y = 0.579 \text{ N/mm}^2$$

$$\text{Vertical pressure at level of bar} = 3.53 \text{ N/mm}^2$$

$$f_b = (2.78 - 0.579) \times 1.2019 = 2.645 \text{ N/mm}^2$$

$$\begin{aligned} \therefore F &= 2.645 \times 78.72 \times \frac{100}{1000} + 0.5 \times \frac{3.53}{2} \times 78.72 \times \frac{100}{1000} \\ &= \underline{27.76 \text{ kN}} \end{aligned}$$

$$(iv) \text{ Pressure} = 11.76 \text{ N/mm}^2$$

$$\sigma_y = 0.869 \text{ N/mm}^2$$

$$\text{Vertical pressure at level of bar} = 5.30 \text{ N/mm}^2$$

$$f_b = (2.78 - 0.869) \times 1.2019 = 2.297 \text{ N/mm}^2$$

$$\begin{aligned} \therefore F &= 2.297 \times 78.72 \times \frac{100}{1000} + 0.5 \times \frac{5.30}{2} \times 78.72 \times \frac{100}{1000} \\ &= \underline{28.51 \text{ kN}} \end{aligned}$$

$$4. \text{ Cover} = 100 \text{ mm} = 4.0 D$$

In this case too, the top cover to the bar governs i.e. $C + D/2 = 50 \text{ mm}$

$$(i) \text{ Pressure} = 0; f_b = 2.78 \times \frac{2.0 D}{1.664 D} = 2.78 \times 1.2019 = 3.34 \text{ N/mm}^2$$

$$F = F_{cr} = 3.34 \times 78.72 \times \frac{100}{1000} = \underline{26.30 \text{ kN}}$$

$$(ii) \text{ Pressure} = 3.92 \text{ N/mm}^2$$

$$\sigma_y = 0.260 \text{ N/mm}^2$$

$$\text{Vertical pressure at level of bar} = 1.65 \text{ N/mm}^2$$

$$f_b = (2.78 - 0.260) \times 1.2019 = 3.029 \text{ N/mm}^2$$

$$\begin{aligned} \therefore F &= 3.029 \times 78.72 \times \frac{100}{1000} + 0.5 \times \frac{1.65}{2} \times 78.72 \times \frac{100}{1000} \\ &= \underline{27.08 \text{ kN}} \end{aligned}$$

$$(iii) \text{ Pressure} = 7.84 \text{ N/mm}^2$$

$$\sigma_y = 0.520 \text{ N/mm}^2$$

$$\text{Vertical pressure at level of bar} = 3.29 \text{ N/mm}^2$$

$$f_b = (2.78 - 0.52) \times 1.2019 = 2.716 \text{ N/mm}^2$$

$$\begin{aligned} \therefore F &= 2.716 \times 78.72 \times \frac{100}{1000} + 0.5 \times \frac{3.29}{2} \times 78.72 \times \frac{100}{1000} \\ &= \underline{27.86 \text{ kN}} \end{aligned}$$

$$(iv) \quad \text{Pressure} = 11.76 \text{ N/mm}^2$$

$$\sigma_y = 0.781 \text{ N/mm}^2$$

$$\text{Vertical pressure at level of bar} = 4.94 \text{ N/mm}^2$$

$$f_b = (2.78 - 0.781) \times 1.2019 = 2.404 \text{ N/mm}^2$$

$$\begin{aligned} \therefore F &= 2.404 \times 78.72 \times \frac{100}{1000} + 0.5 \times \frac{4.94}{2} \times 78.72 \times \frac{100}{1000} \\ &= \underline{28.64 \text{ kN}} \end{aligned}$$

Plough-through force

Bond stress is given by Equation 5.23

$$\text{i.e. } f_b = 0.5 \sqrt{f_t \cdot f_{cu}} \cdot \frac{D_c + 2h}{D}$$

$$f_t = 2.78 \text{ N/mm}^2; \quad f_{cu} = 35 \text{ N/mm}^2; \quad D = 25.06 \text{ mm}$$

$$D_c = 24.08 \text{ mm}; \quad h = 1.20 \text{ mm}$$

$$\therefore f_b = 0.5 \times \sqrt{2.78 \times 35} \cdot \frac{26.48}{25.06} = 5.21 \text{ N/mm}^2$$

$$F = 5.21 \times \pi \times 26.48 \times \frac{100}{1000} = \underline{43.35 \text{ kN}}$$